

BIOSENSING TOTAL BACTERIAL LOAD IN LIQUID MATRICES TO IMPROVE FOOD
SUPPLY CHAIN SAFETY USING CARBOHYDRATE-FUNCTIONALIZED MAGNETIC
NANOPARTICLES FOR CELL CAPTURE AND GOLD NANOPARTICLES FOR
SIGNALING

By

Leann Lerie Matta

A DISSERTATION

Submitted to
Michigan State University
in partial fulfillment of the requirements
for the degree of

Biosystems Engineering – Doctor of Philosophy

2018

ABSTRACT

BIOSENSING TOTAL BACTERIAL LOAD IN LIQUID MATRICES TO IMPROVE FOOD SUPPLY CHAIN SAFETY USING CARBOHYDRATE-FUNCTIONALIZED MAGNETIC NANOPARTICLES FOR CELL CAPTURE AND GOLD NANOPARTICLES FOR SIGNALING

By

Leann Lerie Matta

Economical rapid nano-biosensing methods with expedited electrochemical signaling, were developed using carbohydrate-functionalized magnetic nanoparticles (MNP) and gold-nanoparticles (AuNP) to detect pathogenic bacteria in liquid or homogenized food samples. MNP functionalized with glycan- and amino/glycan ligands were able to rapidly extract bacteria, while concentrated dextrin-coated AuNP labeling improved detection sensitivity. Carbohydrate ligands are more stable than antibodies, permitting long shelf life of MNP at room temperature and minimized AuNP aggregation during simple refrigeration. Transmission electron microscopy (TEM) imaged the electrostatic binding between MNP and *Salmonella* Enteritidis, *E. coli* O157:H7, *Bacillus cereus*, *Listeria monocytogenes* and *E. coli* C3000, which mimics electrostatic binding by antibodies, although with lower specificity.

Capture index (CI) is defined as the parts-per-thousand (ppt) of bacteria extracted per initial bacterial presence. TEM images showed that attached milk matrix components did not interfere with microbial capture. *Salmonella*, *E. coli*, and *Bacillus* (3 to 5 log CFU/mL) capture in three milks was 2 ppt to 120 ppt CI. Capture in beef juice and apple cider was 0.002 ppt to 0.011 ppt for *E. coli* and *Listeria*, respectively, at 10 log cfu/mL due to accelerated microbial growth immediately following the spike. Viscous homogenized eggs, though, impeded MNP-*Salmonella* migration to the magnet during separation. This phenomenon was a motivating factor in creating “dip-sticks”: plastic strips coated in MNP (MNP-strip).

Rapid nano-biosensing of MNP-cell complexes in under 30 min from either suspended or strip capture was possible using electrochemical technology of spectrometry or a simple handheld potentiostat. Capture concentrates bacteria as MNP-cell from large volumes allowing strong cyclic voltammetric (CV) signaling. Normalized peak current responses (NPCR) for microbial detection from simple matrices (PBS and beef juices) showed sample (S) NPCR lower than negative controls (N) ($S/N < 1.0$). Whereas in complex matrices (milk, apple cider, and homogenized eggs), S/N were significantly greater than 1.0. NPCR for negative controls were found to be linearly related to matrix components fats, proteins, and sodium ($R^2 = 0.92$). Except for *E. coli* in beef juices, all S/N were significant ($p < 0.05$) for contamination levels ranging between 6.2 to 12.3 log CFU/mL.

Enhanced signaling of low pathogen presence in food was achieved using electrically active AuNP labeling. Electrochemical detection of MNP-cell-AuNP complexes with spectrophotometry or differential pulse voltammetry (DPV) was significantly more sensitive, detecting 3 log CFU/mL and 5 log CFU/mL *E. coli* contamination in milk ($p < 0.20$), respectively. Food component attachment to the complexes altered, but did not interfere, with distinguishing samples from negative controls.

MNP carbohydrate ligands exposed to refrigerated milk matrix components (fats, lipids, sugars, protein and sodium) for up to 9-days still extracted bacteria. This makes possible future biocompatible tag-on nano-biosensors inside individual food packaging. Pathogen presence could be monitored over the lifetime of the product, reducing consumption of contaminated foods. Reliable frequent testing along the food supply chain would facilitate reduced human disease, while reducing industry financial losses due to foodborne outbreaks. Flexible carbohydrate-based MNP-cell/(CV) and MNP-cell-AuNP/(DPV or spectrometry) nano-biosensing with electrochemical detection can provide a truly rapid, economical test.

Dedicated to my beloved family, supportive husband, Samir, of 32 blessed years of marriage,
and children, Laran Alexi & Andreas Per, Carlos & Alexa Kay, Anastasia and Ibtisam.

ACKNOWLEDGMENTS

This research was funded by The Axia Institute at Michigan State University (formerly MRIVCC) and supported by Dr. Evangelyn C. Alcocilja's Nano-Biosensors Lab.

My sincere gratitude to Dan Jones, Ph.D., for his continued professional guidance, friendship, and encouragement over many years, especially throughout my doctoral studies.

TABLE OF CONTENTS

LIST OF TABLES	ix
LIST OF FIGURES	x
LIST OF SCHEMES.....	xivii
KEY TO ABBREVIATIONS.....	xv
Chapter 1. Introduction	1
1.1 Introduction	1
1.2 Hypotheses	3
1.3 Objectives.....	4
1.4 Innovations	5
Chapter 2. Food Supply Chain Safety Against Pathogenic Microbial Contamination.....	8
2.1 Introduction	8
2.2 Food supply regulation.....	9
2.3 Pathogenic microbial contamination along the food supply chain	10
2.4 Conventional methods in pathogen detection	12
2.5 Conclusions	14
Chapter 3. Emerging Nano-biosensing with Suspended MNP Microbial Extraction and Electrically-Active Nanoparticle Labeling	16
3.1 Introduction	16
3.2 MNP-assisted Biosensing Properties	17
3.3 Suspended MNP-assisted Biosensing	21
3.4 MNP “dip-stick” Strips	24
3.5 Enhanced Biosensing with Electrically-Active Nanoparticles.....	28
3.6 Carbohydrate Ligands Against Microbial Targets	32
3.7 Microbial Surface Epitopes for Carbohydrate-functionalized MNP-cell-AuNP Nano-biosensing.....	34
3.8 Conclusions	39
Chapter 4. Literature Review – Technology.....	41
4.1 Introduction	41
4.2 Electrochemical Signaling Using Cyclic Voltammetry and Differential Pulse Voltammetry	42
4.2.1 MNP-cell-AuNP Detection.....	42
4.2.2 Voltammetric Methods	43
4.2.3 Micro-bio-sensing.....	45
4.2.4 Voltammetry Conventions.....	46
4.2.5 Improved Bio-sensing with Nanoparticles	49
4.2.6 Signal Interpretation	50

4.3 Spectrophotometric Verification of NP Presence and Quantity.....	52
4.3.1 Spectrophotometric Conventions	52
4.3.2 Spectrometry Bio-sensing.....	54
4.3.3 Spectral Integration.....	55
4.4 Conclusion.....	57
Chapter 5. Analysis of Carbohydrate-Functionalized Magnetic Nanoparticles and Dextrin-Coated Gold Nanoparticles Binding Properties to <i>Salmonella</i> , <i>E. coli</i> , <i>Bacillus</i> , and <i>Listeria</i> Using Transmission Electron Microscopy	60
5.1 Introduction	60
5.2 Materials and Methods	61
5.2.1 Materials	61
5.2.2 Microbial Culture	62
5.2.3 MNP Microbial Capture and Deactivation.....	62
5.2.4 Concentrated AuNP Preparation	63
5.2.5 AuNP Labeling of MNP-cell Complexes.....	64
5.2.6 TEM Imaging	64
5.3 Results and Discussion.....	65
5.3.1 Binding Forces Between Nanoparticles and Microbes.....	65
5.3.2 MNP- <i>Salmonella</i> Enteritidis Binding.....	67
5.3.3 MNP- <i>E. coli</i> O157:H7 Binding	68
5.3.4 MNP- <i>Bacillus cereus</i> Binding.....	70
5.3.5 MNP- <i>Listeria monocytogenes</i> Binding	71
5.3.6 AuNP Binding to MNP-cell Complexes	72
5.4 Conclusions	75
Chapter 6. Rapid Extraction of Pathogenic Bacteria from Liquid Foods using Carbohydrate-Functionalized Magnetic Nanoparticles Including Cyclic Voltammetric Detection.....	77
6.1 Introduction	77
6.2 Materials and Methods	80
6.2.1 Materials	80
6.2.2 Bacterial Culture.....	81
6.2.3 Suspended MNP Bacterial Capture in Milk	82
6.2.4 Suspended MNP Multiple Bacterial Capture	83
6.2.5 Matrix Exposure Effects on Suspended MNP Capture	84
6.2.6 Capture Index Calculation for Suspended MNP Capture.....	84
6.2.7 MNP-strip Production.....	85
6.2.8 MNP-strip Bacterial Capture	86
6.2.9 Cyclic Voltammetry Detection of Cell Presence on MNP-strips	87
6.2.10 Statistical Analysis	88
6.3 Results and Discussion.....	89
6.3.1 Aspects of Bacterial Capture.	89
6.3.2 Definition of a Complex Matrix	90
6.3.3 Suspended MNP Capture in Milk Matrices.....	91
6.3.4 Suspended MNP Capture of Multiple Bacteria	94
6.3.5 Milk Matrix Exposure Effects on Suspended MNP Capture.	98

6.3.6 Maximum Capture Index due to Equilibrium.....	100
6.3.7 Suspended MNP Capture in Beef Juices, Apple Cider and Homogenized Egg.....	102
6.3.8 Rapid Detection of Bacteria in Complex Liquids Using Cyclic Voltammetry	103
6.3.9 Confirmation of MNP-strip Bacterial Capture in Simple Buffer	104
6.3.10 Rapid Detection of Bacteria in Complex Liquids Using MNP-strips with Cyclic Voltammetry	107
6.4 Conclusions	111
 Chapter 7. Gold Nanoparticle Enhancement in Differential Pulse Voltammetric and Spectrophotometric Detection of MNP Extracted Bacteria.....	114
7.1 Introduction	114
7.2 Materials and Methods	116
7.2.1 Method of Development for Carbohydrate-based MNP-cell-AuNP Nano-Biosensing	116
7.2.2 Materials	116
7.2.3 Bacterial Culture.....	117
7.2.4 Antibody-functionalized AuNP.....	118
7.2.5 Specificity of Capture of <i>Salmonella</i> Monoclonal Antibody and Cross-reactivity....	119
7.2.6 Concentrated Dextrin-coated d-AuNP.....	119
7.2.7 Temporal Attachment of Concentrated d-AuNP to MNP-cell Complexes	120
7.2.8 Carbohydrate-based MNP-cell-AuNP Nano-biosensing	120
7.2.9 Electrochemical Spectrophotometric or Differential Pulse Voltammetric Detection	121
7.3 Results and Discussion.....	123
7.3.1 Electrochemical Signature Responses for MNP-cell-AuNP Biosensing	123
7.3.2 Specificity of <i>Salmonella</i> Detection Using Antibody-functionalized AuNP.....	127
7.3.3 Dextrin-coated AuNP Biosensing with DPV and Spectrometry	132
7.3.4 Electrochemical Quantification of MNP-cell-AuNP.....	136
7.4 Conclusions	140
 Chapter 8. Conclusions	141
 APPENDIX.....	151
 BIBLIOGRAPHY.....	154

LIST OF TABLES

Table 1.1 Innovative advances in nano-biosensing using carbohydrate-based MNP-cell-AuNP capture and label with electrochemical technology.	7
Table 3.1. Magnetization properties of various magnetic nanoparticles (MNP) with carbohydrate functional groups.	23
Table 3.2 Biosensing methods using suspended functionalized magnetic nanoparticles (MNP).	25
Table 3.3 Nano-biosensing methods with functionalized MNP and NP labeling.	30
Table 3.4 Biosensing methods using carbohydrate functional groups for target capture.	36
Table 6.1 Composition and properties of liquid matrices.	92
Table 6.2 Capture index (CI) of <i>Salmonella</i> , <i>E. coli</i> and <i>Bacillus</i> using suspended MNP-F#1 for large-volume capture (LVC) within three types of undiluted milk (25 mL) and each species' increased cell concentration factor in each milk type following the standard five-fold serial dilution. ⁺ (n=3).	95
Table 6.3 Capture indexes (CI) of <i>Salmonella</i> , <i>E. coli</i> and <i>Bacillus</i> using suspended MNP-F#2 for large-volume capture (LVC) within three types of undiluted milk (25 mL) and each species' increased cell concentration factor in each milk type following the standard five-fold serial dilution. ⁺ (n=3).	96
Table 6.4 Microbial capture indexes using suspended MNP-F#1 for rapid extraction of three competitive bacteria, <i>Salmonella</i> , <i>E. coli</i> and <i>Bacillus</i> , either simultaneously (at 10 ⁻⁶ dilutions of the stock culture) or separately (at 10 ⁻⁵ dilutions) from PBS and vitamin D milk in small-volume capture (SVC)*. (n=3)	97
Table 6.5 Capture indexes for <i>Salmonella</i> in large-volume capture following long-term suspended MNP-exposure ⁺ . (n=3)	100
Table 6.6 Normalized peak current responses (NPCR) for MNP-strip negative controls in simple and complex matrices and the matrix composition used in linear regression statistical analysis. (n=3).	109
Table 7.1 Specificity of <i>Salmonella</i> detection using antibody-functionalized AuNP.	128
Table S7.2 Specificity of <i>Salmonella</i> detection using antibody-functionalized AuNP.	153

LIST OF FIGURES

Figure 3.1 Schematic of the MNP-cell-AuNP biosensor for total bacterial load. Carbohydrate-functionalized MNP extract *E. coli* from artificially contaminated milk, while dextrin-coated EANP attach to captured cells at different cell receptors. Negative controls consist of sterile milk where MNP-EANP complexes form due to carbohydrate attraction between the functional groups. Cell quantification is possible using FDA bacteriological analytical methods (BAM) agar plating (top), where neither MNP nor EANP inhibit bacterial growth and negative controls will have no cell growth present. Rapid biosensing is possible with spectrophotometric or electrochemical signaling, where negative controls will produce larger signals due to higher EANP presence than samples, due to saturation binding of EANP to MNP. 18

Figure 3.2 Examples of hysteresis magnetization for magnetic nanoparticles (MNP) functionalized with carbohydrate groups, (A) from Alocilja Nano-Biosensors lab and (B) used in metal recovery [99] (emu = electromagnetic units). 21

Figure 4.1 Electrochemical systems exemplified with (A) common voltaic cell, (B) miniaturized screen-printed carbon electrode (SPCE) sensor, and (C) a mock-up of voltammetric bio-sensing with an SPCE chip with capture bacteria labeled with AuNP. 44

Figure 4.2 Examples of graphical results of nano-biosensing responses using cyclic voltammetry for microbial detection with MNP-strips on (A) soft plastic or (B) hard plastic. 44

Figure 4.3 Examples of graphical results of nano-biosensing responses using differential pulse voltammetry for microbial detection using MNP-cell-AuNP with (A) positive current convention and (B) negative current convention. 45

Figure 4.4 Equations for general theory of voltammetry including (A) the Nernst Equation which relates the applied potential force, E , across the electrode to the concentration of the reductive and oxidative species, c_R and c_O , respectively, where R is the molar gas constant ($8.3144 \text{ J mol}^{-1}\text{K}^{-1}$), T is the absolute temperature (K), n is the number of electrons transferred, $F =$ Faraday constant ($96,485 \text{ C/equivalents}$), and E^0 is the standard reduction potential for the redox couple; (B) the Butler-Volmer Equation further relates current, i , potential, E , and concentration, c_R and c_O , where $\theta = nF(E - E^0)/RT$, k^0 is the heterogeneous rate constant, a is known as the transfer coefficient, and A is the area of the electrode; and (C) Fick's Law relates the flux of matter, ϕ , which is directly proportional to the analyte concentration gradient, $\partial c_O/\partial x$, where D_O is the diffusion coefficient of oxidative species and x is the distance from the electrode surface [205]. 47

Figure 5.1 Examples of *Salmonella* Enteritidis (A) attachment to MNP-F#1 (B) and MNP-F#2 (C). 68

Figure 5.2 Examples of *E. coli* O157:H7 (A) binding to MNP-F#1 (B) including cell lysing over extended exposure (C) and to MNP-F#2 (D) as well as cell lysing that occurs over extended exposure (E). 69

Figure 5.3 Examples of *Bacillus cereus* (A) binding to MNP-F#1 (B) and MNP-F#2 with short exposure (C) and extended exposure to the MNP (D). 70

Figure 5.4 Examples of *Listeria monocytogenes* (A) binding to MNP-F#1 (B) and MNP-F#2 (C). 71

Figure 5.5 Examples of MNP-F#2-*E. coli* C3000 complex labeling with AuNP250 with excess AuNP250 present (A), showing aggregated AuNP binding to the cell wall (B) and at higher magnification (C) all in TSB, and finally persistence of AuNP binding to the cell structure even during lysing caused by extended MNP exposure in PBS. 733

Figure 5.6 Examples of unconcentrated d-AuNP (A), concentrated AuNP250 coating MNP-F#2 in PBS without prior milk exposure (B), with 2-step “capture” in milk then label in PBS (C), and with 1-step “capture and label” directly in the milk matrix (D). 74

Figure 6.1 Photos of extracted bacterial growth on solid agar for Salmonella on BGA (A), *E. coli* on LBA (B), *Bacillus* on LBA (C), and TEM images of milk contamination bound to MNP (D). 94

Figure 6.2 Evidence of MNP-strip Salmonella capture in PBS through TSB culture (A) and detection using cyclic voltammetry for soft plastic MNP-strips (B) and hard plastic MNP-strips (C), which showed an inverse linear relation ($R^2 = 0.7132$) to cells available for capture (D). Inset plots (B & C) show cathodic peaks in greater detail and the order of concentration listed in the legend (actual units log CFU/mL) follow the order of peak response. 106

Figure 6.3 Effect liquid matrix components upon CV detection for MNP-strip cell capture of *Salmonella* in PBS (6.19 log CFU/mL available cells, S/N = 0.85, p = 0.04) (A) and *E. coli* in beef juices (7.7 log CFU/mL available cells, S/N = 0.92, p = 0.08) (B). All peak current responses here were normalized to the mediator reference run at the time of testing to compare matrix effects upon current responses. (error bars = standard deviation) 108

Figure 6.4 Effect of homogenized egg matrix component upon CV peak current response increased proportionally as the purity of the matrix increased (A) such that MNP-strips exposed homogenized egg diluted with PBS showed higher peak current responses for higher PBS dilutions (B). All peak current responses here were normalized to the mediator reference run at the time of testing to compare matrix effects upon current responses. (error bars = standard deviation) 108

Figure 6.5 Effect of complex liquid matrix components upon CV detection for *Salmonella* in homogenized egg (12.3 log CFU/mL available cells, S/N = 1.25, p = 0.04) (A), *Listeria* in apple cider (7.9 log CFU/mL cells available, S/N = 1.13, p = 0.06) (B), and *E. coli* in vitamin D milk (8.5 log CFU/mL cells available, S/N = 1.08, p = 0.04) (C) showed lower peak current responses for negative controls, while cell presence expended less of the chemical mediator, resulting in

higher peak current responses. All peak current responses here were normalized to the mediator reference run at the time of testing to compare matrix effects upon current responses. (error bars = standard deviation)..... 110

Figure 7.1 Spectral scans of AuNP250 controls combined with MNP (A) and following attachment through the cell capture and labeling method (B)..... 124

Figure 7.2 Signature responses for MNP-cell-AuNP biosensing controls with differential pulse voltammetry. (Se= *Salmonella* Enteritidis) 125

Figure 7.3 Effect of sample complexity upon AuNP current response in DPV biosensing. 127

Figure 7.4 Specificity testing using anti-*Salmonella*-antibody-functionalized AuNP to label MNP-*Salmonella* (Target Se1 at 5.69 log CFU/mL and Se2 at 4.69 log CFU/mL) and MNP-*E. coli* (Non-Target Ec at 5.94 log CFU/mL) complexes, as well as negative controls, for DPV detection of the AuNP label..... 130

Figure 7.5 DPV current responses for concentrated AuNP responses (A) showing a linear relation between current response at 0.4 V and AuNP volume where (B) AuNP responses are indicated with an arrow. 133

Figure 7.6 Spectral absorbance of concentrated AuNP (A) showing an extinction peak at approximately 520 nm; (B) AuNP concentration is linearly related to both the peak height and the step-integrated spectral absorbance between 220 nm to 900 nm (n = 3)..... 134

Figure 7.7 Spectral signaling for carbohydrate-based MNP-cell-AuNP complexes showing (A) shifted AuNP peak from 520 nm slightly masked with the MNP peak at approximately 620 nm where (B) both the AuNP peak height and step-integrated spectral area 220 – 900 nm are linearly related to the time allotted for AuNP attachment. 135

Figure 7.8 Electrochemical nano-biosensing for simultaneous carbohydrate-based MNP-*E. coli*-AuNP rapid extraction from milk and electrically-active labeling followed by (A) DPV or (B) spectral analysis of samples and negative controls for microbial detection in milk (n=3). “e5Ec” = log 5 CFU/mL *E. coli* and “e3Ec” = log 3 CFU/mL *E. coli*..... 137

Figure 7.9 Graphs for electrochemical nano-biosensing for simultaneous carbohydrate-based MNP-*E. coli*-AuNP rapid extraction and electrically-active labeling followed by (A) DPV or (B) spectral analysis of samples and negative controls for microbial detection in milk (n=3). Arrows identify (A) 0.4 V and (B) 520 nm for the AuNP response location. “e5Ec” = log 5 CFU/mL *E. coli* and “e3Ec” = log 3 CFU/mL *E. coli*..... 138

Figure 8.1 Cost-benefit analysis of microbial contamination detection in the food supply chain including (nano-) biosensing methods. (see text for acronym definitions) 148

Figure S8.2 Example of adjusted DPV current response for MNP-F#2-cell-Ab-AuNP nano-biosensing, showing corrected baseline with respect to average current response between 0.9 V to

0.6 V; identifying maximum (average) AuNP response potential (arrow, 0.38 here); and portion of a sample signal for clarity during visual data analysis..... 152

LIST OF SCHEMES

Schematic 6.1. Rapid detection of bacterial contamination in contaminated liquids using MNP-strips and CV detection. MNP-F#2 affixed to plastic strips (MNP-strip) (A) for user-friendly capture in only 10 min (B) by either dipping the strip into microbial contamination within undiluted liquids or applying 250 uL liquid onto the strip (C), then rapid detection by electrochemical testing of reacted chemical mediator on a screen-printed carbon electrode (SPCE) (D) using cyclic voltammetry (E). Results between samples and negative controls are shown in (F)..... 88

KEY TO SYMBOLS AND ABBREVIATIONS

Units

°C = degrees Celsius

μA = microamps

μL = microliter

μM = micromolar

CFU/mL = colony forming units per milliliter

cm = centimeter

cm² = centimeters squared

emu/gm = electromagnetic units per gram

fg/mL = femtogram per milliliter

gm = gram

hr = hour

in Hg = inches mercury

log CFU/mL = log base 10 of colony forming units per milliliter

M = molar

mg = milligram

mg/mL = milligram per milliliter

min = minutes

mL = milliliter

ms = milli seconds

mS/cm = milli-Siemens per centimeter

mV = millivolt

mV/s = millivolts per second

nm = nanometer

nm = nanometers

nM = nanomolar

pM = picomolar

ppm = parts per million

ppt = parts per thousand

rpm = rotations per minute

tbsp = tablespoon

V = volts

v/v = volume of MNP to volume total ratio

Chemical Nomenclature

Ca²⁺ = calcium ion

CoPt₃ = cobalt platinum

Fe₃O₄ = iron oxide

FePt = iron platinum

H₂O₂ = hydrogen peroxide

HCl = hydrochloric acid

Mn²⁺ = manganese ion

O = oxygen

S = Sulphur

Research-Related Acronyms

α = confidence level for statistical tests

1-step biosensing = microbial detection using magnetic nanoparticle capture and gold nanoparticle labeling simultaneously, followed by differential pulse voltammetric detection

2-step biosensing = microbial detection using magnetic nanoparticle capture first, then gold nanoparticle labeling separately, followed by differential pulse voltammetric detection

Ab-AuNP = antibody-functionalized gold nanoparticles

ANOVA = analysis of variance

AuNP = gold nanoparticles

BAM = bacteriological analytical methods

BGA = brilliant green agar

CI = capture index

CV = cyclic voltammetry

d-AuNP = dextrin-coated gold nanoparticles

DPV = differential pulse voltammetry

FORMVAR = trademarked film coating for microscopy grids

LBB = Luria Bertani broth

LVC = large volume capture

MANOVA = multi-variate analysis of variance

MNP = magnetic nanoparticles

MNP/EANP – complexes consisting of magnetic nanoparticle and electrically-active nanoparticles

MNP-AuNP = magnetic nanoparticles labeled with gold nanoparticles

MNP-cell = complexes consisting of magnetic nanoparticles attached to cells

MNP-cell/CV = cyclic voltammetric detection of complexes consisting of magnetic nanoparticles attached to cells

MNP-cell-AuNP – complexes consisting of magnetic nanoparticles attached to cells and labeled with (dextrin-coated) gold nanoparticles

MNP-cell-AuNP/DPV = differential pulse voltammetric detection of complexes consisting of magnetic nanoparticles attached to cells and labeled with (dextrin-coated) gold nanoparticles

MNP-F#1 = glycan-functionalized magnetic nanoparticles

MNP-F#2 = amino/glycan-functionalized nanoparticles

MNP-strip = (amino/glycan-functionalized) magnetic nanoparticles adhered to plastic strips

MNP-strip-cell = cells attached to magnetic nanoparticles adhered to plastic strips

MNP-strip-cell/CV = cyclic voltammetric detection of cells attached to (amino/glycan-functionalized) magnetic nanoparticles adhered to plastic strips

MOX = modified Oxford media

N = negative control

n = number of replicates

NPCR = normalized peak current response

PBS = phosphate buffered solution

PCA = principle component analysis

pH = negative logarithm base ten of the hydrogen concentration

p-value = indicator of the strength of the null hypothesis

R^2 = coefficient of determination representing the variability in the identified dependent variable with respect to a linear combination of independent variable regressors

S = sample

S/N = ratio of the electrochemical current responses of the sample to corresponding negative control

SVC = small volume capture

TEM = transmission electron magnification

TSA = tryptic soy agar

TSB = tryptic soy broth

Literature Review and Background-Related Acronyms

HAACP = Hazard Analysis and Critical Control Point

HPLC-DAD = high-pressure liquid chromatography diode array detection

HRP = horseradish peroxidase

HUS = hemolytic uremic syndrome

i = current response

I_{pa} = anodic peak current

I_{pc} = cathodic peak current

LPS = lipopolysaccharide

M_s = magnetization saturation

OMP = outer membrane protein

PCR = polymerase chain reaction

pKa = acid dissociation constant

QD = quantum dots

RF = radio frequency

RNA = ribonucleic acid

SPEL = signaling pathogens electrically in liquids

SPR = surface plasmon resonance

SWCNT = single-walled carbon nanotubes

TN = titanium oxide nanoparticles

USDA = United States Department of Agriculture

UV-Vis = ultraviolet-visible light

WHO = World Health Organization

Chapter 1. Introduction

1.1 Introduction

Worldwide population growth is estimated to reach 9.8 billion people by 2050 [49]. This growth will further strain our food and water supplies. Currently over 28 billion meals are consumed each day around the globe [50], but foodborne disease sickened 600 million people globally in 2010, causing over 420,000 deaths from foodborne hazards, including those that were bacterial in origin [1]. Unfortunately, children under the age of 5 years represented 40% of these illnesses [51]. Higher mortality rates persistently hit developing countries in African sub-regions, South-East Asia and the Eastern Mediterranean [51], [52], which have limited economical resources to fight these diseases.

Environmental microbial pathogens are therefore a major concern, especially creating a double-edged sword for developing countries. Food and water scarcity create conditions in which contamination is ignored by starving people who can also ill afford to contract diseases. Even in the US, foodborne outbreaks sicken thousands yearly, with the majority caused by three pathogenic bacteria: *Salmonella*, Shiga Toxin-producing *E. coli*, and *Listeria monocytogenes* [53], [54]. Many biosensing assays are too expensive or technically complicated to be economically feasible in many regions of the world. Designing a biosensor to meet more stringent regulations established by the US through the FDA and USDA will ensure rigorous assay performance worldwide. Economical methods will ensure affordability in even developing countries and should require minimal storage and technology, with long shelf life, such as those using carbohydrate-functionalized magnetic nanoparticle (MNP) and dextrin-coated gold nanoparticles (AuNP) [2]–[6].

In ensuring a secure microbial pathogen-free food supply, rapid response detection of microbial contamination is of utmost importance. Many biosensor designs consist of self-contained test strips developed from the base up with complex nanoparticle chemistry and intricate ligand immobilization. Some methods are based upon ELISA 96-well plate technology with fluorescent detection or may use expensive antibody receptors or DNA ligands. Many of these proposed designs are impractical for most users, since they don't first address the broad goals of any biosensor: Field operability, Inexpensive, with Real-time detection that is both Sensitive and Specific to target, while being as Trouble-free as possible (FIRST) [7]. Carbohydrate ligands are inexpensive, robust structures that are increasingly synthesized for higher selectivity. Used in conjunction with optical or electrical detection of gold nanoparticles (AuNP), carbohydrate-functionalized MNP-cell-AuNP nano-biosensing advances the goal of being the FIRST biosensor of choice in detecting microbial pathogens throughout our food supply chain.

Quantifying the level of microbial contamination within a food product using the FDA preferred bacteriological analytical methods (BAM) requires tedious, time-consuming and supply-intensive microbiological methods for decades in the US [8]. Before that, though, humans rarely knew the potential food hazards that may have sickened them, as discussed in food microbiology courses, much less went so far as to investigate their cause[9]. With technological advances made in miniaturizing sensor components in the past twenty years, nano-sized sensors have reduced most aspects of microbial detection. Nano-biosensors are now prevalent within medical, environmental and even personal-use areas [10]–[13]. Within industrialized countries, cost is of little concern to the user; and within under/developing countries, cost is the least of their concerns, since many of the nano-biosensors designed to date also require expensive test equipment, environmentally sensitive components, refrigeration, and advanced knowledge to use [14].

Given the amount of sampling required throughout the food supply chain, reliable rapid methods are of necessity to expedite risk assessment for food products on the market. To improve the process of reliably tracking pathogenic microbial contamination within our food supply, this research evaluated the ability of inexpensive, highly reactive magnetic and gold nanoparticles to develop rapid tests that quantify bacterial levels in liquid food products. Overall, the goal of this research is to apply the capture and biosensing technology of carbohydrate-functionalized MNP and AuNP for rapid detection and quantification of microbial loads in complex liquid food matrices to improve the safety of our highly-integrated food supply chain and thereby reduce incidences of foodborne outbreaks.

1.2 Hypotheses

This research had three hypotheses with regards to carbohydrate-based MNP/AuNP nano-biosensing. First, magnetic nanoparticles (MNP) coated with carbohydrates, without the presence of antibodies, will still rapidly bind, extract, and concentrate microbial pathogens from complex liquid food matrices to reduce the rate of false negatives through increased signal strength without initial sample preparation whether as suspended MNP or immobilized onto plastic strips for broad-based rapid pathogen detection in the liquid food industry. Second, electrochemical instrumentation will simplify testing methods for accelerated pathogen detection of MNP-extracted microbial pathogens from complex food matrices despite the presence of food components. Third, concentrated, dextrin-coated gold nanoparticles, without the presence of antibodies, will rapidly label MNP-extracted microbial pathogens to reduce false positives through increased signaling by better separation from negative controls even in the presence of complex

liquid food matrices through enhanced electrochemical instrumental signaling for improved food security through frequent economical testing.

1.3 Objectives

Objective one of this research was to determine which MNP carbohydrate functional group extracts target bacteria at the highest amount, reported as a capture index (CI). In fulfilling this objective, transmission electron microscopy (TEM) imaging was evaluated as a means to substantiate the capture dynamics of various pathogenic bacteria by the numerous carbohydrate-functionalized magnetic nanoparticles (MNP). Then an evaluation was made of matrix component effects upon microbial extraction from complex matrices with suspended glycan- and amino/glycan-functionalized MNP (MNP-F#1 and MNP-F#2, respectively). To understand if improved microbial extraction from complex matrices would result, MNP-F#2 were affixed to plastic strips (MNP-strips) and then accelerated detection using cyclic voltammetry (CV) signaling was evaluated. Finally, an extensive literature search was done to understand the microbial surface epitope chemistry with respect to binding properties to MNP carbohydrate ligands.

Objective two was to investigate whether AuNP labeling with electrochemical instrumental signaling would enhance pathogen detection. Specificity of *Salmonella* capture by MNP-F#2 using anti-*Salmonella* antibody-functionalized AuNP (Ab-AuNP) was investigated using differential pulse voltammetry (DPV). This antibody-based method was compared to economical carbohydrate ligands dextrin-coated gold nanoparticles (d-AuNP) as a means to enhance DPV signaling (biosensing). Finally, accelerated pathogenic bacteria detection through DPV or spectrophotometric signaling of carbohydrate-based MNP-cell-AuNP complexes was evaluated.

Objective three was to optimize carbohydrate-based MNP-cell-AuNP nano-biosensing parameters, including MNP and AuNP quantity, respective capture and labeling times, and analyze matrix complexity effects upon signaling interpretation. Additionally, electrochemical instrumentation was evaluated to determine if it would reliably detect microbial pathogens extracted directly from complex food matrices of milk, beef juices, apple cider and homogenized eggs using spectrometry, cyclic voltammetry (CV) and DPV.

1.4 Innovations

As will be shown later in sections *3.3 Suspended MNP-assisted Biosensing* and *3.5 Enhanced Biosensing with Electrically-Active Nanoparticles*, many current nano-biosensors use expensive antibodies or DNA ligands, reducing their ability to detect pathogens across a broad spectrum, or use time-consuming and labor-intensive methods with complicated detection schemes. Many reported biosensors are also limited in their ability to reliably detect bacterial loads below 1000 cfu/mL. The goal of this research was to develop an economical microbial assay that minimizes the user-required technology, utilizes novel carbohydrate-functionalized nanoparticles with a proven long shelf-life, and reduces sample handling required to achieve an accurate result within minutes. Selective carbohydrates are an economical means to functionalize nanoparticles used in biosensing applications [15], [16]. Carbohydrate-functionalized MNP overcome matrix interference, easily extracting pathogens from undiluted liquid matrices. FDA prescribed BAM culture methods require substantial sample preparation and dilution and time-consuming centrifugation methods to concentrate cells. These steps are all eliminated with rapid MNP extraction, and these MNP-cell complexes can still be quantified with common agar plating methods. For thicker matrices, such as liquid homogenized eggs, these MNP can be affixed to

plastic strips (MNP-strip) and retain their capture ability. Either MNP extraction method concentrates microbial contamination to enhance microbial signaling, especially for samples with low cell presence. These MNP-cell complexes can be labeled with electrically active d-AuNP. These concentrated MNP-cell-AuNP complexes enhance electrochemical signaling above background noise for either electrochemical voltammetric or spectrophotometric signaling, thereby reducing labor costs and providing real-time results. Table 1.1 highlights these innovations, along with the current state of the art and the particular research question each innovation addresses.

Table 1.1 Innovative advances in nano-biosensing using carbohydrate-based MNP-cell-AuNP capture and label with electrochemical technology.

(Research Question)	Shortcomings of Current Methods	My Contribution to Advance Technology	Literature References & Publication
Question 1 (Hypothesis 1): What matrix effects will complex liquid foods have on the carbohydrate-functionalized MNP capture of pathogenic bacteria for different exposure times?			
Matrix Effects	Require extensive sample preparation for matrix removal before exposure to biosensor	Selectively bind microbial contamination amidst complex components in matrices ¹	References [17]–[20] “Milk Capture” ² [3]
Question 2 (Hypothesis 1): How does MNP affixed to plastic strips affect their ability to extract bacteria from complex liquids? What methods can be used to detect microbial presence?			
MNP-strip Capture	Complex manufacturing methods with specialized materials	Develop cost-effective MNP-strip and verify ability for microbial capture and detection	References [21]–[23] “MNP-strip” [4]
Question 3 (Hypothesis 1): How can literature concerning microbial surface chemistry and MNP-carbohydrate chemistry, along with TEM imaging, allow us to discern the dynamics of carbohydrate-functionalized MNP capture of pathogenic bacteria in simple and complex liquid food matrices?			
Microbial Epitopes	Selective methods depend upon expensive antibodies or DNA/RNA ligands	Present carbohydrate selectivity from literature and outline biosensor selectivity vs cost trade-off	References [24]–[28] “Biosensing Review” [29]
Question 4 (Hypothesis 2): What factors affect selectivity of <i>Salmonella</i> detection using MNP capture, antibody-functionalized gold nanoparticles (Ab-AuNP) labeling and differential pulse voltammetry (DPV)?			
Detection Specificity	Require complex nanoparticle labeling mechanisms for improved detection sensitivity	Determine limitations within MNP-cell-Ab-AuNP/DPV biosensing method for future improvements ³	References [5], [6], [30]–[32]
Question 5 (Hypothesis 3): What factors must be considered when using dextrin-coated gold nanoparticle (d-AuNP) attachment to MNP-cell complexes in liquid foods for (DPV) biosensing or spectral absorbance detection?			
d-AuNP Signaling	Complex nanoparticle antibody or DNA ligand conjugation and extensive sample handling	Developed carbohydrate-based MNP-cell-d-AuNP bio-sensing useful with DPV or spectrophotometry	References [33]–[35] “Biosensing Review” [29]
Question 6 (Hypothesis 3): How can microbial surface attachment and AuNP binding be exploited to detect bacteria within liquids using electrochemical instrumentation?			
Electro-chemical Biosensing	Lack of rapid detection methods	Established electrochemical detection parameters using spectrometry and voltammetry	References [36], [37] “Biosensing Review” [29] & “SPEL” ⁴ [2]

¹ Capture of *Salmonella*, *E. coli*, *Bacillus* and *Listeria* from milk, beef juices, apple cider and homogenized eggs.

² Accepted manuscript by *Journal of Food Protection*, JFP-18-040R1, “Carbohydrate ligands on magnetic nanoparticles for centrifuge-free extraction of pathogenic contaminants in pasteurized milk”, Matta, L.L. & Alocilja, E.C., 2018, awaiting publication fee funds.

³ Limitations to MNP-cell-Ab-AuNP/DPV biosensing is reviewed in chapter 7.

⁴ Research concurrent with wireless radio-frequency (RF) signaling of sensing pathogens electrically in liquids SPEL-cell-AuNP samples, published in *Biosensors & Bioelectronics*.

Chapter 2. Food Supply Chain Safety Against Pathogenic Microbial Contamination

2.1 Introduction

World-wide, governments in developed countries regulate the production and sale of food within their countries to ensure consumers are purchasing food free from microbial health risks [38], [39], whereas in developing countries, food supply regulations are inadequate or poorly enforced [40]. In the US, the FDA regulates larger industry producers, whereas small local sellers are not regulated. Although bacteriological methods recommended by the FDA are highly accurate in detecting microbial contamination, they are time-consuming and labor-intensive [8]. Using an inexpensive rapid microbial test would then substantially reduce both lost product and consumer health risks. For example, nutritionally rich drinks such as milk and fruit juices allow rapid microbial growth. It is estimated that over 210 pounds of dairy products are consumed per US citizen each year, with over 60% in milk form. In the liquid food supply chain, between the farm and fork, there are multiple avenues for pathogens to enter the food product, therefore frequent testing would ensure secure food production methods and reduce consumer risks of illness. But the complex components present in most liquid food products, as well as any homogenized food sample, may interfere with pathogen detection. Many reported nano-biosensing methods require pre-test preparation to reduce this interference so that false negative results are not incurred. Nano-biosensors that bind more selectively to bacteria than surrounding liquid matrix components without any necessary dilution necessary would reduce both sample handling and false negative results.

2.2 Food supply regulation

Worldwide, our food supply is monitored by a variety of agencies and regulations [38], [40], [41]. Unfortunately, the World Health Organization (WHO) reported that in the year 2010 an estimated 600 (95% uncertainty interval 420 – 900) million illnesses occurred. The most frequent foodborne disease agents were norovirus, *Campylobacter*, and non-typhoidal *Salmonella enterica*, causing diarrheal diseases [1]. The European Commission (EC) instituted a Food Safety policy to ensure coherent farm-to-table monitoring of their food supply, including imports. The European Food Safety Authority (EFSA) provides science-based risk assessment to aid the EC in its regulations [38]. Similarly, the Food Standards Agency (FSA) of the United Kingdom monitors food and drink threats [42]. Finally, in the US, several agencies cover our local and imported food supply including the United States Department of Agriculture (USDA), Food and Drug Administration (FDA) and Centers for Disease Control and Prevention (CDC).

The USDA provides inspection of domestic products, imports, and exports, and conduct risk assessments to many areas of food processing and food distribution. Specifically, the USDA's Food Safety Inspection Service (FSIS) monitors our nation's meat, poultry and egg supply against foodborne diseases [43]. Regulations instituted in 2012 requires products must be “tested and held” until it is determined that no microbiological contamination exist. Specifically, the presence of six strains of *E. coli* are banned in ground beef in their “zero tolerance” policy, due to their low infective dose, which has reduced the number of overall recalls required [44], [45].

A foodborne outbreak response network was formed by the FDA in 2011. This network surveils outbreaks and provides post-response activity related to multiple-illness events involving food [46]. To reduce outbreak events, food producers are encouraged to follow the FDA's Hazard Analysis and Critical Control Point (HACCP) method to identify points where contamination can

occur along their food supply chain [47]. To determine any microbial contamination, the FDA also established standardized bacteriological analytical methods (BAM). BAM methods are considered the gold standard that all reported nano-biosensing methods are commonly tested against in the drive to design more expedient means to ensure a safe food supply for consumers.

Regulations instituted by different agencies may vary in different markets. For example, different microbial contamination levels are allowed in milk products in the European Union (EU) versus the USA. In the EU, pasteurized milk may contain no more than 50,000 CFU/mL total bacterial count and less than 5000 coliforms, compared to 20,000 CFU/mL total bacterial load and below 10 coliforms in the US [48]. Suppliers of raw milk sold in the US for pasteurization are required to keep bacterial levels below 200,000 CFU/mL. US groups that have lobbied the FDA to allow interstate raw milk sales, which are currently illegal, even concede the necessity to warn consumers about the presence of potential pathogens [49].

It would be expected that regulations across the globe would vary for most food products. The agencies assigned to protect consumers in each region from foodborne diseases continually monitor threats, occasionally setting new standards for allowed microbial levels, among other contaminants, as new evidence from event investigations and scientific research are reported. As these are reactive actions, one consistent factor, though, is the need to rapidly determine pathogen presence with high reliability

2.3 Pathogenic microbial contamination along the food supply chain

Sustainable food supply chains have a goal of providing a sufficient supply of safe, healthy food while still ensuring economical options for farmers and suppliers alike, along with addressing any environmental concerns during food production [50]. One important aspect of a safe food

supply is the continued monitoring of any pathogenic microbial contamination in our food along the supply chain from farm to fork. This involves the diligent attention of farmers who grow and raise our food sources, packers and food-contact packaging providers, food product manufacturers, commercial sellers and the shipping industry [51], since microbial contamination may be introduced at any step. The Grocery Manufacturers Association encourage programs that focus on prevention and anticipation of potential problems, to ensure a safe finished product. This fits well with the FDA's HACCP methods to identify possible points of contamination entry in the food product.

Common pathogenic bacteria found in our food supply that are tracked by the CDC include those that cause acute intoxication, toxico-infection, or invasive infections with a range of symptoms and possible organ failure. *Clostridium botulinum* spores and *Bacillus cereus* are both uncommon diseases in the US, but *C. botulinum* found in canned food may cause muscle paralysis if the food is not heated appropriately and *B. cereus* can curdle milk products. *Clostridium perfringens* and *Staphylococcus aureus* cause quick onset of diarrhea when consumed in foods such as meatballs, causing up to 10% of foodborne disease in the US. *Listeria monocytogenes* is commonly found in ready-to-eat foods and fresh, unpasteurized apple cider. *L. monocytogenes* causes thousands of invasive infections yearly, similar to *Campylobacter jejuni* found in raw milk and poultry. Together *L. monocytogenes* and *C. jejuni* result in 25% of yearly deaths due to microbial infection.

Strains of *E. coli* cause some of the most serious diseases in the US, particularly enterohemorrhagic *E. coli* (EHEC) strain O157:H7. EHEC is one of the six *E. coli* strains the USDA lists as zero tolerance when found in ground beef since they can cause hemolytic uremic syndrome (HUS). Although most EHEC infections result in bloody diarrhea lasting up to eight

days, HUS results in kidney failure and death for 15% of infected children. *Salmonella*, a common peanut butter contaminant, can also result in HUS, causing over a million deaths a year, equating to 10% of all microbial illnesses and 30% of all deaths.

Common contaminants of milk, an example of a rich, complex food matrix, include several bacteria. *Staphylococcus aureus* is commonly found on human skin and wounds and can easily contaminate milk products post-pasteurization and cause cramps, vomiting, and diarrhea from an infectious dose of 6 log CFU/mL. *Yersinia* is a common pork contaminant that is easily transferred from live hogs to raw milk on farms, causing vomiting and diarrhea for 100,000 US citizens per year, even septicemia for 3% of sufferers. Finally, *Salmonella* was the cause of a landmark outbreak case in 1985 in which cross-contamination of milk from Hillman Farms identified important possible sources of foodborne disease. In fact, the FDA cautions against drinking raw milk and unpasteurized products due to the severity of diseases from over 90 microbial pathogens that may be present [52].

2.4 Conventional methods in pathogen detection

Bacteriological analytical methods (BAM) published by the FDA since 1965 are their preferred laboratory procedures to determine microbiological levels present in food [53]. These gold standard methods have been developed and refined over the years to detect pathogens in our food sources, even though they are time-consuming and require substantial supplies. Additionally, BAM methods are more reactive than proactive in response and used in industrial risk assessments of possible contamination presence. A concerted drive to develop sensitive, miniaturized biosensing methods or stand-alone nano-biosensors has succeeded in addressing numerous aspects of reliable detection, but the economical rapid “microbe trap” is still quite elusive.

Biosensors can technically detect any quantifiable microbial component or biological material, but reliably relating the quantity of bacteria that are present may be problematic. Mandal et. al. reviewed biosensor designs reported throughout the first decade of the 21st century [54]. Sensor limits above 100 CFU/mL limit their application within the food supply industry, especially for zero-tolerance pathogens, referring to the fact that if the pathogen is detected at levels set by the FDA, USDA or FSIS, for example, they may not be sold. Many of these methods may also not distinguish between live and dead cells nor be able to detect cells within complex food matrices.

Numerous current and proposed biosensing methods like those reported later in section 3, below, suffer from matrix interference in achieving strong signaling responses. Particularly, molecular methods that detect biochemical markers and nucleic acid based methods that detect cellular DNA/RNA, causing higher detection limits and limited test applications [12], [20], [55]–[58]. Many biosensors require extensive sample preparation before the final detection step, such as a sandwich-based sensor against *Aeromonas* or nucleic acid molecular beacons to discriminate between *Bacillus* strains [20], [59]. Flow cytometry BactoScan^(R) methods approved by the FDA can detect down to hundreds of cells, but samples must be diluted to prevent system clogging and use more expensive fluorescent-tagged antibody labels if cell differentiation is desired [18], [19], [53], [60], [61]. In addition, flow cytometers are known for the intensive work necessary to obtain reliable results [18]. Multifaceted manufacturing methods using specialized materials make many biosensors effectively uneconomical for broad production and application [21]–[23]. Specialized ligands improve sensitivity, but also increase production and handling costs. Investigation into carbohydrate based ligands that attach to microbial targets is promising more economical options [24], [26], [28], [62].

Electrochemical methods show real promise in improving microbial sensitivity while reducing detection time. Gold nanoparticles are electrically active labels that assist in improving signal strength using electrical signaling, as well as providing strong colorimetric responses for optical sensors [5], [6], [31], [63]. Biosensors incorporating gold nanoparticles into their design may also reduce sensor costs applying carbohydrate ligands for pathogen surface labeling [35], [64].

2.5 Conclusions

Understanding the seriousness of pathogenic bacterial contamination in our food supply to human health makes apparent the importance of reliable microbial detection. In extension, identifying which pathogens are most infective, their prevalence in causing foodborne disease, and which foods they most contaminate will help to reduce human illness. Eliminating how this microbial contamination enters the food supply chain will then reduce supplier costs and improve consumer confidence in the food products. Food regulatory agencies around the world, such as the FDA and USDA, address bacterial limits allowed in foods, as well as steps that are necessary to ensure industry food products meet these levels before sale. Numerous pathogens exist in nature, making their way into our foods, but six strains of *E. coli* have been identified as so detrimental to human health, they are considered “zero tolerance” bacteria. In addition to *E. coli*, complex liquid foods such as milk may contain *Bacillus* or *Listeria*, causing illnesses from mere diarrheic to invasive infections. Emerging nano-biosensors show promise in providing rapid detection of food pathogens, as opposed to the gold standard BAM methods, but many are still uneconomically designed or lack reliability in sensitive detection. Development of economical biosensors that are user-friendly and easily adapted to new pathogen and food combinations may increase food testing

along the food supply chain and further reduce foodborne outbreaks. As more reliable nano-biosensors are designed, food supply safety will be more reliable.

Chapter 3. Emerging Nano-biosensing with Suspended MNP Microbial Extraction and Electrically-Active Nanoparticle Labeling

3.1 Introduction

Many biosensing assays are too expensive or technically complicated to be economically feasible in many regions of the world. Sensor component miniaturization has led to nano-sized microbial biosensors [17], [65]–[69]. Nano-biosensors are now prevalent within medical, environmental and even personal-use areas [70]–[72]. Their cost is of little concern to the industrial user; but in under-developed countries, cost is the least concern. Many nano-biosensors designed to date also require expensive test equipment, environmentally sensitive components, refrigeration, and advanced training [73], [74]. Economical methods should require minimal storage and technology, with long shelf life, such as those developed in our Nano-Biosensors lab using carbohydrate-functionalized MNP and dextrin-coated gold nanoparticles (AuNP). A truly successful biosensor design incorporates high sensitivity with fast responses that are easily deciphered and require little manual labor and supplies.

Current nano-biosensing methods show specificity that ranges from non-selective bacterial attachment to surfaces, to selective capture using monoclonal antibodies or DNA-aptamer binding. Detection methods vary from “visual” reporting of aggregated nanoparticles, to electrical and electrochemical signaling. Magnetic nanoparticles (MNP) are beneficial in all of these applications due to their large surface area to volume ratio and superparamagnetic properties. Immobilized surface ligands capture bacteria, and the MNP-cell complex can then be separated rapidly from even complex solutions [5]. Carbohydrates are becoming an economical ligand option. Cell surfaces and carbohydrate functional groups form non-covalent, electrostatic forces, similar to the antigen-antibody bonds, which then persist throughout the extraction process. Recent development have found carbohydrates with increased specificity to target bacteria [69], [75]. Electrically-active

nanoparticles (EANP) additionally provide more sensitive electrochemical or spectrophotometric detection methods [2], [76], [77].

Reviewed here are state-of-the-art nano-biosensing methods designed for rapid bacterial extraction using suspended MNP. Selective versus non-selective functional groups are compared with respect to their capture ability. Those MNP methods proven in more complex matrices, which closely replicate food sampling, are also evaluated. Some MNP applications additionally use EANP to intensify optical detection or electrochemical methods. Carbohydrate ligands from a broad spectrum of research areas are discussed with regards to selectivity. Finally, a novel rapid (30 min) MNP-cell- AuNP nano-biosensing method is introduced that exclusively uses biocompatible carbohydrate ligands immobilized onto MNP and AuNP to detect the presence of *E. coli* in milk using spectral and electrochemical detection, as shown in Figure 3.1.

3.2 MNP-assisted Biosensing Properties

Functionalized magnetic nanoparticles (MNP) allow rapid capture and extraction of pathogenic bacteria from liquid matrices in real-time, as well as target concentration with minimal liquid handling. MNP have large surface area to volume ratios, providing for high surface functionalization. Many applications conjugate biological compounds to the MNP surface, such as antibodies or nucleic acid aptamers, to improve their specificity [31], [78]–[85] Park et al. MNP-aptamer biosensing was able to visibly detect up to 5 log CFU/mL *Salmonella* [83]. But random DNA orientation or antibody cross-reactivity can reduce assay sensitivity [86]–[88], as also does matrix interference [89].

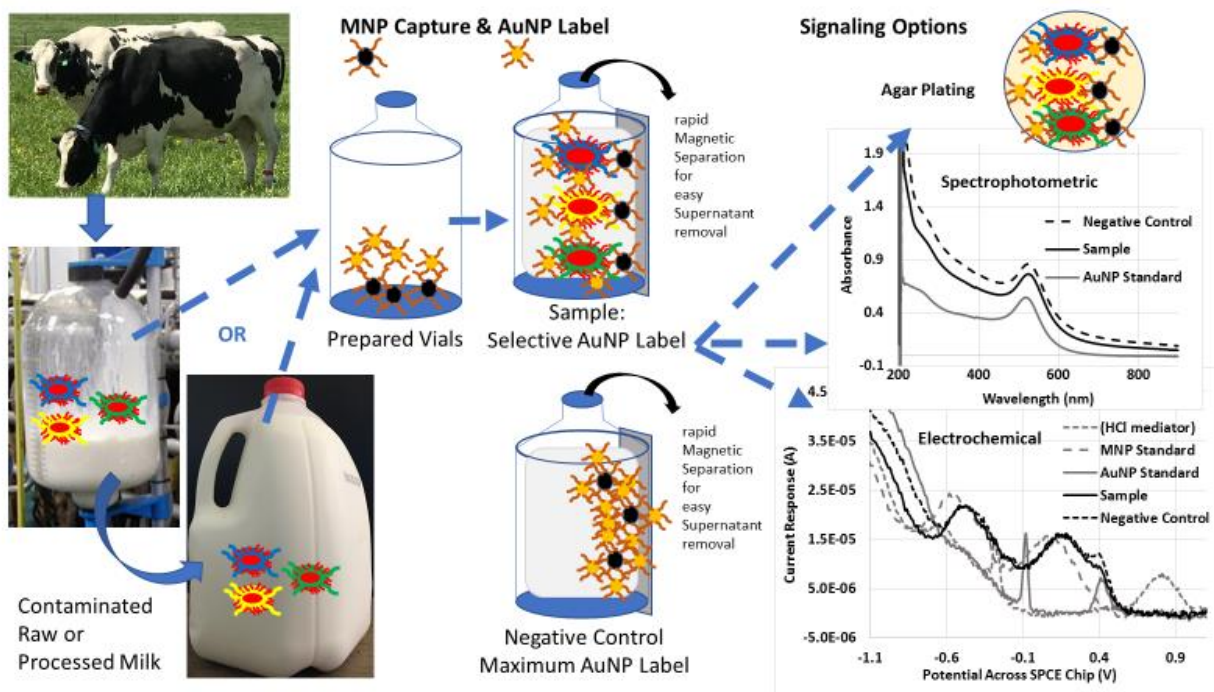


Figure 3.1 Schematic of the MNP-cell-AuNP biosensor for total bacterial load. Carbohydrate-functionalized MNP extract *E. coli* from artificially contaminated milk, while dextrin-coated EANP attach to captured cells at different cell receptors. Negative controls consist of sterile milk where MNP-EANP complexes form due to carbohydrate attraction between the functional groups. Cell quantification is possible using FDA bacteriological analytical methods (BAM) agar plating (top), where neither MNP nor EANP inhibit bacterial growth and negative controls will have no cell growth present. Rapid biosensing is possible with spectrophotometric or electrochemical signaling, where negative controls will produce larger signals due to higher EANP presence than samples, due to saturation binding of EANP to MNP.

MNP are synthesized through a variety of methods, including microemulsion, co-precipitation and thermal decomposition, with a variety of final compositions, including iron oxides such as Fe_3O_4 or alloys such as FePt and CoPt_3 . An excellent review of these synthesis methods was written by Lu et al. [90]. The aforementioned MNP functional groups further protect the nanoparticles from degradation.

Various carbohydrate and amino acid ligands have been used as antibody substitutes, making the MNP more biocompatible for biological sample applications. Examples of carbohydrates, and other carbon-based, ligands include lectins, mannose, oligonucleotides, galactose, glucose, caprylic acid, cysteine and chitosan [86], [91]–[96]. As a group, carbohydrates

retain their structural integrity and chemical reactivity when immobilized onto the surface of MNP. The chemical reactivity of each surfactant then affects MNP suspension and capture dynamics.

Chitosan is a cationic biopolymer derived from chitin with a high percentage of amino groups that aid in MNP suspension. Chitosan may be used directly in MNP preparation using three different methods, micro-emulsion, cross-linking and covalent binding [97]. Amino groups improve nanoparticle suspension in aqueous solution [98], and improve proximity between biological target and MNP. Galhoum et al. functionalized MNP with chitosan crosslinked to cysteine [99], further increasing amino group presence. Reactive chitosan amino groups can form amide bonds with carboxyl groups from carboxylated sugars, such as oligosaccharides [100]. Oleic acid, citrate, and ethylene glycol are other biocompatible coatings used on nanoparticles [101]–[103].

Each carbohydrate displays a different specificity towards biological target epitopes based upon their chemical moieties. Cysteine amino acid has three reactive moieties: carboxyl, amine, and thiol groups. It was proposed that the carboxyl O and thiol S groups bind to the iron oxide nanoparticle core [104], [105], while the positively charged amino group electrostatically binds the highly negative cell surface [95]. Clues to carbohydrate specificity are found studying human cell epitope binding, which microbial cells also bind during infectious disease initiation. Mannose, glucose and galactose sugars show varying specificities to different cell surface markers [100], [106], [107], binding the Fim-H surface molecule on *Escherichia coli* [108].

Although chitosan is a natural antimicrobial agent [109]–[111], its bonding strength to bacterial cells makes it a desirable MNP surfactant for extraction purposes. Its polycationic structure binds easily to the anionic surface markers of microorganisms [109]. The expediency of MNP extraction minimizes any deleterious effects. Also at high pH 10, chitosan is nearly neutral,

but at more neutral conditions such as in many liquid foods (pH 5 to 7) chitosan is more positively charged and more effective in cell attachment [109], [112].

The combination of the selected synthesis method, core composition and surfactant determine the final MNP properties, particularly free space permeability, particle dispersion or aggregation, biocompatibility, and their mechanical and electrochemical stability. MNP magnetization saturation (M_s) properties can be identified using hysteresis magnetization plots (Figs. 3.2A & B), which show that application of an external magnet quickly saturates the nanoparticle magnetic field, aligning the magnetic moments, causing MNP to migrate to the magnetic force [100], [113], [114]. When the applied magnetic field is zero, superparamagnetic nanoparticles do not retain a net magnetic moment. Iron-oxide-MNP display strong superparamagnetism, especially below threshold diameters of 50 nm. These MNP do not aggregate without an external magnet present and therefore MNP are easily suspended evenly into liquid solutions, and following microbial capture, are easily separated from the supernatant upon application of an external magnet. This eliminates the need for time-consuming centrifugation to separate bacteria from food matrices.

Values for MNP M_s vary, due to ferric oxide core diameter and carbohydrate functional group. As shown in Table 3.1, surfactants reduce the magnetic moment response. For example, MNP prepared by Mahdavi et al. without surfactant showed increasing M_s as their diameter increased, but for the largest 25 nm diameter with oleic acid surfactants, M_s dropped from 81 electromagnetic units per gm (emu/gm) to 58 emu/gm. In addition, defects, or “holes” in the iron core also reduce saturation magnetization values. Therefore, a direct relationship between overall diameter and M_s cannot be expected if other parameters vary. In comparing the carbohydrate-

functionalized MNP produced in our Nano-Biosensors Lab against others, the M_s values are relatively strong.

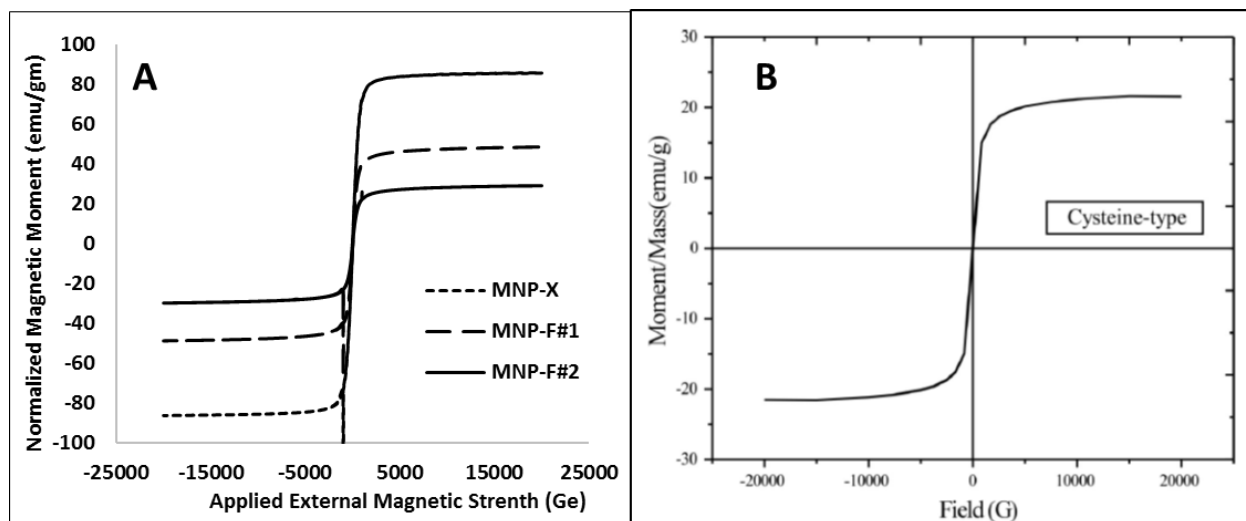


Figure 3.2 Examples of hysteresis magnetization for magnetic nanoparticles (MNP) functionalized with carbohydrate groups, (A) from Alocilja Nano-Biosensors lab and (B) used in metal recovery [99] (emu = electromagnetic units).

3.3 Suspended MNP-assisted Biosensing

MNP's ability to extract and detect targeted biological components depends on their magnetization properties and surface functionalization. Table 3.2 provides detailed information concerning biosensing applications using suspended MNP, functionalized with either selective or non-selective surfactants. Antibody surfactants have higher specificity for their targets, for example against *Listeria monocytogenes* showing a linear detection response between 10^3 to 10^6 colony forming units per mL (CFU/mL [77]). Jansaento et al. designed a deoxy ribonuclease acid (DNA)/polymerase chain reaction (PCR) method that used aptamer-based MNP that achieved a detection limit of 4 log CFU/mL [115]. Although antibodies, genetic aptamers, and fluorescent tags are selective to their targets, improving assay sensitivity, they are expensive, requiring special preparation and storage [116], [93], [115], [74], [89], [117].

Carbohydrate ligands are economical options as MNP surfactants against microbes. Currently many reported carbohydrate ligands are non-selective, but still successfully detect various biological targets. Lin et al. detected 10^1 to 10^8 CFU/mL *E. coli* using MNP-chitosan/glutaraldehyde with wireless magneto-elastic resonance [118]. Vancomycin-polyethylene-glycol-MNP was used to extract *Listeria*, among other Gram-positive bacteria using UV trans-illumination detection [119]. Wang et al. used cetyltrimethylammonium bromide coated MNP to recover up to 1000 ng/L estrogen from pork samples [96], whereas chitosan-MNP recovered over 90%, or up to 720 μ M, of spiked morphine from synthetic urine and processed serum [92]. Work in the Nano-Biosensor Lab found glycan-coated-MNP and cysteine/glycan-coated-MNP captured 2 parts per thousand (ppt) to 120 ppt of microbial contamination directly from undiluted milk, and over 0.002 ppt to 0.011 ppt from beef juices, orange juice and apple cider [29], providing sufficient bacterial presence for sensitive detection.

A major advantage of MNP is their ability to separate biological targets from their matrices, even concentrating captured bacteria, using only an external magnet. Most of these reported methods were tested in simple buffer or food rinsate solutions such as the *E. coli* detection by Liu et al., but food matrix interference was not studied for subsequent detection using refractive index [80], fluorescence spectrometry [127], or cyclic voltammetry [128]. Concentrated MNP-target, though, can improve optical detection [87]. MNP may even be incorporated into subsequent detection steps, such as interdigitated microfluidic impedance [89] or chemiluminescence [82], [85] without signal interference. MNP even provided optical signaling in *Salmonella* quantification [86].

Two pitfalls in suspended MNP biosensing are cross-reactivity against non-target species and matrix interference with detection signaling. Even using selective antibody ligands, *Listeria*

Table 3.1 Magnetization properties of various magnetic nanoparticles (MNP) with carbohydrate functional groups.

Physical Diameter (nm)	Surfactant (functionalization)	Magnetization Saturation (emu/gm)	Synthesis Method	Reference
21	Oleate	17	Thermal Decomposition w/o O ₂	[120]
21	Oleate	74	Thermal Decomposition w/ O ₂	[120]
7.83	None	58	Hydrothermal	[102]
8.29		70		
9.41		78		
< 25	None	81		
	Oleic Acid	58		
120	Glutaraldehyde w/ antibody	~ 60	Solvothermal	[121]
10	Chitosan-coated	45.09	Coprecipitation	[122]
8	Chitosan-coated w/ cellulase enzyme	37.58		
(<2000)	Cysteine-glutaraldehyde /Chitosan	1.15		[123]
7 – 25, with 150-250 aggregation	Chitosan w/ epichlorohydrin crosslink to cysteine	21.51	Coprecipitation	[99]
50 – 55	Alginate	59.3	Coprecipitation	[124]
80 – 120	Chitosan	56.8		
18 - 20	None	62	Coprecipitation	[125]
103	23% Chitosan	39		
58	15% Chitosan	25		
14	Chitosan-FITC fluorescent marker	53	Coprecipitation	[112]
14	None	55		
8.5	None	58	Coprecipitation	[126]
	Low mw chitosan	29		
	High mw chitosan	18		
8	None	61	Thermal Decomposition	
	Low mw chitosan	30		
	High mw chitosan	25		
5 – 15	(none)	83.87	Coprecipitation	[29]
	Amino Acid coating	47.06		
	Amino/Glycan	28.31		

detection showed 50% cross reactivity [88] and a *Staphylococcus* assay showed 40% cross reactivity [87], both against non-target pathogens. Another MNP-antibody method to detect *Listeria* cross-reacted with *Staphylococcus* [86]. Non-selective, carbohydrate surfactants show

broad spectrum capture, but vancomycin-PEG-MNP suffered only 20% cross reaction with Gram-negative bacteria when combined with PCR using *L. monocytogenes* specific primers [119]. When food matrices such as beef wash solution or pork extracts were introduced into the sampling method, detection sensitivity was reduced with capture at 70% [89]. Carbohydrate-functionalized MNP produced in the Alocilja's Nano-Biosensors Lab showed similar matrix interference, but matrix effects were factored in the final signal interpretation using controls.

3.4 MNP “dip-stick” Strips

Even though, superparamagnetic magnetic nanoparticles have been exploited in numerous biotechnology applications, their usefulness may be limited by thick liquid or homogenized food matrices where magnetic separation may be diminished. Affixing or embedding the functionalized MNP onto a support has shown retention of their desirable properties such as thermal magnetic dissipation and easy functionalization while allowing expedited separation of chemicals and bacteria from contaminated liquids. MNP have increased surface area, and functionalized MNP retain their capture ability, with low mass transfer resistance. Methods that exploit immobilized MNP include mixing them into carbon paste to improve optical and electrical properties of electrodes; or embedding them into polydimethylsiloxane to make use of MNP thermal properties by application of an AC magnetic field [132], [133]. MNP functionalized with tridecafluorooctyl triethoxysilane were deposited on various solid and fabric surfaces to create a hydrophobic surface, adhering through a simple air-drying [134]. Once the MNP are affixed to a solid surface, they are available to use for biological extractions within complex matrices, exploiting their numerous properties, but allow easy removal from the matrix following target binding.

Table 3.2 Biosensing methods using suspended functionalized magnetic nanoparticles (MNP).

Biosensor Design & Signal Generation	Ligand and Target & Sample Matrix	Method Aspects	Linear Range	Reference
MNP (30 nm) capture & load polyurethane-coated Metglas w/ resonance frequency shift detection of magneto-elastic sensor loading	Non-selective chitosan/ glutaraldehyde – <i>E. coli</i> in phosphate buffer (8 min incubation)	8 min wireless frequency shift signaling vs untested against food matrix effects	$10^1 - 10^8$ CFU/mL	[118]
MNP (30 nm) capture w/ impedance detection on microfluidic interdigitated gold-microelectrode	Selective antibody – <i>Listeria</i> in phosphate buffer and food rinse water (2 hr incubation)	User-friendly & specific w/ rapid detection vs costly ligand, poor reliability & spiked beef wash solution matrix interference	Threshold detection of $10^3 - 10^7$ CFU/mL (poor reproducibility across range, w/ >70% capture efficiency)	[89]
MNP (10-20 nm) capture and ethanol separation w/ HPLC-DAD detection (1)	Non-selective CTAB-coated MNP@caprylic acid MNP – estrogens in pork (1 min incubation)	Quick target recovery (standards) vs matrix effects upon signaling (food)	5 – 1000 ng/L for standards (w/ > 90% recovery)	[96]
MNP capture & PFBT displacement w/ fluorescence spectrometry detection of unbound PFBT (2)	Non-selective q-MNP-1, 2, or 3/PFBT – 8 bacteria in phosphate buffer (20 min incubation)	Microbial discrimination w/o expensive ligands vs complicated chemistry & linear discriminant analysis	10^7 CFU/mL (poor LDA separation) vs OD600=0.2 (good LDA separation)	[129]
Aptamer/MNP (20 nm) displacement & TMB oxidation w/ absorbance spectrometry detection of supernatant (3)	Selective MNP/ oligo-nucleotide – <i>Salmonella</i> in water (15 min incubation)	Easily modified for new bacteria & simple detection vs complicated 1-step chemistry	Tested at 7.5×10^5 CFU/mL	[83]
MNP (100 nm) capture & PCTE filtration w/ HRP chemiluminescence detection (4)	Selective HRP-MNP-antibody – <i>Salmonella</i> in PBS (30 min incubation)	Minimal sample size vs high negative background signal & expensive PMT luminometer	$10^1 - 10^4$ CFU/mL	[82]
MNP capture & 1.2 μ m pore nitro-cellulose/PDMS vacuum-filtration w/ color intensity (optical density) detection (5)	Selective antibody – <i>Salmonella</i> in PBS (30 min incubation)	Minimal sample size vs vacuum-filtration & specialized ChemiDoc™ MP detection	$10^1 - 10^4$ CFU/mL (varying capture efficiencies of 90 – 8%)	[84]
MNP capture & 1.2 μ m pore nitro-cellulose/PDMS vacuum-filtration w/ color intensity (optical density) detection (5)	Selective antibody – <i>Listeria</i> in PBS (30 min incubation)	Minimal sample size vs vacuum-filtration & cross-reaction with <i>Staphylococcus</i> and <i>Listeria</i> spp.	$10^1 - 10^3$ CFU/mL (varying capture efficiencies of 89 – 48%)	[86]
MNP capture & Au-chip loading w/ SPR detection of change in refractive index (6)	Selective MNP-Ab1-& Au-Chip-Ab2 – <i>Salmonella</i> in PBS (40 min incubation)	Signal amplification w/ MNP sample concentration	$10^1 - 10^9$ CFU/mL (3-order improvement from 10^4 CFU/mL w/o MNP)	[80]

Table 3.2 (cont'd)

Biosensor Design & Signal Generation	Ligand and Target & Sample Matrix	Method Aspects	Linear Range	Reference
MNP capture w/ magnetic resonance relaxometry against a negative control	Selective antibody – <i>Listeria</i> in 2% milk stabilizer (40 min incubation)	Specific Ab-silica-MNP capture vs almost 50% cross reactivity against 4 non-target pathogens	$10^0 - 10^3$ CFU/mL	[88]
MNP extraction, subsequent cell heat release, DNA extraction, PCR & gel electrophoresis w/ UV transillumination of ethidium bromide staining (7)	Non-selective vancomycin-PEG – <i>Listeria</i> & Gram(+) in PBS & lettuce homogenate (45 min incubation)	MNP signal concentration vs vancomycin binds broad-spectrum Gram(+) w/ > 20% Gram(-) false positives & overall 4 hr processing time	Extracted bacteria between $10^1 - 10^6$ CFU/mL at > 70% capture efficiency for PCR	[119]
MNP capture w/ enzymatic chemiluminescence detection of AMPPD (8)	Selective MNP-Ab1 & ALK-Ab2 – <i>E. coli</i> (1 hr processing)	Good specificity w/ little non-target cross reaction against 5 pathogens	Tested at 10^3 CFU/mL	[85]
MNP extraction w/ magnetophoresis separation	Selective antibody – <i>E. coli</i> in PBS	High capture for possible bulk process detection	Tested at 10^3 CFU/mL w/ > 97% capture	[79]
PANi-MNP capture & CNN membrane separation w/ resistance detection (9)	Selective MNP-Ab1 & CNN-Ab2 - <i>E. coli</i> in Tris buffer	Lateral flow design vs minimal stable detection window after 6 min	$10^1 - 10^4$ CFU/mL with threshold detection > 10^5 CFU/mL	[81]
ASMNP separation, PCR & gel electrophoresis w/ UV transillumination of ethidium bromide staining (10)	Non-selective ASMNP & selective DNA PCR in buffer	Broad spectrum DNA extraction (post cell lysis) vs complex sample preparation from contaminated raw milk	Extracted DNA lysed from $10^0 - 10^4$ CFU/mL <i>Salmonella</i> & <i>Listeria</i>	[78]
Au/MNP concentration & LFA inverse color line detection (11)	Selective half-fragment – <i>Salmonella</i> in milk (resuspended in Tween)	Minimal matrix interference vs inverse threshold indicator	Threshold detection above 10^3 CFU/mL	[31]
Au-MNP concentration & 0.8 μ m CA filtration w/ optical density detection (12)	Selective antibody & <i>Staphylococcus</i> in PBS and milk (30 min incubation)	User-friendly, optical detection vs high LOD & 20 – 40% cross reactivity against 4 non-target bacteria	Threshold detection 10^3 CFU/mL in PBS and 10^5 CFU/mL in milk (> 70% capture efficiency)	[87]
CMNP-CPE attachment & filtration w/ ferrocyanide mediated DPV detection (13)	Non-selective chitosan – morphine in PBS or synthetic urine & serum	Improved sensitivity vs required centrifugation/ filtration to minimize matrix interference & 10 mL voltammetric cell volume	0.01 – 2 μ M and 2 – 720 μ M w/ > 90% recovery in synthetic urine & serum	[16]
MNP extraction & PCR amplification w/ optical HRP enzyme fluorescence detection (14)	Selective DNA – <i>Campylobacter</i> (3 hr method) after chicken skin culture in broth (24 hr) & cell lysis	Fast PCR amplification w/ MNP-DNA amplification vs 24-hr enrichment media incubation of chicken skin	pg DNA or 10^4 CFU equivalents/ mL	[115]

Table 3.2 (cont'd)

Biosensor Design & Signal Generation	Ligand and Target & Sample Matrix	Method Aspects	Linear Range	Reference
CMN extraction & CN – electrospun LF biosensor separation w/ resistance detection (15)	Selective CMN-mAb & biosensor-pAb – <i>E. coli</i> O157:H7 in peptone water	Fast lateral flow, real-time detection vs expensive ligand & limited 8-min detection window	$10^1 - 10^4$ CFU/mL	[81]
EAM extraction & electrochemical CV transducer detection (16)	Selective EAM-Ph-Pro-DNA & SPCE-PRO-bio-DNA – amplified <i>Bacillus anthracis</i> DNA in water	High target sensitivity vs extended preparation time (w/ PCR amplification & purification)	Sensitive 0.01 – 10 ng/ μ L DNA	[128]
AMN extraction & TEM analysis (17)	Non-selective glycan carbohydrate – <i>E. coli</i> O157:H7	Cell concentration w/o centrifugation proof-of-concept	(not applicable)	[130]
MNP extraction & electrochemical redox ferrocyanide-mediated CV detection (18)	Broad-based chitosan or chitosan/cysteine – <i>Salmonella</i> , <i>E. coli</i> , <i>Bacillus</i> & <i>Listeria</i> in PBS, milk, beef juices & apple cider (10 min incubation)	Total bacterial quantification from undiluted complex liquids, minimal capture loss due to liquid components & optional dip-stick method vs necessity to calibrate biosensor per liquid type	$10^4 - 10^8$ CFU/mL w/ capture in undiluted liquids of 2 ppt to 120 ppt in milk and 0.002 ppt to 0.11 ppt in beef & apple cider (500 μ L – 25 mL volumes)	[131]

(Table 3.2 biosensing definitions: (1) HPLC-DAD = high performance liquid chromatography diode array detection, CTAB = cetyltrimethyl ammonium bromide; (2) PFBT = in-lab produced anionic polymer functionalized with side-chain carboxylic acid group, q-MNP-1, 2 or 3 = quarterized MNP functionalized 3 types of organic bromides, bacteria = *S. oneidensis*, *V. fischeri*, *M. luteus*, *E. tarda*, *E. coli*, *V. alginolyticus*, *P. aeruginosa*, and *P. pastoris*; LDA = linear discriminant analysis; (3) TMB = 3,3,5,5-tetramethylbenzidine (oxidized via H_2O_2 upon aptamer displacement from MNP); (4) PCTE = 0.6- μ m pore polycarbonate track-etched filter, HRP = horse-radish peroxidase, PMT = photo-multiplier tube; (5) PDMS polydimethylsiloxane film possessing six holes with 3 mm diameters, PBS = phosphate buffered saline; (6) SPR = surface plasmon resonance, Ab1 = monoclonal and Ab2 = polyclonal anti-Salmonella antibodies, Au-chip = gold chip; (7) PEG = polyethylene glycol, Gram(+) = Gram-positive bacteria, Gram(-) = Gram-negative bacteria, PCR = polymerase chain reaction; (8) AMPPD = 3-(2-spiroadamantane)-4-methoxy-4-(3-phosphoryloxy) phenyl-1,2-dioxetane substrate of ALK enzyme, Ab1 = polyclonal anti-E. coli antibody, ALK = alkaline phosphatase enzyme, Ab2 = monoclonal anti-E. coli antibody; (9) PANi-MNP = (electrically conductive) polyaniline MNP, CNN = cellulose nitrate nanofibers, Ab1 = monoclonal anti-E. coli antibody, Ab2 = polyclonal anti-E. coli antibody; (10) ASMNP = amino-modified silica-coated magnetic nanoparticles, PCR = polymerase chain reaction, DNA = deoxyribonucleic acid; (11) Au/MNP = gold-coated magnetic nanoparticles, LFA = lateral flow immunoassay; (12) Au-MNP = gold nanoparticle-coated MNP, CA = cellulose acetate, LOD = limit of detection; (13) CMNP-CPE = chitosan magnetic nanoparticle (functionalized) carbon paste electrode, DPV = differential pulse voltammetry; (14) PCR = polymerase chain reaction, HRP = horse-radish peroxidase enzyme; (15) CMN = conductive magnetic nanoparticles w/ electrically-active PANi shell, CN = cellulose nitrate, LF = lateral flow, mAb = monoclonal antibody, pAb = polyclonal antibody; (16) EAM = electrically-active magnetic nanoparticles w/ electrically-active PANi shell, CV = cyclic voltammetry, Ph-Pro-DNA = phosphorylated DNA probes, SPCE-PRO-bio-DNA = screen printed carbon electrode biotinylated DNA probe; (17) AMN = Alocilja magnetic nanoparticles; (18) CV = cyclic voltammetry, ppt = parts per thousand.)

3.5 Enhanced Biosensing with Electrically-Active Nanoparticles

Electrically-active nanoparticles (EANP) have strong surface plasmon resonance (SPR) properties that make them ideal for nano-biosensing methods. EANP generate local electromagnetic fields through conductance of electrons, detectable by optical, spectral and electrochemical instrumentation. Microbial surfaces labeled with EANP show amplified signaling for higher assay sensitivities and detection limits down to 10^1 CFU/mL. Nanoparticles used in MNP-cell-EANP nano-biosensing (Table 3.3) include those produced from titanium, gold and other transition metals, yttrium and other rare metals, quantum dots from lead sulfide and silica dots [77], [121], [135]–[137].

AuNP surface plasmon resonance (SPR) occurs within the UV-visible region between 380 to 780 nm, making them highly suitable as colorimetric biosensors [34], [35], [63], [138], [139] or microbial concentration can also be determined spectrophotometrically [140]. Particles with diameters below 30 nm show absorbance maximums at approximately 520 nm. Other SPR absorbance maximums are 230 nm for titanium oxide nanoparticles (TN) or 630 nm for quantum dots (QD) photoluminescence. Rare earth metal nanoparticles can be designed to fluoresce at varying wavelengths, allowing simultaneous detection of multiple targeted bacteria [76].

As with MNP, EANP surface ligands determine their binding properties to targeted biological compounds. Citrate is a conventional surfactant for AuNP [138], [141], [142], but other capping agents have been investigated for microbial binding specificity. In evidence of surfactant specificity, cysteine-capped AuNP were able to bind *E. coli* more effectively than citrate-capped AuNP, purportedly from positively charged amino group attraction to negatively charged microbial surfaces [95].

Few reported biosensing methods combine suspended MNP capture with EANP labeling. Notably, many of the reported methods summarized in Table 3.3 target *Salmonella* in their development, using antibody or aptamer ligands on both MNP and EANP with optical or spectral signaling for detection [76], [136], [137]. In direct signaling, the MNP-cell-EANP complex is directly quantified. For example, Duan et al. (2012) used rare earth nanoparticles functionalized with DNA aptamers to detect *Salmonella* and *Staphylococcus* ($10^1 - 10^5$ CFU/mL) from filtered environmental water samples [76]. Inverse methods quantify microbial presence by the level of unbound EANP in the supernatant. Levels of unattached EANP identified *Salmonella* presence ($10^2 - 10^5$ CFU/mL) in diluted milk with AuNP labeling [135], or residual TN quantified *Salmonella* ($10^2 - 10^8$ CFU/mL) in milk [121]. AuNP functionalized with both antibody ligand and urease enzyme was used in a biosensing assay that monitored impedance changes to detect *Listeria* [77].

Dextrin is a novel capping agent used to reduce gold chloride during AuNP production [143], [144]. The prevalent negatively charged hydroxyl groups of dextrin bind to the positively charged surface gold atoms, protecting the nanoparticles against aggregation in liquid suspension. This oligosaccharide coating also improves AuNP/dextrin suspension in aqueous-based solutions by its low molecular weight, pKa of 12.3, and external hydroxyl chemical groups. Dextrin is also biocompatible, for example reducing selenium nanoparticle toxicity from 95% against human cells to 15% [145]. Dextrin-coated AuNP developed in our Nano-Biosensors Lab successfully detected *Salmonella* and *E. coli* from undiluted milk in a proof-of-concept design, described below.

Comparison of MNP-cell (Table 3.2) versus MNP-cell-EANP (Table 3.3) nano-biosensing methods shows EANP SPR properties improves optical and spectral detection. This advances development of rapid, simple and economical microbial assays, improving subjective visual tests

Table 3.3 Nano-biosensing methods with functionalized MNP and NP labeling.

Biosensor Design & Signal Generation	Ligand and Target & Sample Matrix	Method Aspects	Linear Range	Reference
MNP capture & AuNP label w/ optical & absorption spectrometry detection (520 nm) of unbound AuNP (1)	Selective MNP- & AuNP-aptamer ^{1,2} – <i>Salmonella</i> in strained & 1:20 diluted milk (45 min incubation)	User-friendly 1-step specific method w/ simple optical detection vs >25% cross reaction w/ <i>E. coli</i> & <i>Listeria</i> at 10 ⁵ CFU/mL	10 ² – 10 ⁵ CFU/mL (inversely proportional to signaling)	[135]
MNP capture, TN label w/ absorption spectrometry detection (230 nm) of unbound TN (2)	Selective MNP-mono- & TN-poly-clonal antibody – <i>Salmonella</i> in milk (20 min incubation each)	User-friendly & specific w/ simple detection vs costly ligand, 2-step method & non-target signaling	10 ² – 10 ⁸ CFU/mL (inversely proportional to signaling)	[121]
MNP capture & QD labeling w/ photoluminescence spectrometry detection (630 nm) (3)	Selective MNP-Ab1 and QD-Ab2 – <i>Salmonella</i> in phosphate buffer (30 min incubation)	1-step capture-n-label & simple detection vs expensive Ab ligands	10 ³ – 10 ⁸ CFU/mL	[136]
MNP capture & YYbErTmNP labeling w/ fluorescence spectrometry detection (<i>Salmonella</i> at 452 nm; <i>Staphylococcus</i> at 660 nm; for 980 nm excitation) (4)	Selective aptamers DNA1 – <i>Salmonella</i> and DNA2 – <i>Staphylococcus</i> in buffer (40 min incubation)	High specificity w/ easily synthesized aptamer & 1-step batch method vs complicated NP chemistry & high cross-reactivity to <i>E. coli</i> & <i>Enterobacter</i> with DNA1	10 ¹ – 10 ⁵ CFU/mL (>70% capture efficiency from filtered environmental water samples: lake, stream & puddle)	[76]
MNP capture & Blue-SiNP labeling w/ visual optical color density confirmation (5)	Selective MNP-Ab1 & Blue-SiNP-Ab1 – <i>Salmonella</i> in saline (pH 2 to pH 13) (30 min MNP & 15 min Blue-SiNP incubations)	Strong visual calibration & no non-target pathogen cross-reaction vs 2-step capture & label w/ multiple liquid changes	10 ¹ – 10 ⁹ CFU/mL (1 mL mixed target bacteria) 10 ⁴ – 10 ⁹ CFU/mL (20 uL mixed target bacteria)	[137]
MNP capture, AuNP labeling, & urea reaction w/ supernatant impedance change detection of inter-digitated microelectrode loading	Selective MNP-mono- & urease-AuNP-poly-clonal antibodies – <i>Listeria</i> in PBS or lettuce wash (45 min MNP & 30 min AuNP incubations, 30 min urease catalysis)	Small sample and nanoparticle volumes vs multi-step process w/ multiple liquid handling steps	10 ³ – 10 ⁶ CFU/mL (> 90% recovery from spiked lettuce samples at same concentrations; no <i>E. coli</i> cross-reactivity)	[77]
MNP capture & AuNP labeling w/ differential pulse voltammetry (DPV) (6)	Selective MNP-mAb & AuNP-pAb – <i>E. coli</i> in PBS (45 min MNP, AuNP & DPV)	Small samples and expedited detection vs complicated Ab conjugation chemistry and random MNP-AuNP binding	10 ¹ – 10 ⁶ CFU/mL (log-linear between contamination concentration vs DPV-AuNP current response)	[6]

Table 3.3 (cont'd)

Biosensor Design & Signal Generation	Ligand and Target & Sample Matrix	Method Aspects	Linear Range	Reference
MNP capture, AuNP labeling w/ electrochemical HCl-activated DPV (0.4 V) or spectrometry detection (520 nm, or novel step-integrated spectral absorbance)	Broad-based MNP-amino/glycan & AuNP-dextrin carbohydrates – <i>Salmonella</i> & <i>E. coli</i> in PBS & milk (30 min incubation; total 45 min detection)	1-step capture & label of total bacterial load from undiluted complex liquid vs proof-of-concept stage	Tested at $10^3 - 10^5$ CFU/mL	[29]

(Table 3.3 biosensing method definitions: (1) MNP = magnetic nanoparticles, AuNP = gold nanoparticles, aptamer 1 & 2 = Salmonella DNA sequences; (2) MNP= magnetic nanoparticles, TN= titanium oxide nanoparticles, CFU = colony forming units; (3) QD = quantum dot, Ab1 and Ab2 = two different monoclonal anti-Salmonella antibodies; (4) YYbErTmNP = (rare earth metals) yttrium ytterbium erbium thulium nanoparticles which are Lanthanide-doped near-infrared (NIR)-to-visible upconversion-nanoparticles (UCNPs) , DNA1 = aptamer for Salmonella, DNA2 = aptamer for Staphylococcus; (5) Blue-SiNP = silica nanoparticles functionalized with Reactive Blue 14 (Zhejiang Shunlong Chemical Co. Ltd, China).)

and replacing complicated methods requiring expensive instrumentation. Spectral detection of MNP can mask bacterial presence due to their wide absorbance band [2], therefore secondary reactions, such as TMB (3,3,5,5-tetramethylbenzidine) oxidation [83] or HRP (horseradish peroxidase) enzymatic chemiluminescence [82] (Table 3.2) were required.

All selective and non-selective methods suffer false positive results from cross-reactivity, which minimizes assay efficacy. The trade-off between expensive selective ligands, complicated technology and time-consuming procedures versus economical carbohydrate ligands and user-friendly methods with easily-adapted signaling should be a driving force in improving carbohydrate-based MNP-cell-EANP nano-biosensing.

3.6 Carbohydrate Ligands Against Microbial Targets

Carbohydrate ligands with selective binding against targeted pathogens can be identified from many sources. Microbial virulence is initiated through bacterial surface protein lectin attraction to tissue carbohydrate ligands. These protein-carbohydrate interactions can be exploited to target pathogens in our food sources. Selectivity can even be improved by addition of binding moieties to the ligand [146], and synthesis methods are producing a broad range of possible carbohydrate ligands. In 1983, Firon et al. reported that α -glycosides of branched oligosaccharides inhibited type 1 fimbriated *E. coli* attachment to yeast or tissue cells [147]. Higher monosaccharide numbers in the carbohydrate structure, particularly mannose and fucose, improve multivalent interaction to increase binding strength [148]. Table 3.4 lists several of these carbohydrate ligands identified through these glycobiology or synthesis chemistry investigations.

Several seemingly unrelated review articles have identified selective carbohydrate ligand options. Type 1 fimbriated uropathogenic *E. coli* (EPEC) pathogen was inhibited from binding

tissue when monosaccharide bound its terminal α -D-mannoside virulence lectin residue [149]. Tissue cell haemagglutinin lectins associated with bacterial virulence were identified by replicating the protein-carbohydrate binding using glycoconjugate receptors [150]. Researchers found that C-type lectin immulectin-2 from the tobacco hornworm, *Manduca sexta* binds *E. coli* or *Staphylococcus* lipopolysaccharides, peptidoglycan, and β -1,3 glucan [75]. Even a hospital epidemic identified how *Clostridium difficile* strains acquired the ability to bind trehalose, a food substitute [151].

Carbohydrate ligands offer economical options to larger antibodies and DNA ligands. Fratila et al. reviewed magnetic glyconanoparticles with increased carbohydrate functionalization for rapid cell extraction [100], which is a technique utilized in our Nano-Biosensors lab. Various carbohydrate ligands have shown promising binding properties, as summarized in Table 3.4. Several of these biosensing methods use mannose or fucose residues [69], [152]–[155], or plant lectins [156], [157] to target pathogenic bacteria. In addition, the terminal sugar residues of C-type lectins were identified as the primary targets for binding interaction [75], [158].

Protein-carbohydrate bonds identified in Table 3.4 all use electrostatic forces, similar to those used by antibodies. The *E. coli* Fim-H surface molecule uses hydrophobic binding to attach to mannose-rich oligosaccharides [69]. Hydrogen binding forces are present between sugar hydroxyls and amino acid residues in microbial surface C-type lectins [75], [158]. Type 1 piliated *E. coli* HB101 attached organic polymer through multivalent acidic and mannose hydrogen bonds [153]. Some binding schemes also require cation cofactors Ca^{2+} or Mn^{2+} for binding between surface lipopolysaccharides and lectins.

3.7 Microbial Surface Epitopes for Carbohydrate-functionalized MNP-cell-AuNP Nano-biosensing

Microbial pathogens have two main goals: survival and reproduction. A pathogen's survival necessitates its ability to attach, either to surfaces or host organisms; involves secretion of toxins against competitors and regulatory cells; and requires uptake of nutrients for growth, regeneration and reproduction. Microbial cell surfaces are enveloped with molecular structures that fulfill their cellular functions. All of these same microbial surface markers, or epitopes, may also be used to target those microbes that contaminate our environmental and food supply sources. The human immune system itself produces antibodies and complement that target pathogen epitopes. Following is a brief review of these microbial epitopes which can be targeted by carbohydrate ligands in nano-biosensing assays.

Microbial surface epitopes may be attached directly to the membrane surface, transverse the membrane to connect external and internal cellular spaces or are in "association" with the cell surface through non-covalent forces. These molecules are complex, frequently constructed from several sub-structures excreted to the cell surface. Epitopes are temporal structures, changing over time with growth and environmental conditions. Due to the complex nature of surface epitopes, many regions along the structure which are not necessarily used in cellular processes may provide novel areas for selective MNP targeted capture.

Nanoparticles can be functionalized with surfactants that target microbial surface epitopes for extraction and quantification from liquid foods. In immune responses, antibody binding is one of the most specific and strongest non-covalent binding mechanisms in cellular processes [159]. But antibody ligands are quite expensive and time-consuming to produce and require special handling. Current carbohydrate ligands, such as those summarized in Table 3.4, are less selective

in their binding targets but have proven their ability to attach to a broad spectrum of surface epitopes at fractions of the cost of antibodies and DNA. Plus, more selective carbohydrate ligands are being discovered and synthesized.

Lipopolysaccharide (LPS) and peptidoglycan moieties make up a substantial amount of prokaryotic cell wall structure. Gram-negative cell walls contain higher amounts of LPS, whereas Gram-positive cell walls are composed of a thick layer of peptidoglycan. LPS is toxic to the human body [160] and cause antibody immune responses. LPS is composed of a hydrophobic lipid A region, responsible for toxicity, which anchors the structure within the cell membrane, followed by a core polysaccharide region, extending into the O-antigen domain which consists of repeated polysaccharides [161]. Peptidoglycan is composed of sugars and amino acids, with residues of N-acetylglucosamine or N-acetylmuramic acid. Peptidoglycan moieties can be further conjugated to secondary cell wall polymers (SCWP), covalently link to the exposed N-terminus [162].

Spread across the cell walls of all microbial types are peptidases and outer membrane proteins that assist in nutrient flow, pathogenesis, motility and cell wall turnover. Peptidases are specialized proteins secreted to the surface that interact with surface carbohydrates and lipids and act as enzymes with catalytic sites involved in peptidoglycan modification, cell wall turnover and cellular locomotion [164], [165]. Adenosine triphosphate (ATP)-binding cassettes (ABC) are one major group of nutrient transporter proteins. Due to the ABC structure specificity among microbial species they are strong antigens, or targets, for immunogenic responses, resulting in highly selective antibodies [166]. Outer membrane proteins (OMP) are porins that transverse the cell wall providing entry across the cell wall for a broad spectrum of nutrient exchange [161], [167]), using active-transport of nutrients at low-concentration, and more passive diffusion of higher-concentration nutrients. Due to porin discriminatory transport of hydrophilic compounds by size

Table 3.4 Biosensing methods using carbohydrate functional groups for target capture.

Carbohydrate Ligand & Modifications	Microbial Target & Surface Epitope	Identified Binding Moiety	Binding Efficiency	Reference
Mannose-containing oligosaccharides with PTAM, PCAM, DAMP, glucosamine & chitosan; (immobilized onto gold electrodes and SPR surfaces) (1)	FimH of <i>E. coli</i>	Hydrophobic phenyl residues & aliphatic side groups	Relative selectivity for <i>E. coli</i> at 86% vs 2.6% & 8.6% for <i>Citrobacter freundii</i> & <i>Staphylococcus epidermis</i> (detection for MED across 2 to 6 log CFU/mL, or for SPR across 3 to 11 log CFU/mL)	[69]
Organic polymer glycopolythiophene with mannose	Type 1 piliated <i>E. coli</i> HB101 (additional lectin & Influenza virus targets also described)	Multivalent polymer acidic group electrostatic bonding and mannose H-binding along microbial receptors	Visual red-shift with ligand binding to target	[153]
Monovalent α -D-mannose-pyranoside altered w/ attached fluorescent DBD dye (2)	FimH of <i>E. coli</i> DH5 α	(not addressed)	Signal to noise optimized binding at ligand concentration of 10 ⁻¹² mol/L with 10-min binding window	[152]
Plant-based lectins ConA, LCA, WGA, MAL, & UEA; (immobilized onto quartz crystal electrode) (3)	<i>Campylobacter jejuni</i> & <i>Helicobacter pylori</i> LPS of lysed cells (ConA & LCA to mannose & glucose, WGA & MAL to β -N-acetylglucosamine, UEA to fucose)	Binding requires Ca ²⁺ & Mn ²⁺ ions	4 log CFU/mL microbial effect on crystal oscillation frequency against lysed cell samples, e.g. for <i>C. jejuni</i> strains ConA-HS:3 @ 60 Hz; evidence of selective lectin binding	[156]
C-type lectin SSL from Atlantic <i>Salmo salar</i> (4)	<i>Aeromonas salmonicida</i> surface molecule LPS (which is also mannose-binding) and glycans w/ terminal GlcNAc; also binds <i>Pseudomonas fluorescens</i> , <i>A. hydrophilia</i> , <i>Pichia pastoris</i> , & <i>Saccharomyces cerevisiae</i>	3 to 4 hydroxyl groups from the sugar hydrogen bond with acidic and amino acid side chains of LPS in coordination with Ca ²⁺	Western blots showed SSL binding to bacteria & fluorescence-labeled SSL bound 10 glycans w/ GlcNAc terminal labels	[158]
Plant-based lectins from: WGA, Con A, UAE, PNA & MAL (5)	<i>E. coli</i> O157:H7 surface mono- and oligosaccharide polysaccharide structures	SEM imaging of WGA-coated biosensor surface with captured <i>E. coli</i> cells	Linear response between 5 to 8 log CFU/mL for WGA ligand w/ higher signaling than Con A, UEA, PNA & MAL ligands	[157]
Fucose-bearing oligosaccharides Le ^b & blood group H type 1 FMNP (6)	<i>H. pylori</i> J99 BabA cell surface fucose binding adhesin lectin	Monomeric sugar binding to protein	Confocal microscopy evidence of FMNP-cell binding & TEM evidence of FMHP-AAL aggregation	[155]

Table 3.4 (cont'd)

Carbohydrate Ligand & Modifications	Microbial Target & Surface Epitope	Identified Binding Moiety	Binding Efficiency	Reference
Purified immulectin-2 C-type lectin (w/ extended terminal carbohydrate loop) from hemocytes cell surface containing 2 carbohydrate-recognition domains (7)	LPS from <i>E. coli</i> K12 & <i>E. coli</i> 011:B4; peptidoglycan from <i>E. coli</i> K12, <i>Staphylococcus aureus</i> & <i>Bacillus subtilis</i> ; zymosan & mannan from <i>Saccaromyces cerevisiae</i> ; laminarin (β -1,3-glucan)	Glutamate-proline-asparagine motif binds sugar motifs	ELISA confirmation of ligand-target binding in 96 well plate @ 10 nM and 40 nM concentrations	[75]
Mannose monosaccharide equipped with ethanolamine linker to immobilize on microarray	<i>E. coli</i> ORN178	(not addressed)	Levels above 10^6 <i>E. coli</i> ORN178 stained with nucleic acid dye provided signaling above background, whereas <i>E. coli</i> ORN209 showed 4-fold lower binding	[154]
20 D-mannose derivatives (sulfonamides & cinnamides)	<i>Pseudomonas aeruginosa</i> LecB (PA-IIL) surface lectin virulence factor	Via three hydroxy groups from trisaccharide Lewis ^a , w/ ability to target adjacent protein cleft for improved affinity	Inhibition ligand-target testing showed derivatives increased binding 4 to 24-fold, which minimized pathogen tissue binding	[163]
Tridecafullerenes w/ 120-count mannose residues attached to azide-substituted glycofullerene scaffold with alkyl chain linkers (8)	DC-SIGN lectin of EBOV infection	DC-SIGN recognizes multivalent sugar residues on oligosaccharides	100% inhibition of 2.5×10^5 DC-SIGN @ $>10^4$ pM, with IC ₅₀ of 667 nM	[148]

(Table 3.4 biosensing definitions: (1) PTAM = p-thiolphenylaminomannose, PCAM = p-carboxyphenylaminomannose, DAMP = 1-deoxy-1-aminomannopyranoside, SPR = surface plasmon resonance, FimH = mannose-specific fimbrial lectin adhesin molecule, and MED = metal-enhanced electrochemical detection; (2) DBD = [1,3]dioxolo[4,5-f][1,3]benzodioxole; (3) ConA = Concanavalin A, LCA = Lens culinaris agglutinin, WGA = Wheat Germ agglutinin, MAL = Maackia amurensis lectin, UEA = Ulex europaeus agglutinin, & LPS = lipopolysaccharides; (4) SSL = Salmo salar lectin, LPS = lipopolysaccharides, & GlcNAc= N-acetylglucosamine; (5) WGA = Triticum vulgare wheat germ agglutinin, Con A = Canavalia ensiformis jack bean concanavalin A lectin, UAE = flowering plant Ulex europaeus agglutinin,, PNA = Arachis hypogaea peanut agglutinin, MAL = tree species Maackia amurensis leukagglutinin, & SEM = scanning electron microscopy; (6) Le^b = Lewis b, FMNP = fluorescent magnetic nanoparticles, BabA = blood group antigen binding adhesin A & AAL = fucose binding Aleuria aurantia lectin; (7) LPS = lipopolysaccharide; (8) DC-SIGN = dendritic cell-specific intercellular adhesion molecule-3-grabbing non-integrin receptor, EBOV = Ebola virus, & IC₅₀ = 50% inhibition concentration.)

and charge, they are targets of specific antibody production, especially for OmpD porins [168]–[170].

Microbial cells detect their environment through their cellular wall molecular components. Chemotaxis proteins sense signals secreted from other microbes, OmpC porins sense changing osmolarity, and MSCRAMM (microbial surface components recognizing adhesive matrix molecules) recognize connective tissue of mammalian tissue [171]–[173]. Flagella are locomotive organelles attached to the surface of the microbe, composed of monomeric polypeptides with high variability in their protein composition with high specificity per microbial species as H antigens in immuno-reactivity serotyping [164], [174], [175]. Curli and fimbriae are hair-like projections involved in adhesion to surfaces and aggregation with other cells, containing hydrophobic amino acids lysine, proline, and serine, as well as a mannose-binding region [94], [176]–[180]. Pili also acts in surface binding through hydrophobic amino acids that act [28], [181]–[185].

As major nutrients, amino acid and sugars uptake is facilitated by transporter structures. Cysteine transfer across the cell membrane is performed in cystine form for *E. coli* [24], *Bacillus subtilis* [186], and *Listeria monocytogenes* [187]. Glycosylated milk compounds inhibited lectin proteins of *Pseudomonas aeruginosa* from galactose, fucose and mannose uptake [62]. *Chronobacterium violaceum* lectin binding protein binds both fucose and mannose, but at different protein orientations [188].

Chitosan is a polycationic polysaccharide derived from acetylated chitin that easily binds the negative charged surfaces of microbial species, such as seen for *E. coli*, *Pseudomonas*, and *Salmonella* [189], [190]. The positively charged amino groups of chitosan also bind *Bacillus* vegetative cells to block nutrient uptake [191], [192].

3.8 Conclusions

Carbohydrate functionalized MNP are an economical means to expedite microbial extraction in mere minutes from simple and complex matrices such as milk, without the need for time-consuming centrifugation from large sample volumes. Upon extraction, MNP-cell complexes can be concentrated to less than 1 mL, resulting in stronger detection signaling. Although the initial carbohydrate ligands reported here bind and extract the total bacterial load present in samples, higher selectivity is possible through study of the cell surface molecular structures against a range of carbohydrates. Biocompatible ligands are desired as antibody-replacements due to the cost of antibodies, particularly given the persistence of cross-reactions with non-target microbes. Regardless of the ligand used, though, it was shown that several methods were able to significantly quantify microbial presence with the MNP still attached to their target.

Beyond the potentially intensified microbial biosensing via MNP concentration, EANP labeling, such as with quantum dots, TN or AuNP, of the MNP-cell complexes further improves test sensitivity with less complicated spectral and electrochemical detection methods. Microbial contamination along the food supply chain could be detected quickly using this economical method in frequent product checks, assuring suppliers the safety of their product and reducing substantially consumer illness. Additionally, functionalizing MNP and AuNP with inexpensive biocompatible carbohydrates, such as dextrin, further decreases assay costs, while reducing hazardous waste production through green chemistry.

Combining carbohydrate-functionalized MNP cell capture and concentration, along with dextrin-coated AuNP labeling resulted in promising nano-biosensing development towards the goal of feasible, less complicated tests. Much work in nano-biosensing development has focused heavily on designing highly specific, one-time-use “strip” sensors that involve substantial

technology to produce. These are not cost-effective for many worldwide food suppliers, though. Even many of the suspended MNP/EANP biosensing assays reviewed here are still out of reach for many users, requiring special storage or highly technical equipment.

Carbohydrate ligands are easily incorporated onto nanoparticles, and require little special handling, showing a long shelf life at room temperature. As more selective carbohydrate ligands are identified and incorporated into MNP-cell-AuNP assays, consumers can be assured of safer food supplies at affordable costs. While the proof-of-concept test presented here requires optimization for detection at lower cell concentrations, it was successful in detecting *E. coli* presence directly from milk, whereas many reported tests were studied only in simple buffer solutions. The future in nano-biosensing is not in developing more technically complex sensors, but applying technological knowledge to develop inexpensive, user-friendly microbial assays.

Chapter 4. Literature Review – Technology

4.1 Introduction

Designing reliable, user-friendly nano-biosensors to detect pathogenic bacteria does not require intricate combinations of the multitude components that define biosensors. The intricate design of the glucose meter, which uses a sensitive enzymatic reaction to quantify sugar levels in blood samples through miniaturized electronic components, is a bio-sensor style that has not been easily replicated in other biological testing at an economical cost. Instead, separating components of the bio-sensing mechanism while utilizing inexpensive ligands, rapid extraction methods, and affordable signaling instrumentation will allow the design of a sensitive, reliable and adaptable nano-biosensing system to aid in ensuring the safety of food supplies globally.

Carbohydrate-based MNP-cell-AuNP bio-sensing complexes can be used to quantify bacterial presence utilizing either commonly available UV-Vis spectrophotometer technology or an inexpensive handheld potentiostat, which uses electrically produced signaling. As spectrophotometers are more commonly available lab instrumentation, bacterial contamination levels can be rapidly quantified from MNP-cell-AuNP absorbance peaks in the UV-visible spectral region of 900 nm to 200 nm. Within developing countries, though, access to even minimally equipped labs is problematic, therefore, an inexpensive handheld potentiostat for repeated on-site testing is a reliable option.

Electrochemistry is the study of an electroactive specie's electrical response to an applied electrochemical force, such as potential (voltage), current (amps), or due to non-equilibrium chemical concentration. These species are targets being quantified and may be organic or inorganic chemicals [193]–[195], with simple or complex molecular structures [196]–[198], even pharmaceuticals [15], generated through chemical reactions or biological metabolism, and may

even be individual cells of mammalian or microbial origin [199]. Cyclic voltammetry (CV) and differential potential voltammetry are two such electrochemical methods minimally applied in novel biosensing methods, as indicated in Tables 3.2 and 3.3 [6], [92], [128]. These methods provide sensitive detection of nano-levels of compounds with highly technical instrumentation. But, user interpretation of detection results can be designed by developers to provide simplified, straight-forward responses to their contamination concerns.

Spectrophotometry is another electrochemical method that offers a sensitive approach to design rapid microbial contamination detection methods. In the continuing drive to develop improved nano-biosensing methods of pathogenic bacteria, spectrometry is a more simplistic method that uses simple light beam technology [76], [80], [83], [121], [127], [135], [136]. Spectrophotometry measures the absorbance (or transmission) of an incident light beam upon a suspended compound due to its surface plasmon resonance (SPR) [80]. The ultimate success in the application of spectrometry to nano-biosensing likewise depends upon the development of a user-friendly method to interpret signaling responses.

4.2 Electrochemical Signaling Using Cyclic Voltammetry and Differential Pulse Voltammetry

4.2.1 MNP-cell-AuNP Detection

MNP-cell-AuNP species described in the previous chapter are electroactive and their properties can be studied through electrochemical means. In the case of amperometry (electrical current), applied potentials across an electrochemical test cell result in the chemical changes in the form of chemical reduction or oxidation (“redox”) of the species at specific potentials due to electron flow. This electron flow is either positive or negative current that can be monitored using a potentiostat instrument. The redox properties of the species result in characteristic graphs of the

current response versus the applied potential [21], [197], [200], [201]. Common uses of electrochemistry include determination of a specie's standard reduction potential useful in studying chemical redox reactions, along with measurement of reaction kinetics and corresponding chemical coefficients. A specie's absorption properties to an electrode surface can also be studied. Finally, quantification of species is possible through the characteristic current response peak height for either oxidation or reduction, or both [65], [202], [203].

4.2.2 Voltammetric Methods

Voltammetry applies the principles of electrochemistry in the study of the electroactive species, or target analyte. These experiments may be carried out within voltaic cells, which are commonly studied in general chemistry, using separated anodic and cathodic electrodes with a connecting salt bridge for macro-analysis (e.g. Fig. 4.1A). Over the past two decades, though, miniaturized cells have been developed with grafted, printed or etched electrically conductive chemicals forming the separated electrodes, which are then bridged by a micro-volume solution containing the target analyte (e.g. Fig. 4.1B and C). Currently sensors can detect analyte levels as low as nano- and pico-grams or micro-moles, and also analyze the properties of the analyte [132], [195], [197], [204]. Cyclic voltammetry (CV) consists of applying a linearly increasing then decreasing potential (voltage) across the electrode surface and measure the current as a function of applied potential and establishes whether it has reversible electroactive properties (Figs. 4.2A & B). Reversible chemical species are those that can be regenerated even after reaction. Differential pulse voltammetry (DPV) instead applies increasingly (or decreasingly) sized pulses

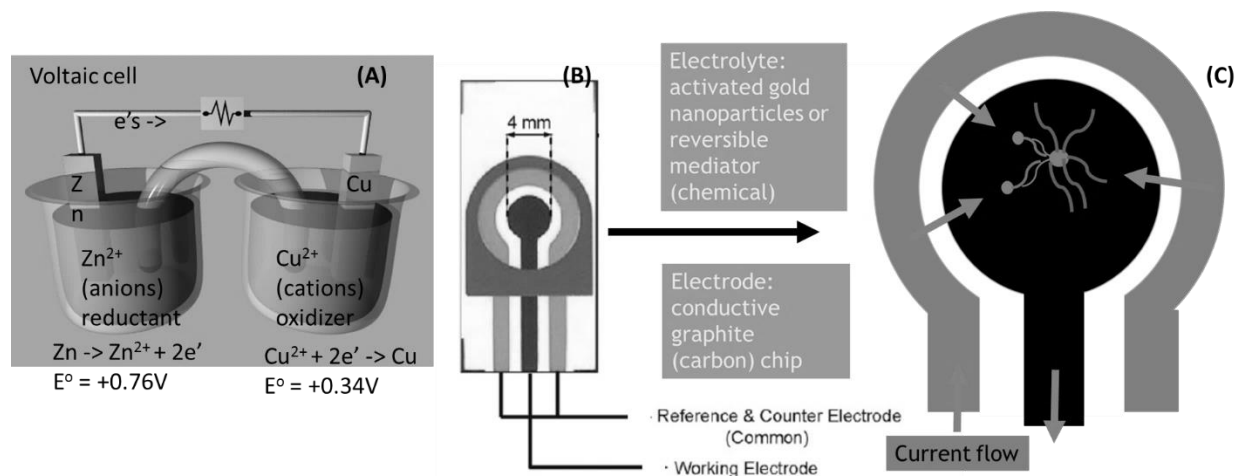


Figure 4.1 Electrochemical systems exemplified with (A) common voltaic cell, (B) miniaturized screen-printed carbon electrode (SPCE) sensor, and (C) a mock-up of voltammetric bio-sensing with an SPCE chip with capture bacteria labeled with AuNP.

of potential (voltage) across the electrode, to measure electrochemical currents from the various components of the sensor and target, since different components will respond at characteristic potentials (Figs. 4.3A & B). DPV additionally provides improved sensitivity for measuring analyte concentrations compared to CV, showing similar current responses of 15 μA to 20 μA for morphine detection for concentrations at one order of magnitude lower, e.g. 0.5 μM in DPV testing versus 50 μM in CV testing [132].

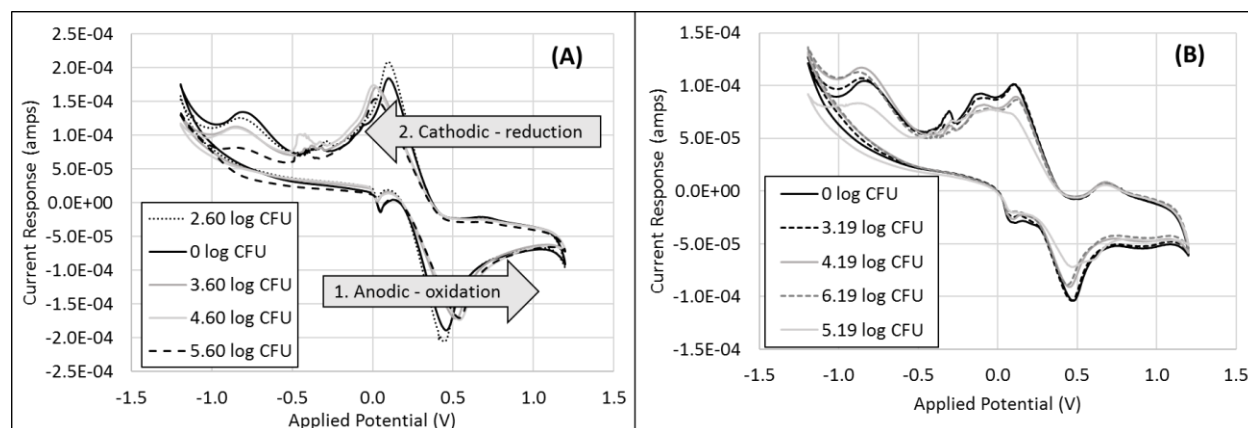


Figure 4.2 Examples of graphical results of nano-biosensing responses using cyclic voltammetry for microbial detection with MNP-strips on (A) soft plastic or (B) hard plastic.

4.2.3 Micro-bio-sensing

Miniaturized sensors consist of a working electrode, reference electrode and counter electrode all contained within squared centimeter areas (Fig. 4.1B). Potential changes are applied across the working and reference electrode, with liquid sample sizes of only microliters bridging the electrode, and the current response monitored at the working electrode. A potentiostat instrument connected to the electrodes provides both the desired potential changes and measures the resulting current response. During a voltammetric experiment, applied potential creates an electrical force across the sensor surface. If the target analyte is in an electrically reduced state and a more positive potential is applied with respect to the working electrode, electrons will be stripped

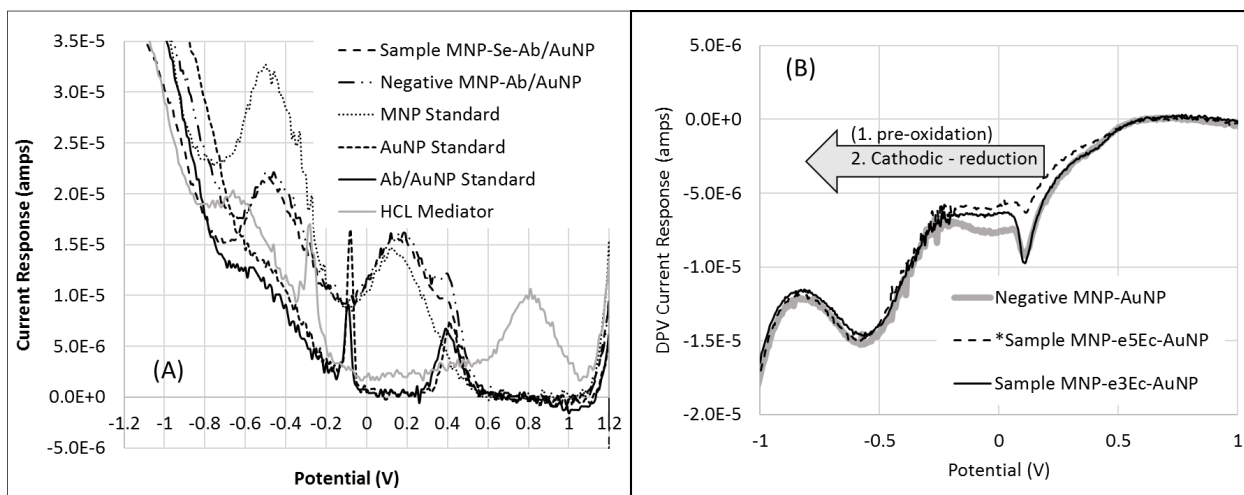


Figure 4.3 Examples of graphical results of nano-biosensing responses using differential pulse voltammetry for microbial detection using MNP-cell-AuNP with (A) positive current convention and (B) negative current convention.

from the analyte, causing oxidation, and flow from the solution into the working electrode. These current responses will be registered as negative with respect to the working electrode, since the electrode is not providing electrons (Fig. 2A). A chemically reversible analyte can then be returned to its reduced state by applying reversed potential differences across the electrodes, resulting in positive current responses as electrons flow out of the working electrode to the analyte.

A similar response is achieved in differential pulse voltammetry, except current convention can vary per instrument (Figs. 4.3A & B). Initially, the activated MNP-cell-AuNP suspension sample applied to the electrode is oxidized. Then, as more positive negative potential is applied across the electrode, electrons will flow from the working electrode to reduce the analytes in the solution. This electron flow may be registered as either positive current (Fig. 4.3A) or negative current (Fig. 4.3B) depending on the direction of the current.

When a reversible analyte is monitored using cyclic voltammetry, the oxidative and reductive redox potentials can be determined (Fig. 4.2A). A reversible analyte is one that rapidly reacts to potential changes so that the system continuously approaches equilibrium for the new conditions. During oxidation of the analyte within the test solution, the analyte at the electrode surface will lose electrons and the speed at which this occurs depends upon the size of the chemical gradient within the solution and diffusive properties of the analyte through the bulk solution to the electrode. When reduced analyte finally reaches zero concentration at the electrode, the absolute peak oxidation current is reached at a characteristic potential. At this time, the chemical gradient is reversed, slowing additional analyte flow to the working electrode and oxidation eventually ceases, tailing off in current response. Upon reversing the potential difference, analyte reduction will begin in reverse order as oxidation.

4.2.4 Voltammetry Conventions

These analyte responses can be described by several physical laws, such as the Nernst equation (Fig. 4.4A) which defines the newly established concentrations of the oxidized and reduced forms of the analyte, c_O and c_R , respectively, due to the applied potential. The Butler-Volmer equation (Fig. 4.4B) further relates these same analyte concentrations to both the applied

potential, E , and the current response, i . In addition, Fick's law (Fig. 4.4C) relates the analyte concentration

Nernst Equation (A)

$$E = E^0 - \frac{RT}{nF} \ln \frac{c_R^0}{c_O^0}$$

Butler-Volmer Equation (B)

$$\frac{i}{nFA} = k^0 \{ c_O^0 \exp[-\alpha\theta] - c_R^0 \exp[(1 - \alpha)\theta] \}$$

Fick's Law (C)

$$\Phi = -AD_O(\partial c_O / \partial x)$$

Figure 4.4 Equations for general theory of voltammetry including (A) the Nernst Equation which relates the applied potential force, E , across the electrode to the concentration of the reductive and oxidative species, c_R and c_O , respectively, where R is the molar gas constant (8.3144 J mol⁻¹K⁻¹), T is the absolute temperature (K), n is the number of electrons transferred, F = Faraday constant (96,485 C/equivalents), and E^0 is the standard reduction potential for the redox couple; (B) the Butler-Volmer Equation further relates current, i , potential, E , and concentration, c_R and c_O , where $\theta = nF(E - E^0)/RT$, k^0 is the heterogeneous rate constant, α is known as the transfer coefficient, and A is the area of the electrode; and (C) Fick's Law relates the flux of matter, Φ , which is directly proportional to the analyte concentration gradient, $\delta c_O / \delta x$, where D_O is the diffusion coefficient of oxidative species and x is the distance from the electrode surface [205].

gradient within the sample solution, $\delta c_O / \delta x$, at the sensor to the flux of matter, Φ [205], and the analytes diffusion coefficient, D_O . In studying a new analyte, these relations provide valuable information into the redox reaction occurring on the sensor, especially during cyclic voltammetry. In some systems, a well-defined electrochemically reversible mediator chemical, or redox probe, such as ferrocene or potassium ferricyanide, may be included into the test sample to assist electron transfer if the analyte shows irreversible chemistry [205]–[207]. In these situations, analyte quantification is determined with respect to its reactive effect on the mediator presence. Reversible mediators allow the easy application of cyclic voltammetry to irreversible or more complex systems when desiring only to quantify analyte.

In voltammetry, polarity convention with respect to the working electrode must be determined before interpreting any resulting voltammograms. Different conventions result in oxidation and reduction peaks assigned to different quadrants of their respective plots [207]. Oxidation occurs when electrons are stripped from the analyte due to increasing potential difference across the electrodes, making the working electrode more positive than the analyte and more attractive to free electrons. This current flow can either be considered as positive into the working electrode, or negative away from the analyte. The opposite is true for reduction, when the working electrode is more negative than the oxidized analyte, the working electrode then supplies excess charge to the analyte, reducing it. Again this current can be defined as negative flowing away from the working electrode, or positive flow to the analyte.

Inclusion of redox probes – reversible mediators – or redox-active receptors into the test sample or directly onto the sensor can improve sensitivity and reduce detection limits of the desired analyte. This is through improved electron transport or flux to the electrode as the strongly oxidizing or reducing mediator causes a large shift of the redox potential to a higher rate constant than the sample system [208], [209]. In addition to chemicals such as potassium ferricyanide mentioned earlier, biological enzymes may be incorporated into a sensing system. In fact, immobilizing catalytic electron-transfer proteins, such as cytochrome C and ferredoxins [208], directly to a sensor surface improves access to the buried catalytic region and improves voltammetry sensing without the need for electroactive intermediates [210]. Similar catalytic proteins may populate the surface of microbial targets, also. Other studies have exploited glucose oxidase and/or horseradish peroxidase to react upon secondary species such as hydrogen peroxide (H_2O_2), glucose or thionine to quantify analyte at concentrations down to 6 pM DNA, 10 μM H_2O_2 , and 3.33 fg/mL alpha fetoprotein within human serum [198], [211], [212]. Even so, adding a redox

probe, such as potassium ferricyanide, to the test sample can aid in improving a system's redox potential, shifting the redox peaks from the autocatalytic potentials to more advantageous regions of the voltammogram [211].

4.2.5 Improved Bio-sensing with Nanoparticles

MNP with high surface area to volume ratio may also improve voltammetric sensing through when present in the sample applied to the flat electrode surface. MNP have a high surface area to volume ratio for increased analyte adsorption to the sensor, and MNP's high surface reactivity promotes electron transfer [132]. In testing morphine levels within urine and serum, the presence of 10% MNP functionalized with chitosan improved DPV current response at 0.4 V for 50 μM morphine over two-fold, a three-fold higher current response over CV signaling for the same sample, as well as allowing reliable detection of 0.5 μM morphine. The combination of MNP and DPV resulted in a detection limit of 0.003 μM morphine, with a linear response for micromolar amounts [132]. Another sensor including MNP, this time functionalized with an N-acetyl-homoserine-lactone (AHL) homologue, was able to detect a limit of 0.1 nM AHL using DPV [213]. Felisilda et. al. were also able to lower the limit of detection for a lysozyme enzyme to 0.010 μM with DPV, versus an earlier limit of 0.030 μM using CV signaling [196]

Incorporating AuNP into the sensor design can also improve electrochemical signaling responses for similar reasons as mentioned for MNP, along with autocatalytic capabilities. Fournier et. al. immobilized cytochrome B enzyme to the surface of an AuNP-modified sensor to study the electron transfer properties of its heme factors, which showed current peaks for reduction at -0.12 V and oxidation at -0.06 V with CV [193]. Improved signal transfer through AuNP is particularly beneficial when using sensors to detect microbial targets. Kang et. al. detected *Bacillus*

bacteria down to 1 log CFU/mL using horseradish peroxidase reduction of H₂O₂ and thionine integrated into an AuNP-antibody-sandwich sensor; this same signaling method was used by Fei et. al. to detect *Salmonella* at a concentration of 4 log CFU/mL using an AuNP-DNA-sandwich sensor; and Cheng et. al. could detect 2 log CFU/mL *Listeria* in milk also using an AuNP antibody-sandwich sensor [21], [200], [214].

4.2.6 Signal Interpretation

In analyzing the current responses from voltammetric interrogation of an electroactive system, DPV measurements provide direct comparison of peak heights between varying analyte concentration and sensor composition. CV measurements of a test sample not only indicate redox potentials but can be used to quantify analyte concentrations through specific anodic and cathodic peak heights. For reversible systems, or an irreversible system that applies a reversible mediator, the cathodic peak response, I_{pc} , for reduction is determined as the distance between the maximum absolute current response and a line extrapolated to the reduction potential of the initial reduction slope. The anodic peak response, I_{pa} , for oxidation is simply the maximum absolute peak current value. A truly reversible system has a ratio of I_{pa}/I_{pc} equal to 1, whereas irreversible systems have a ratio of their anodic and cathodic peak currents greater than 1. Additionally, the sum of I_{pa} and I_{pc} provide a method to compare analyte concentrations between test samples.

Even though pathogenic microbes have a net negative surface charge from the high levels of peptidoglycans or transmembrane lipopolysaccharides (LPS) present, it might be expected that they could be detected directly as analytes within an electrochemical system. Voltammetric signaling of microbial samples, though, requires redox-active moieties to be present in the microbial surface structures, and available for oxidation in a high concentration. This is exemplified by cytochrome c proteins which utilize tyrosine and tryptophan amino acids for

electron transport [215]. But, direct detection of pathogenic microbial electro-activity shows minimal promise with low current responses for biofilm detection of totaled 10 to 20 mA over 10 hr of pathogen detection monitored over 10 to 24 hr in milk enriched with target substrates [216], [217]. Voltammetric methods have been developed, though, that exploit microbial surface enzymes or transport systems connected to metabolic processes to provide electron flux for current response, but these methods suffer in poor rapid extraction of the target [70], [218]–[220].

Recent examples, though, include cytochrome c membrane electron transport of *Shewanella* was connected to a photoanode to supply electrons in which to reduce environmental carbon. The flux of electrons through this proof-of-concept microbial fuel cell circuit was monitored through CV and found to have a reductive peak at -329 mV and oxidative peak at -25 mV with peak sizes relative to the combined microbial electron flux of the system [218]. Antibody-captured *E. coli* were quantified via a surface membrane redox enzyme, D-glucose dehydrogenase, reaction with glucose substrate and ferrocenemethanol to assist in electron transfer which produced an oxidation peak at 0.3 V in CV measurements, able to detect as low as 1 log CFU/mL [70]. *Pseudomonas aeruginosa* was quantified using cellular acridine orange (AO) uptake. Pure AO shows two oxidation peaks within CV at 0.72 and 0.88 V, while DPV interrogation of cells exposed to AO showed a 100 nA peak at 0.8 V for 6 log cfu/mL [219]. Additionally, secreted electroactive molecules detected using CV distinguished between *E. coli* and *Saccharomyces* yeast cells when stimulated with glucose nutrient [220].

4.3 Spectrophotometric Verification of NP Presence and Quantity

4.3.1 Spectrophotometric Conventions

Metallic nanoparticles contain a large surface area to volume ratio, resulting in a high quantity of surface electrons that can be exploited for spectral signaling, compared to bulk materials. Electrical and spectral detection schemes excite these surface electrons, creating a surface plasmon resonance (SPR) phenomenon. For example, the reduced gold nanoparticle surfaces are coated with dextrin which containing an abundance of electrically charged hydroxyl groups and oxygen atoms. When a spectral incident light beam at a resonant wavelength strikes the nanoparticle surface, the electrons flow across the surface, absorbing a fraction of that energy related to their quantity, in dilute systems. SPR is dependent upon the dielectric properties of the sample compound and its environment, among other factors. Changes in the dielectric constant will result in a characteristic reportable change in spectral absorbance. But, plasmon excitations are only possible if the incident light has a longer wavelength, lower energy, than the nanoparticle diameter. Therefore, nanoparticles with diameters smaller than 100 nm show properties different from bulk materials. These nanoparticles can be excited, and thereby measured, using electromagnetic radiation in the visible light spectrum with wavelengths between 400 nm and 700 nm.

Electromagnetic radiation in the form of light waves carries an electric field that oscillates at specific frequencies, causing movement of electrons on the nanoparticle surfaces, creating concentrated negative regions and positive (ion) regions, or surface plasmons. Light photons with the appropriate energy are absorbed by the nanoparticles causing the electron motion across the surface. Maxwell's four equations describe electric and magnetic properties arising from electric charge and current distributions and these equations can be solved for spherical nanoparticles using

Mie's theory for round nanoparticles. These solutions predict that nanoparticles with a diameter of 10 nm will absorb most visible light, whereas those with diameters of 100 nm will scatter most visible light, which results in signature peak absorbances useful in nano-biosensing. The commonly reported spectral absorbance spectrum is more accurately described as an extinction spectrum which measures the amount of light absorbed and scattered at each wavelength. For a given sample, the resulting spectral results represent the maximum, or overall, absorbance value at each wavelength.

Spectrometry of dilute systems is linearly related to concentration and can be used to quantify the amount of compound present in the sample. Increased nanoparticle concentration results in increased surface plasmon, and therefore an increase in absorbance of the incident light. This property can be exploited, for example, in using increases in AuNP labeling to report the amount of target present. Using Beer's Law, the absorbance, A , can be related to the intensity of the scattered light recorded at the spectrometer sensor, I_{sample} , with respect to a reference sample, I_0 , as $A = \log (I_0/ I_{\text{sample}})$. In addition, the nanoparticle concentration, C , can be related to the absorbance through the Beer-Lambert equation $A = \epsilon l C$, where ϵ is the molar absorptivity of the particle and l is the sample cell length of the cuvette. For nanoparticles with a narrow range of diameters in dilute suspensions, their total concentration can be directly related to the maximum peak absorbance, and to their integrated peak area. For gold nanoparticles with a diameter below 30 nm, the peak extinction maximum is approximately 520 nm, whereas magnetic nanoparticles diameters of 200 nm have a peak extinction maximum at approximately 620 nm. Additionally, any nanoparticle aggregation that creates pseudo particles with a larger "effective" diameter with absorbance at higher wavelengths can be monitored with spectrometry.

4.3.2 Spectrometry Bio-sensing

Exploiting nanoparticle surface area properties allows unique nano-biosensing applications. Quantifiable shifts in the spectral absorbance will result in relation to changes within the sampling suspension due to varying surface properties. As discussed earlier, the high surface area to volume ratio provides substantial room to functionalize nanoparticles with surfactants that will be attractive to either a variety or specific biological targets. Therefore, spectrometry provides a means to rapidly evaluate detection parameters when investigating the binding properties of nanoparticle surfactants to microbes. As reported by Bilankohi, as the thickness of the functionalized nanoparticle shell decreases relative to the core metal, surface plasmon increases, causing a “red shift” in absorbance maximum to higher wavelengths. Additionally, it was found that both the core material and its diameter established the location of the peak absorbance maximum [221]. A shift in the peak maximum will also occur as biological targets bind to the surfactant, both in total absorbance and with respect to the wavelength of the incident light, thus providing two measures to quantify target analyte.

Although numerous examples exist in the application of magnetic and/or gold nanoparticles to improve extraction and detection of pathogenic bacteria within environmental samples as shown earlier [6], [21], [31], [74], [89], [93], [121], [127], [201], [222]–[225], a few even apply visual methods to simplify detection [66], [93], [95], [226], but most examples that combine spectral detection with nanoparticle capture are used to target and detect chemicals [34], [72], [138]–[140], with none appearing to use spectrophotometry to directly detect MNP-captured bacteria combined with AuNP enhanced signaling. Biological components show a strong absorbance within the UV-visible spectral range between 200 to 400 nm. Their characteristic absorbance pattern, minus nanoparticle presence, may even allow identifying different species

such as that shown by Ghosh et. al. in identifying 5 species of *Bacillus* using the first derivative of their individual spectra [227]. Although microbes can be easily detected and quantified using spectrophotometry methods, cellular extraction from many environmental samples is tedious, requiring centrifugation or serial dilutions in the initial sample preparation steps. Centrifugation is used to separate the targeted bacteria from the surrounding matrix, concentrating the microbial load and removing chemicals that may interfere with subsequent detection. Serial dilution is necessary when for suspected high microbial concentrations to ensure linear responses during detection steps. Functionalized MNP provide an efficient method to extract bacteria from even complex liquids, but MNP can then mask the spectral properties of captured cells. AuNP attachment to captured cells, though, can provide a strong spectral signal around their peak extinction maximum (520 nm) for the MNP-cell-AuNP complexes.

4.3.3 Spectral Integration

Since the combination of MNP, cells, and AuNP in a spectral sample have overlapping absorbances, spectrum obtained from MNP-cell-AuNP samples show convoluted peaks throughout the spectral range. Additionally, as the nanoparticles aggregate, as will be seen in Chapter 5 through transmission electron microscopy (TEM), the peaks will broaden about their respective maximum extinction peaks, increasing peak convolution, or overlapping, and the difficulty in identifying the true nanoparticle response. The additive effect of the absorbance for the individual MNP, cells and AuNP peaks may also be further compromised by any matrix residue, such as milk components. When cells are included in the MNP-cell-AuNP complexes, the additive effect for all three components causes even more masking of their individual peaks. But step-integration of spectral absorbance for the complex sample across the tested visible region between 220 nm to 900 nm may reliably represent the AuNP peak height signaling. Since

absorbance spectrum incorporate the responses of each component of the MNP-cell-AuNP sample, including any matrix components discussed later, integrating the entire region in a step-integration manner will provide a metric that compares samples based on their complete composition. In contrast, Joo et. al. used MNP to capture *Salmonella* bacteria from a milk matrix, magnetically separated them from the matrix, then further labeled the MNP-cell complexes with titanium nanoparticles (TNP) in fresh buffer solution, but only measured spectral absorbance of the unattached TNP remaining in the supernatant, not the MNP-cell-TNP complexes. TNP peak extinction values at 230 nm were inversely related to the concentration of captured cells. When tested, though, in a complex matrix such as milk, attached milk residue caused noticeable broadening of TNP peaks [121], masking the pure TNP response.

With the necessity to identify more reliable means to interpret convoluted, multi-component spectrum, analysis through absorbance integration was considered. Streit et. al. found that integration across the spectral scans for single walled carbon nanotubes (SWCNT) were more reliable in predicting their concentration in solution in place of peak heights [228]. Even serially diluted fluorescent probes showed a linear relationship between their final concentrations and the integration across their spectral scans [229]. Demissie et. al. agreed with Streit et. al. that using integration across the spectral range was more reliable and found a strong linear relationship to the concentration of caffeine found in green coffee beans. In addition, caffeine spectral peaks were converted from absorbance to the molar decadic absorption coefficient, ϵ , using Beer-Lambert's law, to normalize the quantity across different samples [230].

4.4 Conclusion

Although the US as a developed country has seemingly inexhaustible resources, microbial foodborne diseases occur regularly each year, even given the heavily regulated food industry. Resources and regulations in under/developing countries are both insufficient to protect their populace which live on dollars per day [231], [232]. Feasible methods to determine the safety of a country's food supply require low cost tests with minimal storage requirements, long shelf life, and minimal technological instrumentation and knowledge. Inexpensive, reliable, user-friendly instrumentation would open the door for food suppliers to incorporate more frequent food testing into their supply chain procedures. Rapid identification of pathogen contamination sources and presence in food is possible using voltammetric and spectrophotometric methods with the MNP-cell-AuNP complexes described in the previous chapter. This nano-biosensing method contrasted with the numerous methods also reported earlier that require extensive sample preparation, expensive supplies, and complex instrumentation application.

Electrochemical signaling can provide expedient, reliable and sensitive detection of microbial contamination interrogating MNP-cell-AuNP complexes. This electrochemical signaling may consist of spectrophotometric absorbance of the entire complex, or current responses to activated samples where cyclic voltammetry measures total complex while differential pulse voltammetry reports current responses for individual components. As mentioned earlier, MNP may also be affixed to plastic strips to minimize contaminated liquid handling and expedite extraction of bacteria from more complex liquids, and also tested with CV.

DPV, CV, and spectrophotometric detection methods may use either direct quantification of microbial presence based on sample responses alone, or threshold indicators based upon negative control responses. Ideally, MNP-cell-AuNP nano-biosensing methods would be

developed per microbial target and food matrix, optimizing parameters to obtain linear responses across a range of bacterial contamination. This optimization would be personalized per available instrumentation and required minimal detection levels. For example, *E. coli* O157:H7 and *Listeria monocytogenes* are both zero-tolerance pathogens, requiring detection of even 1 microbe per sample size, or ensuring undetectable levels of pathogen presence of less than 1 microbe in 25 gm samples.

Specifically, these different electrochemical detection methods require different analyses to interpret their instrumental responses in determining target concentration. Calibration is necessary in all applications between the microbial contamination and the particular instrument response to the specific MNP-cell(-AuNP)/matrix samples being tested. In CV, the combined, absolute anodic and cathodic current responses are evaluated; for DPV, the absolute AuNP current response at 0.4 V; and with spectrophotometry, the total step-integrated spectral absorbance (220 nm to 900 nm) is used. Each detection method will also entail its own set of detection limits and range, based not only on the chosen electrochemical method, but also optimizing any chemical mediator or initiator parameters, and mitigating matrix interference through minimizing nanoparticle quantities.

Within new liquid food matrices, rapid detection at threshold levels may be quickly established without extensive development by applying a sample-to-negative ratio detection method. Since negative controls replicate the sample system, but do not contain contamination, a sample response that differs from the negative control indicates microbial presence. Given the pertinent parameters of the microbial-food system, particularly level of microbial tolerance and matrix component effects, the necessary nanoparticle quantities and chemical mediator/initiator can be quickly identified. In this design, fewer parameters would require optimization since only

MNP, and possibly AuNP for DPV detection, would need to be optimized to identify quantities that would allow significant ($p < 0.05$) separation between a contaminated sample and a negative control. Application of this nano-biosensing method could then find broad application across the food supply chain.

Chapter 5. Analysis of Carbohydrate-Functionalized Magnetic Nanoparticles and Dextrin-Coated Gold Nanoparticles Binding Properties to *Salmonella*, *E. coli*, *Bacillus*, and *Listeria* Using Transmission Electron Microscopy

5.1 Introduction

Transmission electron microscopy (TEM) provides a means to assess capture of cells by magnetic nanoparticles (MNP) and labeling by gold nanoparticles (AuNP). As mentioned earlier in chapter 3, the carbohydrate functional groups coating MNP and AuNP surfaces bind to the various surface molecular structures of the cells via ionic attraction, van der Waals forces, dipole-dipole or ion-dipole interactions, or hydrophobic attraction. Although carbohydrate functional groups show less specificity in binding than antibodies, binding between MNP/AuNP and pathogenic cells persists following extraction and labeling. This allow binding patterns between the nanoparticle functional group and targeted microbe to be studied for information regarding quantity and location of nanoparticle attachment. MNP-F#1 are functionalized with larger glycan carbon structures, containing amino and hydroxyl groups, whereas MNP-F#2 have additional amino acid functionalization, increasing the number of carboxyl and amino groups available for binding. Dextrin coating on AuNP (d-AuNP) contains substantial numbers of negatively charged hydroxyl groups, particularly in basic solutions.

Proper steps are necessary in preparing nanoparticle-cell complexes for viewing using TEM. Due to the rigidity of MNP and AuNP structures at the nano-level, common TEM embedding methods used to study tissue structure at the sub-molecular level are not applicable, since nanoparticle presence causes tearing during sectioning. Therefore, negative staining techniques were utilized to image nanoparticle-cell attachment, whereby nanoparticle-cell complexes are deposited to a film-covered copper grid and coated with a heavy uranyl acetate metal stain for contrast in TEM.

Bacteria naturally attach to most surfaces to form biofilms [233]–[237]. Although cells will attach to sample containers, evidence of cell binding to the MNP from TEM images provide initial evidence that bacterial colony growth following MNP extraction are directly related to the true bacterial load within the sample. TEM images of the binding between MNP-F#1, MNP-F#2 and d-AuNP used in this research identified some characteristics specific to the nanoparticles and particular pathogen cell surface. Microbial cells studied were both gram negative, *Salmonella* Enteritidis and *E. coli*, and gram positive, *Bacillus cereus* and *Listeria monocytogenes*. The binding properties of the nanoparticles displayed differences in both cell binding and nanoparticle clumping due to the molecular surface structures and the carbohydrate functional groups.

5.2 Materials and Methods

5.2.1 Materials

Cell strains of *Salmonella* Enteritidis, *E. coli* O157:H7, *E. coli* C3000, *Bacillus cereus*, and *Listeria monocytogenes* were obtained from Evangelyn Alocilja's Nano-Biosensors Lab at Michigan State University (MSU). In-house, proprietary glycan- and amino/glycan-functionalized magnetic nanoparticles (200 nm in diameter, MNP-F#1 and MNP-F#2, respectively) and dextrin-coated gold nanoparticles (approximately 20 nm in diameter, d-AuNP) were used as received from the Nano-Biosensors Lab, MSU, and have been described previously [6], [143]. Phosphate buffer solution, pH 7.4 (Neogen, Lansing, MI), was prepared as directed. Brilliant green agar (BGA), tryptic soy broth (TSB), tryptic soy agar (TSA), Luria Bertani broth (LBB), and Luria Bertani agar (LBA) were purchased from Sigma Aldrich (St. Louis, MO), while CHROMagar™ *E. coli* was purchased from DRG International (Springfield, NJ), and prepared as directed. A Sphero FlexiMag Separator was purchased from Spherotech Inc (Lake Forest, IL). Sodium cacodylate buffer (0.2

M, pH 7.4), paraformaldehyde 16% aqueous solution and glutaraldehyde 25% aqueous solution both in 0.1 M cacodylate buffer, copper grids (200 lines/inch), and FORMVAR 1% solution were purchased from VWR (Radnor, PA).

5.2.2 Microbial Culture

Salmonella Enteritidis, *E. coli* strains, and *Listeria monocytogenes* colonies were rejuvenated from frozen (-70 °C) storage frequently on BGA, CHROMagar™ *E. coli* and LBA, respectively. A transfer loop-full of *Bacillus cereus* was heat-shocked at 75 °C for 15 min in 10 mL LBB in 50 mL flasks, grown with foam stoppers overnight at 37 °C and 100 rpm, then streaked onto LBA. All master plates were incubated at 37 °C overnight and stored at 20 °C for a maximum of 3 months. Microbial cultures were generated fresh for each experiment. A single colony was isolated from the master plate, inoculated into broth and grown overnight at 37 °C. *Salmonella* and *E. coli* were grown in TSB, and *Bacillus* and *Listeria* in LBA, with *Bacillus* heat-shocked at 75 °C for 15 min in 10 mL LBB in 50 mL flasks, grown with foam stoppers overnight at 37 °C and 100 rpm. One milliliter of the liquid culture was transferred to a new tube of appropriate broth (9 mL) and incubated at 37 °C for 4 hr, with shaking for *Bacillus*, before each experiment.

5.2.3 MNP Microbial Capture and Deactivation

Each sample consisted of one type of MNP and one type of bacteria. MNP (5 mg/mL in PBS) were sonicated for 20 min then dispersed with shaking between sampling. Based upon ongoing TEM imaging results, between 100 to 1000 µL of MNP were added to 1000 µL of undiluted microbial culture within a 2 mL flat bottom centrifuge tube. MNP capture was allowed for 10 to 30 min, then MNP-cell complexes were separated with a magnetic separator for 10 min.

The supernatant was removed, and the complexes were resuspended into 500 μL of 2.5% (v/v) glutaraldehyde and paraformaldehyde in 0.1 M cacodylate buffer. Cells were deactivated for 30 min, the complexes re-separated, and suspended into 1000 μL 0.1 M cacodylate. MNP quantity was based upon prior thickness interfering with electron transfer, and deactivated samples may even be subsequently diluted as 10 μL MNP-cell solution into 1000 μL fresh buffer. Additionally, when investigating complex liquid food matrix effects upon capture, only non-pathogenic *E. coli* C3000 bacteria were used, negating the necessity of a deactivation step to eliminate any rinsing effects upon the electrostatic MNP-cell bonds.

5.2.4 Concentrated AuNP Preparation

Concentrated d-AuNP was prepared by removing excess dextrin and solution to improve signaling through increased labeling with minimal dextrin interference. Volumes ranging between 25 to 250 μL of the original d-AuNP suspension were transferred to 2 mL pinched-tip centrifuge tubes, sonicated for 10 min, and centrifuged at 15,000 rpm at 4 °C for 20 min. Following supernatant removal, the remaining 20 μL d-AuNP pellet was sonicated for 15 min to evenly distribute the concentrated d-AuNP evenly, then used as the starting aliquot. Even distribution of the concentrated d-AuNP was assured using spectrophotometric scans (900 - 200 nm wavelength, Shimadzu UV-3101PC, UVProbe software, 1000 μL PBS reference) compared to non-concentrated d-AuNP standards of the same original volume, showing peak values at 520 nm for both and no evidence of nanoparticle aggregation, which was described earlier as dextrin's main purpose during AuNP production. This lack of aggregation therefore also ensures sufficient dextrin coating for subsequent microbial attachment. Tubes were stored at 4 °C and used within 24 hr of

preparation. Concentrated d-AuNP are referred to using their initial volume, e.g. a 75 μL concentrated d-AuNP will be identified as “AuNP75” or simply “AuNP” as appropriate.

5.2.5 AuNP Labeling of MNP-cell Complexes

MNP-cell complexes, following magnetic separation and removal of the supernatant, were resuspended into the appropriate concentrated AuNP. An additional 100 μL of PBS was added to augment mixing and labeling. The complexes were labeled for 30 min, magnetically separated, and the supernatant removed. Labeled complexes were resuspended into 100 to 1000 μL of PBS, depending upon ongoing TEM imaging results. Negative MNP controls consisted of 20 to 100 μL MNP (5 mg/mL in PBS) without cells present, labeled with the same procedure.

5.2.6 TEM Imaging

A 5 μL drop of the MNP-cell or labeled MNP-cell-AuNP complex solution was deposited onto a copper grid coated with FORMVAR film with excess moisture wicked away using filter paper. Complexes were stained with 5 μL micro-filtered 1% uranyl acetate in water, again with excess liquid wicked away using filter paper. Grids were allowed to dry for at least 15 min before imaging. Grids were imaged using a JEOL 100CX TEM instrument (MSU) containing a lanthanum hexaboride, LaB₆, electron gun encased within a vacuum system at magnifications between 5000x to 100,000x. Caution was taken to minimize imaging times of MNP clumps to reduce sample loss due to electron over-excitement.

5.3 Results and Discussion

5.3.1 Binding Forces Between Nanoparticles and Microbes

As described earlier in chapter 3, carbohydrate ligands bind to microbial surfaces using the same electrostatic forces used in antigen-antibody binding, but with less specificity and therefore strength. As libraries of carbohydrates are tested for their selectivity against pathogenic bacteria, those ligands that more tightly bind microbial surface structures will be identified. These carbohydrate ligands will further advance detection methods since their biocompatible properties will allow development of possible individual in-package monitoring throughout the food supply chain.

TEM imaging of the attachment between the carbohydrate coated nanoparticles and microbial cells used in this study provide information into the binding forces present. Current glycan-coated MNP-F#1 and amino/glycan-coated MNP-F#2 that will be shown to expeditiously extract bacteria from simple and complex liquid matrices attached to differing molecular surface structures or locations among the pathogens. Images of dextrin-coated d-AuNP labeled samples, as concentrated AuNP, also lent information, and verified to some extent, unforeseen electrochemical responses achieved by their presence, which is reported later.

MNP clumping appearance is particularly specific to the two types of MNP used. Glycan coating during production of the MNP-F#1 causes a uniform, spherical distribution of the iron oxide (Figs. 5.1A, 5.2B & C, 5.3B, and 5.4B) as it reduces the surface molecules during formation. The presence of an amino acid used in MNP-F#2 production along with the glycan instead causes a more nondescript shape to the nanoparticles (Figs. 5.1C, 5.2D & E, 5.3C & D, and 5.4C). All of these examples are with MNP-cell complexes prepared in PBS for imaging. The nanoparticles also aggregate differently, with MNP-F#1 forming smaller groupings when attached to the gram-

negative microbes, *Salmonella* and *E. coli* (Figs. 5.1A and 5.2B & C), but when binding gram-positive *Bacillus* and *Listeria* microbes they aggregate in larger groupings, with microbes attached around the edges of the grouping (Figs. 5.3B & 5.4B). Meanwhile MNP-F#2 form larger amorphous groupings seemingly covering the bacteria, regardless of the microbial surface structures.

Overall, extended MNP-F#2 exposure to the microbial surfaces caused sufficiently more cell wall lysing than MNP-F#1, particularly for gram-negative cells. Gram-positive cell walls are composed of a single thick layer of peptidoglycan protecting the inner cell membrane, while gram-negative cell walls are composed of an outer membrane that contains higher amounts lipopolysaccharide (LPS) encasing a thinner wall of peptidoglycan. LPS is composed of a hydrophobic lipid A region extending into the O-antigen domain which consists of repeated polysaccharides [238]. Peptidoglycan is composed of sugars and amino acids, with residues of N-acetylglucosamine or N-acetylmuramic acid. Since MNP-F#2 bind all of the microbial surfaces directly, the single layer of LPS for *Salmonella* and *E. coli* is not as resistant to the electrostatic forces that both bind and pull the membrane apart. Most likely the glycan ligand hydrophobically bind the Lipid A regions, while the amino groups then pull at the membrane as they also try to bind the negatively charged surface. Neither microbe, though, showed evidence of lysing after 8 hr exposure to MNP-F#1.

This lysing effect is especially seen with *E. coli*, even though gram-negative cells have a second, albeit thinner, peptidoglycan layer. In fact, *E. coli* cells exposed only to PBS, and likewise bound to MNP-F#1 in PBS, for 8 hr showed substantial cell membrane lysing and cell dissolution (images not shown). *Salmonella* exposed to PBS for 8 hr, though, did not lyse, but did show minimal lysing when exposed to either MNP-F#1 or MNP-F#2 for that length of time.

Similar to how gram-positive microbes resist the forces of acetone or ethanol in removing the peptidoglycan layer, retaining their violet coloring during common staining methods, they also resist the lysing forces of bound MNP-F#2. Therefore, *Bacillus* and *Listeria* are able to retain their cell structure for longer periods of time upon exposure to the MNP. Results did show eventual minimal cell lysing for *Bacillus* and *Listeria* following 8 hr exposure to MNP-F#2 (image not shown), though, when the complexes were suspended in PBS, which does not provide nutrients to repair wall tears. Lysing effects, though, are of minimal concern during any microbial detection as the extraction process is completed within minutes versus the hours needed here.

5.3.2 MNP-*Salmonella* Enteritidis Binding

Salmonella Enteritidis contain significant number of flagella (Fig. 5.1A) that participate in binding to MNP-F#1 (Fig. 5.1B), but MNP-F#2 bind the surfaces of the microbe (Fig. 5.1C). Flagella found on pathogens such as *Salmonella* (Fig. 5.1A) and *Bacillus* (Fig. 5.3A) are locomotive organelles attached to the surface of the microbe that assist in cellular motility. These flagella are composed of monomeric polypeptides and are diphasic, producing two different types of flagella, but never both at the same time. Due to the high variability of their protein composition and micrometers-in-length extension from the surface, they provide high specificity per microbial species as H antigens in immuno-reactivity serotyping [164], [174], [175]. The protein structures along the flagella contain alternating projecting carbonyl electron rich oxygen atoms and amine hydrogens, along with possible aliphatic side chains for binding. The glycan structure in MNP-F#1 seemingly bind in specific locations along the flagella, not coating the entire length. In addition, the flagella do not appear to wrap around the surface of the MNP. Therefore, it may be that regions with high

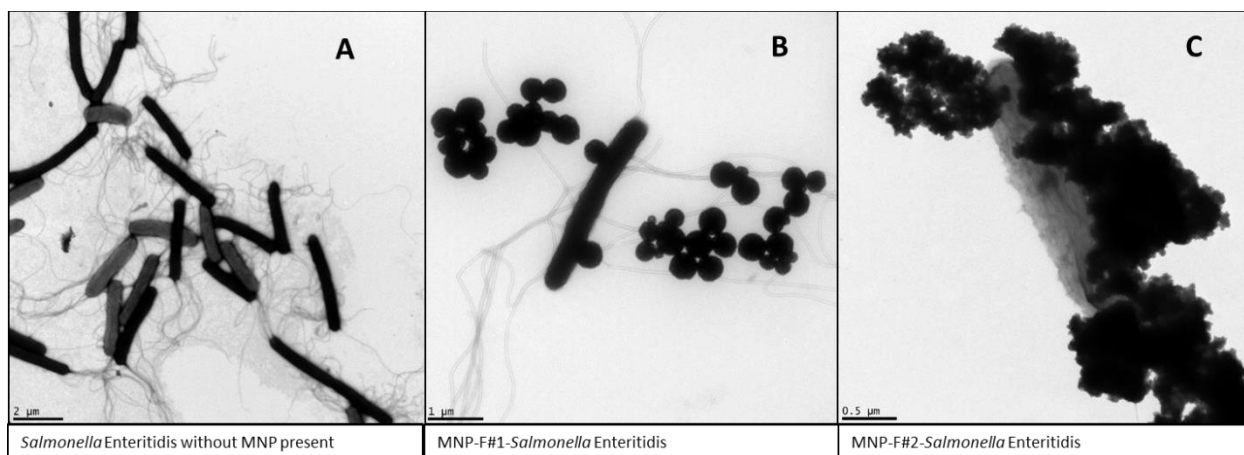


Figure 5.1 Examples of *Salmonella* Enteritidis (A) attachment to MNP-F#1 (B) and MNP-F#2 (C).

content of aliphatic side groups hydrophobically bind to similar carbon chain lengths of the glycan coating.

Although *Salmonella* are peritrichous, with flagella extending from the entire cell surface, no flagella are present when binding to MNP-F#2 (Fig. 5.1C). It is possible that the lysing properties of MNP-F#2 immediately attack the flagella, which are more available for initial binding, lysing flagella faster than seen in cell wall lysing. This lysing may occur during TEM sample preparation during the 30-min deactivation process. Once the flagella have been removed, the MNP-F#2 bind the surface of the cell, with the positive amine groups present in the ligands interacting with the negatively charged cell surface. Aggregation of the MNP against the ionic PBS environment may be the reason that the entire cell surface is not covered, causing an equilibrium between microbial binding and ionic exclusion forces upon the MNP.

5.3.3 MNP-*E. coli* O157:H7 Binding

As stated earlier, exposure of *E. coli* over extended times to PBS or either MNP can have deleterious effects upon the cell membrane causing lysis (Figs. 5.2C & E). These effects do not

occur immediately (Figs. 5.2B & D), which allows for pathogen detection during the timely extraction from liquid matrices. Less aggregation of MNP-F#1 occurs in *E. coli* attachment (Fig. 5.2B) than was present for *Salmonella*, and the nanoparticles bind directly to the cell wall, which was also reported by Lim et al. [130] and MNP-chitosan/glutaraldehyde used by Lin et al. [118]. This probably hastens the eventual lysing effects against the membrane. MNP-F#2 again do not bind the entire surface of the cell (Fig. 5.2C) but aggregate more at the ends than seen for *Salmonella*. Again, there appears to be an equilibrium established between the ionic PBS environment that suspend the complexes and their electrostatic binding of the surface. Additionally, each microbe exudes a varying composition of chemicals which also alter the liquid surrounding the MNP-cell complexes.

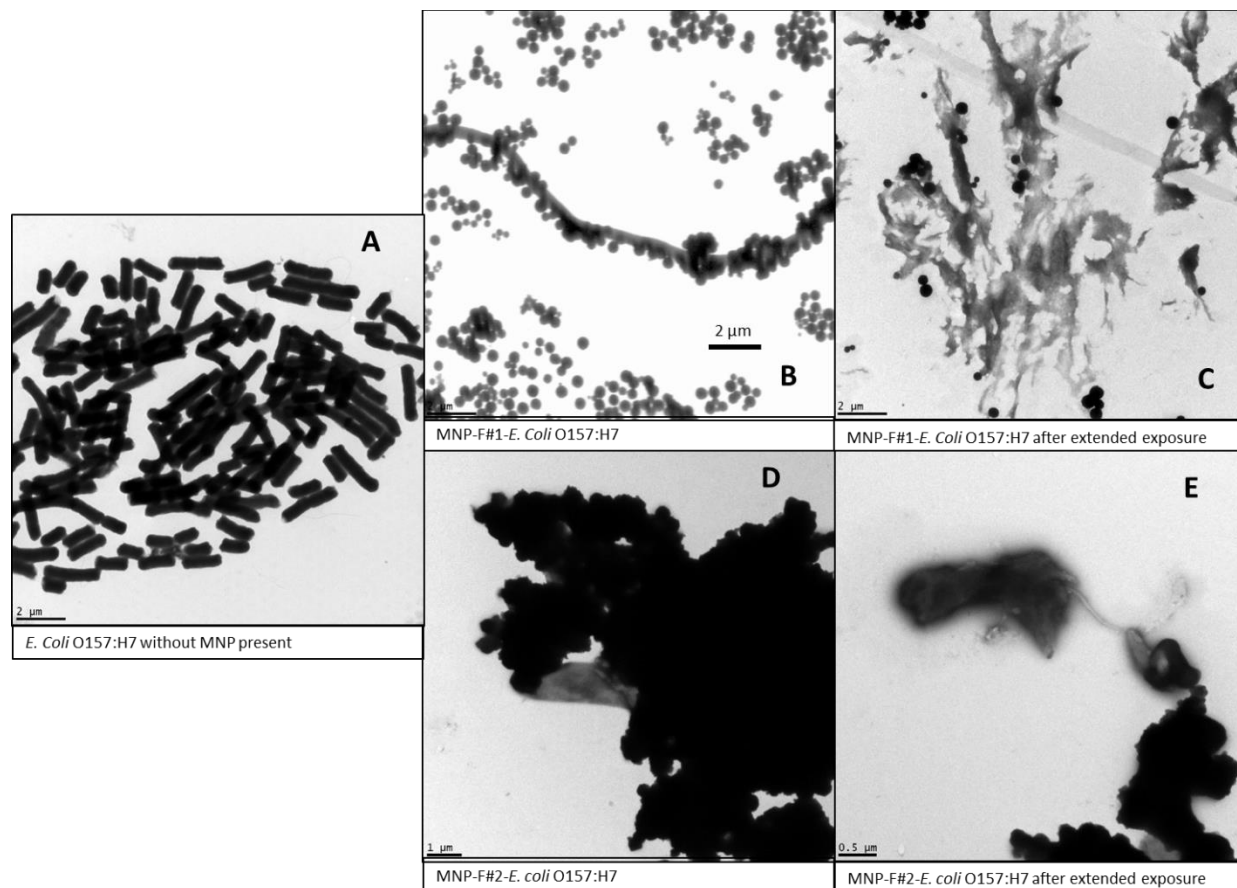


Figure 5.2 Examples of *E. coli* O157:H7 (A) binding to MNP-F#1 (B) including cell lysing over extended exposure (C) and to MNP-F#2 (D) as well as cell lysing that occurs over extended exposure (E).

5.3.4 MNP-*Bacillus cereus* Binding

Bacillus cereus are peritrichous cells (Fig., 5.3A), but flagella are not present when bound to either MNP-F#1 nor MNP-F#2. Whereas MNP-F#1 bound the length of *E. coli*, they bind specific locations along the *Bacillus* cell wall (Fig. 5.3B), again aggregating in smaller groupings similar to that seen to the *Salmonella* flagella when not located next to the larger grouping. Little binding occurs at the cell ends as the pathogen lines the periphery of the aggregated nanoparticles attached along their lengths. MNP-F#2 similarly binds the cell length (Fig. 5.3C), aggregating in

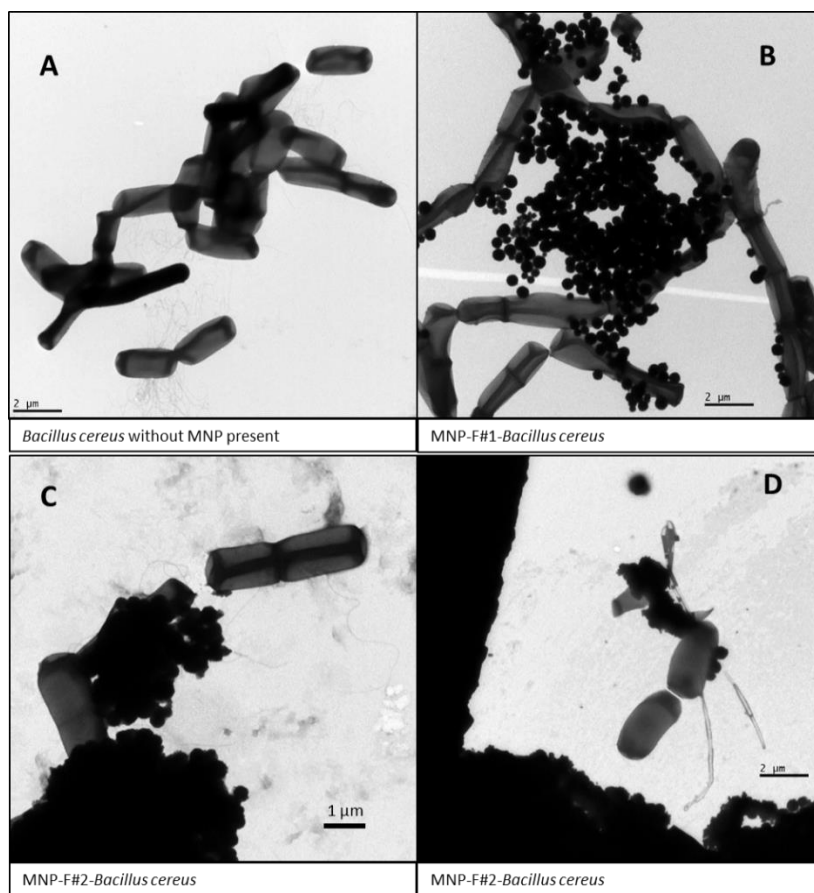


Figure 5.3 Examples of *Bacillus cereus* (A) binding to MNP-F#1 (B) and MNP-F#2 with short exposure (C) and extended exposure to the MNP (D).

larger clumps that also overlay the surface. Some cell lysing is evident when the *Bacillus* cells are exposed to MNP-F#2 for extended periods of time (Fig. 5.3D).

5.3.5 MNP-*Listeria monocytogenes* Binding

Rod-like *Listeria* (Fig. 5.4A) expand in diameter when attached to MNP-F#1 (Fig. 5.4B) and MNP-F#2 (Fig. 5.4C). Their binding to MNP-F#1 are similar to that of *Bacillus*, lining the periphery of the aggregated nanoparticles. MNP-F#2 more clearly show their round appearance comparable to that of MNP-F#1 when bound to the *Listeria* cell surface. Meng et al. studied nanoparticle binding against *Listeria monocytogenes* using MNP-Vancomycin/polyethylene glycol bound in small clumps around the surface of the microbe [119]. The nanoparticles did not aggregate as much, which may be an aspect of the *Listeria* surface molecular structure binding forces pulling the MNP more tightly to the surface as individual particles. Internalins are leucine-rich adhesive proteins that assist pathogenic *Listeria* to insert themselves into epithelial cells and reproduce intracellularly [239], [240], while Ctap is a cysteine binding surface transporter for *Listeria monocytogenes* which is expressed during low cysteine presence [187]. Leucine is rich in methyl groups, creating hydrophobic pockets for targeted binding to the MNP moieties, while MNP-F#2, specifically, will bind Ctap surface epitopes.

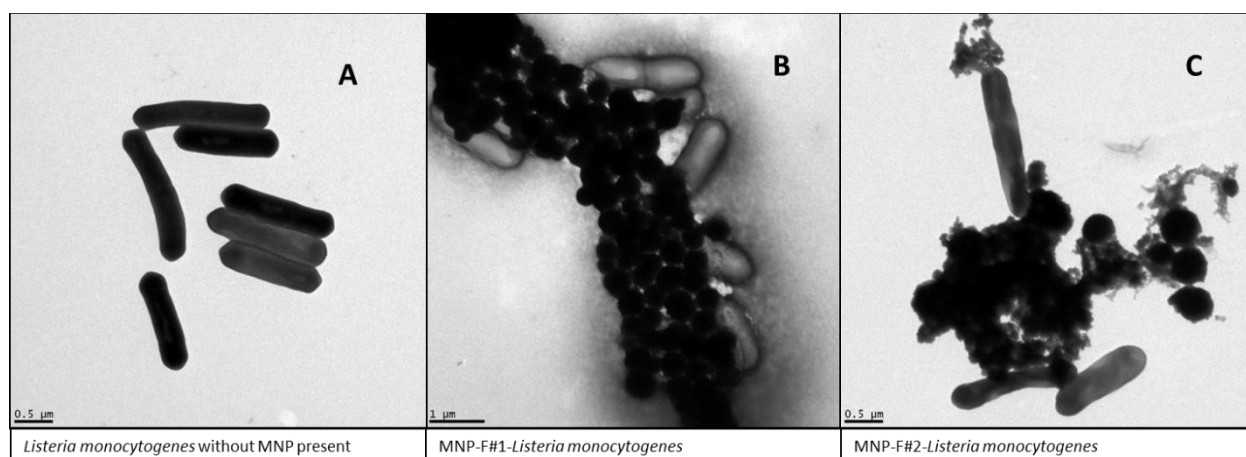


Figure 5.4 Examples of *Listeria monocytogenes* (A) binding to MNP-F#1 (B) and MNP-F#2 (C).

5.3.6 AuNP Binding to MNP-cell Complexes

E. coli C3000 non-pathogenic microbial surrogate cells were used to exemplify binding eliminating the need to deactivate the cells. Due to the non-covalent electrostatic forces between carbohydrate ligands and cell surfaces, a fraction of either MNP-cell and AuNP-cell binding is lost in fresh supernatant. During capture, extraction and labeling, each subsequent suspension of these complexes in fresh liquid matrix results in a new equilibrium established between complexed and separated cells, even during cellular deactivation. This concept will be further elucidated later, but to reduce lost binding during increased rinses, AuNP250 binding properties were studied using *E. coli* C3000 (Figs. 5.5A – D) to eliminate these deactivation steps.

AuNP250 binding to the cellular surface through the dextrin ligand was studied under several conditions. When excess AuNP250 is not rinsed from the *E. coli*-AuNP250 complex (Fig. 5.5A) the AuNP250 nanoparticles can be seen dispersed throughout the remaining dextrin matrix. Magnification of rinsed MNP-F#2-*E. coli*-AuNP250 complexes shows the aggregation of the AuNP into 50 – 100 nm clumps along the cell surface, but seemingly coating the MNP more evenly (Fig. 5.5B). This sample was suspended in nutrient rich TSB to minimize cellular lysis when exposed to MNP-F#2 through cell membrane regeneration. As can be seen in Fig. 5.5C, the AuNP retain their dextrin coating when binding the cell surface structure. These attachments persist even when the cell is allowed to lyse when suspended in PBS (Fig. 5.5D).

Cellular polypeptides contain positively charged amino groups which provide binding sites for the negatively-charged dextrin hydroxyl groups. Pockets of positively charged amino acids within the polypeptide chain will cause AuNP aggregation. MNP-F#2 have a more uniform appearance when bound to the *E. coli* surface within the presence of AuNP (Figs. 5.5A & B) due

to the combined binding properties of dextrin coating individual MNP. Dextrin will saturate the MNP-F#2 surfaces due to the presence of the amino acid ligand. Therefore, binding to the cell

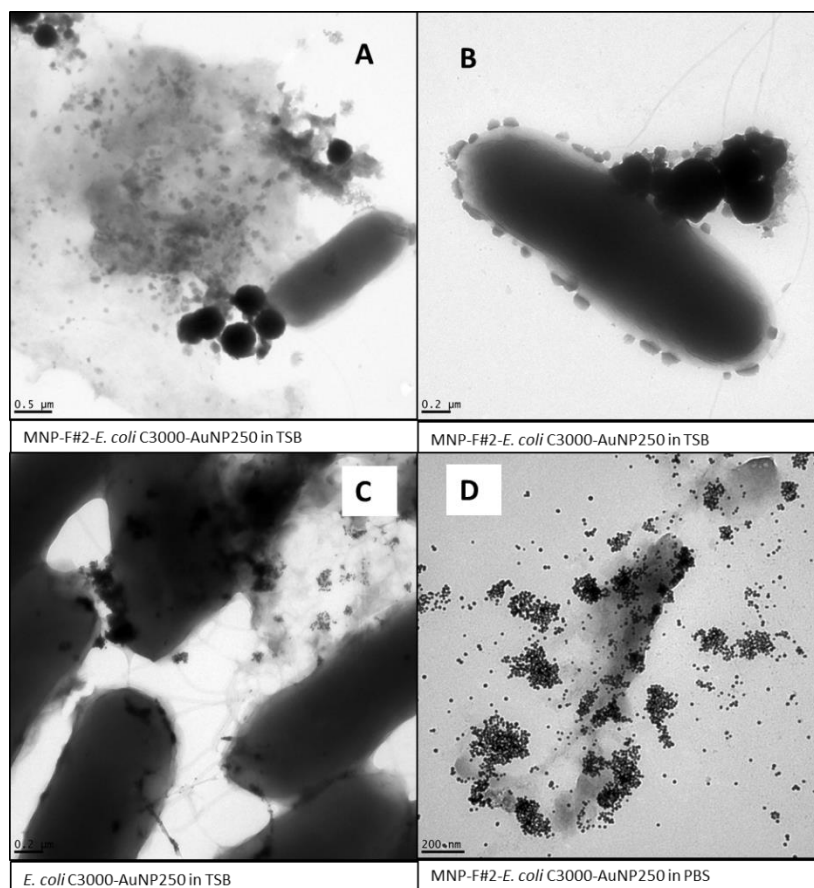


Figure 5.5 Examples of MNP-F#2-*E. coli* C3000 complex labeling with AuNP250 with excess AuNP250 present (A), showing aggregated AuNP binding to the cell wall (B) and at higher magnification (C) all in TSB, and finally persistence of AuNP binding to the cell structure even during lysing caused by extended MNP exposure in PBS.

surface is more selective than to the MNP surface, which will later be shown to cause larger negative control MNP-AuNP electrochemical responses than sample MNP-cell-AuNP responses.

Binding is the transduction event in biosensing that leads to signaling. Electrostatic forces dominate the binding dynamics between targeted microbial cells to the AuNP dextrin-coating, and to the carbohydrate ligand of MNP. Attachment mechanisms are of varying selectivity. The bonds formed during MNP-cell-AuNP nano-biosensing between the cells and the carbohydrate functional groups are non-covalent, electrostatic forces in form, similar to the antigen-antibody

bonds, but of lower strength and specificity. Dextrin's negatively charged hydroxyl groups potentially bind to positively charged amino acid pockets of the cellular surface molecules, leading to seemingly selective attachment of AuNP on *E. coli* cell surfaces (Fig. 5.5B). MNP bind readily to cells and appears to be selective as seen above for each pathogen tested. AuNP also easily bind the MNP functional groups at saturation levels (Figs. 5.6B & C). AuNP saturated binding to the MNP, though, are potentially between the hydroxyl groups of the dextrin to the high number of positively charged amines in the MNP carbohydrates. Binding between MNP and cells, though, impedes d-AuNP binding to both the MNP and cell, reducing AuNP presence in MNP-cell-AuNP

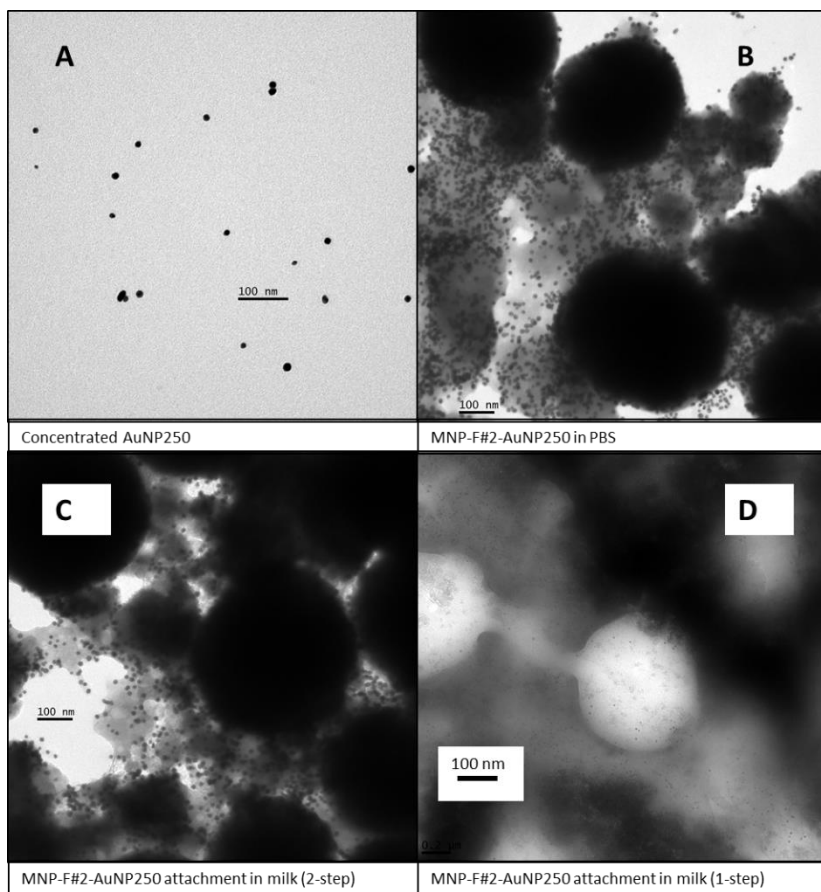


Figure 5.6 Examples of unconcentrated d-AuNP (A), concentrated AuNP250 coating MNP-F#2 in PBS without prior milk exposure (B), with 2-step “capture” in milk then label in PBS (C), and with 1-step “capture and label” directly in the milk matrix (D).

complexes (Figs. 5.5A & B). These binding dynamics will impact signaling interpretation in this biosensing method.

AuNP labeling on MNP-F#2 remains saturating whether carried out in PBS or a complex matrix such as milk. The AuNP used in these experiments were of sizes below 20 nm (Fig. 5.6A) therefore a substantial quantity of the concentrated AuNP may coat MNP-F#2 during labeling (Fig. 5.6B). In experiments when MNP-cell capture is carried out in a milk matrix before AuNP labeling (2-step), versus when MNP cell capture and AuNP labeling is concurrent in milk (1-step), AuNP still saturate the surface of the MNP. In 2-step biosensing, the PBS rinse step following MNP-cell capture removes the attached milk residue from the MNP-F#2 surface, as visualized in Fig. 5.6C compared to the presence of milk residue in Fig. 5.6D. This exposes the MNP surface again to allow saturation amounts of AuNP binding. 1-step biosensing, though, result still in the MNP-F#2 surface being completely covered with AuNP, albeit over the attached milk residue layer. The binding of milk components and AuNP to the samples will be shown later to have created contrasting electrochemical signaling results.

5.4 Conclusions

Along with TEM imaging providing evidence of nanoparticle binding to cellular surfaces, evidence is also found to understand subsequent nano-biosensing results. Of particular interest were the differences in MNP-F#1 and MNP-F#2 binding properties to the different pathogenic bacteria studied, showing selectivity in the surface markers that they attach. This points to different aspects of electrostatic binding between MNP and cell, which are the first steps in distinguishing biocompatible carbohydrate ligands for specific microbial targets. Lysing effects caused by MNP-F#2 attachment to *E. coli*, and to a lesser extent *Salmonella*, over extended times indicate tests

against gram-negative microbial targets will require quick response times of at least less than the 40 min extraction and deactivation time for TEM sample preparation, which are possible through MNP-cell extractions. As important is the verification of saturation binding levels of AuNP to the MNP-F#2 surfaces versus the more selective binding to *E. coli* surfaces, which assisted in explaining later electrochemical responses for MNP-cell-AuNP responses below those of negative controls.

Chapter 6. Rapid Extraction of Pathogenic Bacteria from Liquid Foods using Carbohydrate-Functionalized Magnetic Nanoparticles Including Cyclic Voltammetric Detection

6.1 Introduction

Fluid milk products are consumed at over 100 pounds per year per person in the US [241]. Since raw milk may contain pathogenic bacteria from the pasture, feed or milking equipment [242], [243], USDA regulations require that milk destined for “Grade A” production contain no more than 100,000 CFU/mL [244]. But bacterial contamination may persist through pasteurization or enter through secondary contamination [52], [236], [245]. Whole milk is a complex matrix that is 89% water containing fats, proteins, carbohydrates and enzymes suspended in whey serum [246], [247]. This complex matrix encourages microbial growth, while also interfering with conventional microbial extraction methods and detection sensitivity.

Both raw and pasteurized milk products are consumed in the U.S., even though raw milk was involved in 60% of dairy associated foodborne outbreaks in 2006 [248]. The Food and Drug Administration (FDA) cautions against drinking raw milk and unpasteurized products, due to the severity of diseases that may be contracted from over 90 microbial pathogens that may be present, such as *E. coli*, *Salmonella*, *Streptococcus*, *Staphylococcus*, and *Listeria* [52]. In 2005 – 2006, 80% of children (2 – 11 years) consumed milk [249], but they are especially susceptible to infections. Pasteurized milk products are safer for human consumption, given they are not cross-contaminated post-sterilization, as occurred in numerous foodborne outbreaks between 1976 to 2007 [250]. To protect this valuable commodity and its consumers, farmers and producers alike require rapid, frequent, and reliable testing of milk quality and contamination.

Nanoparticles provide a large surface-to-volume ratio onto which multiple ligand molecules may bind [35], [251]–[254]. Although antibodies are ideal ligands to target pathogenic bacteria, their high cost, short shelf-life and special handling requirements increase detection costs.

Therefore, less expensive, stable antibody-mimics that can selectively attach to bacteria are desired [16], [44]–[46]. Carbohydrate ligands are an economical option, able to attach to bacterial surface markers through stable non-covalent bonds that mimic antibody binding [118], [163], [257]. These inexpensive carbohydrate ligands retain their structural integrity when immobilized onto MNP. Their multivalent moieties can both target pathogenic bacteria and improve suspension within liquids by increasing proximity between MNP and their microbial target.

Magnetic nanoparticles (MNP) functionalized with a variety of bio-recognition ligands have been used to target bacteria from various liquid and gaseous matrices [30]–[33]. MNP from ferrous oxide are superparamagnetic, becoming magnetized in the presence of an external magnetic force, allowing for quick extraction from solution. Admittedly, as mentioned, antibody ligands provide highly selective biosensors, but they require expensive storage with a limited shelf life. In comparison for the same assay performed in our lab, carbohydrate-functionalized MNP cost less than \$0.10 per assay, whereas the cost of the antibody ligands alone used in a similar extraction method [11] increased costs to \$0.40 per assay.

Suspended MNP biosensing methods cover a broad range of ligands, targeted pathogens and detection methods, as extensively reviewed in Tables 3.2 and 3.3 above. Although many studies report on the extractive ability of MNP, most of their work was carried out in simple buffer solutions or following time-consuming pre-sampling steps of over an hour that first removed matrix components [2], [3], [5], [6], [8], [49], [50]. Many of these nano-biosensing applications showed promising results using selective antibodies or oligonucleotides to target *Salmonella*, *E. coli* and *Listeria* [79], [82]–[86], [88], [89], [259] to detect bacterial levels between 10^1 to 10^8 CFU/mL. Initial studies into MNP capture in the complex milk matrix centered around designing a biocompatible MNP-based biosensor to detect microbial pathogens in individual liquid food

packages over the life of the product. This requirement precluded using antibody ligands. Other proposed biosensors have used carbohydrate functional groups on the MNP, such as chitosan/glutaraldehyde [118], which showed a similar range of detection in buffer solutions.

A major advantage of MNP is their ability to separate biological targets from their matrices, even concentrating captured bacteria, using only an external magnet. Concentrated MNP-target, though, can improve optical detection [87]. MNP may even be incorporated into subsequent detection steps, such as interdigitated microfluidic impedance [89] or chemiluminescence [82], [85] without signal interference. Other signaling methods for these biosensing systems included magneto-elastic, HPLC-DAD, optical density and chemiluminescence [84]–[86], [96], [118]. Most of these reported methods required matrix removal pre-detection, instead of identifying matrix effects and incorporating these effects into the signaling. Extensive sample preparation using substantial supplies and time were required to first separate the bacteria from the matrix [12], [20], [55]–[58]. After the bacteria have been removed from the matrix, the final detection step is then rapid.

Functionalized magnetic nanoparticles prepared in the Nano-Biosensors lab with an iron oxide magnetite core functionalized with glycan (MNP-F#1) or amino/glycan (MNP-F#2) carbohydrates were used to extract pathogenic bacteria from complex matrices in suspended and affixed forms. MNP-F#2 were also affixed to plastic strips (MNP-strip) and used to rapidly separate bacteria directly from complex matrices with reduced matrix handling. Capture using either method did not require matrix dilution or complicated pre-separation steps. Electrochemical detection using cyclic voltammetry (CV) was used to expedite detection during MNP-strip biosensing. Suspended MNP extraction provided a rapid means to concentrate bacteria within minutes for improved detection using preferred bacteriological analysis methods (BAM) with agar

growth detection after 18 h incubation. This method is most economical for under/developing locales to determine contamination levels in their liquid food supply. Meanwhile, MNP-strips used in conjunction with a simple handheld potentiostat minimized liquid handling, concentrated targeted bacteria for enhanced signaling, and allowed detection within 30 min. Currently both methods report total cell presence in the liquid food samples. As an initial design, the MNP-strip extraction with CV detection biosensing method provides simple, rapid and affordable microbial detection in complex matrices for higher food security through more testing.

6.2 Materials and Methods

6.2.1 Materials

Cell strains of *Salmonella* Enteritidis, *E. coli* O157:H7, *E. coli* C3000, *Bacillus cereus*, and *Listeria monocytogenes* were obtained from Evangelyn Alocilja's Nano-Biosensors Lab at Michigan State University (MSU). In-house, proprietary glycan- and amino/glycan-functionalized magnetic nanoparticles (200 nm in diameter, MNP-F#1 and MNP-F#2, respectively) and dextrin-coated gold nanoparticles (approximately 50 nm in diameter, d-AuNP) were used as received from the Nano-Biosensors Lab, MSU [6], [143]. Phosphate buffer solution, pH 7.4 (Neogen, Lansing, MI), was prepared as directed. Brilliant Green agar (BGA), tryptic soy broth (TSB), tryptic soy agar (TSA), Luria Bertani broth (LBB), and Luria Bertani agar (LBA) were purchased from Sigma Aldrich (St. Louis, MO), CHROMagar™ *E. coli* was purchased from DRG International (Springfield, NJ), and Oxford Listeria Agar base and Modified Oxford Listeria Supplement for modified Oxford agar (MOX) was purchased from Neogen Corp. (Lansing, MI), and prepared as directed.

Square 1 oz (30 mL) clear glass bottles with phenolic caps were purchased from Thomas Scientific (Swedesboro, NJ). A Sphero FlexiMag Separator was purchased from Spherotech Inc (Lake Forest, IL). Vitamin D, 2% reduced fat, fat free milk, apple cider, and homogenized eggs were purchased from a local commercial seller, while beef juices were procured from the MSU meat store, all stored at 4 °C, and used fresh. Before use, all food containers were sterilized externally using 70% ethanol and the bottles thoroughly mixed by inversion. *Salmonella* Enteritidis, *E. coli* O157:H7 and *E. coli* C3000, *Bacillus cereus*, and *Listeria monocytogenes* were rejuvenated from frozen storage frequently on BGA, CHROMagar™ *E. coli*, LBA following heat shock treatment, and MOX, respectively.

6.2.2 Bacterial Culture

Salmonella Enteritidis, *E. coli* O157:H7 and *E. coli* C3000 were cultured in 10 mL TSB, while *Listeria monocytogenes* was cultured in 10 mL LBB, in 15 mL Eppendorf tubes overnight at 37 °C. *Bacillus cereus* was heat-shocked at 75 °C for 15 min in 10 mL LBB in 50 mL flasks and grown with foam stoppers overnight at 37 °C and 100 rpm. A 10% spike was then grown with the same respective conditions for four hours to log phase immediately preceding all experiments. Tenfold serial dilutions of the stock culture, from 10^{-1} to 10^{-7} , were prepared using PBS before each experiment. Similar tenfold dilutions were made in the appropriate liquid food from 10^{-1} up to 10^{-12} to account for the immediate accelerated bacterial growth during dilutions and used as indicated below for cell capture. Viable cells for both cultures from PBS dilutions and liquid food were enumerated by microbial plating. *Salmonella* was plated on BGA while *E. coli*, *Bacillus*, and *Listeria* were plated on LBA and plates incubated at 37 °C for up to 16 hr. Target plate counts were between 25 and 300 colonies per plate.

6.2.3 Suspended MNP Bacterial Capture in Milk

Each experiment consisted of one type of bacteria and one type of milk. All samples and controls for “large scale capture” (LVC) consisted of 25 gm of food matrix, approximated as 25 mL, used without further dilution. To ensure sample and control volume consistency, all sample and control bottles were first filled with 23 mL of milk, then 750 μL of milk was added to sample and positive control bottles and 1000 μL of milk was added to the negative and positive control bottles. MNP (suspended in the corresponding matrix at 5 mg/mL) were next added to sample and negative control bottles in 1 mL aliquots. Sample and positive bottles were then inoculated with 250 μL of stock culture diluted by 10^{-3} in milk, resulting in a final 10^{-5} dilution for capture.

Bacteria were found to acclimate to the food matrices in under 10 min during the stock culture dilutions, with new microbial growth increasing cell concentrations even three-fold over those in PBS. During the experimental process, separate replicates for each type of MNP were run concurrently, with each replicate spiked from a fresh culture dilution in the appropriate food matrix to minimize differences in the cell concentrations at the time of capture. This increase in concentration was also quantified using agar plate counts from the 10^{-6} dilutions in their respective matrices as:

$$\text{Increased Cell Concentration Factor in Milk} = \frac{\text{CFU agar plate count for stock culture diluted } 10^{-6} \text{ in matrix}}{\text{CFU agar plate count for stock culture diluted } 10^{-6} \text{ in PBS}}$$

“Small volume capture” (SVC) followed the LVC method with either PBS or milk as the matrix with modification. SVC consisted of 50 μL of stock culture diluted 10^{-4} in the appropriate matrix, 250 μL of matrix liquid, and 200 μL of MNP.

Prepared bottles or tubes were mixed for 10 min for LVC or 5 min for SVC and separated on a magnetic rack for 5 min to allow MNP-cell complexes to migrate to the magnetic side of the bottle. Supernatant was removed while the bottles remained on the magnet. All bottles had their contents resuspended in 1 mL of fresh matrix for LVC and 500 μ L for SVC. This in essence concentrated the MNP-cell complexes of samples from 25 mL down to 1 mL. Then 100 μ L was plated onto appropriate agar in duplicate. Resulting positive control colony counts represent those cells that initially affixed to the vessel wall but resuspended in fresh matrix and were reported as “Positive Control Retained Cell Concentration (log CFU/mL)”. All samples and controls were run in triplicate and plate counts were averaged.

For TEM imaging of fungal milk contamination, MNP-cell complexes were inactivated, as described earlier, with a glutaraldehyde-paraformaldehyde solution and resuspended in cacodylate buffer. Then 5 μ L volumes were applied to Formvar[®] coated copper grids and stained with 5 μ L of 1% uranyl acetate immediately before imaging.

6.2.4 Suspended MNP Multiple Bacterial Capture

Using SVC with suspended MNP capture, milk and PBS matrices were inoculated simultaneously with competitive bacteria *Salmonella*, *E. coli* and *Bacillus* to test multiple bacterial capture. These tests were carried out at a final 10^{-6} dilution from culture to provide appropriate final plate counts. Resulting MNP-cell complexes were plated on both BGA and LBA. *Salmonella* were counted from BGA plates, while *E. coli* and *Bacillus* were counted from LBA plates. *Salmonella* appeared as red colonies on BGA, distinguished from yellow *E. coli* colonies, while *Bacillus* did not grow on BGA. All three bacteria on LBA were distinguished by their colony appearance: *E. coli* colonies were larger than *Salmonella*, with a darker outer ring, while the

Bacillus colonies were composed of smaller, conglomerated clear globes. Total target plate counts were 25 to 300 colony forming units. Capture indexes (CI) were calculated both individually per bacterial strain and for total captured bacteria.

6.2.5 Matrix Exposure Effects on Suspended MNP Capture

Cell capture after extended MNP exposure to different fresh milk types was tested. In SVC long-term exposure, MNP was exposed to milk stored at refrigerated (4 °C) conditions for 5 days before inoculation. On day 5, *Salmonella*, *E. coli* or *Bacillus* were separately spiked into the tubes to determine MNP capture ability. In LVC long-term MNP exposure, bottles of milk with MNP were prepared in vitamin D milk, 2% reduced fat milk, and fat free milk (9, 16 and 8 days from expiration, respectively) on day one and refrigerated for 9 days, then spiked with *Salmonella* for capture.

6.2.6 Capture Index Calculation for Suspended MNP Capture

Dilution of the bacterial cultures within the liquid food matrices caused accelerated microbial growth, therefore suspended MNP capture was calculated with respect to stock culture diluted in the corresponding matrix. In addition, as described above the “Increased Cell Concentration Factor in Milk” was calculated by dividing the stock concentration diluted in matrix by that in PBS.

Positive control counts, resulting from inoculated samples without MNP present, represent those cells that originally adhered to the capture vessel but resuspended into the fresh matrix, being therefore unavailable for MNP capture in the sample bottles. Therefore, the resulting positive

control cell concentrations were subtracted from the stock culture concentration to correct for the actual cells available for MNP capture.

Sample and positive control cell concentrations for LVC were determined as:

$$\begin{aligned} \text{captured or positive cells } \left(\frac{CFU}{mL} \right) &= (\text{plate count}) * 10^3 * \frac{1000 \text{ uL}}{250 \text{ uL}} * \frac{1}{100 \text{ uL}} * \frac{1000 \text{ uL}}{1 \text{ mL}} \\ &= \text{plate count} * 10^4 * 4 \end{aligned}$$

where 250 μ L of the 10^{-3} diluted stock culture was inoculated into LVC bottles and concentrated to a final 1000 μ L after magnetic separation and removal of the supernatant, followed by plating 100 μ L of MNP-cell on appropriate agar media.

Capture index (CI) was calculated based on the capture matrix serial dilution cellular concentration, as shown below, and reported with its standard deviation, both as parts per thousand (ppt).

$$\text{capture index (CI)} = \frac{\left(\text{captured cells } \frac{cfu}{mL} \right)}{\left(\text{stock culture } \frac{cfu}{mL} - \text{positive cells } \frac{cfu}{mL} \right)} * 1000 \text{ ppt}$$

6.2.7 MNP-strip Production

Plastic strips (5 x 1 cm) were numbered at the top 1 cm, heated in a vacuum oven at 100 °C and 1.4 in Hg for 1 hr, allowed to cool overnight under vacuum, then weighed. MNP was prepared in sterile water (5 mg/mL) and 250 uL (1.25 mg MNP) was applied to the lower 4 cm length as 5 to 6 evenly-spaced dots. Strips were returned to the pre-heated vacuum oven at 100 °C and 1.4 in Hg for 1 hr, allowed to cool overnight under vacuum, and re-weighed. Resulting MNP weights were calculated and averaged per production batch. Positive control strips were handled in the same manner, except without MNP application.

6.2.8 MNP-strip Bacterial Capture

Each experiment consisted of one type of bacteria and one type of liquid matrix (*Salmonella* in homogenized egg, *Listeria* in apple cider, *E. coli* in milk, or *E. coli* in beef juices). MNP-strip capture followed the method of LVC described above replacing suspended MNP. Samples, negative controls and positive controls consisted of 25 mL of matrix used without further dilution. Bottles were filled with 24 mL of the liquid matrix, then 750 uL of matrix was added to sample and positive control bottles and 1000 uL of the matrix added to the negative control bottles. Sample and positive control bottles were inoculated with 250 uL of log-phase 10^{-2} serially diluted bacterial culture in matrix for a final 10^{-4} dilution. Prepared MNP-strips were inserted into each bottle; positive control strips contained no MNP. Capture in beef juices was carried out in 10 mL volumes, due to limited resources, using the same final 10^{-4} final dilution for *E. coli*.

Bottles were then mixed by inversion several times and incubated for 10 min to allow the MNP-strips to capture bacteria. Then the MNP-strips were removed, rinsed on both sides with 1 mL of PBS over prepared agar plates, and placed individually MNP-side up in a sterile petri dish for cyclic voltammetry (CV) testing. Remaining bacteria within the supernatant were determined by plating 100 uL on appropriate agar. Agar plates were incubated overnight at 37 °C. Target plate counts were between 25 and 300 CFU. All samples and controls were run in triplicate.

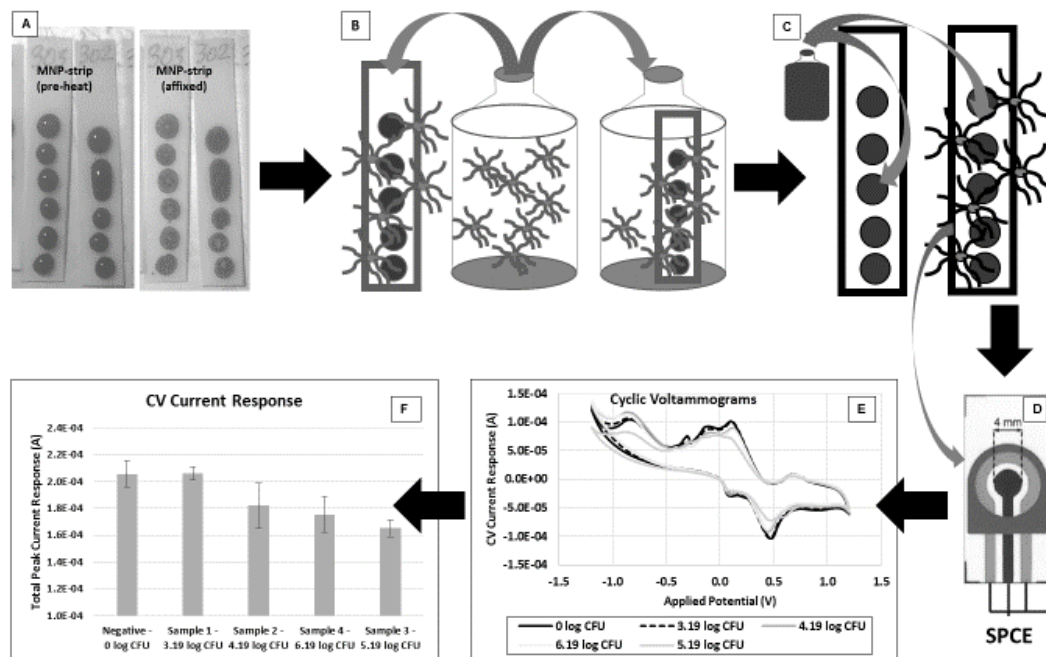
Capture of *Salmonella* in PBS at varying concentrations was carried out using the same method. To verify cell capture, MNP-strips were inserted into 10 mL TSB, incubated at 37 °C for 4 hr, serially diluted twice, and 100 uL plated on TSA, incubated at 37 °C overnight, and counted. Target plate counts were between 25 and 300 CFU. All samples and controls were run in triplicate.

As described above, microbial cells showed new growth in the liquid food matrices and increased concentration above that of their resting concentration in PBS, particularly in

homogenized egg. At the 10^{-4} dilution for capture of *Salmonella* in PBS, *E. coli* in beef juices, *Salmonella* in homogenized egg, *Listeria* in apple cider, and *E. coli* in milk, cell concentrations of available cells were 5.19, 7.72, 12.30, 7.94 and 7.04 log CFU/mL, respectively.

6.2.9 Cyclic Voltammetry Detection of Cell Presence on MNP-strips

Cyclic voltammetry (CV) testing was carried out using a handheld potentiostat (model PG581 Uniscan Instruments, Bio-Logic Scientific Instruments, Seyssinet-Pariset, France), driven by UiE Chem Software. For each test, a disposable screen-printed carbon electrode (SPCE, Gwent Electronic Materials Ltd, United Kingdom) with a surface area of 1 cm^2 , was loaded into the port of the potentiostat. Ferricyanide ($150 \text{ }\mu\text{L}$), a chemical mediator, was applied to the MNP spots on the MNP-strips, reacted for 5 min, then $75 \text{ }\mu\text{L}$ was carefully collected using a pipette and applied to the SPCE. The residual ferricyanide ion concentration in the collected liquid following the reaction was indirectly related to the reactive components on the MNP-strip and was then quantified. CV was run between $+1.2 \text{ V}$ to -1.2 V , applied across the electrode, at a scan rate of 100 mV/s with 30 mV increments for 300 ms step time. A CV voltammogram was recorded for each sample. All sampling was done at room temperature. Total CV voltammogram was calculated by adding the absolute values of the anodic and cathodic peak currents. Averaged sample peak currents were normalized against averaged negative controls as S/N for biosensing results. Sample and negative control peak currents were normalized against the chemical mediator reference peak currents “normalized peak current responses” (NPCR) for matrix effects analysis and reported with corresponding standard deviation. This process is exemplified in Schematic 6.1. All samples and controls were run in triplicate.



Schematic 6.1. Rapid detection of bacterial contamination in contaminated liquids using MNP-strips and CV detection. MNP-F#2 affixed to plastic strips (MNP-strip) (A) for user-friendly capture in only 10 min (B) by either dipping the strip into microbial contamination within undiluted liquids or applying 250 μ L liquid onto the strip (C), then rapid detection by electrochemical testing of reacted chemical mediator on a screen-printed carbon electrode (SPCE) (D) using cyclic voltammetry (E). Results between samples and negative controls are shown in (F).

6.2.10 Statistical Analysis

All suspended MNP capture experiments were run in triplicate, and the average CI was reported with corresponding standard deviation. Two-way ANOVA for LVC was run for milk and bacteria type with replications per MNP type, as well as for either milk or bacteria type against MNP type, and significant differences in the average CI were determined using the q-test, both with significance $p < 0.05$. Unpaired t-tests were run comparing MNP type for LVC and for *Salmonella* capture in fresh versus long-term MNP exposure milks for all MNP and milk types, all with significance of $p < 0.05$.

All MNP-strip experiments were run in triplicate, with NPCR reported with corresponding standard deviations. Two-way ANOVA for matrix type (PBS, beef juices, homogenized egg, apple cider, and milk) and treatment type (sample and negative control NPCR) with three replicates was

run along with linear regressions to analyze matrix component effect upon negative control NPCR. Finally, unpaired t-tests were used to compare sample to negative control NPCR in all matrix types. All tests were run with significance of $p < 0.05$.

6.3 Results and Discussion

6.3.1 Aspects of Bacterial Capture.

MNP capture here is defined as a stable bond between the MNP carbohydrate ligand and the cell membrane, as an MNP-cell complex, allowing rapid extraction of the pathogenic bacteria from liquid food using a simple magnet, in place of time-consuming centrifugation. Carbohydrate-functionalized MNP used in these experiments have hydroxyl, amino, and hydrophobic regions that interact with the bacterial membranes and their surface epitopes forming non-covalent electrostatic bonds similar to those found in antibody bonding [159]. Bacteria have varied transmembrane and surface molecular structures composed of lipids, sugars and proteins that determine their binding dynamics to ligand functional groups such as the F#1 and F#2 carbohydrates [177], [185], [260]–[262]. For example, flagella are composed of polypeptides and extend micrometers from the cell surface, making them highly available for MNP binding [164], [174]. Microbial surface expression varies with respect to their surrounding environment, therefore MNP capture must be evaluated in matrices more representative of the food supply chain, such as milk, when cells are growing versus in buffer solutions, when cells enter a resting state. The positively charged amino groups and negatively charged hydroxyl groups present in the MNP functional groups also aid in MNP suspension within aqueous-based simple and complex matrices such as PBS or milk, improving proximity for MNP and cell binding opportunities.

In the previous section, TEM images showed MNP-cell complexes that were analyzed for their binding properties. For example, *Salmonella* bind MNP-F#1 (Fig. 5.1A) primarily through their flagella in selective areas, with some MNP also adhering to the cell wall, while MNP-F#2 bind along the cell wall (Fig. 5.1B). Also shown were MNP-F#1 clearly binding both *E. coli* (Fig.5.2B) and *Bacillus* (Fig. 5.3B) cell membranes, while MNP-F#2 aggregate along their walls (Figs. 5.2D and 5.3C, respectively).

As will be shown below, user-friendly MNP used in this study rapidly extracted pathogenic bacteria from undiluted milk, beef juices and apple cider. This was in part due to their superparamagnetic property. Superparamagnetic particles show random electron spins in the absence of an external magnet, allowing them to disperse easily within liquids. As shown in earlier (Fig. 3.2A), both MNP types display strong magnetization in the presence of an external magnet, comparable to a similarly carbohydrate-functionalized MNP [99], but when this external magnetic force is removed, or zero, MNP lose magnetization. Therefore, MNPs are easily suspended in most liquid foods and likewise rapidly separated. Other methods to rapidly detect pathogenic bacteria have proposed various bioreceptors and support materials, including antibodies [10], [16], [63]–[68], but most proposed methods are only “rapid” in their final steps. These methods require time-consuming separation of the target bacteria from the food matrix to minimize signal interference, or culturing to first increase target quantity.

6.3.2 Definition of a Complex Matrix

As mentioned earlier in the literature review, numerous biosensors work well against various species of pathogenic bacteria in simple buffer and water suspensions or following extensive cell-matrix separation steps. In this work, the freely suspended MNP and MNP-strips

were able to directly extract bacteria from liquid matrices that contained high amounts of carbohydrates in the form of fats, sugars and/or proteins. In addition, as will be shown later, this biosensing method was able to distinguish between samples and negative controls ($p < 0.05$), even though there was evidence of matrix binding to the MNP see in Fig. 5.6D.

Most food-based liquids are rich in carbohydrates, as well as minerals. Even though milk, apple cider and homogenized egg are all over 80% water-based, they contain substantial amounts of carbohydrates and other nutrients (Table 6.1). In a single serving (240 mL), milk has 28 gm of sugars, lipids and proteins in a whey serum, while, apple cider has 30 gm of sugars. In the same volume, homogenized eggs contain over 32 g of carbohydrates, most as protein.

These matrices, therefore, are here defined as complex liquids since their carbohydrates will be electrostatically attracted and attach to the MNP carbohydrate ligand. The binding between the matrix and ligand carbohydrates are through electrostatic forces due to their similar chemistries. In contrast, PBS does not contain carbohydrates, and beef juices have minimal myoglobin proteins released from the muscle. These differences in the complexity of the matrix will be shown to have different results on nano-biosensing using MNP.

6.3.3 Suspended MNP Capture in Milk Matrices

Both MNP-F#1 and MNP-F#2 were able to extract bacteria directly from undiluted milk, which is a thick, nutritionally rich and chemically complex matrix. Capture indexes (CI) and increased cell concentration factors for large volume capture (LVC) in milk are listed in Table 6.2 for MNP-F#1 and Table 6.3 for MNP-F#2. *Salmonella*, and *E. coli* capture in all milks was between 2 ppt to 20 ppt CI. Meanwhile, *Bacillus* showed significantly higher capture of 40 ppt to 120 ppt across all milk types ($p < 0.05$) regardless of MNP type, except in fat free milk with MNP-

F#2. These CI for capture in complex milk matrices were for samples spiked with 3 to 5 log CFU/mL bacteria and compared well with capture of *Salmonella* in PBS, a simple matrix, at 20 ppt (20 ppt \pm 6 ppt at 3.78 log CFU/mL, n=3). Capture for *Bacillus*, a Gram-positive microbe, may be higher than *Salmonella* and *E. coli*, both Gram-negative microbes, due to the higher

Table 6.1 Composition and properties of liquid matrices.

Composition	Milk	Beef Juice	Apple Cider	Homogenized Egg	PBS
Serving Size	1 cup (240 mL)		8 oz (240 mL)	8 oz (240 mL) [#]	
Calories (Kcal)	150		120	133	
Fat (gm)	8*		0	0	
Cholesterol (gm)	25		0	0	
Sodium (gm)	105		135	480	
Potassium (gm)	0		60	373	
Carbohydrate (gm)	12 (sugars)		30 (sugars)	5	
Protein (gm)	8	+	0	26	
Water (%)	~80	~75	~80	~80	100
pH (25 °C)	6.54	5.27	3.21	8.58	7.44
Conductivity (mS/cm)	4.92	11.84	19.2	8.83	14.2

* 8 gm for Vitamin D, 5 gm for 2% reduced fat and 0 gm for fat free milks

+ minimal amount of myoglobin proteins released from muscle tissue

based upon reported 3 tablespoon (tblsp) (46 gm) serving size; 3 tblsp = 1.5 oz

concentration of lipopolysaccharide in its cell wall which may bind the common glycan ligand present on each MNP. The highest accelerated bacterial growth rates in milk were 2.26 for *Salmonella* in 2% reduced fat milk; 2.86 for *E. coli* in both 2% reduced fat milk and fat free milk; and 1.38 for *Bacillus* in fat free milk.

Naturally bacteria attach to most surfaces to form biofilms [233]–[237]. But even though cells will attach to sample containers, evidence of cell binding to the MNP were shown in the

previous section, ensuring that the colony growth following MNP extraction was directly related to the true bacterial load within the sample.

Statistically, no relation was found between MNP type and either milk or bacteria type for capture, except *Bacillus* as mentioned above, nor any significant difference in capture between MNP type for all milk and bacteria types ($\alpha = 0.05$). Within a particular MNP, though, there were significant differences in capture between milk and bacteria types and these differences are noted in Tables 6.2 and 6.3. Specifically, for MNP-F#1 there are true differences in the higher capture of *Bacillus* in vitamin D and fat free milks. Extraction using MNP-F#2 also showed a true difference existed in capture of *Bacillus* in 2% fat free milk. All of these combinations have CI greater than 75 ppt and show that biocompatible carbohydrate ligands may be identified to increase targeted pathogen detection, particularly Gram-positive *Bacillus* using the amino/glycan-functional groups for capture in milk.

Conventional bacteriological methods are time-consuming [54], [268], whereas MNP extraction efficiently replaces cumbersome dilution and centrifugation steps in liquid food sampling, while rapidly concentrating bacteria from large volumes, improving test sensitivity. Bacterial elution from MNP was even unnecessary since its presence does not affect cell growth on agar plates following capture; and MNP was even safely included in polymerase chain reaction (PCR) without altering DNA amplification [70]. As mentioned in the methods section, *Salmonella* colonies were enumerated on BGA (Fig. 6.1A), while *E. coli* colonies (Fig. 6.1B) and *Bacillus* colonies (Fig. 6.1C) were enumerated on LBA. Capture was carried out at a five-fold serial dilution of the stock culture, resulting in 3 to 4 log CFU/mL final concentrations in fresh milk reported in

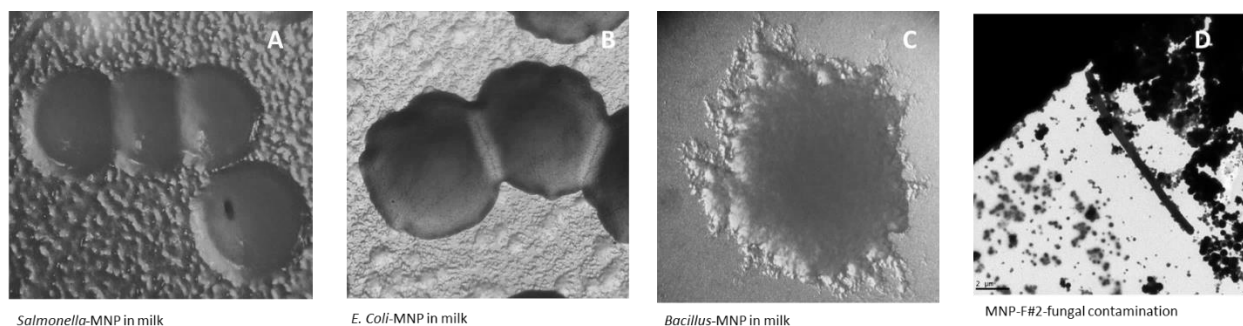


Figure 6.1 Photos of extracted bacterial growth on solid agar for *Salmonella* on BGA (A), *E. coli* on LBA (B), *Bacillus* on LBA (C), and TEM images of milk contamination bound to MNP (D).

Tables 6.2 and 6.3, which is in the range of maximum contamination acceptable for raw milk (100,000 CFU/mL) and allowed for pasteurized milk (20,000 CFU/mL) [244]. After capture, MNP-cell complexes were concentrated to a final 1 mL volume. Bacterial concentration also reduces sample handling since microbial pre-enrichment is not necessary.

Occasionally fungal colonies would appear on incubated media plates following milk sampling (Fig. 6.1D). Numerous spoilage and pathogenic bacteria have been reported in raw and pasteurized milk and milk products [52], [269], [270]. The fungal colonies consisted of aggregated clear globes but did not appear in every experiment. These colonies were cultured in TSB and imaged with TEM, showing rod-like cells of 10 to 20 μm in length (Fig. 6.1D). No appreciable effect was seen on the capture indexes (CI) for the target pathogens when this milk contamination was present. Additionally, data for any milk product that tested positive for the presence of other pre-existing non-fungal contamination was rejected and the experiment repeated.

6.3.4 Suspended MNP Capture of Multiple Bacteria

Products contaminated with multiple types of competitive bacterial species occur infrequently in the food industry but results here show that each different species present could

Table 6.2 Capture index (CI) of *Salmonella*, *E. coli* and *Bacillus* using suspended MNP-F#1 for large-volume capture (LVC) within three types of undiluted milk (25 mL) and each species' increased cell concentration factor in each milk type following the standard five-fold serial dilution.+ (n=3)

Milk	Bacteria	Concentration at Capture (log CFU/mL)	Capture Index Average (ppt)	Standard Deviation (ppt)	Positive Control Retained Cell Concentration (log CFU/mL)	Increased Cell Concentration Factor in Milk
Vitamin D	<i>Bacillus cereus</i> ^m	2.93	118.81 ^b	6.75	-0.18	1.03
	<i>E. coli</i> O157:H7	4.46	5.92 ^a	2.03	1.98	2.09
	<i>Salmonella</i> Enteritidis	4.33	7.50 ^a	1.13	2.07	3.42
2% Reduced Fat	<i>Bacillus cereus</i>	3.96	111.66 ^b	20.54	1.84	0.94
	<i>E. coli</i> O157:H7	3.61	8.63 ^a	4.71	1.47	3.86
	<i>Salmonella</i> Enteritidis	4.17	16.66 ^a	1.18	2.59	2.26
Fat Free	<i>Bacillus cereus</i>	3.84	21.36 ^a	6.44	1.33	1.38
	<i>E. coli</i> O157:H7	4.40	4.19 ^a	0.76	1.88	3.87
	<i>Salmonella</i> Enteritidis	4.28	6.63 ^a	0.26	2.26	1.31

* Means followed by the same letter are not significantly different from each other ($\alpha = 0.05$)

+ Negative control colony counts per experiment: $m = 1$ CFU and 1 CFU on separate plates.

still be simultaneously extracted with high reliability using MNP. Little loss in capture capacity was experienced for simultaneous capture of *Salmonella*, *E. coli* and *Bacillus* using MNP-F#1. Simultaneous capture in small volume capture (SVC, Table 6.4) showed high CI in PBS (268 ppt) and vitamin D milk (67 ppt) with each species at equal concentrations, and total bacterial concentrations of over 3 log CFU/mL. The CI for each of the species in the combined mixture compared well with their individual SVC for the corresponding matrix (Table 6.4).

MNP have a high surface area to volume ratio resulting in a high quantity of available ligand for capture. As described earlier, an equilibrium is established for each type of bacteria between the supernatant and those attached to MNP. Therefore, the ligands are not saturated with

cell attachment for a particular microbe, causing a maximum amount of capture per cellular concentration. Combined with the varied MNP-cell binding between different microbial species

Table 6.3 Capture indexes (CI) of *Salmonella*, *E. coli* and *Bacillus* using suspended MNP-F#2 for large-volume capture (LVC) within three types of undiluted milk (25 mL) and each species' increased cell concentration factor in each milk type following the standard five-fold serial dilution.⁺ (n=3)

Milk	Bacteria	Concentration at Capture (log CFU/mL)	Capture Index Average (ppt)	Standard Deviation (ppt)	Positive Control Retained Cell Concentration (log CFU/mL)	Increased Cell Concentration Factor in Milk
Vitamin D	<i>Bacillus cereus</i> ^m	2.93	39.30 ^a	19.00	-0.18	1.03
	<i>E. coli</i> O157:H7	4.46	4.48 ^a	2.33	1.92	2.09
	<i>Salmonella</i> Enteritidis	4.25	6.41 ^a	1.47	1.93	3.42
2% Reduced Fat	<i>Bacillus cereus</i>	3.96	76.63 ^b	40.47	1.82	0.94
	<i>E. coli</i> O157:H7	3.61	6.71 ^a	0.86	1.58	3.86
	<i>Salmonella</i> Enteritidis	4.09	16.63 ^a	1.42	2.49	2.26
Fat Free	<i>Bacillus cereus</i>	3.84	5.36 ^a	1.37	1.42	1.38
	<i>E. coli</i> O157:H7	4.40	3.42 ^a	0.14	1.84	3.87
	<i>Salmonella</i> Enteritidis	4.28	5.90 ^a	0.35	2.25	1.31

* Means followed by the same letter are not significantly different from each other ($\alpha = 0.05$)

+ Negative control colony counts per experiment: $m = 4$ CFU.

discussed earlier, MNP can therefore simultaneously extract various bacterial species. As more selective carbohydrate groups are identified in future work, these pathogens can then be reliably separated at lower costs than antibodies [75], [163].

Comparing values for CI in SVC were higher than corresponding LVC by an order of magnitude for individual capture in vitamin D milk using MNP-F#1, except for *Bacillus*. Similarly, capture of *Salmonella* in PBS in using MNP-F#1 in LVC was 20.13 ppt (20.13 ppt +/- 6.16 ppt), again an order of magnitude lower than CI, 132 ppt, for SVC (Table 6.4). Capture in LVC was in

25 mL total volume, as opposed to 500 μ L for SVC which will affect the opportunity for interaction between the microbes and MNP. With 1 mL of MNP used in 25 mL LVC, or 4% of the volume, this is an order of magnitude less than 200 μ L of MNP used in 500 μ L SVC, or 40% of the volume.

Table 6.4 Microbial capture indexes using suspended MNP-F#1 for rapid extraction of three competitive bacteria, *Salmonella*, *E. coli* and *Bacillus*, either simultaneously (at 10^{-6} dilutions of the stock culture) or separately (at 10^{-5} dilutions) from PBS and vitamin D milk in small-volume capture (SVC)*. (n=3)

Matrix	Bacteria	Concentration at Capture (log CFU/mL)	Capture Index Average (ppt)	Standard Deviation (ppt)	Positive Control Retained Cell Concentration (log CFU/mL)
PBS	Total Combined Bacteria	3.17	268	284	1.60
	<i>Salmonella</i> Enteritidis fraction	2.71	163	156	1.22
	<i>E. coli</i> O157:H7 fraction	2.91	342	416	0.52
	<i>Bacillus cereus</i> fraction	2.19	143	-	1.30
Milk ^a	Total Combined Bacteria	3.72	67	12	2.59
	<i>Salmonella</i> Enteritidis fraction	3.20	59	8	2.14
	<i>E. coli</i> O157:H7 fraction	3.50	70	23	2.34
	<i>Bacillus cereus</i> fraction	2.73	113	97	1.52
PBS	<i>Salmonella</i> Enteritidis alone	3.99	132	59	2.64
	<i>E. coli</i> O157:H7 alone ^b	3.58	51	18	2.12
	<i>Bacillus cereus</i> alone	3.75	624	444	3.06
Milk	<i>Salmonella</i> Enteritidis alone	3.89	80	36	2.68
	<i>E. coli</i> O157:H7 alone ^c	4.22	47	8	2.82
	<i>Bacillus cereus</i> alone ^d	3.73	85	60	0.00

* Negative control colony counts: *a* 3 CFU *E. coli*, 1 CFU *Bacillus*, and 1 CFU fungi; *b* 1 CFU; *c* 3 CFU and 2 CFU on separate plates with 2 CFU, 1 CFU and 1 CFU fungi on separate plates; *d* 1 CFU and 6 CFU fungi on separate plates.

6.3.5 Milk Matrix Exposure Effects on Suspended MNP Capture.

Initially the goal of this project was the design of a nano-biosensor that may be inserted into individual food packaging to monitor pathogenic bacteria presence. Therefore, the effect that extended exposure of the complex matrix would have on the MNP was necessary to quantify. Binding between the MNP and targeted cells is the transduction element for this nano-biosensing method. Therefore, any noticeable reduction in attachment would likewise reduce detection responses.

Capture indexes following nine-day long-term exposure of MNP to each milk type in LVC for *Salmonella* are shown in Table 6.5. Compared to *Salmonella* capture in fresh milk (Tables 6.2 and 6.3), CI were reduced to 1 ppt to 3 ppt, except for MNP-F#2 capture in fat free milk at 6 ppt. All reductions in CI were significant ($p < 0.05$), except for MNP-F#2 in fat free milk. Overall, vitamin D milk exposure caused an approximate 5 ppt loss in CI, 2% reduced fat milk caused up to a 15 ppt loss in capture, and fat free milk caused a 3 ppt decrease in MNP-F#1 capture. Whereas, in SVC, long-term exposure of MNP-F#1 suspended in vitamin D milk for five days actually showed an increase in *Salmonella* CI (100 ppt +/- 22 ppt), while *E. coli* and *Bacillus* capture did decrease (37 ppt +/- 8 ppt and 38 ppt +/- 16 ppt, respectively) from individual capture values reported in Table 6.4, all at comparable cell concentrations of approximately 4 log CFU/mL.

Following long-term MNP exposure for LVC, a flocculated sludge residue on the MNP-F#1 was formed in vitamin D milk and fat free milk, and fat free milk samples did not magnetically separate as easily as in fresh milk. Re-suspension of the MNP-cell complexes into fat free milk was also difficult. Milk is a complex mixture of lipids and fat globules suspended in whey, along with phagocytes and casein micelles. The phagocytes and caseins act enzymatically against the lipids and fats, causing lipolytic hydrolysis of triacylglycerides and casein proteolysis over time.

This degradation of the milk components most likely contributed heavily to altered properties of the milk.

Salmonella dilutions carried out in nine-day old milk for LVC, showed accelerated cell growth by factors of 17 to 22, depending upon the milk (Table 6.5). These were an order of magnitude increase over those reported for fresh milk in Tables 6.2 & 6.3, resulting in 1 to 2 log CFU/mL higher cell concentrations for MNP capture after long-term milk exposure. This increased accelerated growth over that in fresh milk is most likely due to the substantial amount of degraded fat and lipid products available for bacterial growth. These degraded products would require less microbial metabolic exertion.

At over 1 ppt, MNP displayed reliable capture capacity in various milk matrices, in both SVC and LVC, for individual or combined bacterial loads between 2 to 5 log CFU/mL, and even after MNP experienced extended milk exposure. Other researchers doing studies in milk reported accelerated bacterial growth [271], [272], and MNP used in this study still captured at these higher concentrations. All milk types provided rich, nutritional environments for microbial growth. In an 8 oz serving, all three milk types had the same fraction of whey product and all contained 8 gm protein, but their fat content varied with 8 gm fat in vitamin D milk, 5 gm fat in 2% reduced fat milk, and 0 gm fat in fat free milk.

Even though MNP functionalized with carbohydrate ligands suspend easier within milk matrices due to the similar chemical composition, it was shown that the milk fats and proteins will not interfere with cellular binding. CI in milk was not adversely affected, even following extended MNP exposure to refrigerated milk over days. Since MNP capture is unaffected by matrix exposure, this makes possible the development of a biosensor-patch using biocompatible

carbohydrate-functionalized MNP, that may be affixed within liquid food containers to signal contamination when integrated with an external magnetometer sensor.

Table 6.5 Capture indexes for Salmonella in large-volume capture following long-term suspended MNP-exposure+. (n=3)

Milk Type	MNP Type	Concentration at Capture (log CFU/mL)	Capture Index Average (ppt)	Standard Deviation (ppt)	Positive Control Retained Cell Concentration (log CFU/mL)	Increased Cell Concentration Factor in Milk
Vitamin D	F#1	5.29	1.37	0.08	2.16	22
	F#2	5.29	1.01	0.18	2.08	
2% Reduced Fat	F#1	5.23	1.20	0.14	2.52	19
	F#2	5.23	2.16	0.39	2.76	
Fat Free	F#1	5.17	2.73	1.03	2.20	17
	F#2	5.17	6.00	1.46	2.54	

+ Negative control colony counts were zero for all replicates.

6.3.6 Maximum Capture Index due to Equilibrium

By instinct, MNP should extract the same number of cells from liquids no matter the concentrations of cells present given otherwise the same sampling conditions. During capture, the supernatant consistently contained a fraction of targeted cells, and when extracted MNP-cell complexes were resuspended into fresh matrix, additional cells would be released into the fresh supernatant. There is a type of cellular “equilibrium” that is established during capture as the bonds between the microbial target surface epitopes and carbohydrate functional groups are formed, which has been seen in other detection methods [273]. This is similar to a chemical reaction that is at equilibrium, with the forward product formation reaction (MNP-cell bonding) matching the reverse reactant formation from the product (MNP and cell detachment). Multiple factors will define this equilibrium, or capture snapshot, between cells in MNP-cell complexes and those

remaining in the supernatant, particularly the matrix composition, MNP to sample volumes ratio, as well as the ligand-microbial-surface-epitope pair involved in bonding.

Microbial capture equilibrium could be seen in SVC experiments where it was found that the ratio of captured cells to those in the supernatant varied both by microbial target and matrix. In simple PBS, *Salmonella*, *E. coli*, and *Bacillus* had on average ratios of 0.25, 0.07 and 0.96, respectively, captured cells in MNP-cell complexes compared to those in the supernatant. These ratios were 0.10, 0.09 and 0.14, respectively, for these same microbial targets in vitamin D milk. The trends in these ratios of course mimicked the change in CI reported in Table 6.4 for these same matrix-microbe pairs, which ranged from 47 ppt to 624 ppt. In a separate experiment looking at cell loss from MNP-cell complexes in fresh matrix, *Salmonella* captured in fat free milk using MNP-F#1 and MNP-F#2 showed an order of magnitude loss of the captured cells to the supernatant, shown in the resulting CI from 4.61 ppt to 0.99 ppt and 2.72 ppt to 0.54 ppt, respectively with just one change of fresh matrix.

Binding between MNP carbohydrate groups and cells is through non-covalent, electrostatic forces that may create a dynamic environment, with multiple forces pulling at the cell from the MNP and matrix. Equilibrium within this dynamic environment of MNP extraction would then be defined as reaching the point where cellular detachment from MNP is balanced with MNP-cell re-attachment. Cell concentration, the ratio of sample volume to MNP volume, and the matrix composition will all affect the rate and possibility of forming an MNP-cell bond. At higher cell concentrations, MNP proximity to cells increases, but sufficient MNP presence may limit extraction. For example, *Salmonella* captured using LVC at three concentrations in 2% reduced fat milk (3.3, 4.3, and 5.3 log CFU/mL), showing higher capture at lower cell concentrations (12.19 ppt, 7.86 ppt, and 1.09 ppt, respectively). When multiple microbial targets are present during

capture, as seen in the simultaneous multiple bacteria capture reported in Table 6.4, equilibrium is also established between the MNP and each type of microbe present resulting.

Decreases that were seen in microbial capture for LVC (Tables 6.2 and 6.3), compared to SVC (Table 6.4) for the otherwise same conditions, were likely due to the reduced proximity of cells to MNP. Individual bacterial capture on both scales was carried out at a standardized serial five-fold dilution of the stock culture, resulting in cellular concentrations of 3 to 5 log CFU/mL in their respective solution (25 mL for LVC and 500 μ L for SVC). SVC had a 40% v/v MNP to matrix concentration (200 μ L MNP into 500 μ L total volume) whereas LVC was one order of magnitude less at 4% v/v MNP to matrix concentration (1000 μ L MNP into 25 mL total volume). But CI for capture in milk was only reduced at most by 15% CI for LVC for the same microbe-matrix-MNP combination, showing the capacity of MNP to capture in large volumes. Work in the Nano-Biosensors lab has shown that 1 mL of MNP suspension can capture bacteria with high CI and concentrate them from raw sewage, river water, and emulsified foods with volumes of 100 mL to 400 mL.

6.3.7 Suspended MNP Capture in Beef Juices, Apple Cider and Homogenized Egg

As discussed earlier, complex matrices are rich in a variety of nutrients. As shown earlier in Table 6.1, in a single serving (240 mL), milk has 28 gm of sugars, lipids and proteins in a whey serum, while, apple cider has 30 gm of sugars. Beef juices, though, contain a minimal amount of myoglobin proteins released from muscle tissue. In the same volume, homogenized eggs contain over 31 gm of carbohydrates, most as protein. In fact, it is this high protein content in homogenized egg that may have been the reason that MNP-cell complexes did not migrate to the magnet during separation. This prevented calculation of capture indexes in homogenized egg for *Salmonella*

extraction. Also, this magnetic resistance result was one driving force in the development of an MNP-strip biosensing method, which will be introduced later.

As reported above, microbial capture in milk was above 3 ppt, up to 120 ppt for *Bacillus*, for a variety of pathogenic bacteria, milk types and two MNP, even when the MNP were exposed to the aging fresh milk over days. In initial tests, though, suspended MNP-F#2 extraction of *E. coli* O157:H7 from beef juices and *Listeria monocytogenes* from apple cider were at substantially lower amounts of 2.5 parts-per-million (ppm) and 11.4 ppm, respectively (n=3, data not shown). In *Salmonella* capture from homogenized eggs, the minimal (< 10%) of MNP-cell complexes collected in magnetic separation due to their close proximity to the magnet even showed 0.3 ppm CI on average (n=3, data not shown). Both milk and homogenized egg have high fractions of protein as indicated in Table 6.1, while beef juices and apple cider have essentially none.

Further comparing the matrices used in microbial capture, milk has a more neutral pH, similar to PBS, whereas beef juices and apple cider are more acidic. Capture in PBS (20 ppt in LVC) and milk was higher for all bacteria and MNP (Tables 6.2, 6.3 & 6.4) than those CI for beef juices and apple cider. During capture, the acidic environment may alter the binding properties of the glycan and amino acid ligands immobilized onto the MNP, reducing their ability for hydrogen bonding to the cell surface structure, resulting in lower bacterial extraction.

6.3.8 Rapid Detection of Bacteria in Complex Liquids Using Cyclic Voltammetry

Cyclic voltammetry detection was investigated as a more rapid signaling method following rapid MNP extraction, even from complex liquid matrices. Suspended MNP-cell complexes from LVC were tested following the method described for MNP-strips. Here, 100 μ L of the concentrated sample was resuspended into 150 μ L of chemical mediator, then magnetically separated from the

MNP-cell complexes. A volume of 75 μL of the chemical mediator was then tested for remaining strength using CV. Initial sampling found the sample-to-negative-control ratio (S/N) for *E. coli* O157:H7 detection in beef juices of 0.72, *Salmonella* detection in Vitamin D milk of 0.98, and *Listeria* detection in apple cider of 1.07. Capture of *E. coli* in beef juices showed significant separation between the sample and negative control responses ($p < 0.05$), whereas *Salmonella* in milk and *Listeria* in cider were significantly separated from their respective negatives at $p < 0.15$. These CV tests for sampling in complex matrices were the first to indicate matrix effects in CV testing with $S/N > 1.00$, as opposed to testing in PBS that is commonly carried out in the Nano-Biosensors lab which consistently showed $S/N < 1.00$. Additionally, as mentioned above, MNP-*Salmonella* complexes were unable to be magnetically separated from the thicker homogenized egg matrix. This was a motivating factor to instead optimize resources and focus development on the MNP-strip technology with CV detection discussed next.

6.3.9 Confirmation of MNP-strip Bacterial Capture in Simple Buffer

Simultaneous to suspended MNP testing, development was ongoing to design tag-on biosensors for individual food packages. The goal in this work was to boost consumer confidence in food security along the supply chain using MNP-strips functionalized with carbohydrate ligands. These would provide a viable option for biocompatible detection as opposed to utilizing antibody ligands due to their negative association with creating “super-bugs”. Carbohydrate-functionalized MNP-strips would eliminate this concern, and using it for improved microbial extraction would eliminate the need for supernatant handling.

During development of the MNP-strip, it was determined that MNP-F#2 affixed to plastic strips extracted on average two-times more bacteria than MNP-F#1, using MNP-cell growth in

TSB as described earlier (data not shown). The amino acid and glycan carbohydrate ligands alone did not adhere to the plastic strips without being first immobilized onto the MNP surface. Only when the ligands were immobilized onto the MNP did they adhere to the plastic strips in the economical method used. On average, 1.03 ± 0.51 mg of the MNP-F#2 were immobilized per MNP-strip, while the weight change of positive control strips, with no MNP, was -0.12 ± 0.36 mg. This level of functionalization was slightly below the target of 1.25 mg of MNP-F#2 per strip for the method described above.

Immobilization of the amino/glycan-functionalized MNP onto the plastic strips would presumably provide higher capture ability for the ligands due to the high surface area to volume ratio for the 200 nm MNP. The amino/glycan ligand used in this study had shown preferential attachment to cells over complex matrix components as reported earlier, able to capture over 3 ppt of bacteria in different milks in suspended form. In addition, the biosensing method was able to distinguish between samples with cells against negative controls.

Initial capture testing with MNP-strips was carried out in PBS. *Salmonella* cultures were diluted between 2 to 6 log CFU/mL in 25 mL of PBS and extracted using the MNP-strips. Capture was confirmed through subsequent *Salmonella* growth in TSB from the MNP-strip-cell complexes and was directly related to the concentration of available cells in PBS ($R^2 = 0.9307$, Fig. 6.2A). Negative control MNP-strips that were exposed to PBS with no cells present did not grow bacteria when cultured in TSB.

Separate MNP-strip capture experiments were run to investigate rapid bacterial load detection using cyclic voltammetry (CV) signaling. In these experiments both soft plastic (Fig. 6.2B) and hard plastic (Fig. 6.2C) strip types were used to capture *Salmonella* in PBS. In these preliminary tests, MNP-strips were exposed to 100 μ L of diluted culture in PBS. Upon capture,

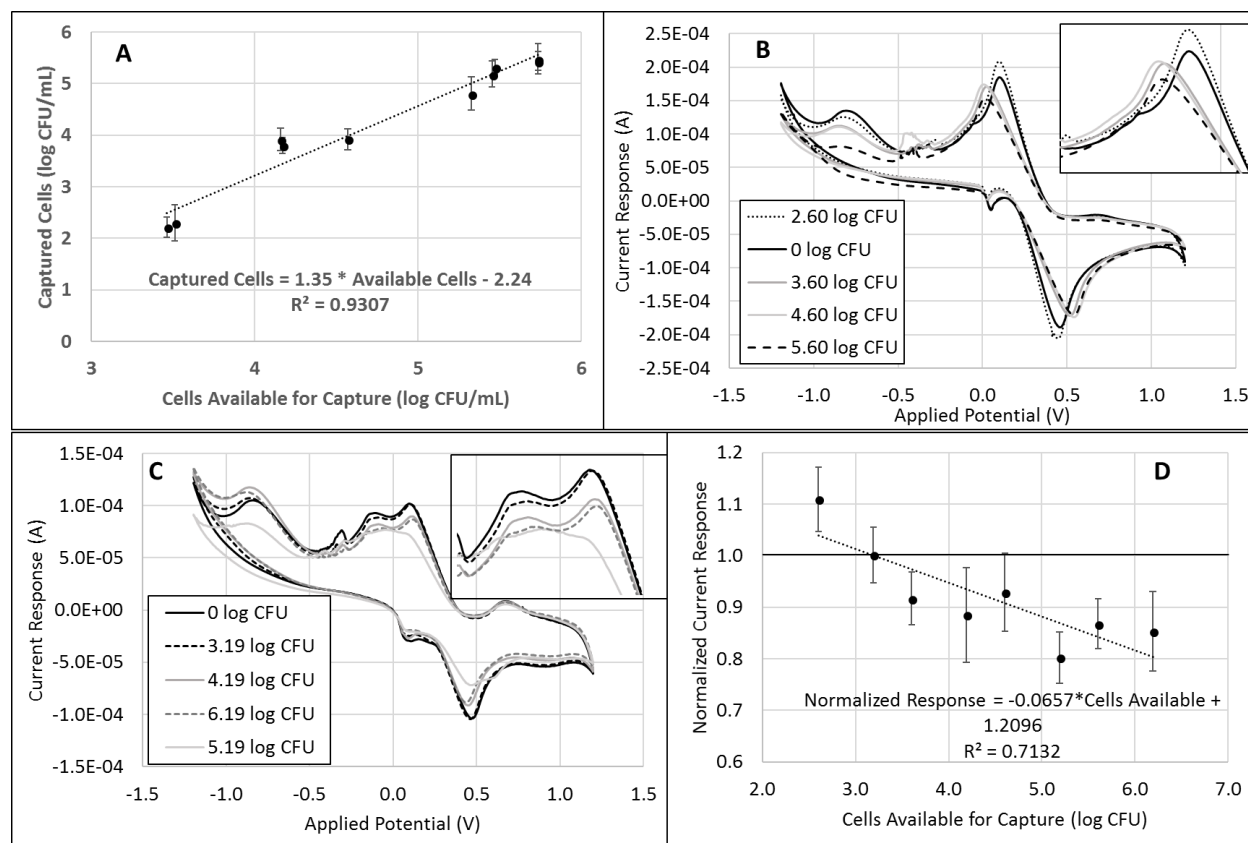


Figure 6.2 Evidence of MNP-strip *Salmonella* capture in PBS through TSB culture (A) and detection using cyclic voltammetry for soft plastic MNP-strips (B) and hard plastic MNP-strips (C), which showed an inverse linear relation ($R^2 = 0.7132$) to cells available for capture (D). Inset plots (B & C) show cathodic peaks in greater detail and the order of concentration listed in the legend (actual units log CFU/mL) follow the order of peak response.

the MNP-strip-cell structures were then reacted with chemical mediator as described above. The remaining chemical mediator strength was then determined using CV, finding that normalized current response (S/N) decreased linearly as available cell presence increased ($R^2 = 0.7132$, Fig. 6.2D). As cell presence on the MNP-strip increased, more of the chemical mediator was reduced, thereby resulting in lower CV normalized current responses.

High variance in the normalized CV response was most likely due to the variation seen in immobilized MNP weights on the MNP-strips. In future work, higher amounts of immobilized MNP-F#2 on the strips covering more of the plastic surface area should reduce the amount of variability in MNP immobilization, improving test reproducibility. In addition, the volume of

chemical mediator used on the strip should then be optimized to allow for better distinction between bacterial loads. These changes would allow more significant separation between CV responses for 1 log CFU/mL differences in contamination.

6.3.10 Rapid Detection of Bacteria in Complex Liquids Using MNP-strips with Cyclic Voltammetry

As described above, cyclic voltammetry (CV) allowed quick detection of cell presence on the MNP-strips, when compared to a negative control. Following capture, a chemical mediator was applied to the MNP spots and reaction between the chemical mediator and the MNP-strip contents reduced the mediator for both samples and negative controls. The resulting reduction in chemical reactivity for the mediator translated into a lower CV normalized peak current response (NPCR) for that MNP-strip. When complex matrix components were present on the MNP-strip, additional reduction in the chemical reactivity resulted in even lower NPCR.

Matrix effects upon CV peak current responses can be investigated best by comparing the negative control to the chemical mediator responses. When simple matrix components attach to the negative control MNP-strip from PBS (Fig. 6.3A) and beef juices (Fig. 6.3B) they deplete at most 10% of the chemical mediator reactivity, in addition to any mediator reaction with the amino-glycan carbohydrate ligands on the immobilized MNP and exposed plastic stripping. Whereas, the effect of a complex matrix such as homogenized egg showed substantial reduction in the chemical mediator CV peak current response as the percent of the egg solution increased (Figs. 6.4A & B). In fact, complex matrices reduced the chemical mediator response to 58% for homogenized egg (Fig. 6.4A), 75% for apple cider (Fig. 6.5B), and 65% for vitamin D milk (Fig. 6.5C). This

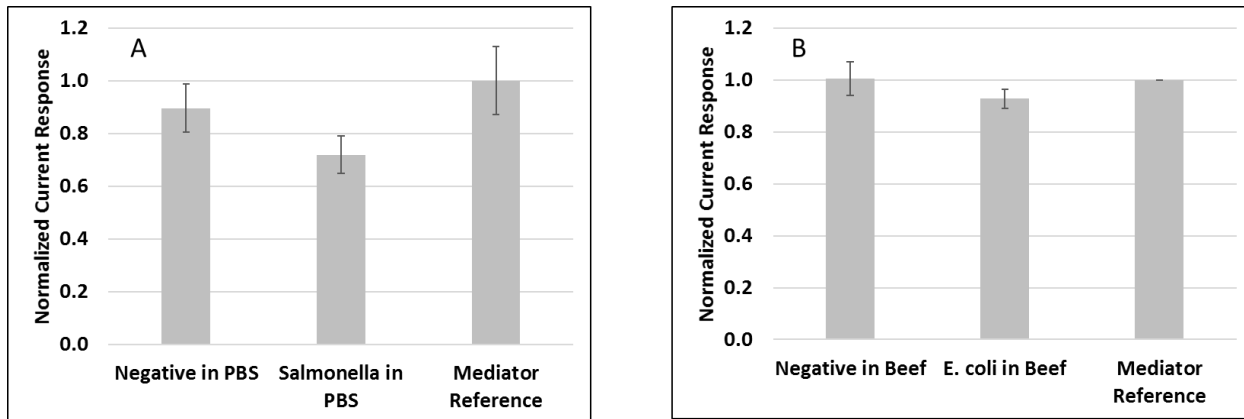


Figure 6.3 Effect liquid matrix components upon CV detection for MNP-strip cell capture of *Salmonella* in PBS (6.19 log CFU/mL available cells, S/N = 0.85, $p = 0.04$) (A) and *E. coli* in beef juices (7.7 log CFU/mL available cells, S/N = 0.92, $p = 0.08$) (B). All peak current responses here were normalized to the mediator reference run at the time of testing to compare matrix effects upon current responses. (error bars = standard deviation)

contrasted with the matrix effects upon CV responses for suspended MNP testing discussed earlier where beef juices depleted over 20% of the mediator, vitamin D milk had no effect, and apple cider reduced it by 30%. Clearly differences between suspended and affixed MNP CV responses must be acknowledged in future selecting the optimal test design.

PBS had a larger effect on the peak current response compared to beef juices due to its available sodium content which can reduce the peak current response of the chemical mediator.

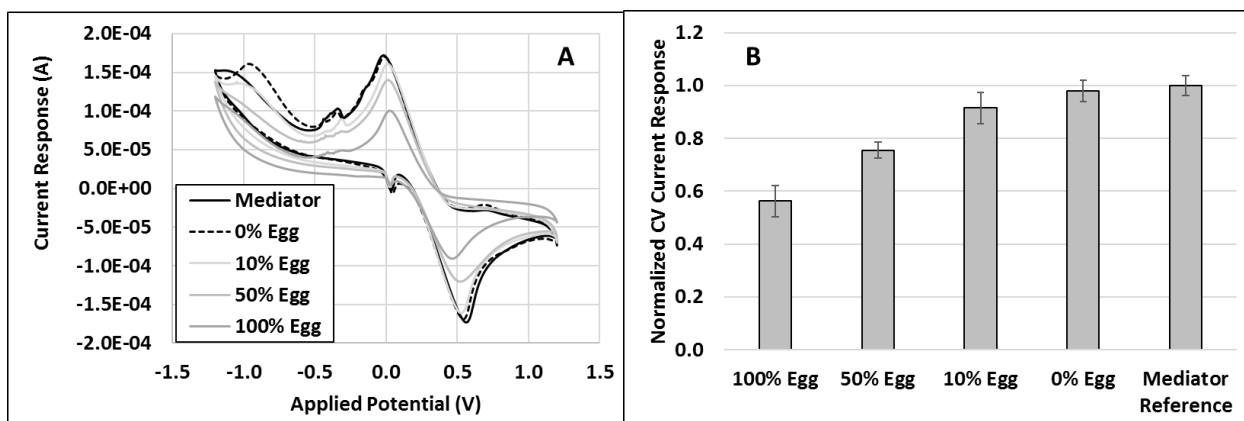


Figure 6.4 Effect of homogenized egg matrix component upon CV peak current response increased proportionally as the purity of the matrix increased (A) such that MNP-strips exposed homogenized egg diluted with PBS showed higher peak current responses for higher PBS dilutions (B). All peak current responses here were normalized to the mediator reference run at the time of testing to compare matrix effects upon current responses. (error bars = standard deviation)

Since the simple matrices used in this study did not contain appreciable carbohydrates, the sodium present may then bind to negative pockets within the MNP carbohydrate ligand and subsequently react with the chemical mediator. Beef has approximately 60 mg of sodium per serving, similar to the level in the PBS, but this sodium is mostly bound to the meat, and therefore may not dissolve into the water solution that is tested with the MNP-strip. In fact, the conductivity of PBS was 14.2 mS/cm, whereas beef juices conductivity was only 11.8 mS/cm.

Table 6.6 Normalized peak current responses (NPCR) for MNP-strip negative controls in simple and complex matrices and the matrix composition used in linear regression statistical analysis. (n=3)

Combination	Normalized Peak Current Responses (NPCR)	Sodium (mg)	Fats (gm)	Carbohydrates* (gm)	Proteins (gm)
PBS	0.87	100	0	0	0
	0.93	100	0	0	0
	0.90	100	0	0	0
Egg	0.65	470	0	5.3	26.5
	0.53	470	0	5.3	26.5
	0.56	470	0	5.3	26.5
Cider	0.71	135	0	30	0
	0.73	135	0	30	0
	0.83	135	0	30	0
Beef	0.94	60	0	0	1
	1.01	60	0	0	1
	1.07	60	0	0	1
Milk	0.64	105	8	12	8
	0.68	105	8	12	8
	0.64	105	8	12	8

*carbohydrates were determined to be have an insignificant effect upon NPCR; subsequent linear regression was run after carbohydrates being removed

Overall, the matrix components that showed a significant effect upon the level of chemical mediator expended by the negative controls were sodium, fats and proteins (Table 6.6, $p < 0.05$).

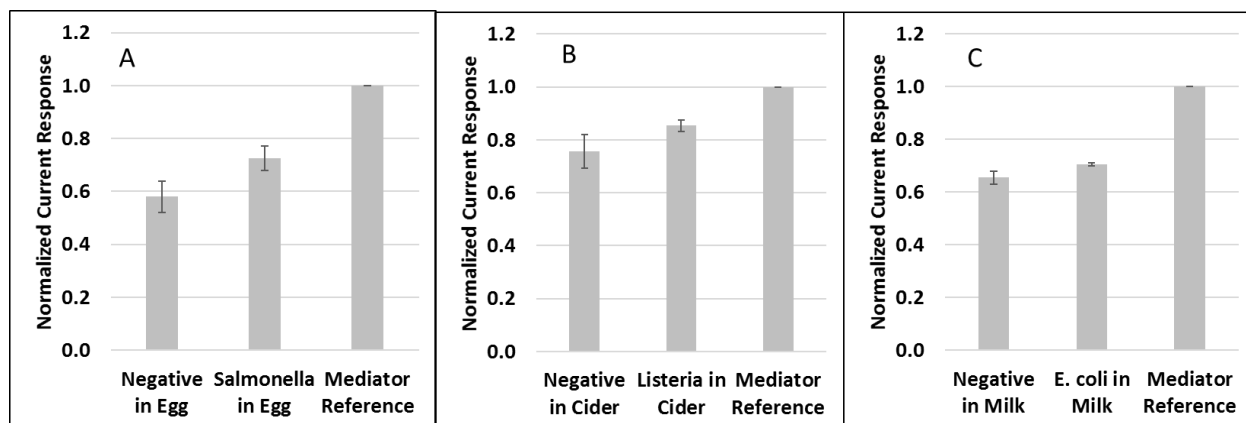


Figure 6.5 Effect of complex liquid matrix components upon CV detection for *Salmonella* in homogenized egg (12.3 log CFU/mL available cells, S/N = 1.25, p = 0.04) (A), *Listeria* in apple cider (7.9 log CFU/mL cells available, S/N = 1.13, p = 0.06) (B), and *E. coli* in vitamin D milk (8.5 log CFU/mL cells available, S/N = 1.08, p = 0.04) (C) showed lower peak current responses for negative controls, while cell presence expended less of the chemical mediator, resulting in higher peak current responses. All peak current responses here were normalized to the mediator reference run at the time of testing to compare matrix effects upon current responses. (error bars = standard deviation)

Sodium and fats had a negative effect upon the level of NPCR for the negative controls, while proteins showed a positive effect ($R^2 = 0.9253$). Carbohydrates showed no significant effect ($p = 0.32$) upon NPCR and were removed from the final linear regression.

Finally, the presence of cells in the matrix has opposing effects depending upon the complexity of the matrix. When cells are present in simple matrices such as PBS (Fig. 6.3A) or beef juices (Fig. 6.3B), the level of chemical mediator expended is increased above that of the negative controls, resulting in lower sample NPCR. For significant separation between sample (S) and negative controls (N) in simple matrices, S/N ratios would be less than 1.0. But, cell presence in complex matrices reduced the amount of expended chemical mediator, since the carbohydrate ligands on the MNP-strips preferentially bind to the cells over the matrix components. This results in samples NPCR that are higher than corresponding negative controls NPCR as seen for capture in homogenized egg (Fig. 6.5A), apple cider (Fig. 6.5B), and milk (Fig. 6.5C). Therefore, for significant separation, S/N ratios would be greater than 1.0 in complex matrices. For the biosensing

tests in this pilot study, all averaged NPCR for samples were significantly different from corresponding negative controls ($p < 0.05$) except in beef juices. As noted in the captions of Figs. 6.3 and 6.5, the presence of any microbial nutrient caused higher cell concentrations available for capture due to accelerated cell growth. All sampling was carried out at four-fold dilutions of the culture spiked into the appropriate matrix, but accelerated growth occurred in beef juices (Fig. 6.3B), homogenized egg (Fig. 6.5A), apple cider (Fig. 6.5B), and vitamin D milk (Fig. 6.5C), for microbial concentrations at the time of capture of 7.7 to 12.3 log CFU/mL.

6.4 Conclusions

Two pitfalls in most published MNP biosensing methods reviewed earlier were cross-reactivity against non-target species and matrix interference with detection signaling. Even using selective antibody ligands, *Listeria* detection showed 50% cross reactivity [88] and a *Staphylococcus* assay showed 40% cross reactivity [87], both against non-target pathogens. Another MNP-antibody method to detect *Listeria* cross-reacted with *Staphylococcus* [86]. Non-selective, carbohydrate surfactants show broad spectrum capture, but vancomycin-PEG-MNP suffered only 20% cross reaction with Gram-negative bacteria [119]. When food matrices such as beef wash solution or pork extracts were introduced into the sampling methods, detection sensitivity was reduced with capture at 70% [89]. Carbohydrate-functionalized MNP produced in the Alocilja Nano-Biosensors Lab showed similar matrix interference, but matrix effects were factored in the final CV signal interpretation using controls.

Glycan- and amino/glycan-functionalized MNP were used here to extract a broad spectrum of pathogenic bacteria from milk to demonstrate the ability of economical carbohydrate ligands to rapidly bind microbes in undiluted complex matrices. Many nano-biosensing methods are vetted using either simple buffer solutions or following removal of food matrix components. Suspended

MNP-F#1 and -F#2 extracted over 3 ppt of three of the pathogenic bacteria (Tables 6.2 & 6.3), at concentrations of 2 to 5 log CFU/mL within minutes and concentrated them into 1 mL volumes. High CI occurred when multiple bacteria were present (Table 6.4) or even following MNP extended exposure to the milk matrix (Table 6.5).

Through microbial concentration, electrochemical detection had shown increased sensitivity with initial CV detection tests in the Nano-Biosensors Lab using suspended MNP (data not shown), even, as reported, at low levels of contamination [82], [92], [118]. In addition, although MNP can be used directly in many detection steps, the non-covalent electrostatic binding of the MNP-cell complexes can be safely broken for further cell study.

MNP-strips were designed using these biocompatible amino/glycan ligands affixed to magnetic nanoparticles (MNP-F#2). A rapid detection method was then successfully developed using cyclic voltammetry (CV) with ferricyanide chemical mediator. Overall, the MNP-strip capture and CV analysis nano-biosensing method allowed cell detection in under 30 min, without the necessity of first separating the target cells from the food matrix before extraction. This “dip-stick” also successfully distinguished between samples and negative controls extracted from homogenized egg, as well as the other liquid food matrices, eliminating additional liquid supernatant handling experienced in suspended MNP methods.

MNP-strip have additional benefits over more common methods. Gel electrophoresis with ethidium bromide detection and fluorescent ELISA methods require special handling and technical knowledge. Carbohydrate functional groups show a long shelf-life, without special storage conditions. But work is needed in improving detection limits at low cell concentrations. Improvements would include increased MNP-F#2 coverage along the plastic strip as well as optimizing the volume of chemical mediator. Using a handheld potentiostat will allow this rapid

“dip-stick” nano-biosensing approach to be field portable for bacterial detection close to contamination sites thereby improving decision making processes for implementing food safety mitigation strategies.

In this work, cell capture was directly quantified using BAM plating methods for suspended MNP capture, in place of methods such as genomic DNA detection using PCR. Future work that would correlate MNP-cell quantification with BAM to that of PCR or electrochemical detection means would additionally decrease detection times. Thus, rapid extraction of total bacterial load from complex matrices is possible. Although antibody ligands may show higher specificity against targeted bacteria, their use in food packaging would create consumer concern about superbugs[274]. Therefore, as more selective carbohydrate ligands against pathogens are identified, greater selectivity will be possible [69], [75], [255] with higher detection sensitivity, and more economical assays to protect our food supply chain will be possible with greater selectivity.

Chapter 7. Gold Nanoparticle Enhancement in Differential Pulse Voltammetric and Spectrophotometric Detection of MNP Extracted Bacteria

7.1 Introduction

Since the mid-1800's, our agricultural products have been monitored by the US government using chemical analysis. In 1906 the Pure Food and Drugs Act was passed, then the Federal Drug Administration (FDA) was created in 1930, to further the efforts of the US government to secure our food supplies, among many other human health goals. The FDA began publishing a set of accepted methods to detect pathogens in our food and cosmetics in 1965. Although these bacteriological analytical methods (BAM) are held as the gold standard for pathogen detection, they require extensive supplies and entail time-consuming steps.

In our fast-paced world, the food on our supper table may have been harvested just days earlier and from half-way around the world. Whereas the standardized methods published in the editions of BAM are more reactive to pathogen presence due to their time-consuming steps, food suppliers and consumers alike desire pro-active rapid microbial detection. Nano-biosensors have been the purported answer for rapid microbial detection, but many of the sensors developed are either economically infeasible or require expensive highly-technical instruments in their design.

Returning to more simplistic nano-biosensing methods that are easily adjusted to new targets, stable over long periods and utilize affordable instrumentation will more rapidly meet the needs of industry and consumers. Combining electrically active nanoparticles such as gold nanoparticles (AuNP) for enhanced detection signaling with proven rapid MNP microbial extraction which are both functionalized with biocompatible carbohydrate ligands will provide economically feasible nano-biosensing methods for both developed and under/developing countries to ensure a safe food supply.

AuNP find numerous uses in microbiological areas, from medical diagnostic applications to detecting pathogens for food and environmental safety [6], [30], [68]. Capping agents such as citrate or dextrin provide AuNP stability against electrostatic forces in solution, reducing aggregation, and provide support for subsequent functionalization with various ligands such as DNA, antibodies, or microbiological components [6], [275]. Although applications using unmodified dextrin-capped nanoparticles of carbon, selenium, and silver have been developed [141], [145], [276], and dextrin-stabilized gold colloids [277], none of these applications use dextrin-coated AuNP (d-AuNP) in conjunction with spectrophotometric or differential pulse voltammetric (DPV) detection.

In this work, d-AuNP standards were first characterized with respect to their electrochemical signaling using spectrometry and DPV, including in the presence of MNP and cells. Detection using anti-*Salmonella* antibody functionalization of d-AuNP is then investigated as a means to show specificity in pathogenic detection. Finally, a rapid nano-biosensing for microbial contamination in milk, a complex matrix, is described. This method used carbohydrate-functionalized (amino/glycan) magnetic nanoparticles (MNP-F#2) and concentrated dextrin-coated gold nanoparticles (AuNP) for rapid detection of *E. coli* C3000 in undiluted vitamin D milk using both spectrometry and electrochemical detection. These economical carbohydrate-based nano-biosensors currently show broad selectivity in pathogen detection for total load of bacterial contamination present. As more selective carbohydrate ligands are designed, they can easily be applied to this method with little increase in detection costs.

7.2 Materials and Methods

7.2.1 Method of Development for Carbohydrate-based MNP-cell-AuNP Nano-Biosensing

Steps taken in investigating the ability of carbohydrate-based MNP and AuNP to detect pathogenic bacteria in complex matrices were carried out in a logical progression. Initially, AuNP were functionalized with selective antibody in attempts to prove specificity of *Salmonella* Enteritidis capture by MNP-F#2. Subsequently, total carbohydrate-based nano-biosensing was pursued, using *E. coli* C3000 for easier TEM imaging reported above. Improved signaling was first addressed by concentrating the dextrin-coated AuNP and removing excess dextrin solution. Spectral and differential pulse voltammetry (DPV) responses to concentrated AuNP were tested. Then the time-spans required to ensure sufficient AuNP coverage of MNP-cell complexes for sensitive spectral and DPV responses, including when complex matrix components are present. At this point, it was necessary to investigate and develop novel “step-integrated spectral absorbance” to interpret scans in which signature peaks were masked by complex matrix components. Finally, the combined carbohydrate-based MNP-cell-AuNP with spectral and DPV signaling was tested at two microbial cell concentrations.

7.2.2 Materials

Cell strains of *Salmonella* Enteritidis, *E. coli* O157:H7, *E. coli* C3000, *Bacillus cereus*, and *Listeria monocytogenes* were obtained from Evangelyn Alocilja’s Nano-Biosensors Lab at Michigan State University (MSU). In-house, proprietary glycan- and amino/glycan-functionalized magnetic nanoparticles (200 nm in diameter, MNP-F#1 and MNP-F#2, respectively) and dextrin-coated gold nanoparticles (approximately 50 nm in diameter, d-AuNP) were used as received from the Nano-Biosensors Lab, MSU [6], [143]. Phosphate buffer solution, pH 7.4 (Neogen, Lansing,

MI), was prepared as directed. Brilliant Green agar (BGA), tryptic soy broth (TSB), tryptic soy agar (TSA), Luria Bertani broth (LBB), and Luria Bertani agar (LBA) were purchased from Sigma Aldrich (St. Louis, MO), CHROMagar™ *E. coli* was purchased from DRG International (Springfield, NJ), and Oxford Listeria Agar base and Modified Oxford Listeria Supplement for modified Oxford agar (MOX) was purchased from Neogen Corp. (Lansing, MI), and prepared as directed.

A Sphero FlexiMag Separator was purchased from Spherotech Inc (Lake Forest, IL). Square 1 oz (30 mL) clear glass bottles with phenolic caps were purchased from Thomas Scientific (Swedesboro, NJ). Vitamin D, 2% reduced fat, fat free milk, apple cider, and homogenized eggs were purchased from a local commercial seller, while beef juices were procured from the MSU meat store, all stored at 4 °C, and used fresh. Before use, all containers were sterilized externally with 70% ethanol and the contents thoroughly mixed by inversion.

7.2.3 Bacterial Culture

Salmonella Enteritidis, *E. coli* O157:H7 and *E. coli* C3000, *Bacillus cereus*, and *Listeria monocytogenes* were rejuvenated from frozen storage (-70 °C) frequently on BGA, CHROMagar™ *E. coli*, LBA following heat shock treatment, and MOX, respectively, as master plates. A single colony was isolated, inoculated into 10 mL media as follows. *Salmonella* Enteritidis, *E. coli* O157:H7 and *E. coli* C3000 were cultured in 10 mL TSB, while *Listeria monocytogenes* was cultured in 10 mL LBB, in 15 mL Eppendorf tubes overnight at 37 °C. *Bacillus cereus* was heat-shocked at 75 °C for 15 min in 10 mL LBB in 50 mL flasks and grown with foam stoppers overnight at 37 °C and 100 rpm. A 10% spike was then grown with the same respective conditions for four hours to log phase immediately preceding all experiments.

Tenfold serial dilutions of the stock culture, from 10^{-1} to 10^{-7} , were prepared using PBS before each experiment. Similar tenfold dilutions were made in the appropriate liquid food from 10^{-1} up to 10^{-12} to account for the immediate accelerated bacterial growth during dilutions and used as indicated below for cell capture. Viable cells for both cultures from PBS dilutions and liquid food were enumerated by microbial plating. *Salmonella* was plated on BGA while *E. coli*, *Bacillus*, and *Listeria* were plated on LBA and plates incubated at 37 °C for up to 16 hr. Target plate counts were between 25 and 300 colonies per plate.

Diluted cultures were used as indicated below, with all testing done in triplicate and at room temperature.

7.2.4 Antibody-functionalized AuNP

Dextrin-coated gold nanoparticles (d-AuNP) were used as received from the Nanobiosensors Lab [143] and functionalized with antibody using the method of Wang et. al. [6]. Volumes of 1000 μ L of the original d-AuNP suspension were transferred to 2 mL pinched-tip centrifuge tubes, sonicated for 10 min, and centrifuged at 15,000 rpm at 4 °C for 20 min. Following removal of the supernatant, the remaining 20 μ L “AuNP” pellet was sonicated for 15 min to evenly distribute the concentrated d-AuNP evenly. No additional sonication was performed. Protein A (from *Staphylococcus aureus*, 1000 μ L, 0.25 mg/mL in PBS, Sigma-Aldrich, St. Louis, MO) was added and the AuNP hybridized on a shaker rotator at 350 rpm for 1 hr. Following each step that follows, the tube was centrifuged at 13,000 rpm at 4 °C for 12 min and the supernatant removed. AuNP were washed with 1000 μ L PBS, resuspended in 500 μ L of *Salmonella* polyclonal antibody (1.25 mg/mL in PBS, Thermo Scientific, Rockford, IL), and hybridized as before. The resulting Ab-AuNP pellet was resuspended in 0.1% bovine serum albumin (BSA) in PBS as a blocking

agent and hybridized for 30 min. The final pellet was resuspended in 1000 uL 0.1% BSA, stored at 4 °C in aluminum foil and used within 24 hr.

7.2.5 Specificity of Capture of *Salmonella* Monoclonal Antibody and Cross-reactivity

Ab-AuNP were tested for their ability to prove target *Salmonella* Enteritidis capture using carbohydrate-functionalized MNP-F#2, as well as their cross-reactivity against non-target *E. coli* O157:H7, as MNP-cell-Ab-AuNP complexes using both spectrometry and differential pulse voltammetry (DPV) detection. In a 2 mL centrifuge tube, 80 uL of MNP (5 mg/mL in PBS) were exposed to 100 µL of either diluted target at 4 or 5 log CFU/mL or non-target at 4 log CFU/mL. After capture for 5 min, 100 uL of 0.1% BSA was added and allowed to block open MNP carbohydrate ligands for 5 min. Samples were magnetically separated, resuspended in 200 uL of Ab-AuNP for DPV testing or 100 uL of Ab-AuNP for spectrometry samples, and labeling allowed for 5 min. The MNP-cell-Ab-AuNP complexes were magnetically separated and resuspended into 200 uL of 0.1% BSA and 800 uL of PBS. Samples and negative controls, prepared in the same manner without cells present, were run in triplicate, unless otherwise stated. All samples and negative controls were analyzed for electrochemical responses using either differential pulse voltammetry (DPV) or spectrophotometric signaling responses, as indicated later.

7.2.6 Concentrated Dextrin-coated d-AuNP

Dextrin-coated gold nanoparticles (d-AuNP) were analyzed for their ability to provide sufficient signaling shifts at various concentrations. Concentrated d-AuNP was prepared by removing excess dextrin and solution. Volumes ranging between 25 to 250 µL of the original d-AuNP suspension were transferred to 2 mL pinched-tip centrifuge tubes, sonicated for 10 min, and

centrifuged at 15,000 rpm at 4 °C for 20 min. Following supernatant removal, the remaining 20 μL d-AuNP pellet was sonicated for 15 min to evenly distribute the concentrated d-AuNP evenly, then used as the starting aliquot. Tubes were stored at 4 °C and used within 24 hr of preparation. Concentrated d-AuNP are referred to using their initial volume, e.g. a 75 μL concentrated d-AuNP will be identified as “AuNP75” or simply “AuNP” as appropriate.

7.2.7 Temporal Attachment of Concentrated d-AuNP to MNP-cell Complexes

Amino/glycan carbohydrate-functionalized magnetic nanoparticles (MNP-F#2, or MNP), was used to capture either *Salmonella* or *E. coli* C3000 to study concentrated d-AuNP temporal attachment to the cell and MNP surface using spectrometry. This procedure was in conjunction with collaborative research, and therefore used minimized sample sizes to mimic design parameters. MNP (20 μL of 5 mg/mL) were exposed to 20 μL of cell culture diluted in PBS to 5 log CFU/mL plus 100 μL PBS for 5 min, magnetically separated and re-suspended in AuNP250 plus 40 μL PBS. AuNP250 attachment was allowed for 10, 20, and 30 min incubation times. The MNP-cell-AuNP complexes were re-suspended in 1000 μL PBS. Negative controls followed the same procedure except without cells (n = 3).

7.2.8 Carbohydrate-based MNP-cell-AuNP Nano-biosensing

E. coli C3000 culture serially diluted in milk (50 μL) was simultaneously exposed to MNP (50 μL of 5 mg/mL prepared in buffer) and AuNP250, plus 100 μL PBS for 30 min, magnetically separated and re-suspended in 100 μL PBS for electrochemical detection or 1000 μL PBS for spectral detection, as indicated below. Negative controls followed the same procedure except

without cells. Sample cell concentrations at the time of capture were determined to be 3 log CFU/mL and 5 log CFU/mL through BAM plate counts.

7.2.9 Electrochemical Spectrophotometric or Differential Pulse Voltammetric Detection

Differential Pulse Voltammetry

DPV were run using a Uniscan PG581 potentiostat with a 1 cm² screen-printed carbon electrode (SPCE), driven by UiEChem software. Samples and negative controls were oxidized for 2 min at 1.2 V then current response was recorded for applied potentials between +1.2 V to -1.2 V, with a pulse height and width of 0.5 V for 50 ms, at a scan rate of 33.3 mV/s. A DPV voltammogram was recorded for each sample. Sample (S) and negative control (N) responses were averaged and S/N ratio calculated (n = 3).

Spectrophotometry

Spectrophotometric scans were run from 900 nm to 200 nm wavelength (Shimadzu UV-3101PC, UVProbe software), against a reference of 200 uL of 0.1% BSA diluted with 800 uL PBS. Total spectral absorbance was calculated by step-integration between 220 nm to 900 nm. A spectral scan was recorded for each sample. Step-integration involves multiplying the 0.5 nm wavelength step-size by the resulting absorbance at that new wavelength and summing these areas.

MNP-F#2 Specificity and Ab-AuNP Cross reactivity

Both MNP-cell-Ab-AuNP samples and MNP-Ab-AuNP negative controls to determine MNP-F#2 specificity and Ab-AuNP cross-reactivity were prepared for differential pulse voltammetry (DPV) where a volume of 500 uL of the sample was magnetically separated and

reacted with 100 μ L of 1 M HCl for 5 min, and the entire contents transferred to the SPCE (n = 3). Whereas, spectrophotometry was run on the samples and negative controls as prepared above (n = 3).

Temporal Attachment of AuNP250

Samples were tested as prepared above using spectrometry. Peak absorbances for MNP (620 nm) and AuNP (520 nm) were monitored for the 10, 20 and 30 min MNP-cell-AuNP and MNP-AuNP complexes. Both AuNP peak height and step-integrated spectral area were compared with respect to time using linear regression (n=3).

Carbohydrate-based MNP-cell-AuNP Nano-biosensing

Carbohydrate-based MNP-*E. coli*-AuNP samples and corresponding negative controls were tested as prepared above.

Peak absorbances for MNP (620 nm) and AuNP (520 nm) were monitored. All spectra were numerically step-integrated between 900 to 220 nm and averaged MNP-cell-AuNP sample step-integrations were compared to averaged MNP-AuNP negative controls (n = 3).

Samples and negative controls were magnetically separated and resuspended in 100 μ L 1 M HCl, reacted for 5 min, then the entire contents were applied to the SPCE. Maximum absolute AuNP current response was determined between 0.3 V to 0.5 V. Averaged sample peak currents were compared to averaged negative controls (n=3).

Sample responses were compared to negative control responses using a t-test for unpaired samples and p-values reported below.

7.3 Results and Discussion

7.3.1 Electrochemical Signature Responses for MNP-cell-AuNP Biosensing

Gold nanoparticle (AuNP) labeling is an effective method to intensify electrochemical responses in nano-biosensing applications [6], [135]. In combination with rapid MNP extraction, microbial presence within liquid matrices can be identified within 45 min. Both MNP and AuNP have distinctive signature responses in both spectrophotometric detection and differential pulse voltammetry (DPV) signaling. This ensured that the AuNP response would not be masked by MNP presence, eliminating the need to separate MNP from the cell-AuNP complexes before detection for DPV. Complex matrix components, though, may attach and mask spectral signaling, necessitating development of a novel data analysis technique presented below.

Binding dynamics between carbohydrate-based MNP and AuNP, and targeted cells, were presented earlier in TEM images. The AuNP were of diameters smaller than 20 nm and seemingly aggregated in small 50 nm clumps when binding cell surfaces (Fig. 5.5B) but saturated the surface of the MNP (Fig. 5.6B). These binding properties were evident in both the spectral detection or DPV signaling, as will be discussed below.

Maximum spectral responses for the concentrated dextrin-coated AuNP used in this work occurred at approximately 520 nm (AuNP250 Fig. 7.1A), whereas MNP peaks were located at approximately 620 nm (MNP Fig. 7.1A). When the two nanoparticles were prepared in a control mix in simple PBS, the stronger AuNP response persisted, while the MNP presence only shifted total absorbance to higher levels in an additive manner (AuNP250 & MNP mix Fig. 7.1A). But as can be seen in Figure 7.1B, spectral scans of carbohydrate-based MNP-cell-AuNP and MNP-AuNP complexes following capture and labeling in PBS show lower absorbance levels, even though the same initial quantities of MNP and AuNP were used. This is the result of non-

complexed unattached nanoparticles loss during supernatant removal. Non-complexed MNP residue may not be separated from the matrix due to insufficient vessel wall space next to the magnet. This loss accounted for at least 50% signal loss in MNP absorbance in Figure 7.1B. Substantial loss in AuNP signal is also apparent due to the limits of attachment between AuNP and the MNP or cell target. As noted in the prior chapter, a dynamic chemical equilibrium is established between attached nanoparticles and the surrounding supernatant, causing limited attachment.

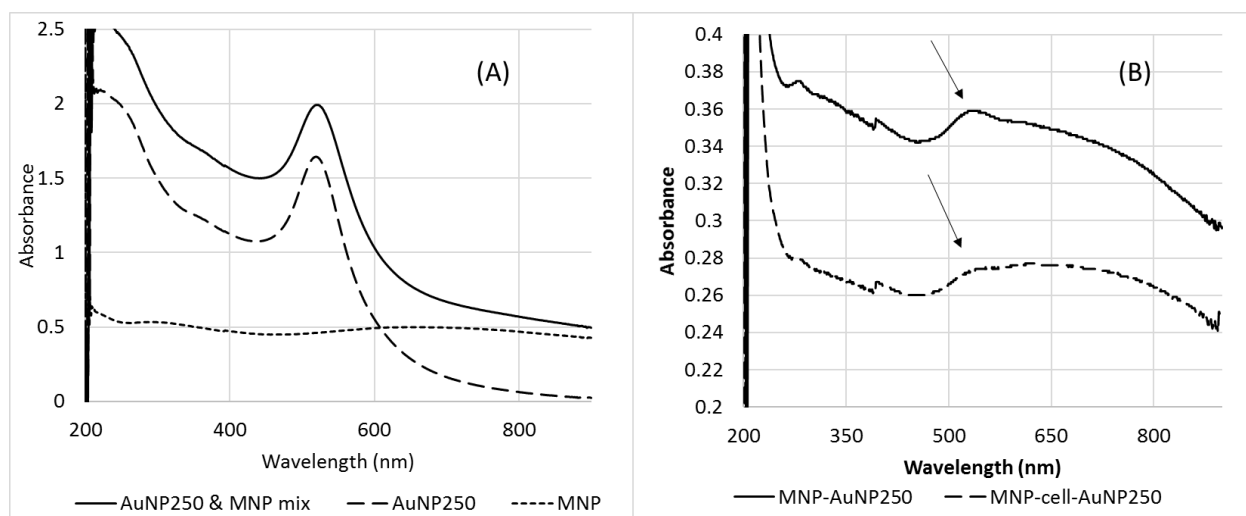


Figure 7.1 Spectral scans of AuNP250 controls combined with MNP (A) and following attachment through the cell capture and labeling method (B).

Although substantial nanoparticle loss was experienced in MNP-cell-AuNP nanobiosensing in Figure 7.1B, sufficient AuNP labeling occurs to preserve its signature peak at 520 nm in both the MNP-AuNP negative control and MNP-cell-AuNP scans. As seen in Figure 5.5B, aggregated AuNP were selectively attached to the cell surface molecular structures and its presence minimized the MNP attachment, which results in the lower MNP-cell-AuNP absorbance seen in Figure 7.1B. In contrast, AuNP was seen saturating the surface of the MNP in Figure 5.6B, which

translated to higher spectral absorbance for MNP-AuNP in Figure 7.1B, along with a more prominent AuNP peak at 520 nm.

DPV analysis of MNP-cell-AuNP complexes show similar distinctive signature current responses for the individual components present. Figure 7.2 shows current responses for these components both individually and combined in complex. The activator chemical, HCl, has a strong response at approximately 0.8 V, while dextrin-coated AuNP or antibody-functionalized Ab-AuNP show a response at 0.4 V, and MNP responds at +0.1 V. Each type of sample and control is first reacted with HCl to activate the sample for electrochemical detection. Any residual, unreacted, HCl presence in the sample then shows a secondary peak at -0.5 V. Additionally, a secondary AuNP response occurs at -0.1 V. Finally, all DPV scans are normalized with respect to their baseline between 0.9 V to 0.6 V which has no HCl peak present when standards, samples with cells or negative controls are present. In normalization, the current responses between 0.9 V and 0.6 V were averaged, then all current responses in the scan, from +1.2 V to -1.2 V, were

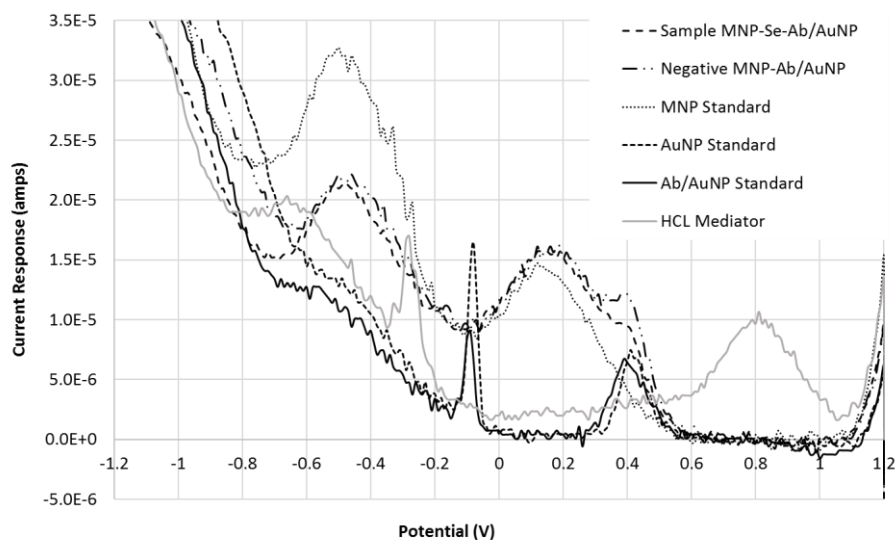


Figure 7.2 Signature responses for MNP-cell-AuNP biosensing controls with differential pulse voltammetry. (Se= *Salmonella* Enteritidis)

divided by this averaged value. This would allow all scans results to be evaluated on a level basis.

DPV current responses for samples (MNP-cell-AuNP complexes) and negative controls (MNP-AuNP complexes) result in convoluted AuNP and MNP peaks, with AuNP commonly appearing as a shoulder at 0.4 V on the MNP peak at +0.1 V (Fig. 7.2). MNP-cell-AuNP/DPV nano-biosensing methods compare the AuNP current responses between the sample complexes that have pathogenic bacteria present to those of the negative controls prepared from uncontaminated standards of the same matrix. During analysis, raw DPV data is corrected with respect to the baseline, as stated above, then the potential that results in the maximum average AuNP current response is located between 0.3 V to 0.5 V. An example of corrected DPV responses is presented in Figure S8.2, where the potential for maximum averaged AuNP current response is at 0.38 V (arrow). Finally, replicates of sample (S) and negative control (N) responses are averaged and the S/N ratio calculated.

As the complexity of the DPV sample increases, the AuNP peak height decreases due to HCl mediator reaction in proportion to all components present. As shown in Figure 7.3 when pure AuNP concentrated standards without any MNP present are tested (“Standards in PBS w/o MNP”), the largest AuNP response is recorded, increasing in response as volume of concentrated AuNP increases. This indicates that HCl is not limiting in the activation step. The presence of MNP in the standards reduces the overall AuNP response (“Standards in PBS w/ MNP”), since the HCl mediator reacts with all components present, including the carbohydrate ligands. Finally, the “Sampling in Milk w/ MNP” samples show the lowest AuNP response due to cell presence, as well as milk matrix components which will be discussed later. Method optimization for MNP, AuNP and HCl quantities would be a major factor in designing a reliable test for pathogen detection.

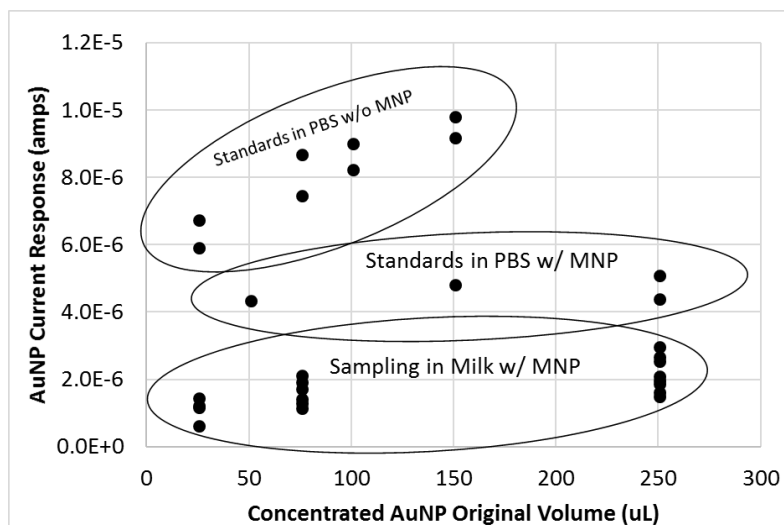


Figure 7.3 Effect of sample complexity upon AuNP current response in DPV biosensing.

7.3.2 Specificity of *Salmonella* Detection Using Antibody-functionalized AuNP

Validation of target capture is an important aspect of nano-biosensor development, particularly when dealing with detection of pathogenic bacteria in our food supply. Antibody ligands are one of the selective methods used to ensure target capture, but they may still result in false positive and false negative results. In addition, antibody functionalization results in higher test costs, requires special test kit handling and shortens shelf life. Wang et. al designed a nano-biosensing test targeting *E. coli* O157:H7 using antibody ligands for both MNP extraction and AuNP labeling [6]. Using DPV signaling, they were able to detect target bacteria as low as 1 log CFU/mL target in broth in an 1 h, although testing against a non-target bacteria for false positive results was not reported.

Applying this same technique, the dextrin carbohydrate coating on the AuNP was replaced with antibody ligand functionalization (Ab-AuNP). This specific label was used in attempts to validate specificity of *Salmonella* Enteritidis detection using carbohydrate-functionalized MNP-

F#2 for microbial extraction. Results consistently showed unreliable, non-reproducible DPV signaling responses for samples consisting of MNP-cell-Ab-AuNP complexes (Tables 7.1 & S8.2).

Table 7.1 Specificity of Salmonella detection using antibody-functionalized AuNP.

Trial	Capture Matrix	Pathogen*	n Samples	Cells Available for Capture (log CFU/mL)	MNP Capture Index (ppt) [@]	Post Ab-AuNP Capture Index (ppt)	t-test ⁺ p-value	AuNP Peak S/N [#] ave.
1	PBS	Se Target	3	3.12	170	40	0.11	0.87
2	PBS	Se Target	6	2.76	520	76	0.02	0.83
3	Milk	Se Target	6	3.40	763	21	0.39	0.96
4	Milk	Se Target	6	3.30	935	346	0.49	0.99
5	Milk	Se Target	6	5.14	14.4	0.9	0.49	1.00
6	Milk	Se Target	3	9.08	1.48	0.01	0.04	0.60
		Se Target	3	8.08	0.62	0.01	0.02	0.45
		Se Target	3	7.08	1.45	0.03	0.36	0.90
7	Milk	Se Target	3	6.95	0.23	0.00	0.16	0.86
		Se Target	3	5.95	0.99	0.04	0.06	1.12
		Se Target	3	4.95	1.33	0.00	0.04	0.82
8	Milk	Se Target	3	5.57	7640	135	0.10	1.32
		Se Target	3	4.57	8108	622	0.05	1.72
		Se Target	3	3.57	8108	751	0.44	0.97
9	PBS	Se Target	3	5.69	NA	12	0.01	0.74
		Se Target	3	4.69	NA	14	0.01	0.70
		Ec Non-target	3	5.94	NA	1	0.08	0.79
10	PBS	Se Target	3	4.90	NA	103	0.27	0.90
		Ec Non-target	3	5.63	NA	0.08	0.39	0.97

* Se = *Salmonella* Enteritidis, Ec = *E. coli* O157:H7; @ standard deviations for MNP Capture Index are not shown for brevity of data comparison (see Table S7.2); + reported one-tail p-values for t-test ran for unpaired samples and negative controls within same trial test, assuming equal variances; # S/N = AuNP current response ratio for Samples to Negative controls.

Numerous test parameters were adjusted throughout development of the test, including capture volume (180 μ L – 25 mL), MNP-F#2 quantity (80 μ L – 1000 μ L), cellular concentration (2.76 log CFU/mL – 9.08 log CFU/mL), liquid matrix (PBS & milk), Ab-AuNP quantity (100 μ L

to 250 μL), total volume during Ab-AuNP attachment (100 μL to 800 μL), stock culture dilution (10^{-2} – 10^{-6}), diluted culture spike volume (50 μL – 250 μL), and total test volume reacted with HCl (100 μL to 700 μL) used in DPV signaling.

Attempted optimization of the various parameters listed above, in efforts to develop a sensitive nano-biosensing method, focused on improving the separation between sample and negative control AuNP current responses at 0.4 V in DPV signaling in. This involved reducing the MNP-F#2 response at +0.1 V, while still maintaining an initially high MNP capture index. The biosensing method, though, was not able to reliably detect *Salmonella* pathogen presence, even though a specific anti-*Salmonella* antibody was used. In fact, resulting S/N values from the AuNP current responses were not significantly affected by MNP-F#2 quantity, capture volume, diluted culture spike volume, cellular concentration, MNP-captured cell counts, Ab-AuNP quantity, total volume during Ab-AuNP attachment, nor total test volume reacted with HCl. Subsequent analysis of the data using principle component analysis (PCA) and multi-variate analysis of variance (MANOVA) was also unable to identify any of these parameters as significant in distinguishing samples from negative controls.

Applying the earlier descriptions of MNP and AuNP binding, it appeared that the antibody ligand on the AuNP were not binding only the targeted *Salmonella* cells. In most of the trials, the AuNP current responses for the negative controls were stronger than those of the samples that contained MNP-*Salmonella*-Ab-AuNP complexes (Table S7.2). Stronger AuNP current response is indicative of higher AuNP presence, which is shown in Table S7.2 for most of the negative controls. In addition, the Wang et. al method applied here for antibody functionalization uses an ionic PBS matrix, which was found post-project to cause AuNP aggregation. This aggregation possibly limited Protein A and antibody exposure to the AuNP surface during functionalization.

Non-selective binding of any remaining dextrin coating would also increase negative control MNP-Ab-dextrin-AuNP signaling. This resulted in S/N values in Table 7.1 that are less than 1.0. Seemingly the anti-*Salmonella* polyclonal antibody bound the MNP amino/glycan ligands at a higher concentration than the selective binding occurring on the MNP-extracted *Salmonella*.

In the final trials 9 and 10, non-target *E. coli* O157:H7 were included to further investigate attachment of the Ab-AuNP. As can be seen in Figure 7.4, the AuNP current responses for both target and non-target MNP-cell-Ab-AuNP complexes are the same. Samples “Target Se1” and “Target Se2” in Figure 7.4 represent those from trial 9 listed in Table 7.1, which were each shown to be significantly different from the negative control ($p < 0.05$), but neither target sample were significantly different from the non-target *E. coli* sample. Also, the negative control, again, shows greater AuNP current response than any of the samples. Similar results were seen for the samples in trial 10 (Table 7.1), with the negative control showing greater AuNP current response, although not at a significant difference from the target and non-target samples. Clearly the Ab-AuNP were

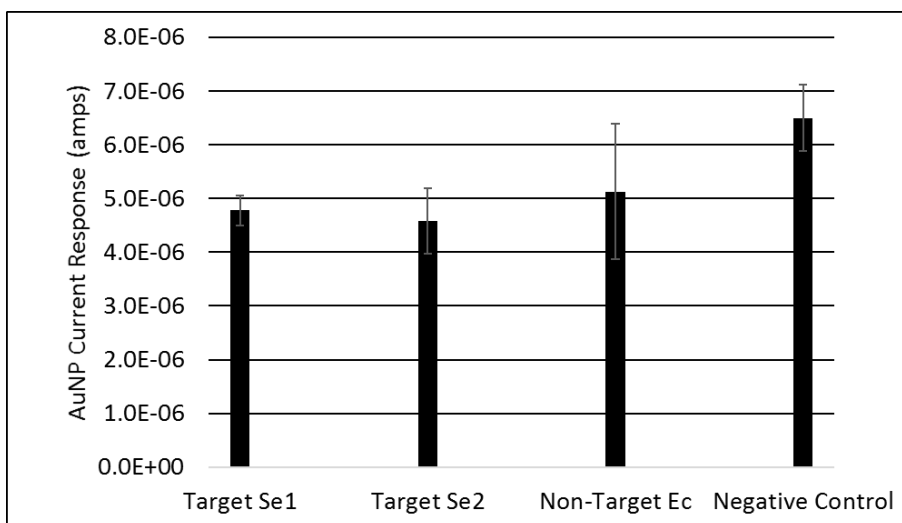


Figure 7.4 Specificity testing using anti-*Salmonella*-antibody-functionalized AuNP to label MNP-*Salmonella* (Target Se1 at 5.69 log CFU/mL and Se2 at 4.69 log CFU/mL) and MNP-*E. coli* (Non-Target Ec at 5.94 log CFU/mL) complexes, as well as negative controls, for DPV detection of the AuNP label.

equally binding both *Salmonella* and *E. coli* surface markers, and heavily saturating the MNP-F#1 carbohydrate ligands.

Another potential aspect causing the insignificant biosensing separation concerns the optimal non-covalent binding properties of carbohydrate ligands. As discussed in chapter 6, the electrostatic bonds between MNP-F#2 and the microbial surface molecular structures are non-covalent, similar to antibody-antigen binding, but at significantly lower specificity and strength. When the MNP-cell complexes are suspended into fresh matrix, fractional levels of the cells release and come to a new equilibrium between the MNP-cell complexes and the fresh matrix, causing a fractional loss of cells to the supernatant. During the multiple rinse steps required in the antibody-based specificity method, a large fraction of the MNP-captured cells was lost, as indicated in Table 7.1. Comparing the MNP capture index and post Ab-AuNP capture index data it can be seen that capture indexes drop by an approximate one to two orders of magnitude across trials 1 through 8. Since the Ab-AuNP seemingly saturate the MNP surface, as more cells are lost through rinsing, the final MNP-cell-AuNP complexes will have similar AuNP current responses as the negative control MNP-AuNP responses.

Some minor success was accomplished with the later trials. The method used in trial 9 was able to retain a sufficient fraction of the cells, with capture indexes over 10 ppt for the target MNP-cell-AuNP complexes. This method minimized all volumes and matrix changes, using only 80 μL of MNP combined with 100 μL of diluted culture spike volume. The MNP-cell complexes were directly resuspended into 200 μL of Ab-AuNP, with the separated MNP-cell-Ab-AuNP complexes diluted directly into 1000 μL for spectrometry. Less rinsing was utilized since the realization that the goal of the method was to detect pathogen bacteria, not just stronger bound microbes. DPV tests were run from spectral samples, where for trial 9 a volume of 500 μL of the diluted sample

was separated and directly reacted with HCl and significantly distinguished between *Salmonella* samples and the negative controls. But this method was still not able to distinguish from non-target *E. coli* O157:H7.

Given the cross-reactivity of the anti-*Salmonella* antibody ligand with both the MNP ligands and non-target *E. coli*, the cost, limited shelf-life, special storage, and even “superbug” concerns inherent with antibody ligands seem exclusionary as a nano-biosensing mechanism. In the drive to design a biocompatible user-friendly biosensing method to detect pathogenic bacteria in our food supply, efforts would be best placed in incorporating emerging carbohydrate-based methods. Although the electrostatic binding forces of the carbohydrate ligands is less than that of antibody ligands, the limitations of these inexpensive ligands can be built into the method to provide robust initial detection methods for broader industry and consumer rapid testing application.

7.3.3 Dextrin-coated AuNP Biosensing with DPV and Spectrometry

As seen in TEM images Figures 5.5A-D, amino/glycan and dextrin carbohydrate ligands attach to the cell surfaces, which enables rapid MNP extraction and increased AuNP labeling of bacteria for enhanced nano-biosensing electrochemical responses. MNP were shown to extract pathogens with capture indexes of over 3 parts-per-thousand (ppt) in milk but only over 2.5 parts-per-million (ppm) in beef juices and apple cider. AuNP labeling increases signaling, since their dextrin coating binds readily to the microbial surface molecular structures and their approximate 20 μ L diameter allows for extensive coverage, especially when excess dextrin solution was removed. The high quantity of the electrically-active AuNP coverage then afforded stronger

electrochemical responses. In addition, concentrated dextrin-coated AuNP signaling was linearly related to the DPV current response at 0.4 V and spectral peak absorbance at 520 nm.

DPV signaling of AuNP presence was found to be linearly related to the resulting current response. As identified in the specificity Ab-AuNP research in the previous section, minimized volumes of the MNP-cell-AuNP components actually improved biosensing signals since cell proximity to the nanoparticles was increased. Therefore, standards were prepared using only 20 μL of MNP-F#2, 10 μL of cell culture diluted 10^{-5} in PBS, 10 μL milk matrix, and varying volumes of concentrated AuNP, from 5 μL to 20 μL . The relation between AuNP current response at 0.4 V and the volume of AuNP showed a linear relation ($R^2 = 0.96$, Fig. 7.5A). These responses were taken from DPV current responses shown in Figure 7.5B.

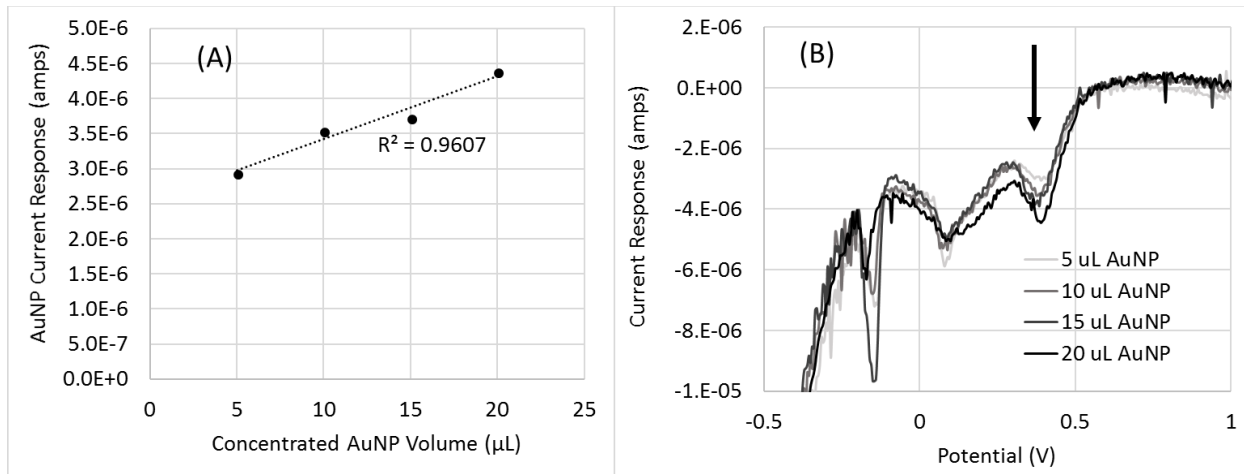


Figure 7.5 DPV current responses for concentrated AuNP responses (A) showing a linear relation between current response at 0.4 V and AuNP volume where (B) AuNP responses are indicated with an arrow.

Likewise, concentrated AuNP responses in spectral signaling showed linear responses between absorbance and the volume of AuNP. Figure 7.6A shows sharp peaks for AuNP standards that were concentrated as described above then resuspended into 1000 μL PBS for spectrophotometric scanning. To ensure that the concentrated AuNP do not aggregate when the excess dextrin is removed, concentrated AuNP75 spectral absorbance was compared to an

unconcentrated sample, both diluted to 1000 μL in PBS. The concentrated AuNP does not show a red shift to higher wavelength, but shares the same spectral characteristics, except for the excess

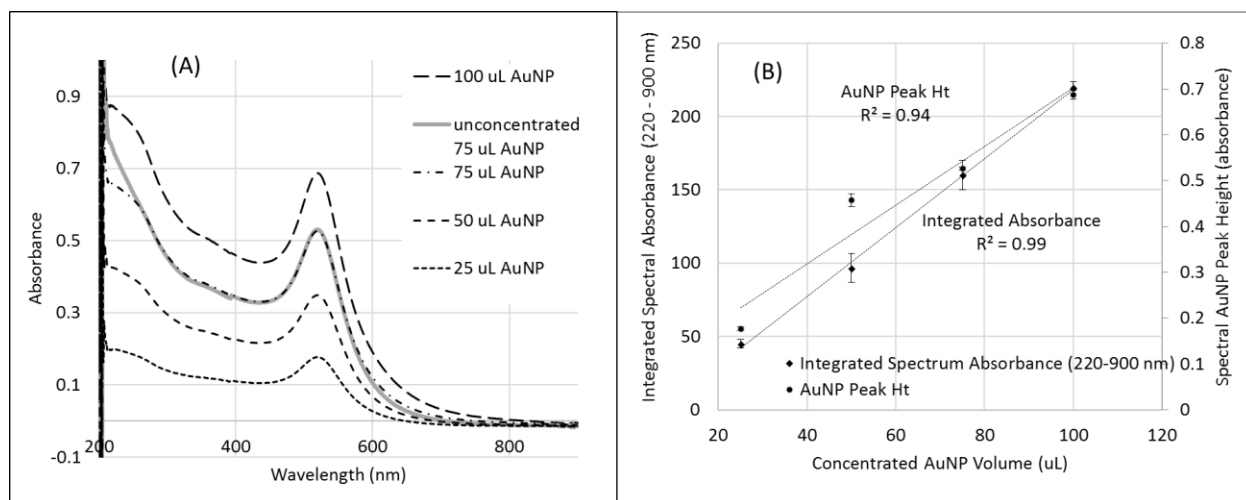


Figure 7.6 Spectral absorbance of concentrated AuNP (A) showing an extinction peak at approximately 520 nm; (B) AuNP concentration is linearly related to both the peak height and the step-integrated spectral absorbance between 220 nm to 900 nm ($n = 3$).

dextrin absorbance between 200 nm to 250 nm. The peak extinction absorbance of the concentrated AuNP at 520 nm were linearly related to their original volume ($R^2 = 0.94$), but when samples are more complex, the AuNP peak may not be as readily visible, as shown in Figure 7.1B. It was found that when the spectrum were step-integrated between 220 nm to 900 nm, the resulting area was also linearly related to the original AuNP volume ($R^2 = 0.99$)

In spectral signaling for carbohydrate-based MNP-cell-AuNP complexes, the presence of MNP can mask the AuNP peak, as discussed earlier and seen in Figures 7.1B and 7.7A. Optimal concentrated AuNP attachment to extracted MNP-cell complexes were determined over 10 to 30 min. Spectral absorbance of the resulting complexes showed a linear relation between the shifted AuNP peak and attachment time ($R^2 = 0.99$). The AuNP peak shifted due to the presence of cells and MNP, as well as possible AuNP aggregation that was seen in Figure 5.5B. AuNP extinction peaks were at 548 nm, 535 nm, 542 nm and 532.5 nm for 10, 20, and 30 min for the samples and

30 min for the negative control, respectively. As discussed for Figure 7.1B, spectral step-integration between 220 nm to 900 nm for the samples was also linearly related to the attachment

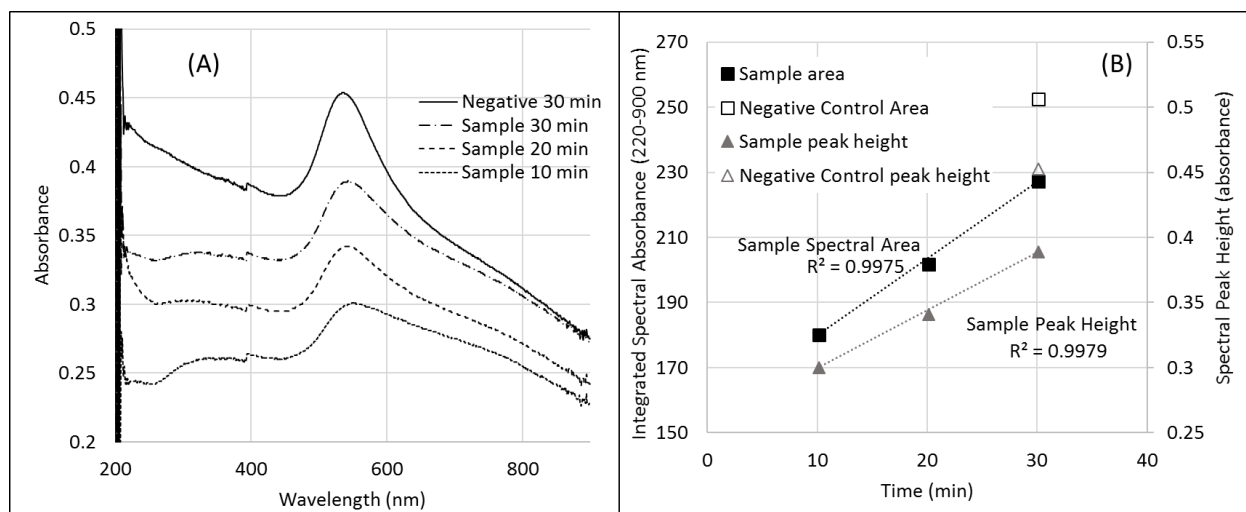


Figure 7.7 Spectral signaling for carbohydrate-based MNP-cell-AuNP complexes showing (A) shifted AuNP peak from 520 nm slightly masked with the MNP peak at approximately 620 nm where (B) both the AuNP peak height and step-integrated spectral area 220 – 900 nm are linearly related to the time allotted for AuNP attachment.

time ($R^2 = 0.99$).

Binding between the dextrin coating on AuNP and amino/glycan ligands of MNP in the negative controls again showed saturation levels in Figure 7.7A. This binding dynamic results in negative controls with higher AuNP signaling than for the sample MNP-cell-AuNP complexes, seen in the 30-min sample response. Both the AuNP peak height and step-integrated spectral area for the negative controls showed greater response at 30 min than for the samples at 30 min (Fig. 7.7B). Although this dynamic can create an inherent detection limit for bacterial presence in liquid food samples, these limitations may be overcome using optimized levels of MNP and AuNP in electrochemical nano-biosensing.

7.3.4 Electrochemical Quantification of MNP-cell-AuNP

Economical carbohydrate-based nano-biosensors currently show broad selectivity in pathogen detection for total load of bacterial contamination present. As more selective carbohydrate ligands are identified, though, they can easily be applied to a proof-of-concept method described here. This method uses amino/glycan-functionalized magnetic nanoparticles (MNP-F#2) for rapid microbial extraction and concentrated dextrin-coated gold nanoparticles (AuNP) for electrically-active labeling, coupled with electrochemical signaling. Testing was carried out in undiluted vitamin D milk to demonstrate the ability of the biosensor to perform rapid detection of bacterial presence in a complex matrix.

In conjunction with another project, non-pathogenic *E. coli* C3000 was used as a model microbe strain to allow easier transfer of samples between colleagues without pathogenic contamination concerns. Applying the properties of minimized volumetric sampling discussed earlier for trial 9 in Table 7.1, 50 μL of serially diluted cell culture was simultaneously exposed to 50 μL of MNP and 250 μL of concentrated AuNP (“AuNP250”), plus 100 μL PBS. Negative controls followed the same procedure except without cells. The resulting MNP-cell-AuNP or MNP-AuNP complexes were magnetically separated and re-suspended in 100 μL PBS for DPV detection or 1000 μL PBS for spectral detection.

Sample complexes were significantly distinguished from negative controls in both electrochemical DPV (Fig. 7.8A for 5 log CFU/mL) and spectral signaling (Fig. 7.8B for 3 log CFU/mL) ($p < 0.2$) using this one-step simultaneous capture-n-label process in undiluted milk. As covered earlier, binding dynamics showed more seemingly selective AuNP attachment to the cell surface as seen in Figure 5.5B while saturating the MNP surface (Fig. 5.6B). Meanwhile, cell attachment to the MNP limits the AuNP exposure to the MNP surface. These binding patterns

resulted in higher signaling for negative controls (MNP-AuNP) than for samples “MNP-e5Ec-AuNP” for DPV signaling and “MNP-e3Ec-AuNP” for spectral signaling, as seen in Figures 7.8A & B, respectively.

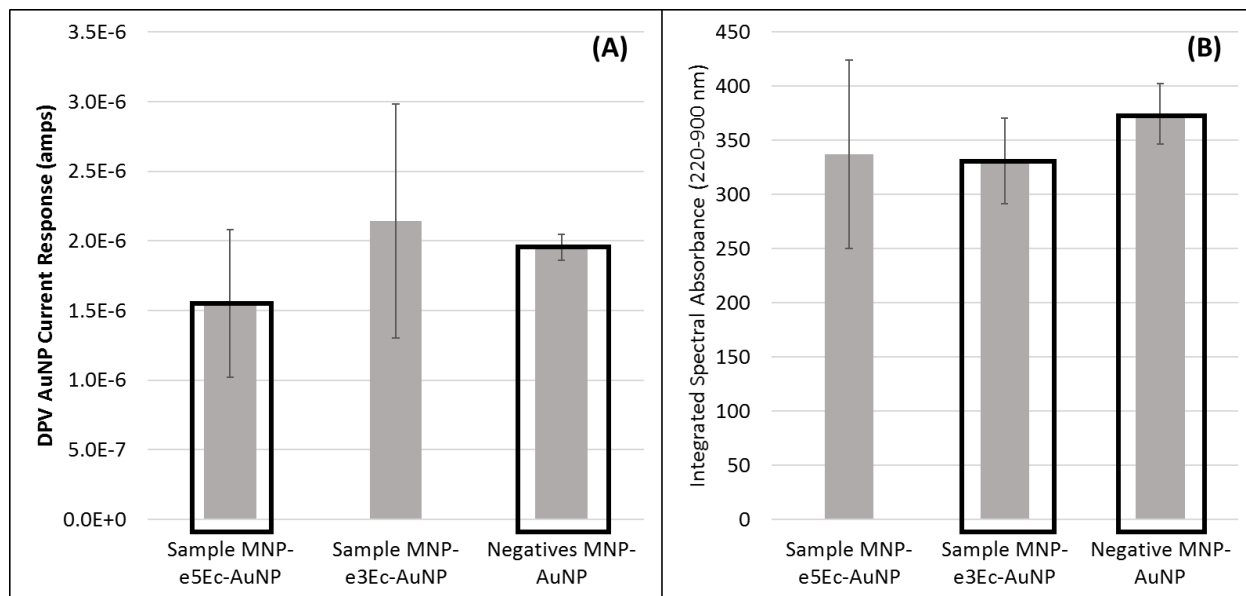


Figure 7.8 Electrochemical nano-biosensing for simultaneous carbohydrate-based MNP-*E. coli*-AuNP rapid extraction from milk and electrically-active labeling followed by (A) DPV or (B) spectral analysis of samples and negative controls for microbial detection in milk (n=3). “e5Ec” = log 5 CFU/mL *E. coli* and “e3Ec” = log 3 CFU/mL *E. coli*.

For both signaling methods, DPV and spectral, current responses and spectral absorbances were inversely related to cell concentration, due to the selective binding of AuNP to cell surface markers. Even though spectral signaling was able to detect at 3 log CFU/mL, samples that contained 5 log CFU/mL *E. coli* showed similar step-integrated spectral absorbance (Fig. 7.8B). This was due to a high response of one replicate, which also caused insignificant separation from negative controls ($p = 0.28$). Meanwhile samples that contained 3 log CFU/mL *E. coli* in DPV sampling showed insignificant separation ($p = 0.37$) from the negative control. DPV biosensing was less sensitive for the current method parameters most likely due to insufficient HCl to react

with the AuNP present in the negative controls, reducing separation (Fig. 7.8B). Separation between the two DPV samples at the different concentrations was significant though ($p < 0.2$).

Reproducibility within the sample replicates is lower (greater standard deviation) than for negative controls in both detection methods, as can be seen in Figures 7.8A & B. In addition, the current sampling method resulted in minimal separation in current response or spectral absorbance between samples and negative control responses (Figs. 7.9A & B). Only $0.4 \text{ E-}6$ amps separated DPV samples at 5 log CFU/mL from the negative controls for the AuNP current response. Spectral scans between both samples and the negative control were separated by an absorbance of 0.05 and step-integrated spectral absorbance of approximately 40. This aspect would need to be addressed in future method optimization to both improve detection sensitivity and increase significance in sample and negative control separation. Particularly for samples, though, cell sizes are much greater than nanoparticle sizes, showing the robust MNP extraction properties. But in the current minimized volume method, as pathogenic bacteria cell concentrations decrease, too few cells may

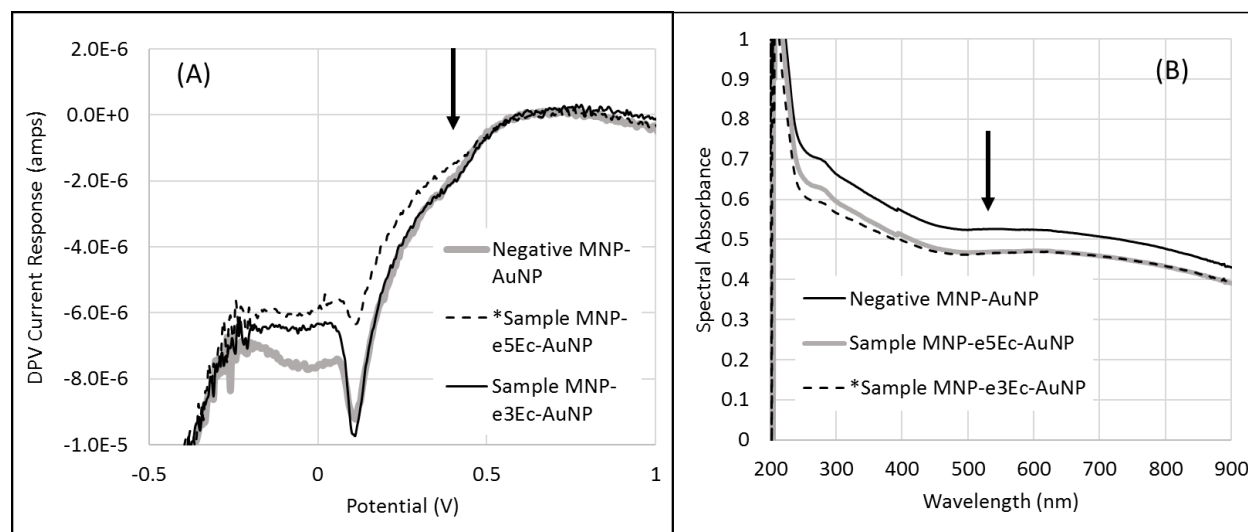


Figure 7.9 Graphs for electrochemical nano-biosensing for simultaneous carbohydrate-based MNP-*E. coli*-AuNP rapid extraction and electrically-active labeling followed by (A) DPV or (B) spectral analysis of samples and negative controls for microbial detection in milk ($n=3$). Arrows identify (A) 0.4 V and (B) 520 nm for the AuNP response location. “e5Ec” = $\log 5 \text{ CFU/mL } E. coli$ and “e3Ec” = $\log 3 \text{ CFU/mL } E. coli$.

be extracted to prevent saturation binding of AuNP to the exposed MNP surface to distinguish from negative controls.

The spectral method here may be more sensitive than DPV, detecting 3 log CFU/mL, since spectral scans do not require activation of the AuNP with HCl, but detect total sample contents. DPV biosensing was not able to distinguish between 3 log CFU/mL and zero cells most likely due to the expense of the MNP and milk component reactions with HCl, reducing the overall AuNP activation. In addition, the amount of bound AuNP onto MNP in negative controls may exceed the reactive character of HCl for complete activation, arbitrarily reducing the negative control response itself. Future work would focus on optimizing the assay to improve sensitivity of the tests in microbial detection focusing initially on improving negative control signaling separation from sample signaling. During early development work in PBS, the AuNP peak was clearly visible in spectrometry (Fig. 7.7A) and DPV detection (Fig. 7.5B). But in milk, the MNP-cell-AuNP peaks are masked since milk components also attached to both MNP and AuNP (Figures 7.9A & B). Optimization work would also include determining the volume of HCl required to react with all components present in the MNP-cell-AuNP complex. As more selective carbohydrate ligands are identified, such as described earlier in the literature review, greater specificity will also improve limits of detection for targeted pathogens. Finally, identifying common complex matrix component effects upon sampling would allow faster application to new liquid or homogenized foods. This rapid, economical MNP-cell-AuNP biosensing method could then be easily applied to other liquid foods which would make our food supply more secure through affordable rapid detection.

7.4 Conclusions

Combining carbohydrate-functionalized MNP cell capture, MNP-cell concentration, and concentrated dextrin-coated AuNP labeling resulted in promising nano-biosensing development towards the goal of feasible, less complicated tests. Much work in nano-biosensing development has focused heavily on designing highly specific, one-time-use “strip” sensors that involve substantial technology to produce. These are not cost-effective for many worldwide food suppliers, though. Even many of similarly suspended MNP/EANP biosensing assays that utilized antibodies or DNA ligands are still out of reach for many users, requiring special storage or highly technical detection equipment.

Carbohydrate ligands are easily incorporated onto nanoparticles, and require little special handling, showing a long shelf life at room temperature. As more selective carbohydrate ligands are identified and incorporated into MNP-cell-AuNP assays, consumers can be assured of safer food supplies free of targeted pathogens at affordable costs. While the proof-of-concept test presented here requires optimization for detection at lower cell concentrations, it was successful in detecting *E. coli* presence directly from milk within 45 min, whereas many reported tests reviewed earlier were studied only in simple buffer solution, or required extensive sample handling before the final “rapid” step. The future in nano-biosensing is not in developing more technically complex sensors, but applying technological know-how to develop inexpensive, user-friendly microbial assays.

Chapter 8. Conclusions

Frequent and reliable detection of foodborne pathogens would provide both consumer food security and supplier economic safety. As cautioned earlier though, biosensing must FIRST address the broad goals of any biosensor: Field operability, Inexpensive, with Real-time detection that is both Sensitive and Specific to target, while being as Trouble-free as possible (FIRST). Throughout development of these biosensing assays focus was placed on economical solutions to microbial assays that minimize sample handling and user-required technology while making use of stable carbohydrate-functionalized nanoparticles to provide broad-based detection. MNP-strip and MNP-cell-AuNP biosensing methods developed here use versatile magnetic nanoparticle (MNP) extraction, electrically active nanoparticles (EANP) labeling, and carbohydrate-based ligand chemistry.

Nano-biosensing can be an economical method to both detect and quantify the presence of pathogenic bacteria, when developed with the mindset that sometimes the beauty of a test is not in the amount of technology that is incorporated into the biosensing method or biosensor design that only one person can interpret, but that this technology is used to design a simple biosensing method and result that can be understood by all. Inexpensive food carbohydrate functional groups can reliably attach to pathogenic bacteria, and when immobilized onto MNP, easily extract, and concentrate, them from liquid/liquified food samples using a common magnet. Further, MNP-strips functionalized with carbohydrate ligands provide a viable option when faced with homogenized food products that are too thick and resist magnetic pull during separation. The amino/glycan ligand used in this study preferentially bound cells over complex matrix components. Gold nanoparticles coated with dextrin, another carbohydrate, also attach to captured bacteria and provide an inexpensive, quick method to substantially increase detection signal

strength, whether by electrochemical or spectrophotometric means. Nano-biosensing using these three options: MNP-cell, MNP-strip-cell or MNP-cell-AuNP, was then able to quickly distinguish between samples with cells against negative controls without cells present.

Electrochemical detection, although complicated in theory, can easily be reduced to positive and negative results. CV and DPV detection require a simple hand-held potentiostat unit that utilizes cheap, disposable printed chips to quantify the captured bacterial response, with or without the presence of AuNP. Spectrophotometers are more commonly available in even smaller research and food industry testing laboratories. AuNP presence provided enhanced signaling in electrochemical DPV detection as well as spectrophotometric methods. MNP-strip with CV could detect *E. coli* in milk at 8.5 log CFU/mL (S/N = 1.08, $p < 0.05$), whereas MNP-cell-AuNP with DPV could detect 5 log CFU/mL (S/N = 0.79, $p < 0.20$) or with spectrophotometry could detect 3 log CFU/mL (S/N = 0.88, $p < 0.20$). A nano-biosensor that is not designed as a self-contained unit for a single test, but takes advantage of reusable technology, along with taking only minutes to prepare, would greatly assist countries in ensuring safe food supplies.

Even though TEM imaging of MNP-cell complexes could identify differences in attachment for MNP-F#1 and MNP-F#2 to the cell surface, both MNP showed no significant difference in suspended capture in either simple or complex matrices. As development continued though, it was necessary to identify one preferred MNP to minimize expended resources. During capture in homogenized egg, it was apparent that suspended MNP capture had its limits, as the MNP-*Salmonella* complexes were unable to migrate to the magnet for separation. MNP-strips were prepared using both MNP-F#1 and MNP-F#2 and compared for their ability to capture bacteria. MNP-F#2-strips outperformed all other types (non-functionalized and amino or glycan

alone without MNP), specifically capturing over two times the cells as MNP-F#1-strips. Therefore, research was carried forward focusing only on MNP-F#2.

Just as homogenized egg prevented suspended MNP-cell migration during magnetic separation, complex matrix components were found to effect CV responses. The liquid food matrices evaluated were milk, beef juices, apple cider and homogenized egg, with varying amounts of carbohydrates, fats, proteins and sodium. Although carbohydrates showed no significant effect upon CV signaling, sodium and fats had a negative effect, while proteins had a positive effect. Most of all, complexity showed the greatest effect, where PBS and beef juices, containing minimal salts and proteins, respectively, resulted in negative control signals higher than corresponding samples. These matrices were mostly composed of water, with beef juices having minimal proteins to bind and PBS containing minimal phosphates, sodium- and potassium-chloride to interfere with signaling. Whereas, milk, apple cider, and of course homogenized eggs, all rich in sodium among other components, caused negative control signaling that was lower than corresponding samples since attached matrix components expended significantly more of the chemical mediator.

Electrically active AuNP were applied as a means to intensify electrochemical signaling. Anti-*Salmonella* antibody were immobilized onto d-AuNP (Ab-AuNP) in attempts to use MNP-cell-Ab-AuNP complexes as a means to specificity of MNP capture of *Salmonella* microbes in a complex milk matrix. DPV results, though, were unreliable across a range of parameters. Principal component analysis (PCA) of the data across ten trials showed that there was a closer relationship between samples and negative controls from a particular trial, than even samples of different trials prepared at the same microbial concentration. Eventually, it was determined that several parameters created the unreliable performance. Although the electrostatic bonds between the carbohydrate ligands and cell surface molecules are similar to antibody binding, the current

amino/glycan carbohydrate ligands bind at weaker strength. A fraction of these bonds also break upon each new suspension in fresh matrix, creating a “chemical” equilibrium between MNP-cell complexes and cells suspended in the matrix, reducing cell presence with each rinse. Additionally, the antibody was found to equally bind both target *Salmonella* and non-target *E. coli* cells, as well as saturating the MNP carbohydrate ligands for negative controls.

Although carbohydrate ligands will show less selectivity and lower binding strength than antibody ligands, nano-biosensing using carbohydrate-based nanoparticles such as with MNP-F#2-*E. coli*-AuNP showed the ability to detect microbial presence with an economical method. Having identified capture concerns due weak electrostatic binding allowing cell loss with rinsing steps in early experimental work, the MNP capture and AuNP labeling steps were thereafter carried out simultaneously, or as a “one-step” method. Minimal sampling volumes were also used to reduce cell loss to the surrounding matrix and increase cell-nanoparticle vicinity. Additionally, excess dextrin coating was removed from the AuNP, concentrating them while allowing enhanced labeling of samples. Resulting DPV and spectrometer signaling successfully allowed detection at lower microbial concentrations than MNP-cell signaling with CV.

Specifically addressing the hypotheses of this research, hypothesis one dealt with testing that magnetic nanoparticles (MNP) coated with carbohydrates, without the presence of antibodies, will still rapidly bind, extract, and concentrate microbial pathogens from complex liquid food matrices to reduce the rate of false negatives without initial sample preparation whether as suspended MNP or immobilized onto plastic strips. MNP functionalized with glycan (MNP-F#1) or amino/glycan (MNP-F#2) ligands were able to bind pathogenic bacteria *Salmonella*, *E. coli*, and *Bacillus* in both simple PBS and complex milk matrices and concentrate them into 1 mL (for larger volume capture, LVC) and 500 μ L (for small volume capture, SVC) volumes. LVC was

used to simulate BAM methods requiring sample sizes of 25 gm, which was approximated with 25 mL of liquid matrix. In LVC, both MNP were able to capture over 3 ppt and up to 120 ppt of the bacteria present, while even capturing up to 600 ppt in SVC with single or multiple bacteria present. In more acidic matrices such as beef juices or apple cider, capture was approximately 10 ppm. Immobilized MNP-F#2 onto plastic strips (MNP-strip) captured bacteria in PBS and reliably reported their concentration from 3 to 5 log CFU/mL using a 4-hr liquid media growth and plating detection method.

Second, it was hypothesized that electrochemical instrumentation will simplify testing methods for accelerated pathogen detection of MNP-extracted microbial pathogens from complex food matrices despite the presence of food components. Electrochemical cyclic voltammetry (CV) detection takes only 30 min from assay start and eliminates the time required to grow the captured bacteria on agar media for suspended MNP capture or in liquid media for MNP-strip capture. Suspended MNP capture showed significant separation between samples and negative controls for *E. coli* capture in beef juices ($p < 0.05$), and capture of *Salmonella* in milk and *Listeria* in apple cider ($p < 0.15$). CV also similarly expedited MNP-strip detection of *Salmonella* presence in PBS, showing a linear response between 2 to 6 log CFU/mL ($R^2 = 0.71$) with a limit of detection for true positive response ($S/N < 1.0$) at 3.6 log CFU/mL ($S/N = 0.92$). MNP-strip capture in complex matrices clearly showed the effect of matrix composition on the resulting CV signaling. This was due to the binding of matrix components to the MNP-strip ligands, with simple matrices PBS or beef juices resulting in $S/N < 1$, while milk, apple cider or homogenized egg components caused $S/N > 1$. CV biosensing was able to distinguish between sample capture and negative control responses for capture of *Salmonella* in PBS, *E. coli* in beef juices, *Salmonella* in homogenized egg, *Listeria* in apple cider, and *E. coli* in vitamin D milk ($p < 0.10$). These results in the initial

MNP-strip design were for microbial concentrations between 6.19 to 12.3 log CFU/mL, all above industry testing standards, but show good progress in developing a rapid, accurate microbial assay requiring minimal sample preparation and little liquid handling. Additional advance in the assay design was made in identifying the effect that the sodium, fats and proteins present in the liquid matrices had upon the normalized peak current response (NPCR).

Finally, it was shown that concentrated, dextrin-coated gold nanoparticles, without the presence of antibodies, will rapidly label MNP-extracted microbial pathogens to reduce false positives by better separation from negative controls even in the presence of complex liquid food matrices through enhanced electrochemical instrumental. This biosensing method was most successful when carried out in smaller volumes and in a simultaneous MNP-capture with AuNP-label procedure. Dextrin-coated AuNP labeling was found to saturate the surface of MNP and selectively bind the microbial surfaces more selectively. This resulted in electrochemical signaling that showed higher signaling for negative controls (MNP/AuNP) than samples (MNP-cell-AuNP) which creates a limit to significantly detecting a microbial load when too few are present. The current design was able to detect *E. coli* in vitamin D milk at 3 log CFU/mL using spectral signaling, but only 5 log CFU/mL using differential pulse voltammetry (DPV) ($p < 0.20$). Although these limits meet testing needs within the milk industry in providing a rapid assay without sample preparation, improving this assay to detect at 1 log CFU/mL, or even 1 CFU/mL would require optimizing the amount of MNP and AuNP present.

Nano-biosensing microbial contamination in liquid foods using MNP-strip-cell/CV or MNP-cell-AuNP/DPV/spectral methods can provide the food industry with economical, rapid assays and under/developing countries with simple, affordable assays to minimize microbial foodborne outbreak events. A cost-benefit analysis, comparing assay cost with the technology

required for detection shown in Fig. 8.1 identifies the niche that these methods fill. Although the current carbohydrate ligands target broad-based microbial presence, they have proven their ability to detect microbes without the necessity of first removing the food components or the need to increase the microbial load, reducing both testing time and supplies cost. They are also user-friendly, requiring little training to apply, while using more common spectral instrumentation or inexpensive potentiostat technology. MNP-strip/CV detection allows minimal sample handling when suspected bacterial loads are higher than 6 log CFU/mL. Significant separation between the negative control and sample NPCR currently requires a higher bacterial load, but entire assay time from extraction to detection is under 30 min and allows a yes/no response. If minimal sample handling is still desired for suspected lower microbial load between 3 to 5 log CFU/mL, the cells captured on the MNP-strip may be grown in liquid media for 4 hr, recaptured with a fresh MNP-strip and then tested for microbial presence with CV. More sensitive direct detection is possible using the one-step MNP/AuNP capture and labeling method, currently for loads between 3 to 5 log CFU/mL, using samples even under 500 μ L, with detection possible by either handheld potentiostat for DPV or spectrometry. DPV detection does allow for immediate testing in the field using a simple magnet to separate the prepared sample from the matrix and a handheld potentiostat. Whereas when bulk sample processing is preferred, numerous samples may be simultaneously handled, and spectral detection completed in minimal time, such as 30 samples tested in 1 hr.

Food safety for people in both the US and worldwide has repeatedly proven elusive as we experience multiple microbial foodborne outbreaks each year that threaten the safety of our food supplies. In the US, the CDC monitors foodborne outbreaks and noted that between 1996 and 2010 microbial outbreaks did decrease but still reported over 19,000 infections and 71 deaths in 2014 from the ten top microbial pathogens [278]. Worldwide, the WHO reports on the status of the

human population, including the occurrence of over 400,000 deaths in 2010 from microbial, viral and protozoan sources [1]. The United Nations officials assert that food safety is entwined with food security and that ensuring the securing safe food supplies will also improve human economic growth [279] through reduced medical costs due to disease and increased work hours for a healthy populace. Frequent testing along the food supply chain, from source to store, will more readily identify contaminated product before it reaches the consumer, increasing consumer confidence that they are purchasing a safe food product. The affordable, user-friendly nano-biosensor assays developed in this research will advance this goal of a more secure food supply since it combines emerging robust carbohydrate-ligands with user-friendly nanoparticle technology and rapid electrochemical detection, as summarized earlier. Simply determining whether a food product is free from a microbial load, or below a specific tolerance level, using these broad-based detection

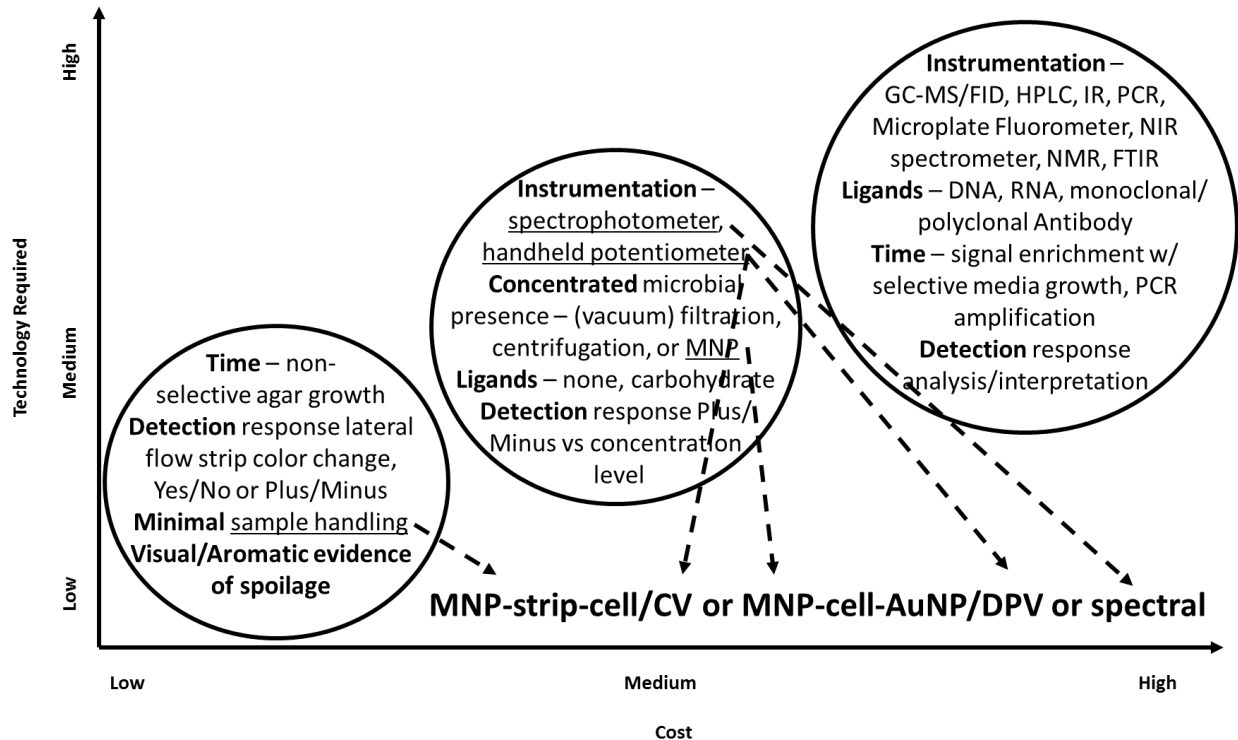


Figure 8.1 Cost-benefit analysis of microbial contamination detection in the food supply chain including (nano-) biosensing methods. (see text for acronym definitions)

assays will allow this product to continue along the food supply chain.

Future improvements in these MNP-based nano-biosensing methods will require focus on the FIRST considerations identified earlier. Of utmost importance is improving the level of capture experienced by the MNP above the current 100 ppt and 10 ppm levels. This will in turn improve the level of detection and reliability of the test, which must be addressed in the design of final assay for pathogenic bacteria in a liquid food sample. False negative results can be reduced by minimizing the quantity of MNP required to capture microbial loads below 5 log CFU/mL, thereby eliminating the masking effect of excessive MNP in electrochemical testing. Identification of more effective carbohydrate ligands which will both bind more readily and securely to the targeted pathogens will further increase secure capture and allow additional reduction in MNP. The search for tighter-binding, yet still economically-feasible, carbohydrate ligands can be achieved through exclusion assays comparing novel carbohydrate-functionalized MNP extraction levels in selected complex matrices for statistically significant improvement. Broad-based capture is still desirable since these assays, as an initial test for possible microbial presence, keep testing costs lower in comparison to selective antibodies, while improving detection at lower levels of food contamination. For food suppliers that handle both small and large quantities of perishable liquid product, these simpler nano-biosensing methods also allow high throughput product movement since the assay will provide a response within 30 min.

Reliability and reproducibility go hand-in-hand in assay design, but first reliability must be addressed in future MNP/AuNP nano-biosensing improvements. Current assay reliability has only been tested at microbial levels that targeted 3 log CFU/mL concentrations in PBS with respect to diluting log-growth culture at approximately 8 log CFU/mL by 10^{-5} . Within complex matrices rich in nutrients, though, the actual level of bacterial presence during assay conditions was between 3

to 5 log CFU/mL for milk, and as high as 6 log CFU/mL in beef juices and apple cider, due to accelerated bacterial growth. In these early stages of MNP/AUNP assay development, reliable capture across a broad range of microbial concentrations was not investigated, therefore reliability at different concentrations will need to be established. In addition, MNP capture showed minimal reproducibility, with only 2 out of 3 replicates for LVC within one standard deviation of the mean. Both accuracy and precision of the assays would need to be improved beyond this first design stage, again through increased extraction capability at lower microbial contamination levels more pertinent to the food industry and optimization of the MNP quantity to sample volume ratio per matrix type.

MNP capture and AuNP labeling of bacteria takes advantage of the drive of pathogenic microbes to survive. Microbial cell surfaces provide numerous molecular structures for their attachment to other cells or surfaces so that they may extract nutrients for survival from the surrounding environment. As more selective carbohydrates are identified that attach to targeted bacteria, their application as ligands for MNP-cell-AuNP nano-biosensing will substantially increase selectivity and specificity of the assay. Optimization of the significant parameters must be considered for particular matrices, especially the complexity of the matrix components and their effect upon voltammetric signaling. In addition, capture volume, MNP and AuNP quantities, and HCl volume will require optimization to further improve both reliability and sensitivity of this biosensing method. Used in conjunction with optical or electrical detection of gold nanoparticles (AuNP), carbohydrate-functionalized MNP-cell-AuNP nano-biosensing advances the goal of being the FIRST biosensor of choice in detecting microbial pathogens throughout our food supply chain.

APPENDIX

Supplementary Data

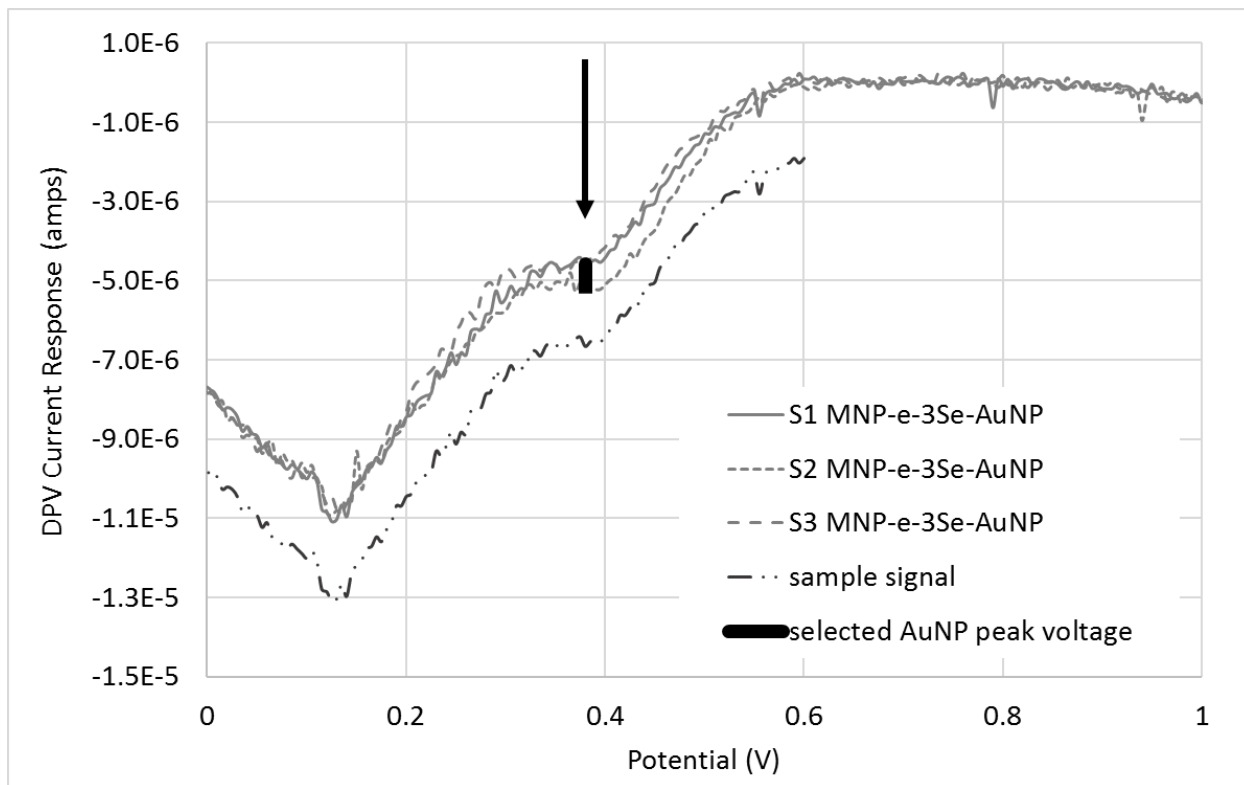


Figure S8.2 Example of adjusted DPV current response for MNP-F#2-cell-Ab-AuNP nano-biosensing, showing corrected baseline with respect to average current response between 0.9 V to 0.6 V; identifying maximum (average) AuNP response potential (arrow, 0.38 here); and portion of a sample signal for clarity during visual data analysis.

Table S7.2 Specificity of *Salmonella* detection using antibody-functionalized AuNP.

Trial	Capture Matrix	Pathogen*	n Samples	Cells Available for Capture (log CFU/mL)	MNP Capture Index +/- St. Dev. (ppt)	Post Ab-AuNP Capture Index (ppt) [®]	Sample AuNP Peak Ht. Ave. (amps)	Sample AuNP Peak Ht. St. Dev. (amps)	Negative AuNP Peak Ht. Ave. (amps)	Negative AuNP Peak Ht. St. Dev. (amps)	t-test [†] p-value	AuNP Peak S/N Ave.
1	PBS	Se Target	3	3.12	170 +/- 28	40	1.17E-05	8.47E-13	1.35E-05	3.12E-12	0.23	0.87
2	PBS	Se Target	6	2.76	520 +/- 214	76	1.05E-05	7.04E-14	1.26E-05	2.42E-12	0.04	0.83
3	Milk	Se Target	6	3.40	763 +/- 285	21	6.32E-06	1.23E-12	6.57E-06	3.76E-13	0.79	0.96
4	Milk	Se Target	6	3.30	935 +/- 159	346	5.87E-06	2.79E-12	5.92E-06	2.65E-12	0.97	0.99
5	Milk	Se Target	6	5.14	14.4 +/- 3	0.9	4.76E-06	7.44E-13	4.74E-06	5.14E-13	0.98	1.00
6	Milk	Se Target	3	9.08	1.48 +/- 0.21	0.01	3.83E-06	1.89E-12	6.36E-06	1.51E-12	0.08	0.60
		Se Target	3	8.08	0.62 +/- 0.09	0.01	2.88E-06	2.71E-12	6.36E-06	1.51E-12	0.04	0.45
		Se Target	3	7.08	1.45 +/- 0.22	0.03	5.72E-06	6.76E-12	6.36E-06	1.51E-12	0.72	0.90
7	Milk	Se Target	3	6.95	0.23 +/- 0.13	0.00	7.57E-06	2.63E-12	8.81E-06	8.23E-13	0.31	0.86
		Se Target	3	5.95	0.99 +/- 0.22	0.04	9.86E-06	2.04E-14	8.81E-06	8.23E-13	0.12	1.12
		Se Target	3	4.95	1.33 +/- 0.71	0.00	7.24E-06	4.56E-13	8.81E-06	8.23E-13	0.07	0.82
8	Milk	Se Target	3	5.57	7640 +/- 1282	135	5.43E-06	1.41E-13	4.12E-06	1.98E-12	0.19	1.32
		Se Target	3	4.57	8108 +/- 8108	622	7.09E-06	3.46E-12	4.12E-06	1.98E-12	0.09	1.72
		Se Target	3	3.57	8108 +/- 8108	751	3.99E-06	1.49E-13	4.12E-06	1.98E-12	0.88	0.97
9	PBS	Se Target	3	5.69	NA	12	4.78E-06	7.75E-14	6.50E-06	3.76E-13	0.01	0.74
		Se Target	3	4.69	NA	14	4.58E-06	3.68E-13	6.50E-06	3.76E-13	0.02	0.70
		Ec Non-target	3	5.94	NA	1	5.12E-06	1.58E-12	6.50E-06	3.76E-13	0.16	0.79
10	PBS	Se Target	3	4.90	NA	103	3.32E-06	3.52E-13	3.69E-06	5.49E-13	0.54	0.90
		Ec Non-target	3	5.63	NA	0.08	3.56E-06	1.41E-14	3.69E-06	5.49E-13	0.79	0.97

* Se = *Salmonella* Enteritidis, Ec = *E. coli* O157:H7; + reported two-tail p-values for t-test ran for unpaired samples and negative controls within same trial test, assuming equal variances; # S/N = AuNP current response ratio for Samples to Negative controls.

BIBLIOGRAPHY

BIBLIOGRAPHY

- [1] WHO, “WHO estimates of the global burden of foodborne diseases,” *Food Safety*, 2015. [Online]. Available: http://www.who.int/foodsafety/areas_work/foodborne-diseases/ferg/en/.
- [2] L. L. Matta, S. Karuppuswami, P. Chahal, and E. C. Alocilja, “AuNP-RF Sensor: An innovative application of RF technology for sensing pathogens electrically in liquids (SPEL) within the food supply chain,” *Biosens. Bioelectron.*, p. 12, 2018.
- [3] L. L. Matta and E. C. Alocilja, “Carbohydrate Ligands on Magnetic Nanoparticles for Centrifuge-Free Extraction of Pathogenic Contaminants in Pasteurized Milk,” *J Food Prot*, vol. 00, no. 00, p. 10, 2018.
- [4] L. L. Matta, J. Harrison, G. Deol, and E. C. Alocilja, “Carbohydrate-functionalized Nano-Biosensor for Rapid Extraction of Pathogenic Bacteria Directly from Complex Liquids with Quick Detection Using Cyclic Voltammetry,” *Ieee Trans. Nanotechnol.*, vol. Special Issue 2018, p. 9, 2018.
- [5] Y. Wang, P. A. Fewins, and E. C. Alocilja, “Electrochemical Immunosensor Using Nanoparticle-Based Signal Enhancement for Escherichia Coli O157:H7 Detection,” *IEEE Sens. J.*, vol. 15, no. 8, pp. 4692–4699, Aug. 2015.
- [6] Y. Wang and E. C. Alocilja, “Gold nanoparticle-labeled biosensor for rapid and sensitive detection of bacterial pathogens,” *J. Biol. Eng.*, vol. 9, no. 16, pp. 1–7, Dec. 2015.
- [7] E. C. Alocilja, “BE 445/845 –Biosensors for Medical Diagnostics,” presented at the BE 845 Biosensors for Medical Diagnostics, Michigan State University, 12-Jan-2015.
- [8] FDA, “Bacteriological Analytical Manual (BAM),” *U.S. Department of Health and Human Services*, 2003. [Online]. Available: <https://www.fda.gov/Food/FoodScienceResearch/LaboratoryMethods/ucm2006949.htm>. [Accessed: 18-Apr-2017].
- [9] M. Adams, M. O. Moss, and P. McClure, *Food Microbiology*. 2015.
- [10] R. Koncki, “Recent developments in potentiometric biosensors for biomedical analysis,” *Anal. Chim. Acta*, vol. 599, no. 1, pp. 7–15, Sep. 2007.
- [11] S. Roy and Z. Gao, “Nanostructure-based electrical biosensors,” *Nano Today*, vol. 4, no. 4, pp. 318–334, Aug. 2009.

- [12] J. W.-F. Law, N.-S. Ab Mutalib, K.-G. Chan, and L.-H. Lee, "Rapid methods for the detection of foodborne bacterial pathogens: principles, applications, advantages and limitations," *Front. Microbiol.*, vol. 5, Jan. 2015.
- [13] M. Pumera, S. Sánchez, I. Ichinose, and J. Tang, "Electrochemical nanobiosensors," *Sens. Actuators B Chem.*, vol. 123, no. 2, pp. 1195–1205, May 2007.
- [14] R. Fogel and J. Limson, "Developing Biosensors in Developing Countries: South Africa as a Case Study," *Biosensors*, vol. 6, no. 1, p. 5, Feb. 2016.
- [15] S. Dehdashtian, M. B. Gholivand, M. Shamsipur, A. Azadbakht, and Z. Karimi, "Fabrication of a highly sensitive and selective electrochemical sensor based on chitosan-coated Fe₃O₄ magnetic nanoparticle for determination of antibiotic ciprofloxacin and its application in biological samples," *Can. J. Chem.*, vol. 94, no. 10, pp. 803–811, Oct. 2016.
- [16] S. Dehdashtian, M. B. Gholivand, M. Shamsipur, and S. Kariminia, "Construction of a sensitive and selective sensor for morphine using chitosan coated Fe₃O₄ magnetic nanoparticle as a modifier," *Mater. Sci. Eng. C*, vol. 58, pp. 53–59, Jan. 2016.
- [17] A. M. Fernandes *et al.*, "Development of highly sensitive electrochemical genosensor based on multiwalled carbon nanotubes-chitosan-bismuth and lead sulfide nanoparticles for the detection of pathogenic *Aeromonas*," *Biosens. Bioelectron.*, vol. 63, pp. 399–406, Jan. 2015.
- [18] D. Galbraith, "Crap in, crap out: Flushing Out The Problems in Your Flow Cytometry Data," *Bitesize Bio*, 09-Sep-2014.
- [19] T. S. Gunasekera, P. V. Attfield, and D. A. Veal, "A Flow Cytometry Method for Rapid Detection and Enumeration of Total Bacteria in Milk," *Appl. Environ. Microbiol.*, vol. 66, no. 3, pp. 1228–1232, Mar. 2000.
- [20] A. V. Hadjinicolaou, V. L. Demetriou, J. Hezka, W. Beyer, T. L. Hadfield, and L. G. Kostrikis, "Use of molecular beacons and multi-allelic real-time PCR for detection of and discrimination between virulent *Bacillus anthracis* and other *Bacillus* isolates," *J. Microbiol. Methods*, vol. 78, no. 1, pp. 45–53, Jul. 2009.
- [21] X. Kang, G. Pang, Q. Chen, and X. Liang, "Fabrication of *Bacillus cereus* electrochemical immunosensor based on double-layer gold nanoparticles and chitosan," *Sens. Actuators B-Chem.*, vol. 177, pp. 1010–1016, Feb. 2013.
- [22] Z. Li, Y. Li, X.-F. Qian, J. Yin, and Z.-K. Zhu, "A simple method for selective immobilization of silver nanoparticles," *Appl. Surf. Sci.*, vol. 250, no. 1–4, pp. 109–116, Aug. 2005.
- [23] Y. Sun *et al.*, "Direct immobilization of DNA probes on non-modified plastics by UV irradiation and integration in microfluidic devices for rapid bioassay," *Anal. Bioanal. Chem.*, vol. 402, no. 2, pp. 741–748, Oct. 2011.

- [24] E. A. Berger and L. A. Heppel, "A binding protein involved in the transport of cystine and diamino pimelic acid in *Escherichia coli*," *J. Biol. Chem.*, vol. 247, no. 23, pp. 7684–7694, 1972.
- [25] P. Chen, Y. Li, T. Cui, and R. Ruan, "Nanoparticles based sensors for rapid detection of foodborne pathogens," *Int. J. Agric. Biol. Eng.*, vol. 6, no. 1, pp. 28–35, Mar. 2013.
- [26] K. C. de Souza, G. F. Andrade, I. Vasconcelos, I. M. de Oliveira Viana, C. Fernandes, and E. M. B. de Sousa, "Magnetic solid-phase extraction based on mesoporous silica-coated magnetic nanoparticles for analysis of oral antidiabetic drugs in human plasma," *Mater. Sci. Eng. C*, vol. 40, pp. 275–280, Jul. 2014.
- [27] E. Lesman-Movshovich and N. Gilboa-Garber, "Pseudomonas aeruginosa lectin PA-IIL as a powerful probe for human and bovine milk analysis," *J. Dairy Sci.*, vol. 86, no. 7, pp. 2276–2282, 2003.
- [28] L. A. Pratt and R. Kolter, "Genetic analysis of *Escherichia coli* biofilm formation: roles of flagella, motility, chemotaxis and type I pili," *Mol. Microbiol.*, vol. 30, no. 2, pp. 285–293, 1998.
- [29] L. L. Matta and E. C. Alocilja, "Emerging nano-biosensing with suspended MNP microbial extraction and EANP labeling," *Biosens. Bioelectron.*, vol. 117, pp. 781–793, Oct. 2018.
- [30] L. A. Dykman and N. G. Khlebtsov, "Gold Nanoparticles in Biology and Medicine: Recent Advances and Prospects," *Acta Naturae*, vol. 3, no. 2, pp. 34–55, 2011.
- [31] J. Hwang, D. Kwon, S. Lee, and S. Jeon, "Detection of Salmonella bacteria in milk using gold-coated magnetic nanoparticle clusters and lateral flow filters," *Rsc Adv.*, vol. 6, no. 54, pp. 48445–48448, 2016.
- [32] Y.-L. Kuo *et al.*, "Functional gold nanoparticle-based antibacterial agents for nosocomial and antibiotic-resistant bacteria," *Nanomed.*, vol. 11, no. 19, pp. 2497–2510, Oct. 2016.
- [33] Y. Liu, Y. Du, and C. M. Li, "Direct Electrochemistry Based Biosensors and Biofuel Cells Enabled with Nanostructured Materials," *Electroanalysis*, vol. 25, no. 4, pp. 815–831, Apr. 2013.
- [34] N. Sattarahmady, G. H. Tondro, M. Gholchin, and H. Heli, "Gold nanoparticles biosensor of *Brucella* spp. genomic DNA: Visual and spectrophotometric detections," *Biochem. Eng. J.*, vol. 97, pp. 1–7, May 2015.
- [35] M. S. Verma, J. L. Rogowski, L. Jones, and F. X. Gu, "Colorimetric biosensing of pathogens using gold nanoparticles," *Biotechnol. Adv.*, vol. 33, no. 6, Part 1, pp. 666–680, Nov. 2015.
- [36] S. Bhadra, D. J. Thomson, and G. E. Bridges, "A Wireless Passive pH Sensor for Real-Time In Vivo Milk Quality Monitoring," 2012.

- [37] L. Ramsahoi, A. Gao, M. Fabri, and J. A. Odumeru, "Assessment of the application of an automated electronic milk analyzer for the enumeration of total bacteria in raw goat milk," *J. Dairy Sci.*, vol. 94, no. 7, pp. 3279–3287, Jul. 2011.
- [38] European Commission, "Food Law General Principles - Food Safety - European Commission," *Food Safety*, 2017. [Online]. Available: /food/safety/general_food_law/principles_en.
- [39] FDA Dairy Guidance Document, "Guidance Documents & Regulatory Information by Topic - Guidance for Industry: Dairy Farms, Bulk Milk Transporters, Bulk Milk Transfer Stations and Fluid Milk Processors: Food Security Preventive Measures Guidance," 2007. [Online]. Available: <http://www.fda.gov/Food/GuidanceRegulation/GuidanceDocumentsRegulatoryInformation/ucm083049.htm>. [Accessed: 29-Oct-2015].
- [40] World Health Organization and Foodborne Disease Burden Epidemiology Reference Group, *WHO estimates of the global burden of foodborne diseases*. 2015.
- [41] European Commission, "General Food Law - Food Safety - European Commission," *Food Safety*, 2017. [Online]. Available: /food/safety/general_food_law_en.
- [42] J. Ridler, "FSA releases guide to protect food chain from attack," *foodmanufacture.co.uk*, 21-Nov-2017. [Online]. Available: <https://www.foodmanufacture.co.uk/Article/2017/11/21/Food-supply-chain-guide-to-protect-businesses-from-attack>. [Accessed: 31-Jul-2018].
- [43] USDA Food Safety, "Food Safety | USDA," 2016. [Online]. Available: <http://www.usda.gov/wps/portal/usda/usdahome?navid=food-safety>. [Accessed: 23-May-2016].
- [44] FDA, "Standards for the Growing, Harvesting, Packing, and Holding of Produce for Human Consumption," *US Food & Drug Administration: FSMA Final Rule on Produce Safety*, 26-Jan-2016. [Online]. Available: <https://www.fda.gov/food/guidanceregulation/fsma/ucm334114.htm>. [Accessed: 26-Oct-2018].
- [45] L. Pirofski and A. Casadevall, "What is infectiveness and how is it involved in infection and immunity?," *BMC Immunol.*, vol. 16, no. 1, p. 13, 2015.
- [46] FDA, "Outbreaks: Investigation, Response & Evaluation," 19-Jul-2018. [Online]. Available: <https://www.fda.gov/food/recallsoutbreaksemergencies/outbreaks/default.htm>. [Accessed: 31-Jul-2018].

- [47] FDA, “Federal Register | Hazard Analysis and Critical Control Point (HAACP); Procedures for the Safe and Sanitary Processing and Importing of Juice,” *Fed. Regist.*, vol. 66, no. 13, Jan. 2001.
- [48] J. E. Hillerton and E. A. Berry, “2004: QUALITY OF THE MILK SUPPLY: EUROPEAN REGULATIONS VERSUS PRACTICE - qualityeuro.pdf,” 2014. [Online]. Available: <http://www.nmconline.org/articles/qualityeuro.pdf>. [Accessed: 23-May-2016].
- [49] D. Flynn, “FDA asked to allow interstate sales of raw milk with warnings,” *Food Safety News*, 19-May-2017. [Online]. Available: <http://www.foodsafetynews.com/2017/05/fda-asked-to-allow-interstate-sales-of-raw-milk-with-warnings/>. [Accessed: 30-Jun-2017].
- [50] B. G. Smith, “Developing sustainable food supply chains,” *Philos. Trans. R. Soc. B Biol. Sci.*, vol. 363, no. 1492, pp. 849–861, Feb. 2008.
- [51] GMA, “Food Supply Chain Handbook.” Grocery Manufacturers Association, 16-Apr-2008.
- [52] V. Deperrois-Lafarge and T. Meheut, “Use of the rpoB gene as an alternative to the V3 gene for the identification of spoilage and pathogenic bacteria species in milk and milk products: Use of the rpoB gene as an alternative to the V3 gene,” *Lett. Appl. Microbiol.*, vol. 55, no. 2, pp. 99–108, Aug. 2012.
- [53] FDA, “Bacteriological Analytical Manual (BAM),” 2003. [Online]. Available: <http://www.fda.gov/Food/FoodScienceResearch/LaboratoryMethods/ucm2006949.htm>. [Accessed: 29-Oct-2015].
- [54] P. K. Mandal, A. K. Biswas, K. Choi, and U. K. Pal, “Methods for Rapid Detection of Foodborne Pathogens: An Overview,” *Am. J. Food Technol.*, vol. 6, no. 2, pp. 87–102, Feb. 2011.
- [55] R. S. Bejhed, T. Z. G. De la Torre, M. Donolato, M. F. Hansen, P. Svedlindh, and M. Stromberg, “Turn-on optomagnetic bacterial DNA sequence detection using volume-amplified magnetic nanobeads,” *Biosens. Bioelectron.*, vol. 66, pp. 405–411, Apr. 2015.
- [56] A. M. Fernandes *et al.*, “Development of highly sensitive electrochemical genosensor based on multiwalled carbon nanotubes-chitosan-bismuth and lead sulfide nanoparticles for the detection of pathogenic *Aeromonas*,” *Biosens. Bioelectron.*, vol. 63, pp. 399–406, Jan. 2015.
- [57] Z. Li, Y. Fu, W. Fang, and Y. Li, “Electrochemical Impedance Immunosensor Based on Self-Assembled Monolayers for Rapid Detection of *Escherichia coli* O157:H7 with Signal Amplification Using Lectin,” *Sensors*, vol. 15, no. 8, pp. 19212–19224, Aug. 2015.
- [58] B. Wang, Q. Wang, Z. Cai, and M. Ma, “Simultaneous, rapid and sensitive detection of three food-borne pathogenic bacteria using multicolor quantum dot probes based on multiplex

- fluoroimmunoassay in food samples,” *LWT - Food Sci. Technol.*, vol. 61, no. 2, pp. 368–376, May 2015.
- [59] A. Petrosova *et al.*, “Development of a highly sensitive, field operable biosensor for serological studies of Ebola virus in central Africa,” *Sens. Actuators B Chem.*, vol. 122, no. 2, pp. 578–586, Mar. 2007.
- [60] C. Grenvall, J. R. Folkenberg, P. Augustsson, and T. Laurell, “Label-free somatic cell cytometry in raw milk using acoustophoresis,” *Cytometry A*, vol. 81A, no. 12, pp. 1076–1083, Dec. 2012.
- [61] R. A. Hoffman, “Flow Cytometry: Instrumentation, Applications, Future Trends and Limitations,” in *Standardization and Quality Assurance in Fluorescence Measurements II*, vol. 6, U. Resch-Genger, Ed. Berlin, Heidelberg: Springer Berlin Heidelberg, 2008, pp. 307–342.
- [62] E. Lesman-Movshovich and N. Gilboa-Garber, “Pseudomonas aeruginosa lectin PA-III as a powerful probe for human and bovine milk analysis,” *J. Dairy Sci.*, vol. 86, no. 7, pp. 2276–2282, 2003.
- [63] J. Contreras, L. Fernando, E. Alocilja, F. Salazar, and B. Bacay, “Fabrication of a Nanoparticle-based Sensor for the Detection of Dengue Virus-3 in *Aedes aegypti*,” *Int. J. Sci. Basic Appl. Res. IJSBAR*, vol. 26, no. 3, pp. 138–157, Apr. 2016.
- [64] T. Wang, L. Wang, J. Tu, H. Xiong, and S. Wang, “Direct electrochemistry and electrocatalysis of heme proteins immobilised in carbon-coated nickel magnetic nanoparticle-chitosan-dimethylformamide composite films in room-temperature ionic liquids,” *Bioelectrochemistry*, vol. 94, pp. 94–99, Dec. 2013.
- [65] C. H. Gayathri, P. Mayuri, K. Sankaran, and A. S. Kumar, “An electrochemical immunosensor for efficient detection of uropathogenic *E. coli* based on thionine dye immobilized chitosan/functionalized-MWCNT modified electrode,” *Biosens. Bioelectron.*, vol. 82, pp. 71–77, Aug. 2016.
- [66] H. Liu, F. Zhan, F. Liu, M. Zhu, X. Zhou, and D. Xing, “Visual and sensitive detection of viable pathogenic bacteria by sensing of RNA markers in gold nanoparticles based paper platform,” *Biosens. Bioelectron.*, vol. 62, pp. 38–46, Dec. 2014.
- [67] E. B. Settingerton and E. C. Alocilja, “Electrochemical Biosensor for Rapid and Sensitive Detection of Magnetically Extracted Bacterial Pathogens,” *Biosensors*, vol. 2, no. 4, pp. 15–31, Jan. 2012.
- [68] S. A. Vetrone, M. C. Huarng, and E. C. Alocilja, “Detection of Non-PCR Amplified *S. enteritidis* Genomic DNA from Food Matrices Using a Gold-Nanoparticle DNA Biosensor: A Proof-of-Concept Study,” *Sensors*, vol. 12, no. 12, pp. 10487–10499, Aug. 2012.

- [69] I. Yazgan, N. M. Noah, O. Toure, S. Zhang, and O. A. Sadik, "Biosensor for selective detection of E. coli in spinach using the strong affinity of derivatized mannose with fimbrial lectin," *Biosens. Bioelectron.*, vol. 61, pp. 266–273, Nov. 2014.
- [70] M. S. Cheng, S. H. Lau, V. T. Chow, and C.-S. Toh, "Membrane-Based Electrochemical Nanobiosensor for Escherichia coli Detection and Analysis of Cells Viability," *Environ. Sci. Technol.*, vol. 45, no. 15, pp. 6453–6459, Aug. 2011.
- [71] M. Kimura, H. Fukushima, Y. Sagawa, K. Setsu, H. Hara, and S. Inoue, "An Integrated Potentiostat With an Electrochemical Cell Using Thin-Film Transistors," *IEEE Trans. Electron Devices*, vol. 56, no. 9, pp. 2114–2119, Sep. 2009.
- [72] M. S. Webster *et al.*, "Detection of bacterial metabolites for the discrimination of bacteria utilizing gold nanoparticle chemiresistor sensors," *Sens. Actuators B-Chem.*, vol. 220, pp. 895–902, Dec. 2015.
- [73] L. Chen, N. Mungroo, L. Daikuara, and S. Neethirajan, "Label-free NIR-SERS discrimination and detection of foodborne bacteria by in situ synthesis of Ag colloids," *J. Nanobiotechnology*, vol. 13, p. 45, Jun. 2015.
- [74] L. Malic *et al.*, "Polymer-based microfluidic chip for rapid and efficient immunomagnetic capture and release of *Listeria monocytogenes*," *Lab Chip*, vol. 15, no. 20, pp. 3994–4007, 2015.
- [75] X.-Z. Shi and X.-Q. Yu, "The extended loop of the C-terminal carbohydrate-recognition domain of *Manduca sexta* immulectin-2 is important for ligand binding and functions," *Amino Acids*, vol. 42, no. 6, pp. 2383–2391, Jun. 2012.
- [76] N. Duan *et al.*, "Dual-color upconversion fluorescence and aptamer-functionalized magnetic nanoparticles-based bioassay for the simultaneous detection of *Salmonella Typhimurium* and *Staphylococcus aureus*," *Anal. Chim. Acta*, vol. 723, pp. 1–6, Apr. 2012.
- [77] D. Wang *et al.*, "Efficient separation and quantitative detection of *Listeria monocytogenes* based on screen-printed interdigitated electrode, urease and magnetic nanoparticles," *Food Control*, vol. 73, pp. 555–561, Mar. 2017.
- [78] Y. Bai *et al.*, "A rapid method for the detection of foodborne pathogens by extraction of a trace amount of DNA from raw milk based on amino-modified silica-coated magnetic nanoparticles and polymerase chain reaction," *Anal. Chim. Acta*, vol. 787, pp. 93–101, Jul. 2013.
- [79] H. Huang *et al.*, "Magnetic Nanoparticle Based Magnetophoresis for Efficient Separation of E. Coli O157:h7," *Trans. ASABE*, vol. 54, no. 3, pp. 1015–1024, Jun. 2011.

- [80] X. Liu, Y. Hu, S. Zheng, Y. Liu, Z. He, and F. Luo, "Surface plasmon resonance immunosensor for fast, highly sensitive, and in situ detection of the magnetic nanoparticles-enriched *Salmonella enteritidis*," *Sens. Actuators B Chem.*, vol. 230, pp. 191–198, Jul. 2016.
- [81] Y. Luo *et al.*, "Novel Biosensor Based on Electrospun Nanofiber and Magnetic Nanoparticles for the Detection of *E. coli* O157:H7," *Ieee Trans. Nanotechnol.*, vol. 11, no. 4, pp. 676–681, Jul. 2012.
- [82] S. Mun and S.-J. Choi, "Detection of *Salmonella typhimurium* by antibody/enzyme-conjugated magnetic nanoparticles," *Biochip J.*, vol. 9, no. 1, pp. 10–15, Mar. 2015.
- [83] J. Y. Park, H. Y. Jeong, M. I. Kim, and T. J. Park, "Colorimetric Detection System for *Salmonella typhimurium* Based on Peroxidase-Like Activity of Magnetic Nanoparticles with DNA Aptamers," *J. Nanomater.*, p. Article ID 527126, 2015.
- [84] W.-B. Shim, J.-E. Song, H. Mun, D.-H. Chung, and M.-G. Kim, "Rapid colorimetric detection of *Salmonella typhimurium* using a selective filtration technique combined with antibody-magnetic nanoparticle nanocomposites.," *Anal. Bioanal. Chem.*, vol. 406, no. 3, pp. 859–866, 2014.
- [85] L. Zhiyang *et al.*, "An Applied Approach in Detecting *E. coli* O157:H7 Using Immunological Method Based on Chemiluminescence and Magnetic Nanoparticles," *Acta Chim. Sin.*, vol. 68, no. 3, pp. 251–256, Feb. 2010.
- [86] W.-B. Shim, C.-W. Lee, M.-G. Kim, and D.-H. Chung, "An antibody-magnetic nanoparticle conjugate-based selective filtration method for the rapid colorimetric detection of *Listeria monocytogenes*," *Anal. Methods*, vol. 6, no. 22, pp. 9129–9135, 2014.
- [87] Y. J. Sung, H.-J. Suk, H. Y. Sung, T. Li, H. Poo, and M.-G. Kim, "Novel antibody/gold nanoparticle/magnetic nanoparticle nanocomposites for immunomagnetic separation and rapid colorimetric detection of *Staphylococcus aureus* in milk," *Biosens. Bioelectron.*, vol. 43, pp. 432–439, May 2013.
- [88] Y. Zhao *et al.*, "Rapid detection of *Listeria monocytogenes* in food by biofunctionalized magnetic nanoparticle based on nuclear magnetic resonance.," *Food Control*, vol. 71, pp. 110–116, 2017.
- [89] D. A. Kanayeva *et al.*, "Efficient separation and sensitive detection of *Listeria monocytogenes* using an impedance immunosensor based on magnetic nanoparticles, a microfluidic chip, and an interdigitated microelectrode," *J. Food Prot.*, vol. 75, no. 11, pp. 1951–1959, Nov. 2012.
- [90] A.-H. Lu, E. L. Salabas, and F. Schüth, "Magnetic Nanoparticles: Synthesis, Protection, Functionalization, and Application," *Angew. Chem. Int. Ed.*, vol. 46, no. 8, pp. 1222–1244, Feb. 2007.

- [91] S. Cho, H. Y. Shin, and M. Il Kim, "Nanohybrids consisting of magnetic nanoparticles and gold nanoclusters as effective peroxidase mimics and their application for colorimetric detection of glucose," *Biointerphases*, vol. 12, no. 1, p. 401, Mar. 2017.
- [92] S. Dehdashtian, M. B. Gholivand, M. Shamsipur, and S. Kariminia, "Construction of a sensitive and selective sensor for morphine using chitosan coated Fe₃O₄ magnetic nanoparticle as a modifier," *Mater. Sci. Eng. C*, vol. 58, pp. 53–59, Jan. 2016.
- [93] S. Li, H. Liu, Y. Deng, L. Lin, and N. He, "Development of a magnetic nanoparticles microarray for simultaneous and simple detection of foodborne pathogens," *J. Biomed. Nanotechnol.*, vol. 9, no. 7, pp. 1254–1260, Jul. 2013.
- [94] C.-C. Lin *et al.*, "Selective Binding of Mannose-Encapsulated Gold Nanoparticles to Type 1 Pili in *Escherichia coli*," *J. Am. Chem. Soc.*, vol. 124, no. 14, pp. 3508–3509, Apr. 2002.
- [95] V. Raj, A. N. Vijayan, and K. Joseph, "Cysteine capped gold nanoparticles for naked eye detection of *E. coli* bacteria in UTI patients," *Sens. Bio-Sens. Res.*, vol. 5, pp. 33–36, Sep. 2015.
- [96] J. Wang, Z. Chen, Z. Li, and Y. Yang, "Magnetic nanoparticles based dispersive micro-solid-phase extraction as a novel technique for the determination of estrogens in pork samples," *Food Chem.*, vol. 204, pp. 135–140, Aug. 2016.
- [97] M. Leitgeb, K. Heržič, G. H. Podrepšek, A. Hojski, A. Crnjac, and Ž. Knez, "Toxicity of magnetic chitosan micro and nanoparticles as carriers for biologically active substances.," *Acta Chim. Slov.*, vol. 61, no. 1, 2014.
- [98] K. L. B. Chang, G. Tsai, J. Lee, and W.-R. Fu, "Heterogeneous N-deacetylation of chitin in alkaline solution," *Carbohydr. Res.*, vol. 303, no. 3, pp. 327–332, Sep. 1997.
- [99] A. Galhoum *et al.*, "Cysteine-Functionalized Chitosan Magnetic Nano-Based Particles for the Recovery of Light and Heavy Rare Earth Metals: Uptake Kinetics and Sorption Isotherms," *Nanomaterials*, vol. 5, no. 1, pp. 154–179, Feb. 2015.
- [100] R. M. Fratila, M. Moros, and J. M. de la Fuente, "Recent advances in biosensing using magnetic glyconanoparticles," *Anal. Bioanal. Chem.*, vol. 408, no. 7, pp. 1783–1803, Mar. 2016.
- [101] G. Basina *et al.*, "Synthesis of Biocompatible Magnetic Iron Oxide (γ -Fe₂O₃ and Fe₃O₄) Nanoparticles by a Modified Polyol Process for Biomedical Applications," *MRS Proc.*, vol. 1256, Jan. 2010.
- [102] M. Mahdavi *et al.*, "Synthesis, Surface Modification and Characterisation of Biocompatible Magnetic Iron Oxide Nanoparticles for Biomedical Applications," *Molecules*, vol. 18, no. 7, pp. 7533–7548, Jun. 2013.

- [103] N. K. Prasad, D. Panda, S. Singh, M. D. Mukadam, S. M. Yusuf, and D. Bahadur, "Biocompatible suspension of nanosized γ -Fe₂O₃ synthesized by novel methods," *J. Appl. Phys.*, vol. 97, no. 10, p. 10Q903, May 2005.
- [104] R. Ahmadi, E. Ranjbarnodeh, and N. Gu, "Synthesizing cysteine-coated magnetite nanoparticles as MRI contrast agent: Effect of pH and cysteine addition on particles size distribution," *Mater. Sci.-Pol.*, vol. 30, no. 4, pp. 382–389, Dec. 2012.
- [105] R. Ahmadi, N. Gu, and H. R. M. Hosseini, "Characterization of cysteine coated magnetite nanoparticles as MRI contrast agent," *Nano-Micro Lett.*, vol. 4, no. 3, pp. 180–183, 2012.
- [106] D. Horák *et al.*, "D-mannose-modified iron oxide nanoparticles for stem cell labeling," *Bioconjug. Chem.*, vol. 18, no. 3, pp. 635–644, 2007.
- [107] N. Sharon, Y. Eshdat, F. J. Silverblatt, and I. Ofek, "Bacterial adherence to cell surface sugars," *Ciba Found. Symp.*, vol. 80, pp. 119–141, 1981.
- [108] S. Trungkathan, D. Polpanich, S. Smanmoo, and P. Tangboriboonrat, "Magnetic polymeric nanoparticles functionalized by mannose-rhodamine conjugate for detection of *E. coli*," *J. Appl. Polym. Sci.*, vol. 131, no. 6, pp. 1–9, Mar. 2014.
- [109] M. Kong, X. G. Chen, K. Xing, and H. J. Park, "Antimicrobial properties of chitosan and mode of action: A state of the art review," *Int. J. Food Microbiol.*, vol. 144, no. 1, pp. 51–63, Nov. 2010.
- [110] M. Mukherjee and S. De, "Investigation of antifouling and disinfection potential of chitosan coated iron oxide-PAN hollow fiber membrane using Gram-positive and Gram-negative bacteria," *Mater. Sci. Eng. C*, vol. 75, pp. 133–148, Jun. 2017.
- [111] S. Shi *et al.*, "Reduced Staphylococcus aureus biofilm formation in the presence of chitosan-coated iron oxide nanoparticles," *Int. J. Nanomedicine*, vol. Volume 11, pp. 6499–6506, Dec. 2016.
- [112] Y. Ge, Y. Zhang, S. He, F. Nie, G. Teng, and N. Gu, "Fluorescence Modified Chitosan-Coated Magnetic Nanoparticles for High-Efficient Cellular Imaging," *Nanoscale Res. Lett.*, vol. 4, no. 4, pp. 287–295, Apr. 2009.
- [113] B. Issa, I. Obaidat, B. Albiss, and Y. Haik, "Magnetic Nanoparticles: Surface Effects and Properties Related to Biomedicine Applications," *Int. J. Mol. Sci.*, vol. 14, no. 11, pp. 21266–21305, Oct. 2013.
- [114] I. Obaidat, B. Issa, and Y. Haik, "Magnetic Properties of Magnetic Nanoparticles for Efficient Hyperthermia," *Nanomaterials*, vol. 5, no. 1, pp. 63–89, Jan. 2015.

- [115] W. Jansaento, K. Jangpatarapongsa, D. Polpanich, and W. Wonglumsom, "Detection of *Campylobacter* DNA using magnetic nanoparticles coupled with PCR and a colorimetric end-point system," *Food Sci. Biotechnol.*, vol. 25, no. 1, pp. 193–198, Feb. 2016.
- [116] X. Wang, Y. Huang, S. Wu, N. Duan, B. Xu, and Z. Wang, "Simultaneous detection of *Staphylococcus aureus* and *Salmonella typhimurium* using multicolor time-resolved fluorescence nanoparticles as labels," *Int. J. Food Microbiol.*, vol. 237, pp. 172–179, Nov. 2016.
- [117] W. Zhang, Q. Hu, Y. Su, and X. Zheng, "Biocompatible nanostructured poly(xanthurenic acid)-Fe₂O₃/reduced graphene oxide platform for genosensing application," *J. Electroanal. Chem.*, vol. 719, pp. 72–76, Apr. 2014.
- [118] H. Lin, Q. Lu, S. Ge, Q. Cai, and C. A. Grimes, "Detection of pathogen *Escherichia coli* O157:H7 with a wireless magnetoelastic-sensing device amplified by using chitosan-modified magnetic Fe₃O₄ nanoparticles," *Sens. Actuators B Chem.*, vol. 147, no. 1, pp. 343–349, May 2010.
- [119] X. Meng, F. Li, F. Li, Y. Xiong, and H. Xu, "Vancomycin modified PEGylated-magnetic nanoparticles combined with PCR for efficient enrichment and detection of *Listeria monocytogenes*," *Sens. Actuators B Chem.*, vol. 247, pp. 546–555, Aug. 2017.
- [120] M. Unni *et al.*, "Thermal Decomposition Synthesis of Iron Oxide Nanoparticles with Diminished Magnetic Dead Layer by Controlled Addition of Oxygen," *ACS Nano*, vol. 11, no. 2, pp. 2284–2303, Feb. 2017.
- [121] J. Joo *et al.*, "A facile and sensitive detection of pathogenic bacteria using magnetic nanoparticles and optical nanocrystal probes," *The Analyst*, vol. 137, no. 16, p. 3609, 2012.
- [122] J. Sanchez-Ramirez *et al.*, "Cellulases immobilization on chitosan-coated magnetic nanoparticles: application for *Agave Atrovirens* lignocellulosic biomass hydrolysis," *Bioprocess Biosyst. Eng.*, vol. 40, no. 1, pp. 9–22, Jan. 2017.
- [123] Y. G. Abou El-Reash, "Magnetic chitosan modified with cysteine-glutaraldehyde as adsorbent for removal of heavy metals from water," *J. Environ. Chem. Eng.*, vol. 4, no. 4, pp. 3835–3847, Dec. 2016.
- [124] J. Castelló, M. Gallardo, M. A. Busquets, and J. Estelrich, "Chitosan (or alginate)-coated iron oxide nanoparticles: A comparative study," *Colloids Surf. Physicochem. Eng. Asp.*, vol. 468, pp. 151–158, Mar. 2015.
- [125] G. Unsoy, S. Yalcin, R. Khodadust, G. Gunduz, and U. Gunduz, "Synthesis optimization and characterization of chitosan-coated iron oxide nanoparticles produced for biomedical applications," *J. Nanoparticle Res.*, vol. 14, no. 11, pp. 1–13, Nov. 2012.

- [126] P. I. P. Soares *et al.*, “Thermal and magnetic properties of chitosan-iron oxide nanoparticles,” *Carbohydr. Polym.*, vol. 149, pp. 382–390, Sep. 2016.
- [127] Y. Wan, Y. Sun, P. Qi, P. Wang, and D. Zhang, “Quaternized magnetic nanoparticles-fluorescent polymer system for detection and identification of bacteria,” *Biosens. Bioelectron.*, vol. 55, pp. 289–293, May 2014.
- [128] S. Pal and E. C. Alocilja, “Electrically active magnetic nanoparticles as novel concentrator and electrochemical redox transducer in *Bacillus anthracis* DNA detection,” *Biosens. Bioelectron.*, vol. 26, no. 4, pp. 1624–1630, Dec. 2010.
- [129] Y. Wan, Y. Sun, P. Qi, P. Wang, and D. Zhang, “Quaternized magnetic nanoparticles–fluorescent polymer system for detection and identification of bacteria,” *Biosens. Bioelectron.*, vol. 55, pp. 289–293, May 2014.
- [130] D. Lim *et al.*, “Alocilja Magnetic Nanoparticles Efficiently Capture *Escherichia coli* O157:H7 Isolates,” *Philipp. J. Pathol.*, vol. 2, no. 2, p. 47, Nov. 2017.
- [131] L. L. Matta and E. C. Alocilja, “Carbohydrate Ligands on Magnetic Nanoparticles as Antibody-mimics for the Expedient Extraction of 5 *Salmonella* Enteritidis, *E. coli* O157:H7 and *Bacillus cereus* from Pasteurized Milk,” *Manuscr. Prep. Publ.*, Dec. 2017.
- [132] S. Dehdashtian, M. B. Gholivand, M. Shamsipur, and S. Kariminia, “Construction of a sensitive and selective sensor for morphine using chitosan coated Fe₃O₄ magnetic nanoparticle as a modifier,” *Mater. Sci. Eng. C-Mater. Biol. Appl.*, vol. 58, pp. 53–59, Jan. 2016.
- [133] J. A. Kim, S. H. Lee, H. Park, J. H. Kim, and T. H. Park, “Microheater based on magnetic nanoparticle embedded PDMS,” *Nanotechnology*, vol. 21, no. 16, p. 165102, Apr. 2010.
- [134] J. Fang, H. Wang, Y. Xue, X. Wang, and T. Lin, “Magnet-Induced Temporary Superhydrophobic Coatings from One-Pot Synthesized Hydrophobic Magnetic Nanoparticles,” *ACS Appl. Mater. Interfaces*, vol. 2, no. 5, pp. 1449–1455, May 2010.
- [135] N. Duan, B. Xu, S. Wu, and Z. Wang, “Magnetic Nanoparticles-based Aptasensor Using Gold Nanoparticles as Colorimetric Probes for the Detection of *Salmonella typhimurium*,” *Anal. Sci.*, vol. 32, no. 4, pp. 431–436, Apr. 2016.
- [136] H. Kuang *et al.*, “A One-Step Homogeneous Sandwich Immunosensor for *Salmonella* Detection Based on Magnetic Nanoparticles (MNPs) and Quantum Dots (QDs),” *Int. J. Mol. Sci.*, vol. 14, no. 4, pp. 8603–8610, Apr. 2013.
- [137] Q. Sun, G. Zhao, and W. Dou, “An optical and rapid sandwich immunoassay method for detection of *Salmonella pullorum* and *Salmonella gallinarum* based on immune blue silica nanoparticles and magnetic nanoparticles,” *Sens. Actuators B Chem.*, vol. 226, pp. 69–75, Apr. 2016.

- [138] M. R. Hormozi-Nezhad, E. Seyedhosseini, and H. Robotjazi, "Spectrophotometric determination of glutathione and cysteine based on aggregation of colloidal gold nanoparticles," *Sci. Iran.*, vol. 19, no. 3, pp. 958–963, Jun. 2012.
- [139] G. Liu *et al.*, "Spectrophotometric and visual detection of the herbicide atrazine by exploiting hydrogen bond-induced aggregation of melamine-modified gold nanoparticles," *Microchim. Acta*, vol. 182, no. 11–12, pp. 1983–1989, Aug. 2015.
- [140] M. Lepoitevin, M. Lemouel, M. Bechelany, J.-M. Janot, and S. Balme, "Gold nanoparticles for the bare-eye based and spectrophotometric detection of proteins, polynucleotides and DNA," *Microchim. Acta*, vol. 182, no. 5–6, pp. 1223–1229, Apr. 2015.
- [141] K. Afshinnia, M. Sikder, B. Cai, and M. Baalousha, "Effect of nanomaterial and media physicochemical properties on Ag NM aggregation kinetics," *J. Colloid Interface Sci.*, vol. 487, pp. 192–200, Feb. 2017.
- [142] Shuguang Wang, R. Lawson, P. C. Ray, and Hongtao Yu, "Toxic effects of gold nanoparticles on *Salmonella typhimurium* bacteria," *Toxicol. Ind. Health*, vol. 27, no. 6, pp. 547–554, Jul. 2011.
- [143] M. J. Anderson, E. Torres-Chavolla, B. A. Castro, and E. C. Alocilja, "One step alkaline synthesis of biocompatible gold nanoparticles using dextrin as capping agent," *J. Nanoparticle Res.*, vol. 13, no. 7, pp. 2843–2851, Jul. 2011.
- [144] K. Bankura *et al.*, "Dextrin-mediated synthesis of Ag NPs for colorimetric assays of Cu²⁺ ion and Au NPs for catalytic activity," *Int. J. Biol. Macromol.*, vol. 80, pp. 309–316, Sep. 2015.
- [145] S. Malhotra, M. N. Welling, S. B. Mantri, and K. Desai, "*In vitro* and *in vivo* antioxidant, cytotoxic, and anti-chronic inflammatory arthritic effect of selenium nanoparticles: *In vitro* and *in vivo* effect of SeNP," *J. Biomed. Mater. Res. B Appl. Biomater.*, vol. 104, no. 5, pp. 993–1003, Jul. 2016.
- [146] S. R. Haseley, "Carbohydrate recognition: a nascent technology for the detection of bioanalytes," *Anal. Chim. Acta*, vol. 457, no. 1, pp. 39–45, 2002.
- [147] N. Firon, I. Ofek, and N. Sharon, "CARBOHYDRATE SPECIFICITY OF THE SURFACE LECTINS OF *Escherichia coli*, *Klebsiella pneumoniae*, AND *Salmonella typhimurium*," *Carbohydr. Res.*, vol. 120, pp. 235–249, 1983.
- [148] A. Muñoz *et al.*, "Synthesis of giant globular multivalent glycofullerenes as potent inhibitors in a model of Ebola virus infection," *Nat. Chem.*, vol. 8, no. 1, pp. 50–57, Jan. 2016.

- [149] T. K. Lindhorst, "Studies on type 1-fimbriated bacteria to understand and combat bacterial adhesion," in *Carbohydrate Chemistry: Chemical and Biological Approaches, Vol 37*, vol. 37, A. P. Rauter and T. K. Lindhorst, Eds. Cambridge: Royal Soc Chemistry, 2011, pp. 194–207.
- [150] K. Ramalingam, "Pathological and immunological significance of receptor determinant molecules of cell surface and binding specificities of lectins (haemagglutinins) in disease," *Biochem. Cell. Arch.*, vol. 5, no. 2, pp. 137–143, Oct. 2005.
- [151] J. Collins *et al.*, "Dietary trehalose enhances virulence of epidemic *Clostridium difficile*," *Nature*, vol. 553, no. 7688, pp. 291–294, Jan. 2018.
- [152] D. Bader, D. T. Klier, C. Hettrich, F. F. Bier, and P. Wessig, "Detecting carbohydrate–lectin interactions using a fluorescent probe based on DBD dyes," *Anal. Methods*, vol. 8, no. 6, pp. 1235–1238, 2016.
- [153] M.-G. Baek, R. C. Stevens, and D. H. Charych, "Design and Synthesis of Novel Glycopolymers for Colorimetric Detection of Influenza Virus and *E. coli*," *Bioconjug. Chem.*, vol. 11, no. 6, pp. 777–788, Nov. 2000.
- [154] M. D. Disney and P. H. Seeberger, "The Use of Carbohydrate Microarrays to Study Carbohydrate-Cell Interactions and to Detect Pathogens," *Chem. Biol.*, vol. 11, no. 12, pp. 1701–1707, Dec. 2004.
- [155] S. Park *et al.*, "Probing Cell-Surface Carbohydrate Binding Proteins with Dual-Modal Glycan-Conjugated Nanoparticles," *J. Am. Chem. Soc.*, vol. 137, no. 18, pp. 5961–5968, May 2015.
- [156] G. Safina, M. Vanlier, and B. Danielsson, "Flow-injection assay of the pathogenic bacteria using lectin-based quartz crystal microbalance biosensor," *Talanta*, vol. 77, no. 2, pp. 468–472, Dec. 2008.
- [157] Y. Wang, Z. Ye, C. Si, and Y. Ying, "Monitoring of *Escherichia coli* O157:H7 in food samples using lectin based surface plasmon resonance biosensor," *Food Chem.*, vol. 136, no. 3–4, pp. 1303–1308, Feb. 2013.
- [158] E. Uribe, T. J. Steele, R. C. Richards, and K. V. Ewart, "Ligand and pathogen specificity of the Atlantic salmon serum C-type lectin," *Biochim. Biophys. Acta BBA - Gen. Subj.*, vol. 1830, no. 1, pp. 2129–2138, Jan. 2013.
- [159] N. Sinha, S. Mohan, C. A. Lipschultz, and S. J. Smith-Gill, "Differences in Electrostatic Properties at Antibody-Antigen Binding Sites: Implications for Specificity and Cross-Reactivity," *Biophys. J.*, vol. 83, no. 6, pp. 2946–2968, Dec. 2002.

- [160] V. A. Kulshin, U. Zahringer, B. Linkner, K.-E. Jager, B. A. Dmitriev, and E. T. Rietschel, "Structural characterization of the lipid A component of *Pseudomonas aeruginosa* wild-type and rough mutant lipopolysaccharides," *Eur. J. Biochem.*, vol. 198, no. 3, pp. 697–704, 1991.
- [161] S. Galdiero *et al.*, "Microbe-host interactions: structure and role of Gram-negative bacterial porins," *Curr. Protein Pept. Sci.*, vol. 13, no. 8, pp. 843–854, 2012.
- [162] T. Candela *et al.*, "Environmental and Biofilm-dependent Changes in a *Bacillus cereus* Secondary Cell Wall Polysaccharide," *J. Biol. Chem.*, vol. 286, no. 36, pp. 31250–31262, Sep. 2011.
- [163] R. Sommer *et al.*, "Cinnamide Derivatives of d-Mannose as Inhibitors of the Bacterial Virulence Factor LecB from *Pseudomonas aeruginosa*," *ChemistryOpen*, vol. 4, no. 6, pp. 756–767, Dec. 2015.
- [164] T. M. Joys, "The Covalent Structure of the Phase-1 Flagellar Filament Protein of *Salmonella typhimurium* and Its Comparison with Other Flagellins*," *J. Biol. Chem.*, vol. 260, no. 29, pp. 16758–16761, 1985.
- [165] S. L. Tran, E. Guillemet, M. Gohar, D. Lereclus, and N. Ramarao, "CwpFM (EntFM) Is a *Bacillus cereus* Potential Cell Wall Peptidase Implicated in Adhesion, Biofilm Formation, and Virulence," *J. Bacteriol.*, vol. 192, no. 10, pp. 2638–2642, May 2010.
- [166] A. Muller *et al.*, "An ATP-binding cassette-type cysteine transporter in *Campylobacter jejuni* inferred from the structure of an extracytoplasmic solute receptor protein," *Mol. Microbiol.*, vol. 57, no. 1, pp. 143–155, Jul. 2005.
- [167] H. Nikaido, "Molecular basis of bacterial outer membrane permeability revisited," *Microbiol. Mol. Biol. Rev. MMBR*, vol. 67, no. 4, pp. 593–656, Dec. 2003.
- [168] A. Diaz-Quiñonez, N. Martin-Orozco, A. Isibasi, and V. Ortiz-Navarrete, "Y Two *Salmonella* OmpC Kb-Restricted Epitopes for CD8+-T-Cell Recognition," *Infect. Immun.*, vol. 72, no. 5, pp. 3059–3062, May 2004.
- [169] C. Gil-Cruz *et al.*, "The porin OmpD from nontyphoidal *Salmonella* is a key target for a protective B1b cell antibody response," *Proc. Natl. Acad. Sci.*, vol. 106, no. 24, pp. 9803–9808, Jun. 2009.
- [170] R. Koebnik, K. P. Locher, and P. Van Gelder, "Structure and function of bacterial outer membrane proteins: barrels in a nutshell," *Mol. Microbiol.*, vol. 37, no. 2, pp. 239–253, Jul. 2000.
- [171] C. Chagnot, A. Listrat, T. Astruc, and M. Desvaux, "Bacterial adhesion to animal tissues: protein determinants for recognition of extracellular matrix components: ECM recognition by bacterial MSCRAMMs," *Cell. Microbiol.*, vol. 14, no. 11, pp. 1687–1696, Nov. 2012.

- [172] M. Gohar *et al.*, “The PlcR virulence regulon of *Bacillus cereus*,” *PLoS One*, vol. 3, no. 7, p. e2793, 2008.
- [173] S. P. Singh, S. R. Singh, Y. U. Williams, L. Jones, and T. Abdullah, “Antigenic determinants of the OmpC porin from *Salmonella typhimurium*,” *Infect. Immun.*, vol. 63, no. 12, pp. 4600–4605, Dec. 1995.
- [174] McDonough, “Amino Acid Composition of Antigenically Distinct *Salmonella* Flagellar Proteins,” *J Mol Biol*, vol. 12, pp. 342–355, 1965.
- [175] J. P. Piette and E. S. Idziak, “Role of flagella in adhesion of *Pseudomonas fluorescens* to tendon slices,” *Appl. Environ. Microbiol.*, vol. 57, no. 6, pp. 1635–1639, 1991.
- [176] S. K. Collinson, S. C. Clouthier, J. L. Doran, P. A. Banser, and W. W. Kay, “*Salmonella enteritidis* agfBAC Operon Encoding Thin, Aggregative Fimbriae,” 1996.
- [177] S. Jain and J. Chen, “Attachment and biofilm formation by various serotypes of *Salmonella* as influenced by cellulose production and thin aggregative fimbriae biosynthesis,” *J. Food Prot.*, vol. 70, no. 11, pp. 2473–2479, 2007.
- [178] M. Kukkonen *et al.*, “Identification of two laminin-binding fimbriae, the type 1 fimbria of *Salmonella enterica* serovar typhimurium and the G fimbria of *Escherichia coli*, as plasminogen receptors,” *Infect. Immun.*, vol. 66, no. 10, pp. 4965–4970, 1998.
- [179] S. G. Stahlhut *et al.*, “Comparative Structure-Function Analysis of Mannose-Specific FimH Adhesins from *Klebsiella pneumoniae* and *Escherichia coli*,” *J. Bacteriol.*, vol. 191, no. 21, pp. 6592–6601, Nov. 2009.
- [180] K. Waalen, K. Sletten, L. O. Fro’holm, V. Vaisanen, and T. K. Korhonen, “The N-terminal amino acid sequence of type 1 fimbria (pili) of *Salmonella typhimurium* LT2,” *FEMS Microbiol. Lett.*, vol. 16, pp. 149–151, 1983.
- [181] J. P. Desrosier and J. C. Lara, “Isolation and properties of pili from spores of *Bacillus cereus*,” *J. Bacteriol.*, vol. 145, no. 1, pp. 613–619, 1981.
- [182] T. K. Korhonen, K. Lounatmaa, H. Ranta, and N. Kuusi, “Characterization of type 1 pili of *Salmonella typhimurium* LT2,” *J. Bacteriol.*, vol. 144, no. 2, pp. 800–805, 1980.
- [183] J.-R. Neeser, B. Koellreutter, and P. Wuersch, “Oligomannoside-type glycopeptides inhibiting adhesion of *Escherichia coli* strains mediated by type 1 pili: preparation of potent inhibitors from plant glycoproteins,” *Infect. Immun.*, vol. 52, no. 2, pp. 428–436, 1986.
- [184] V. Oxaran *et al.*, “Pilus Biogenesis in *Lactococcus lactis*: Molecular Characterization and Role in Aggregation and Biofilm Formation,” *PLoS ONE*, vol. 7, no. 12, p. e50989, Dec. 2012.

- [185] H. Xu *et al.*, “Characterizing Pilus-Mediated Adhesion of Biofilm-Forming *E. coli* to Chemically Diverse Surfaces Using Atomic Force Microscopy,” *Langmuir*, vol. 29, no. 9, pp. 3000–3011, Mar. 2013.
- [186] P. Burguiere, S. Auger, M. F. Hullo, A. Danchin, and I. Martin-Verstraete, “Three different systems participate in L-cystine uptake in *Bacillus subtilis*,” *J. Bacteriol.*, vol. 186, no. 15, pp. 4875–4884, Aug. 2004.
- [187] B. Xayarath, H. Marquis, G. C. Port, and N. E. Freitag, “*Listeria monocytogenes* CtaP is a multifunctional cysteine transport-associated protein required for bacterial pathogenesis,” *Mol. Microbiol.*, vol. 74, no. 4, pp. 956–973, Nov. 2009.
- [188] M. Pokorná *et al.*, “Unusual Entropy-Driven Affinity of *Chromobacterium violaceum* Lectin CV-III toward Fucose and Mannose $\dagger \cdot \ddagger$,” *Biochemistry*, vol. 45, no. 24, pp. 7501–7510, Jun. 2006.
- [189] I. M. Helander, E.-L. Nurmiäho-Lassila, R. Ahvenainen, J. Rhoades, and S. Roller, “Chitosan disrupts the barrier properties of the outer membrane of Gram-negative bacteria,” *Int. J. Food Microbiol.*, vol. 71, no. 2, pp. 235–244, 2001.
- [190] H. Mellegard, C. From, B. E. Christensen, and P. E. Granum, “Inhibition of *Bacillus cereus* spore outgrowth and multiplication by chitosan,” *Int. J. Food Microbiol.*, vol. 149, no. 3, pp. 218–225, Oct. 2011.
- [191] J. C. Fernandes, P. Eaton, A. M. Gomes, M. E. Pintado, and F. Xavier Malcata, “Study of the antibacterial effects of chitosans on *Bacillus cereus* (and its spores) by atomic force microscopy imaging and nanoindentation,” *Ultramicroscopy*, vol. 109, no. 8, pp. 854–860, Jul. 2009.
- [192] L. Manni, O. Ghorbel-Bellaaj, K. Jellouli, I. Younes, and M. Nasri, “Extraction and Characterization of Chitin, Chitosan, and Protein Hydrolysates Prepared from Shrimp Waste by Treatment with Crude Protease from *Bacillus cereus* SV1,” *Appl. Biochem. Biotechnol.*, vol. 162, no. 2, pp. 345–357, Sep. 2010.
- [193] E. Fournier *et al.*, “Creation of a gold nanoparticle based electrochemical assay for the detection of inhibitors of bacterial cytochrome bd oxidases,” *Bioelectrochemistry*, vol. 111, pp. 109–114, Oct. 2016.
- [194] A. Motaharian, F. Motaharian, K. Abnous, M. R. M. Hosseini, and M. Hassanzadeh-Khayyat, “Molecularly imprinted polymer nanoparticles-based electrochemical sensor for determination of diazinon pesticide in well water and apple fruit samples,” *Anal. Bioanal. Chem.*, vol. 408, no. 24, pp. 6769–6779, Sep. 2016.
- [195] N. Nesakumar, S. Sethuraman, U. M. Krishnan, and J. B. B. Rayappan, “Cyclic voltammetric acetylcholinesterase biosensor for the detection of captan in apple samples with the aid of chemometrics,” *Anal. Bioanal. Chem.*, vol. 407, no. 16, pp. 4863–4868, Jun. 2015.

- [196] B. M. B. Felisilda, E. A. de Eulate, and D. W. M. Arrigan, "Investigation of a solvent-cast organogel to form a liquid-gel microinterface array for electrochemical detection of lysozyme," *Anal. Chim. Acta*, vol. 893, pp. 34–40, Sep. 2015.
- [197] T. Gu, J. Wang, H. Xia, S. Wang, and X. Yu, "Direct Electrochemistry and Electrocatalysis of Horseradish Peroxidase Immobilized in a DNA/Chitosan-Fe₃O₄ Magnetic Nanoparticle Bio-Complex Film," *Materials*, vol. 7, no. 2, pp. 1069–1083, Feb. 2014.
- [198] A. Salimi, S. Khezrian, R. Hallaj, and A. Vaziry, "Highly sensitive electrochemical aptasensor for immunoglobulin E detection based on sandwich assay using enzyme-linked aptamer," *Anal. Biochem.*, vol. 466, pp. 89–97, Dec. 2014.
- [199] A. Ravalli and G. Marrazza, "Gold and Magnetic Nanoparticles-Based Electrochemical Biosensors for Cancer Biomarker Determination," *J. Nanosci. Nanotechnol.*, vol. 15, no. 5, pp. 3307–3319, May 2015.
- [200] J. Fei, W. Dou, and G. Zhao, "A sandwich electrochemical immunosensor for *Salmonella pullorum* and *Salmonella gallinarum* based on a screen-printed carbon electrode modified with an ionic liquid and electrodeposited gold nanoparticles," *Microchim. Acta*, vol. 182, no. 13–14, pp. 2267–2275, Oct. 2015.
- [201] R. Das *et al.*, "An electrochemical genosensor for *Salmonella typhi* on gold nanoparticles-mercaptopilane modified screen printed electrode," *J. Biotechnol.*, vol. 188, pp. 9–16, Oct. 2014.
- [202] A. N. Kozitsina *et al.*, "An enzyme-free electrochemical method for the determination of E-coli using Fe₃O₄ nanocomposites with a SiO₂ shell modified by ferrocene," *J. Anal. Chem.*, vol. 70, no. 5, pp. 540–545, May 2015.
- [203] C. M. Ruan, L. J. Yang, and Y. B. Li, "Rapid detection of viable *Salmonella typhimurium* in a selective medium by monitoring oxygen consumption with electrochemical cyclic voltammetry," *J. Electroanal. Chem.*, vol. 519, no. 1–2, pp. 33–38, Feb. 2002.
- [204] S. Nourani, H. Ghourchian, and S. M. Boutorabi, "Magnetic nanoparticle-based immunosensor for electrochemical detection of hepatitis B surface antigen," *Anal. Biochem.*, vol. 441, no. 1, pp. 1–7, Oct. 2013.
- [205] S. P. Kounaves, *Voltammetric techniques*. Prentice Hall, Upper Saddle River, NJ, USA, 1997.
- [206] M. M. Radhi, E. A. Jaffar Al-Mulla, and W. T. Tan, "Electrochemical characterization of the redox couple of Fe(III)/Fe(II) mediated by grafted polymer electrode," *Res. Chem. Intermed.*, vol. 40, no. 1, pp. 179–192, Jan. 2014.

- [207] UMass Boston, “Cyclic Voltammetry of Ferrocene, [Ru(bpy)₃]²⁺, [Co(bpy)₃]²⁺ and Iodide Introduction.” Chem 371 Advanced Inorganic Chemistry Laboratory, 2017.
- [208] T. E. Meyer *et al.*, “Correlation between rate constant for reduction and redox potential as a basis for systematic investigation of reaction mechanisms of electron transfer proteins.,” *Proc. Natl. Acad. Sci.*, vol. 80, no. 22, pp. 6740–6744, Nov. 1983.
- [209] P. D. Beer, P. A. Gale, and G. Z. Chen, “Mechanisms of electrochemical recognition of cations, anions and neutral guest species by redox-active receptor molecules,” *Coord. Chem. Rev.*, vol. 185–186, pp. 3–36, May 1999.
- [210] S. Guo and E. Wang, “Synthesis and electrochemical applications of gold nanoparticles,” *Anal. Chim. Acta*, vol. 598, no. 2, pp. 181–192, Aug. 2007.
- [211] S. Hrapovic, Y. Liu, K. B. Male, and J. H. T. Luong, “Electrochemical Biosensing Platforms Using Platinum Nanoparticles and Carbon Nanotubes,” *Anal. Chem.*, vol. 76, no. 4, pp. 1083–1088, Feb. 2004.
- [212] F. Li, J. Han, L. Jiang, Y. Wang, Y. Li, Y. Dong, and Q. Wei, “An ultrasensitive sandwich-type electrochemical immunosensor based on signal amplification strategy of gold nanoparticles functionalized magnetic multi-walled carbon nanotubes loaded with lead ions,” *Biosens. Bioelectron.*, vol. 68, pp. 626–632, Jun. 2015.
- [213] H. Jiang, D. Jiang, J. Shao, and X. Sun, “Magnetic molecularly imprinted polymer nanoparticles based electrochemical sensor for the measurement of Gram-negative bacterial quorum signaling molecules (N-acyl-homoserine-lactones),” *Biosens. Bioelectron.*, vol. 75, pp. 411–419, Jan. 2016.
- [214] C. Cheng *et al.*, “Rapid detection of *Listeria monocytogenes* in milk by self-assembled electrochemical immunosensor,” *Sens. Actuators B-Chem.*, vol. 190, pp. 900–906, Jan. 2014.
- [215] T. D. Pfister, A. J. Gengenbach, S. Syn, and Y. Lu, “The Role of Redox-Active Amino Acids on Compound I Stability, Substrate Oxidation, and Protein Cross-Linking in Yeast Cytochrome c Peroxidase,” *Biochemistry*, vol. 40, no. 49, pp. 14942–14951, Dec. 2001.
- [216] J. Deepika, S. Meignanalakshmi, and W. R. Thilagaraj, “A study on bioelectricity production by the synergistic action of *Bacillus tequilensis* DMR-5 and *Pseudomonas aeruginosa* DMR-3 isolated from rumen fluid.,” *Am. J. Environ. Sci.*, vol. 9, no. 5, pp. 424–430, 2013.
- [217] Y.-M. Huang, H.-Y. Hsu, and C.-L. Hsu, “Development of electrochemical method to detect bacterial count, *Listeria monocytogenes*, and somatic cell count in raw milk,” *J. Taiwan Inst. Chem. Eng.*, vol. 62, pp. 39–44, May 2016.

- [218] F. Qian, H. Wang, Y. Ling, G. Wang, M. P. Thelen, and Y. Li, "Photoenhanced Electrochemical Interaction between *Shewanella* and a Hematite Nanowire Photoanode," *Nano Lett.*, vol. 14, no. 6, pp. 3688–3693, Jun. 2014.
- [219] T. Kinoshita, Y. Hatsuoka, D. Q. Nguyen, R. Iwata, H. Shiigi, and T. Nagaoka, "Electrochemical Response of Acridine Orange in Bacterial Cell," *Electrochemistry*, vol. 84, no. 5, pp. 334–337, 2016.
- [220] R. Y. A. Hassan, M. M. Mekawy, P. Ramnani, and A. Mulchandani, "Monitoring of microbial cell viability using nanostructured electrodes modified with Graphene/Alumina nanocomposite," *Biosens. Bioelectron.*, vol. 91, pp. 857–862, May 2017.
- [221] S. M. Bilankohi, "Optical Scattering and Absorption Characteristics of Silver and Silica/Silver Core/shell Nanoparticles," *Orient. J. Chem.*, vol. 31, no. 4, pp. 2259–2263, 2015.
- [222] J. H. Chien *et al.*, "A RFID tag based remote DNA sensing system," in *Nano/Micro Engineered and Molecular Systems, 2006. NEMS'06. 1st IEEE International Conference on*, 2006, pp. 278–282.
- [223] M. A. Hoppens *et al.*, "Maghemite, silver, ceragenin conjugate particles for selective binding and contrast of bacteria," *J. Colloid Interface Sci.*, vol. 413, pp. 167–174, Jan. 2014.
- [224] K. Kleo, D. Schaefer, S. Klar, D. Jacob, R. Grunow, and F. Lisdat, "Immunodetection of inactivated *Francisella tularensis* bacteria by using a quartz crystal microbalance with dissipation monitoring," *Anal. Bioanal. Chem.*, vol. 404, no. 3, pp. 843–851, Aug. 2012.
- [225] P. M. Reddy, K.-C. Chang, Z.-J. Liu, C.-T. Chen, and Y.-P. Ho, "Functionalized magnetic iron oxide (Fe₃O₄) nanoparticles for capturing gram-positive and gram-negative bacteria," *J. Biomed. Nanotechnol.*, vol. 10, no. 8, pp. 1429–1439, Aug. 2014.
- [226] H. Su, Q. Ma, K. Shang, T. Liu, H. Yin, and S. Ai, "Gold nanoparticles as colorimetric sensor: A case study on *E. coli* O157:H7 as a model for Gram-negative bacteria," *Sens. Actuators B Chem.*, vol. 161, no. 1, pp. 298–303, Jan. 2012.
- [227] S. B. Ghosh, K. Bhattacharya, S. Nayak, P. Mukherjee, D. Salaskar, and S. P. Kale, "Identification of different species of *Bacillus* isolated from Nisargruna Biogas Plant by FTIR, UV-Vis and NIR spectroscopy," *Spectrochim. Acta Part -Mol. Biomol. Spectrosc.*, vol. 148, pp. 420–426, Sep. 2015.
- [228] J. K. Streit, S. M. Bachilo, S. Ghosh, C.-W. Lin, and R. B. Weisman, "Directly Measured Optical Absorption Cross Sections for Structure-Selected Single-Walled Carbon Nanotubes," *Nano Lett.*, vol. 14, no. 3, pp. 1530–1536, Mar. 2014.

- [229] Y. Wan *et al.*, “Compact characterization of liquid absorption and emission spectra using linear variable filters integrated with a CMOS imaging camera,” *Sci. Rep.*, vol. 6, no. 1, Sep. 2016.
- [230] E. G. Demissie, G. W. Woyessa, and A. Abebe, “UV/VIS spectrometer determination of caffeine in green coffee beans from Haraghe, Ethiopia, using Beer-Lambert's Law and integrated absorption coefficient techniques,” *Sci. Study Res. Chem. Chem. Eng. Biotechnol. Food Ind.*, vol. 17, no. 2, p. 109, 2016.
- [231] WHO, “Food safety,” *World Health Organization*, 31-Oct-2017. [Online]. Available: <http://www.who.int/news-room/fact-sheets/detail/food-safety>. [Accessed: 20-Nov-2018].
- [232] Pew Research Center, “World Population by Income,” *Pew Research Center*, 08-Jul-2015. [Online]. Available: <http://www.pewglobal.org/interactives/global-population-by-income/>. [Accessed: 20-Nov-2018].
- [233] Y.-M. Bae, L. Zheng, J.-E. Hyun, K.-S. Jung, S. Heu, and S.-Y. Lee, “Growth Characteristics and Biofilm Formation of Various Spoilage Bacteria Isolated from Fresh Produce,” *J. Food Sci.*, vol. 79, no. 10, pp. M2072–M2080, Oct. 2014.
- [234] M. A. Bayoumi, R. M. Kamal, S. F. Abd El Aal, and E. I. Awad, “Assessment of a regulatory sanitization process in Egyptian dairy plants in regard to the adherence of some food-borne pathogens and their biofilms,” *Int. J. Food Microbiol.*, vol. 158, no. 3, pp. 225–231, Sep. 2012.
- [235] N.-Y. Choi, B.-R. Kim, Y.-M. Bae, and S.-Y. Lee, “Biofilm formation, attachment, and cell hydrophobicity of foodborne pathogens under varied environmental conditions,” *J. Korean Soc. Appl. Biol. Chem.*, vol. 56, no. 2, pp. 207–220, Apr. 2013.
- [236] S. Marchand, J. De Block, V. De Jonghe, A. Coorevits, M. Heyndrickx, and L. Herman, “Biofilm Formation in Milk Production and Processing Environments; Influence on Milk Quality and Safety,” *Compr. Rev. Food Sci. Food Saf.*, vol. 11, no. 2, pp. 133–147, Mar. 2012.
- [237] S. G. Parkar, S. H. Flint, J. S. Palmer, and J. D. Brooks, “Factors influencing attachment of thermophilic bacilli to stainless steel,” *J. Appl. Microbiol.*, vol. 90, pp. 901–908, 2001.
- [238] S. Galdiero *et al.*, “Microbe-host interactions: structure and role of Gram-negative bacterial porins,” *Curr. Protein Pept. Sci.*, vol. 13, no. 8, pp. 843–854, 2012.
- [239] A. Camejo, F. Carvalho, O. Reis, E. Leitão, S. Sousa, and D. Cabanes, “The arsenal of virulence factors deployed by *Listeria monocytogenes* to promote its cell infection cycle,” *Virulence*, vol. 2, no. 5, pp. 379–394, Sep. 2011.

- [240] P. Cossart, J. Pizarro-Cerdá, and M. Lecuit, “Invasion of mammalian cells by *Listeria monocytogenes*: functional mimicry to subvert cellular functions,” *Trends Cell Biol.*, vol. 13, no. 1, pp. 23–31, 2003.
- [241] B.-H. Lin, J. C. Buzby, T. D. Anekwe, and J. T. Bentley, “U.S. Food Commodity Consumption Broken Down by Demographics, 1994-2008,” Mar-2016. [Online]. Available: http://www.ers.usda.gov/media/2053482/err-206_summary.pdf. [Accessed: 23-May-2016].
- [242] E. E. Jackson *et al.*, “Detection and Enumeration of Four Foodborne Pathogens in Raw Commingled Silo Milk in the United States,” *J. Food Prot.*, vol. 75, no. 8, pp. 1382–1393, Aug. 2012.
- [243] L. H. Ledenbach and R. T. Marshall, “Microbiological Spoilage of Dairy Products,” in *Compendium of the Microbiological Spoilage of Foods and Beverages*, W. H. Sperber and M. P. Doyle, Eds. New York, NY: Springer New York, 2009, pp. 41–67.
- [244] USDHHS, “Grade ‘A’ Pasteurized Milk Ordinance, 2015 Revision.” U.S. Food and Drug Administration, 2015.
- [245] M. L. Ranieri and K. J. Boor, “Short communication: Bacterial ecology of high-temperature, short-time pasteurized milk processed in the United States,” *J. Dairy Sci.*, vol. 92, no. 10, pp. 4833–4840, Oct. 2009.
- [246] B. Ismail and S. S. Nielsen, “Invited review: Plasmin protease in milk: Current knowledge and relevance to dairy industry,” *J. Dairy Sci.*, vol. 93, no. 11, pp. 4999–5009, Nov. 2010.
- [247] N. Silanikove, U. Merin, and G. Leitner, “Physiological role of indigenous milk enzymes: An overview of an evolving picture,” *Int. Dairy J.*, vol. 16, no. 6, pp. 533–545, Jun. 2006.
- [248] A. J. Langer, T. Ayers, J. Grass, M. Lynch, F. J. Angulo, and B. E. Mahon, “Nonpasteurized Dairy Products, Disease Outbreaks, and State Laws—United States, 1993–2006,” *Emerg. Infect. Dis.*, vol. 18, no. 3, pp. 385–391, Mar. 2012.
- [249] R. S. Sebastian and others, “Fluid Milk Consumption in the United States.” NHANES 2005-2006, Sep-2010.
- [250] FDA, “Buy, Store & Serve Safe Food: Raw Milk Misconceptions and the Danger of Raw Milk Consumption,” 01-Nov-2011. [Online]. Available: <https://www.fda.gov/Food/FoodborneIllnessContaminants/BuyStoreServeSafeFood/ucm247991.htm>. [Accessed: 21-Apr-2017].
- [251] S. Ding, A. A. Cargill, I. L. Medintz, and J. C. Claussen, “Increasing the activity of immobilized enzymes with nanoparticle conjugation,” *Curr. Opin. Biotechnol.*, vol. 34, pp. 242–250, Aug. 2015.

- [252] D. A. D. Giusto and G. C. King, "Special-Purpose Modifications and Immobilized Functional Nucleic Acids for Biomolecular Interactions," in *Immobilisation of DNA on Chips II*, C. Wittmann, Ed. Springer Berlin Heidelberg, 2005, pp. 131–168.
- [253] S.-Y. Lee, J.-H. Lee, J.-H. Chang, and J.-H. Lee, "Inorganic nanomaterial-based biocatalysts," *BMB Rep.*, vol. 44, no. 2, pp. 77–86, Feb. 2011.
- [254] A. Alishahi, "Application of Nanotechnology in Marine-Based Products: A Review," *J. Aquat. Food Prod. Technol.*, vol. 24, no. 5, pp. 533–543, Jul. 2015.
- [255] M. D. Disney and P. H. Seeberger, "The Use of Carbohydrate Microarrays to Study Carbohydrate-Cell Interactions and to Detect Pathogens," *Chem. Biol.*, vol. 11, no. 12, pp. 1701–1707, Dec. 2004.
- [256] M. Leitgeb, K. Herzig, G. H. Podrepsek, A. Hojski, A. Crnjac, and Knez, "Toxicity of Magnetic Chitosan Micro and Nanoparticles as Carriers for Biologically Active Substances," 2014.
- [257] S. Park *et al.*, "Probing Cell-Surface Carbohydrate Binding Proteins with Dual-Modal Glycan-Conjugated Nanoparticles," *J. Am. Chem. Soc.*, vol. 137, no. 18, pp. 5961–5968, May 2015.
- [258] D. Wang *et al.*, "Efficient separation and quantitative detection of *Listeria monocytogenes* based on screen-printed interdigitated electrode, urease and magnetic nanoparticles.," *Food Control*, vol. 73, no. Part B, pp. 555–561, 2017.
- [259] M. Q. Carter *et al.*, "Functional Metagenomics of *Escherichia coli* O157:H7 Interactions with Spinach Indigenous Microorganisms during Biofilm Formation," *PLoS ONE*, vol. 7, no. 9, p. e44186, Sep. 2012.
- [260] P. Klemm, R. M. Vejborg, and O. Sherlock, "Self-associating autotransporters, SAATs: Functional and structural similarities," *Int. J. Med. Microbiol.*, vol. 296, no. 4–5, pp. 187–195, Aug. 2006.
- [261] J. D. Barak, C. E. Jahn, D. L. Gibson, and A. O. Charkowski, "The role of cellulose and O-antigen capsule in the colonization of plants by *Salmonella enterica*," *Mol. Plant. Microbe Interact.*, vol. 20, no. 9, pp. 1083–1091, 2007.
- [262] T. Candela *et al.*, "Environmental and Biofilm-dependent Changes in a *Bacillus cereus* Secondary Cell Wall Polysaccharide," *J. Biol. Chem.*, vol. 286, no. 36, pp. 31250–31262, Sep. 2011.
- [263] I.-H. Cho, P. Bhandari, P. Patel, and J. Irudayaraj, "Membrane filter-assisted surface enhanced Raman spectroscopy for the rapid detection of *E-coli* O157:H7 in ground beef," *Biosens. Bioelectron.*, vol. 64, pp. 171–176, Feb. 2015.

- [264] P.-T. Chu, M.-F. Hsieh, S.-Y. Yin, and H.-W. Wen, "Development of a rapid and sensitive immunomagnetic-bead based assay for detecting *Bacillus cereus* in milk," *Eur. Food Res. Technol.*, vol. 229, no. 1, pp. 73–81, May 2009.
- [265] D. C. Vanegas, Y. Rong, N. Schwalb, K. D. Hills, C. Gomes, and E. S. McLamore, "Rapid detection of listeria spp. using an internalin A aptasensor based on carbon-metal nanohybrid structures," 2015, pp. 948708-1 to – 7.
- [266] L. Wang, W. Zhao, M. B. O'Donoghue, and W. Tan, "Fluorescent nanoparticles for multiplexed bacteria monitoring," *Bioconjug. Chem.*, vol. 18, no. 2, pp. 297–301, Apr. 2007.
- [267] J. Wu, Y. X. Ben, and H. C. Chang, "Particle detection by electrical impedance spectroscopy with asymmetric-polarization AC electroosmotic trapping," *Microfluid. Nanofluidics*, vol. 1, no. 2, pp. 161–167, May 2005.
- [268] R. I. Merker, "Bacteriological Analytical Manual (BAM), 8th Edition, Revision A." Office of Special Research Skills, CFSAN, USFDA, 1998.
- [269] E. Czerwińska and W. Piotrowski, "Potencjalne źródła skażenia mleka wpływające na jego jakość spożywczą (Potential Sources of Milk Contamination Influencing its Quality for Consumption)," *Rocz. Ochr. Śr.*, vol. 13, pp. 633–651, 2011.
- [270] S. N. Masiello, N. H. Martin, A. Trmčić, M. Wiedmann, and K. J. Boor, "Identification and characterization of psychrotolerant coliform bacteria isolated from pasteurized fluid milk," *J. Dairy Sci.*, vol. 99, no. 1, pp. 130–140, Jan. 2016.
- [271] S. Migeemanathan, R. Bhat, L. Min-Tze, and W.-N. Wan-Abdullah, "Effects of Temperature Abuse on the Survival, Growth, and Inactivation of *Salmonella typhimurium* in Goat Milk," *Foodborne Pathog. Dis.*, vol. 8, no. 11, pp. 1235–1240, Nov. 2011.
- [272] L. Necidová *et al.*, "Growth and enterotoxin production of *Bacillus cereus* in cow, goat, and sheep milk," *Acta Vet. Brno*, vol. 83, no. 10, pp. S3–S8, 2015.
- [273] B. I. Escudero-Abarca, S. H. Suh, M. D. Moore, H. P. Dwivedi, and L.-A. Jaykus, "Selection, Characterization and Application of Nucleic Acid Aptamers for the Capture and Detection of Human Norovirus Strains," *PLoS ONE*, vol. 9, no. 9, p. e106805, Sep. 2014.
- [274] NIH, "Stop the Spread of Superbugs Help Fight Drug-Resistant Bacteria," *NIH News in Health*, Feb-2014. [Online]. Available: <https://newsinhealth.nih.gov/issue/feb2014/feature1>. [Accessed: 22-Jul-2016].
- [275] A. M. Alkilany and C. J. Murphy, "Toxicity and cellular uptake of gold nanoparticles: what we have learned so far?," *J. Nanoparticle Res.*, vol. 12, no. 7, pp. 2313–2333, Sep. 2010.
- [276] X. Hua, Y. Du, J. Chen, G. Xu, T. Yu, and Q. Zhang, "Evaluation of the enantioselectivity of carbon nanoparticles-modified chiral separation systems using dextrin as chiral selector

by capillary electrokinetic chromatography: CE and CEC,” *ELECTROPHORESIS*, vol. 34, no. 13, pp. 1901–1907, Jul. 2013.

[277] F. Porta, “Gold nanostructured materials for the selective liquid phase catalytic oxidation,” *J. Mol. Catal. Chem.*, vol. 204–205, pp. 553–559, Sep. 2003.

[278] CDC, “Multistate Outbreaks,” *Foodborne Outbreaks*, 2015. [Online]. Available: <http://www.cdc.gov/foodsafety/outbreaks/multistate-outbreaks/index.html>. [Accessed: 31-Oct-2015].

[279] C. Beach, “U.N. officials say food safety is entwined with food security,” *Food Safety News*, 09-Jun-2016. [Online]. Available: <http://www.foodsafetynews.com/2016/06/u-n-officials-say-food-safety-is-entwined-with-food-security/>. [Accessed: 28-Jun-2017].